Tampere University

SINI EEROLA

The Role of PIM Kinases in Prostate Cancer

Promoting and Inhibiting Factors

Tampere University Dissertations 563

Tampere University Dissertations 563

SINI EEROLA

The Role of PIM Kinases in Prostate Cancer

Promoting and Inhibiting Factors

ACADEMIC DISSERTATION
To be presented, with the permission of
the Faculty of Medicine and Health Technology
of Tampere University,
for public discussion in the auditorium F115
of the Arvo building, Arvo Ylpön katu 34, Tampere,
on 11th of March 2022, at 12 o'clock.

ACADEMIC DISSERTATION
Tampere University, Faculty of Medicine and Health Technology
Finland

Responsible supervisor and Custos	Professor Tapio Visakorpi Tampere University Finland	
Supervisors	Adjunt professor Päivi Koskinen University of Turku Finland	Adjunt professor Leena Latonen University of Eastern Finland Finland
Pre-examiners	Adjunt professor Tuomas Mirtti University of Helsinki Finland	Adjunt professor Päivi Östling Åbo Akademi Finland
Opponent	Professor Juha Klefström University of Helsinki Finland	

The originality of this thesis has been checked using the Turnitin OriginalityCheck service.

Cover design: Roihu Inc.

ISBN 978-952-03-2315-8 (print)
ISBN 978-952-03-2316-5 (pdf)
ISSN 2489-9860 (print)
ISSN 2490-0028 (pdf)
http://urn.fi/URN:ISBN:978-952-03-2316-5

PunaMusta Oy – Yliopistopaino
Joensuu 2021

ABSTRACT

Prostate cancer is the most common cancer in males, and it is one of the leading causes of death in developed countries. Although, the five-year life expectancy of all diagnosed cases is usually good, prostate cancer is still a fatal disease. Prostate cancer is often diagnosed based on elevated prostate specific antigen (PSA) values, digital rectal examinations (DRE), and needle biopsies of the prostate. The most common therapy options for prostate cancer are surgery or radiation therapy, androgen deprivation therapy (ADT), and chemotherapy. As altered androgen receptor (AR) signaling is central in the development and progression of prostate cancer, ADT as primary therapy is initially functional. However, eventually cancer develops to a castration-resistant form for which there is no curative treatment available. In prostate cancer, formation of metastases to distant organs, especially to adjacent lymph nodes and bones is an unfavorable and difficult characteristic in terms of functional therapy options (Teo et al. 2019).

PIM kinases are well-known oncoproteins promoting cell proliferation, migration, and survival as well as stimulating activities of several transcription factors that can contribute to tumorigenesis. PIM kinases form a family of serine/threonine kinases that consists of three members, PIM1, PIM2, and PIM3. The functions and expression patterns of these three family members are partially overlapping. Enhanced expression of PIM family members has been detected both in hematopoietic malignancies and in solid tumors such as prostate cancer, where PIM overexpression has been shown to correlate with tumor aggressiveness and thereby also with worse prognosis of patients. In this thesis, the expression levels of different PIM family members were studied during prostate cancer progression, and prostate cancer cell lines and xenograft models were used to evaluate the effects of PIM inhibition on tumor growth and metastatic motility. We demonstrated that higher expression levels of PIM kinases increase tumor growth and cancer cell motility and thereby enhance the formation of metastases. By contrast, inhibition of PIM kinases by specific PIM-selective inhibitors decreased tumor growth and metastatic potential of prostate cancer. In prostate cancer patient samples, expression of all PIM kinases

was increased compared to benign prostate samples. Moreover, PIM1 and PIM2 protein levels were further increased during prostate cancer development from hormone-naïve primary tumor into castration-resistant prostate cancer.

The NFATC1 transcription factor is one of the PIM1 kinase substrates whose transactivation potential is enhanced by PIM1-dependent phosphorylation. In the immune system, NFATC transcription factors transcriptionally regulate the activation, development, and differentiation of helper T-cells. In addition, upregulated activities of both PIM and NFATC1 have been shown to promote tumorigenesis by regulating cell proliferation, migration, invasion, and angiogenesis. In this thesis, PIM kinases have been demonstrated to enhance NFATC1 activity through phosphorylation of seven serine and three threonine residues, leading to increased migration and invasion of prostate cancer cells. Additionally, we have identified alpha 5 integrin (ITGA5) as a potent target of the interplay between PIM and NFATC1 in prostate cancer, where it increases invasion of cancer cells.

To exert their oncogenic functions in cancer cells, PIM kinases co-operate with other tumorigenic proteins. In prostate cancer, these proteins include the MYC and ERG transcription factors which are commonly overexpressed there. Here, we examined co-expression of all PIM kinases with these oncoproteins and evaluated how they regulate PIM-dependent signaling. Our data suggests that both *PIM1* and *PIM3* cooperate with *MYC* in prostate tumorigenesis. Moreover, our results indicate that ERG associates with and regulates the expression of all three PIM kinases in prostate cancer cells.

Altogether, results presented in this thesis indicate that PIM kinases have an important role in the development and progression of prostate cancer. Moreover, inhibition of the PIM signaling pathway may provide benefits especially for such patients who have high PIM expression levels and metastatic cancer. As PIM kinases co-operate with several other oncoproteins, their targeted inhibition in combinations may be more profitable than monotherapies. However, additional studies will be needed to evaluate the efficacy of such combinatorial therapies.

TIIVISTELMÄ

Eturauhassyöpä on miesten yleisin syöpä ja on yksi merkittävimmistä kuolemaan johtavista syistä kehittyneissä maissa. Vaikka viiden vuoden eliniänodote diagnoosin jälkeen on yleensä hyvä, eturauhassyöpä voi silti myös olla kuolemaan johtava sairaus. Eturauhassyöpä diagnosoidaan usein kohonneen PSA-arvon (prostate specific antigen), eturauhasen tunnustelun (tuseeraus per rectum) ja eturauhasesta otettujen ohutneulanäytteiden perusteella. Tärkeimmät eturauhassyövän hoitomuodot tällä hetkellä ovat leikkaus tai sädehoito sekä hormonaalinen hoito ja solusalpaajat. Muutokset androgeenireseptori (AR) -välitteisessä signalointireitissä ovat keskeisiä eturauhassyövän synnyssä ja kehityksessä. Näin ollen androgeenihormonin esto eli kastraatio onkin aluksi toimiva hoitokeino, mutta lopulta syöpä kehittyy kastraatioresistentiksi eturauhassyöväksi, jolle ei ole parantavaa hoitomuotoa. Yksi eturauhassyöpäkasvainten hoidollisesti hankalimmista ominaisuuksista on, että ne lähettävät etäpesäkkeitä eri puolille elimistöä, etenkin luihin ja viereisiin imusolmukkeisiin.

PIM-kinaasit ovat tunnettuja syöpäproteiineja, jotka vaikuttavat syövän etenemiseen edistämällä solujen jakautumista, estämällä solukuolemaa ja stimuloimalla monien sellaisten transkriptiotekijöiden aktiivisuutta, jotka osaltaan edistävät syövän kehitystä. PIM-kinaasit muodostavat seriini/treoniini-kinaasiperheen, johon kuuluu kolme jäsentä, PIM1, PIM2 ja PIM3. Näiden perheenjäsenten toiminta ja ilmeneminen ovat osittain päällekkäisiä. Kaikkien PIM-kinaasien on havaittu ilmenevän liiallisesti niin verisolusyövissä kuin kiinteissä kasvaimissakin, kuten eturauhassyövässä, jossa niiden yli-ilmeneminen korreloi huonon tautiennusteen ja syövän pahanlaatuisuuden kanssa. Tässä väitöskirjatyössä kartoitettiin tarkemmin eri PIM-kinaasien roolia eturauhassyövän etenemisessä ja havainnoitiin PIM-inhibition vaikutuksia syöpäsolujen liikkuvuuteen ja etäpesäkkeiden muodostumiseen eri syöpämalleissa. Huomasimme, että korkeammat PIM-kinaasien ilmenemistasot lisäävät syöpäkasvainten kasvua, syöpäsolujen liikkuvuutta ja etäpesäkkeiden muodostumista. Sitä vastoin spesifiset PIM-inhibiittorit hidastavat eturauhaskasvainten kasvua ja kykyä muodostaa etäpesäkkeitä. Eturauhassyöpänäytteissä kaikkien PIM-proteiinien ilmenemistasot kasvoivat

verrattuna hyvänlaatuisiin eturauhasnäytteisiin. Lisäksi PIM1 ja PIM2 -ilmenemistasot voimistuivat eturauhassyövän edetessä primaarisesta syövästä kastraatioresistenttiin muotoon.

NFATC1-transkriptiotekijä on yksi PIM1-kinaasin substraateista, jonka transaktivaatiokykyä PIM1-välitteinen fosforylaatio voimistaa. Säätelemällä geenien transkriptiota NFATC-proteiinit vaikuttavat oleellisesti immuunijärjestelmän toimintaan ja erityisesti auttaja-T-solujen aktivaatioon, kehitykseen ja erilaistumiseen. Lisäksi tutkimuksissa on havaittu, että sekä PIM- että NFATC1-proteiinien liiallinen aktivoituminen tehostaa syövän kehitystä stimuloimalla syöpäsolujen jakautumista, liikkuvuutta ja kykyä muodostaa verisuonia. Tässä väitöskirjassa osoitettiin, että PIM-kinaasit voimistavat NFATC1-transkriptiotekijän aktiivisuutta fosforyloimalla siitä seitsemän seriini- ja kolme treoniinitähdettä, minkä seurauksena eturauhassyöpäsolujen liikkuvuus ja invasoituminen lisääntyvät. Lisäksi havaitsimme, että integriini alfa 5 (ITGA5) on potentiaalinen PIM- ja NFATC1-proteiinien vuorovaikutuksen kohdegeeni, joka vaikuttaa eturauhassyöpäsolujen invaasiokykyyn.

Välittääkseen vaikutuksensa syöpäsoluissa, PIM-kinaasit toimivat yhteistyössä muiden syöpää aiheuttavien proteiinien, kuten MYC- ja ERG-syöpäproteiinien kanssa, joiden liiallinen ilmeneminen on hyvin yleistä eturauhassyövässä. Tässä väitöskirjassa tutkittiin näiden syöpäproteiinien ja PIM-kinaasien yhteisekspressiota sekä sitä, miten ne säätelevät PIM-signaalinvälitysreittiä. Tulostemme mukaan PIM1- ja PIM3-kinaasit edistävät MYCin kanssa eturauhassyövän kehittymistä. Tuloksemme osoittivat, että myös ERG-proteiinin ekspressio voimistuu yhdessä kaikkien PIM-kinaasien ilmenemisen kanssa. Lisäksi havaitsimme, että ERG voi säädellä kaikkien kolmen PIM-kinaasin ilmenemistä eturauhassyöpäsoluissa.

Yhteenvetona tämän väitöskirjan tulokset osoittavat, että PIM-kinaaseilla on oleellinen merkitys eturauhassyövän synnyssä ja kehityksessä. Lisäksi PIM-signalointireitin estolääkityksestä voisi olla hyötyä etenkin sellaisille eturauhassyöpäpotilaille, joilla PIM-tasot ovat korkealla ja joilla on etäpesäkkeitä. Koska PIM-kinaasit toimivat yhteistyössä muiden syöpäproteiinien kanssa, voisi niiden yhteisestosta olla hyötyä potilaiden hoidossa. Lisää tutkimuksia kuitenkin tarvitaan tällaisten terapeuttisten mahdollisuuksien arvioimiseksi.

CONTENTS

List of Figures

List of Tables

ABBREVIATIONS

ACTB	actin beta
ADT	androgen deprivation therapy
ADP	adenosine diphosphate
AKT	v-akt murine thymoma viral ongogene homolog
AR	androgen receptor
ATP	adenosine 5'-triphosphate
BA	benzo [*cd*] azulene
BAD	BCL2-associated agonist of cell death
BCL2	B-cell lymphoma 2
BPH	benign prostatic hyperplasia
CDK	cyclin-dependent kinase
CK	casein kinase
CRPC	castration-resistant prostate cancer
CsA	cyclosporin A
CXCR	chemokine (C-X-C motif) receptor
CXCL	chemokine (C-X-C motif) ligand
DDR	DNA damage responsive
DHPCC-9	1,10-dihydropyrrolo[2,3-a]carbazole-3-carbaldehyde compound 9 (a pan-PIM inhibitor)
DHT	dihydrotestosterone
DM	double mutant NFATC1
DMA	N, N-dimethylacetamine
DMSO	dimethyl sulfoxide
DN	dominant negative
DYRK	dual-specificity tyrosine phosphorylation-regulated kinase
ECM	extra cellular matrix
EMT	epithelial-mesenchymal transition
ERG	ETS transcription factor 1/ ETS-related gene 1

ETS	E26 transformation specific family of transcription factors
GFP	green fluorescent protein
GG	Gleason grade
GS	Gleason score
GSK	glycogen synthase kinase
GST	glutathione S-transferase
IFN	interferon
IHC	immunohistochemistry
IKKε	inhibitor of nuclear factor kappa-B kinase subunit epsilon
IL	interleukin
IM	ionomycin
ITGA5	integrin alpha 5
JAK	Janus kinase
KLF	krüppel-like factor
KLK3	kallikrein-related peptidase 3
mCRPC	metastatic CRPC
MM	multimutant NFATC1
MMPs	matrix metalloproteinases
mSRR	constitutively active mutant of NFATC1
MYC	v-myc avian myelocytomatosis viral oncogene homolog
NFAT	Nuclear Factor of Activated T-cells
PARPi	Poly(ADP-ribose) polymerase inhibitor
PCR	polymerase chain reaction
PI3K	phosphatidylinositol-3-kinase
PIM	proviral integration site for Moloney murine leukemia virus
PIN	prostatic intraepithelial neoplasia
PKA	protein kinase A
PSA	prostate-specific antigen
STAT	signal transducer and activator of transcription
PTEN	phosphatase and tensin homolog
RB	retinoblastoma protein
RT-qPCR	reverse transcription quantitative PCR

TBP	TATA-binding protein
TMPRSS2	transmembrane serine protease 2
TP53	tumor protein P53
TPA	12-0-tetradecanoyl-phorbol-13-asetate
TR	triple mutant NFATC1
UTR	untranslated region
WT	wild-type

ORIGINAL PUBLICATIONS

Publication I Santio NM, Eerola SK, Paatero I, Yli-Kauhaluoma J, Anizon F, Moreau P, Tuomela J, Härkönen P, Koskinen PJ. Pim kinases promote migration and metastatic growth of prostate cancer xenografts by employing the CXCL12/CXCR4 pathway. PLOS One, 2015; 10(6): e0130340.

Publication II Eerola SK, Santio NM, Rinne S, Kouvonen P, Corthals G, Scaravilli M, Scala G, Serra A, Greco D, Ruusuvuori P, Rainio EM, Latonen L, Visakorpi T, Koskinen PJ. Phosphorylation of NFATC1 at multiple sites is essential for its ability to promote prostate cancer cell migration and invasion. Cell Communication and Signaling, 2019; 17(1):148.

Publication III Eerola SK, Kohvakka A, Tammela TLJ, Koskinen PJ, Latonen L, Visakorpi T. Expression and ERG-regulation of PIM kinases in prostate cancer. Cancer Medicine, 2021; 10(10):3427-3436.

THE AUTHOR'S CONTRIBUTION

Publication I MSc Sini Eerola and Dr. Niina Santio together planned and performed all the animal experiments with mice, and partly together acquired and analysed data from them. The manuscript was mainly prepared by Dr. Niina Santio and Adj. Prof. Päivi Koskinen, but Eerola also partly contributed there. These studies were carried out in the University of Turku, Finland.

Publication II MSc Sini Eerola concepted and designed the study, acquired, and analysed the data together with her supervisors. Eerola had an important role in interpreting the results and she drafted and revised the manuscript together with her supervisors, Dr. Eeva Rainio, and Dr. Niina Santio. These studies were initiated in the University of Turku, Finland and finalized in the Tampere University, Finland.

Publication III MSc Sini Eerola designed the experiments together with her supervisors. Eerola also performed the experiments and analyzed the data. Exceptionally, RT-qPCR-samples were prepared and analyzed by MSc Annika Kohvakka. Eerola had an important role in interpreting the results and she drafted and revised the manuscript together with her supervisors. These studies were carried out in the Tampere University, Finland.

This thesis work was supervised by Prof. Tapio Visakorpi, Adj. Prof. Päivi Koskinen and Adj. Prof. Leena Latonen.

1 INTRODUCTION

Prostate cancer is one of the most common cancers in males, with approximately 1.3 million new diagnoses worldwide every year (GBD 2017 Disease and Injury Incidence and Prevalence Collaborators, Sung et al. 2021). Prostate cancer is often localized and thus relatively indolent with high overall survival (Rawla, 2019). However, some prostate tumors express an aggressive phenotype with rapid progression; therefore, men with this type of disease have shorter overall survival (Sandhu et al. 2021). Prostate cancer incidence is strongly age-related. The average age at the time of diagnosis is approximately 66 years. Other known risk factors are ethnicity of African descent, positive family history, and there is probable evidence of increased risk from taller height. Moreover, obesity, smoking, environmental factors–particularly a high fat, high processed carbohydrate diet, and low physical activity increase the risk of advanced or lethal prostate cancer (Pernar et al. 2018). In addition, genetic factors may have an impact on prostate cancer incidence (Rawla, 2019). Prostate cancer is often diagnosed without any symptoms, based solely on elevated prostate-specific antigen (PSA) values. However, increased PSA levels do not always indicate the presence of prostate cancer, as benign prostate diseases, such as inflammation or benign prostatic hyperplasia, often raise the levels of serum PSA (Lilja et al. 2008). Therefore, elevated PSA levels are not an accurate way to diagnose prostate cancer and may even lead to overtreatment. The prognosis and treatment options depend mainly on the stage of the prostate cancer. Therapy options for prostate cancer are surgery, androgen deprivation therapy, radiation, and chemotherapy (Sandhu et al. 2021). The androgen receptor (AR) signaling pathway is central in the development and progression of prostate cancer. Initially, androgen deprivation is an efficient treatment in prostate cancer, but eventually, the disease develops into castration-resistant prostate cancer (CRPC). For CRPC, there is no curative treatment available.

Different gene expression pathways have important roles in prostate cancer progression. Normal, noncancerous cells grow under strong surveillance, and when they become carcinogenic, their normal phenotype is first transformed due to genetic

changes that affect proteins involved in cell proliferation and cell death. Both acquired and inherited genetic alterations result in the malfunction of genes. These genes are generally divided into two main classes in cancer biology: oncogenes and tumor suppressors. Increased activation of oncogenes stimulates the proliferation of cancer cells. Tumor suppressor genes regulate multiple cellular processes, and they are often inactivated in cancer cells (Sherr, 2004, Kontomanolis et al. 2020). Most oncogenic signaling pathways also contain activated transcription factors that control gene expression patterns affecting tumor formation and progression as well as metastasis. To prevent prostate cancer progression, it is extremely important to understand and inhibit these cancer-promoting molecular events and signaling pathways, with inactivated tumor suppressors and activated oncogenes.

One of the most malignant properties of prostate cancer cells is that they metastasize from the prostate to other parts of the body, especially to bones and lymph nodes. Metastases are the cause of approximately 90% of human cancer deaths (Guan et al. 2015, Fares et al. 2020). Preventing cancer cell migration and invasion and thereby the formation of metastasis would be an extremely effective way to stop prostate cancer from progressing to a fatal stage.

More research is still needed for the molecular characterization of localized, recurrent, and progressive disease, as it would have an impact on clinical therapy options. Hence, new molecular markers and drug targets are needed for diagnostics and therapeutic purposes.

2 REVIEW OF THE LITERATURE

2.1 Development and progression of cancer

2.1.1 Oncogenesis

The development of cancer is a stepwise process that involves several physiological alterations in cells. In normal cells, cell division and cell death are carefully regulated. However, during cancer progression, these important regulatory mechanisms are disturbed. The hallmarks of cancer are well known (Hanahan & Weinberg 2000, Hanahan & Weinberg 2011, Hanahan 2022) and include several traits acquired by the cells to promote their transformation into cancer cells. First, cancer cells become self-sufficient in growth signals, which means that they are capable of producing or mimicking important growth signals that are needed for them to proliferate. Second, cancer cells are insensitive to antigrowth signals, which normally block proliferation according to the cell cycle clock. In addition, cancer cells evade apoptosis (programmed cell death) and have limitless potential to replicate.

To achieve limitless replication, telomerase enzyme must prevent shortening of chromosomal telomeres. Telomeres are DNA sequences at the ends of chromosomes, and they usually shorten by 50-100 bp in every cell division, thereby functioning as limiting factors for cell division. In addition, for tumor formation and the progression of cancer, cells must sustain angiogenesis, as the vasculature provides crucial oxygen and nutrients for cancer cells. One main characteristic of cancer is the ability of cancer cells to invade and form metastases. Moreover, tumor growth-enabling characteristics include genome instability involving dynamic changes in the genome. Due to aberrant cell proliferation, the possibility of genomic changes and mutations increases and contributes to the damage of genes regulating cell division and tumor suppression. Oncogenic mutations produce this interference, which induces signals directing cell division and the spread of transformed cell populations to adjacent tissues, and as a contrasting effect, reduces cell death (Hanahan & Weinberg 2000, Hanahan & Weinberg 2011). Tumor-promoting

inflammation can also contribute to cancer progression by supplying bioactive molecules to the tumor microenvironment, including survival, growth and proangiogenic factors and extracellular matrix-modifying enzymes (Hanahan and Weinberg 2011).

Normal differentiated cells predominantly utilize mitochondrial oxidative phosphorylation to generate the energy needed for different cellular processes. In contrast, most cancer cells rely on reprogrammed energy metabolism, as they use the glycolytic pathway to degrade glucose to lactate in the cytoplasm even in the presence of oxygen (aerobic glycolysis). This phenomenon is named the Warburg effect. Cancer cells have the ability to metabolize glucose anaerobically rather than aerobically, even when oxygen is available. The utilization of glycolysis assists under hypoxic conditions that are common within many tumors. In addition, evading immune destruction enables cancer progression. Normally, immune surveillance enables the recognition and elimination of incipient cancer cells and thus prevents tumor initiation. However, immunogenic cancer cells may evade immune destruction by incapacitating components of the immune system (Hanahan and Weinberg 2011).

2.1.2 Oncogenes and tumor suppressors

Proto-oncogenes are essential for normal cell activity, and their protein products play a role in the regulation of the proliferation, apoptosis, and cell differentiation. Genetic errors or mutations may alter proto-oncogenes to more active oncogenes, resulting in cancer. Activation of an oncogene leads to the formation of abnormally active protein or enhanced expression of the protein. Chromosomal translocations may lead to the production of fusion proteins, which have abnormal activities. Protein overexpression may be due to gene amplifications or mutations in the regulatory regions. In addition, point mutations within coding sequences may create protein products, that are constitutively active. Translocation may also transfer the proto-oncogene under the control of a more active promoter and thereby lead to protein overexpression. However, activation of a single oncogene may not be enough to cause cancer formation, for which several oncogenic events are usually required (Hanahan and Weinberg 2011, Kontomanolis et al. 2020).

In contrast to proto-oncogenes and oncogenes, most tumor suppressor genes decrease cell proliferation or survival. Tumor suppressor genes encode proteins

transmitting signals that control cell division (Hanahan & Weinberg 2000, Hanahan and Weinberg 2011, Chen et al. 2020, Kontomanolis et al. 2020). Cancer development often begins as a result of the accumulation of consecutive somatic mutations (Jolly & Van Loo, 2018). Normal cells usually undergo both gain-of-function mutations in oncogenes and loss-of-function mutations in tumor suppressor genes before cancer initiation (Knudson 1971, Knudson 2001). Diploid organisms, such as humans, undergo gain-of-function mutations that are mostly dominant, while loss-of-function mutations are often recessive. The two-hit hypothesis of oncogenesis suggests that tumor progression starts with the loss of both alleles of a tumor suppressor gene, indicating a recessive mutation (Knudson et al. 2001). Inactivation of tumor suppressor genes therefore leads to tumor development when negative regulation is prevented. In many cases, tumor suppressor proteins inhibit the same cell regulatory pathways that are stimulated by oncogenes. The first tumor suppressor identified was a protein known as retinoblastoma protein (RB) and its corresponding gene, *RB1*. The activity of retinoblastoma protein terminates the expression of genes needed for progression of the cell cycle; hence, its inactivation leads to uncontrolled cell division (Classon & Harlow, 2002, Linn et al. 2021). Moreover, one of the most commonly mutated gene in human tumors and the most well-known tumor suppressor is tumor protein p53 (*TP53*).

2.2 Prostate cancer

The prostate is small approximately 15-20 grams weighing male reproductive gland involved in fertility. The main function of the prostate is the secretion of fluid that contains proteolytic enzymes, prostatic acid phosphatase (PAP/ACPP), alkaline phosphatase (AP), and prostate-specific antigen/kallikrein-related peptidase 3 (PSA/KLK3) into semen to make it favorable to the normal function of spermatozoa (Bauer 1988). The prostate is located below the urinary bladder and attached to the neck of the bladder. The prostate surrounds the prostatic urethra and ejaculatory ducts. The prostatic capsule covers the prostate, which is formed of small glands (acini) and connective tissue. The prostate is divided into four anatomic regions or zones described by McNeal 1981. These zones of the prostate are called the peripheral zone (PZ), the central zone (CZ), the transition zone (TZ), and the anterior fibromuscular stroma (AFMS) (McNeal 1981). Moreover, the periurethral zone (PuZ) surrounds the urethra within the transitional zone (Figure 1).

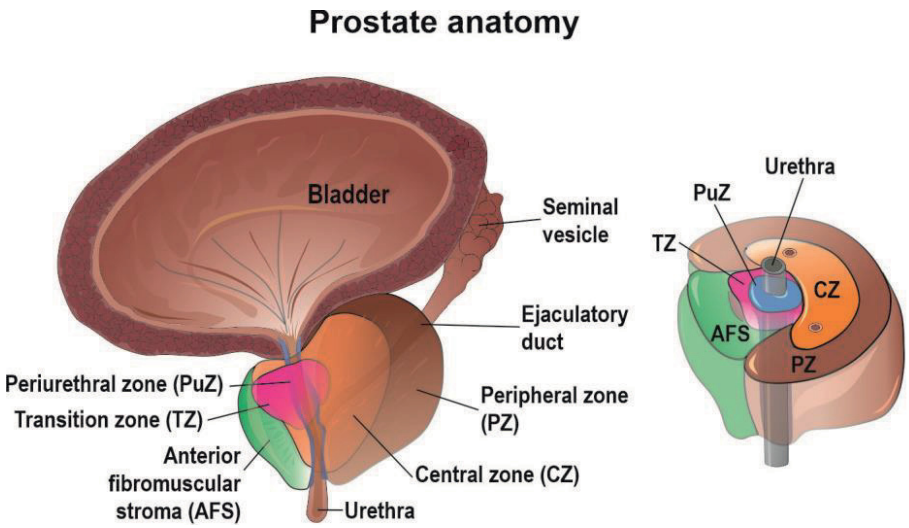

Figure 1. Anatomy of the prostate.

(This figure is based on the Urological Illustrations by Fairman Studios for American Urological Association patient education materials, 2021, https://medika.life/the-prostate-gland/)

Prostatic disorders include enlargement, inflammation, infection, and cancer. Most often, prostate cancer arises from the PZ in the back of the prostate near the rectum. The CZ constitutes most of the base of the prostate and surrounds the ejaculatory ducts. Only a small portion of cancers arise from this region. TZ carcinomas represent approximately one-fifth of the tumor cases. Moreover, the pathogenesis of nonmalignant enlargement of the prostate gland, benign prostatic hyperplasia (BPH), is initiated in the TZ. (McNeal et al. 1988, Aaron et al. 2016) The prostate consists of stroma and epithelial cells. Stroma consists of smooth muscle cells, fibroblasts and endothelial cells, while epithelial cells include secretory, basal and neuroendocrine cells.

2.2.1 Diagnostics of prostate cancer

Prostate cancer is often primarily detected by measuring prostate-specific antigen (PSA) (Wang et al. 1979) levels (ng/ml). The main purpose of PSA test is to observe evidence of a recurrence after the prostate cancer treatment. However, the PSA level is also used as a prognostic marker for prostate cancer survival and the formation of metastases (Kuriyama et al. 1981, Lomas and Ahmed 2020). PSA testing was first approved to monitor disease status by the United States Food and Drug

Administration (FDA) in 1986. Later, it was authorized in the diagnosis process after research findings by Catalona et al. 1994. PSA is not a cancer-specific marker and its testing easily causes over diagnostics, therefore it is not used for population level screening. In addition to the determination of serum PSA, digital rectal examinations (DRE) and transrectal ultrasound-guided needle biopsies are utilized for the diagnosis, localization, and histopathological scoring of the tumorous tissue (Weaver et al. 1991). Usually, 12 needle biopsies are systematically taken from the prostate. Because of the lack of specific prostate cancer markers, pre-imaging risk-stratification tools like magnetic resonance imaging (MRI) and PET-CT have risen to higher role. In addition, there are several molecular biomarkers that can be assessed from blood, body fluid, or tumor tissue to estimate risk for prostate cancer or to detect it, and also to determine prognosis and estimate responses for different treatment options (Bekelman et al. 2018). Currently commercially available biomarker panels include Oncotype Dx Prostate, Prolaris, Decipher, Decipher PORTOS, ProMark (Eggner et al. 2019), and Stockholm-3 model (S3M) (Ström et al. 2018). All men with metastatic prostate cancer should be provided germline and tumor genetic testing, as it is known that there is high incidence of germline and somatic gene alterations in advanced prostate cancer (Sandhu et al. 2021). However, these assays are not yet recommended to be routinely used in localized prostate cancers, as they do not provide significant improvement for long-term outcomes like survival (Eggner et al. 2019).

2.2.2 Histology of the prostate

Prostatic glands are composed of pilar-shaped luminal epithelial cells and more flattened basal cells, which are surrounded by smooth muscle. In addition, neuroendocrine cells are interspersed within the prostate epithelium. The normal gland contains a basal cell layer and an intraluminal section of secretory epithelial cells (Figure 2A-B).

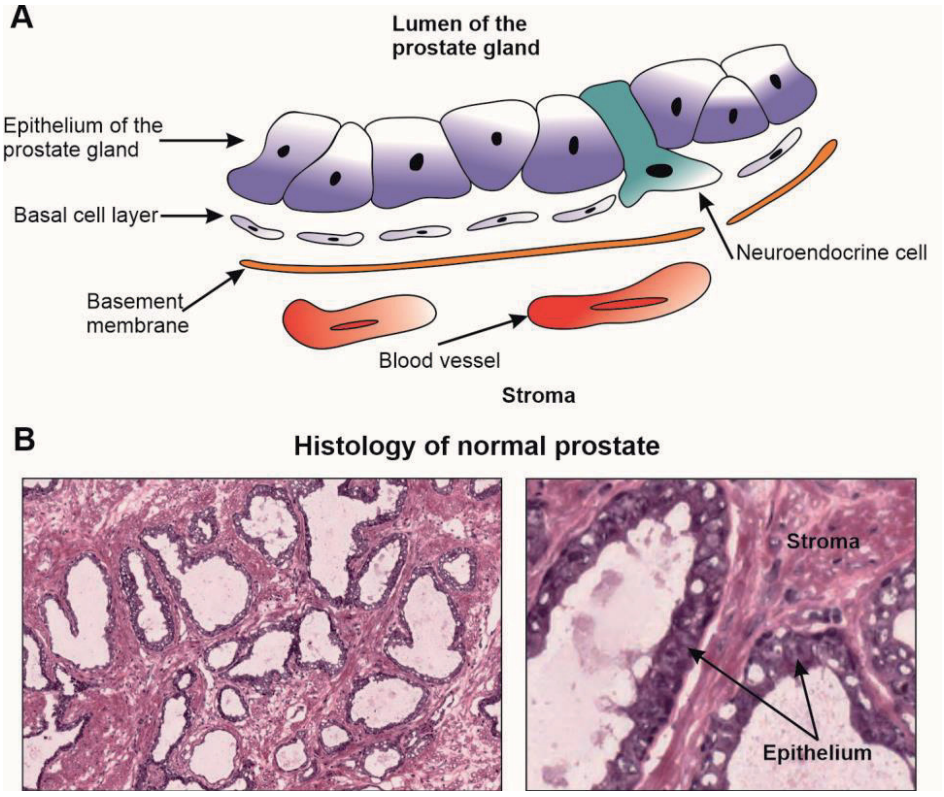

Figure 2. Structure (A) and histology (B) of the prostate gland.

Based on a histological examination of prostate specimens, in benign prostatic hyperplasia (BPH), the amounts of epithelial and stromal components are increased, the structure of the prostate is nodular, and the epithelial layer may also become flattened as the stromal section increases (Foster 2000) (Figure 3A). Prostatic intraepithelial neoplasia (PIN) is a premalignant stage of prostate cancer and is defined by neoplastic growth of epithelial cells within pre-existing benign prostatic glands (Brawer 2005) (Figure 3B). Adenocarcinoma can be distinguished from benign glands by the absence of basal cells. Moreover, prostate cancer cells have nuclear atypia, determined by enlargement of nuclei and prominent nucleoli. Furthermore, the glandular form of the glands disappears or becomes unidentifiable when the tumor becomes more malignant (Magi-Galluzzi 2018) (Figure 3C). Castration-resistant prostate cancer (CRPC) is histologically often poorly differentiated, the glandular structure of the prostate glands is unrecognizable and cancer cells are dispersed (Figure 3D).

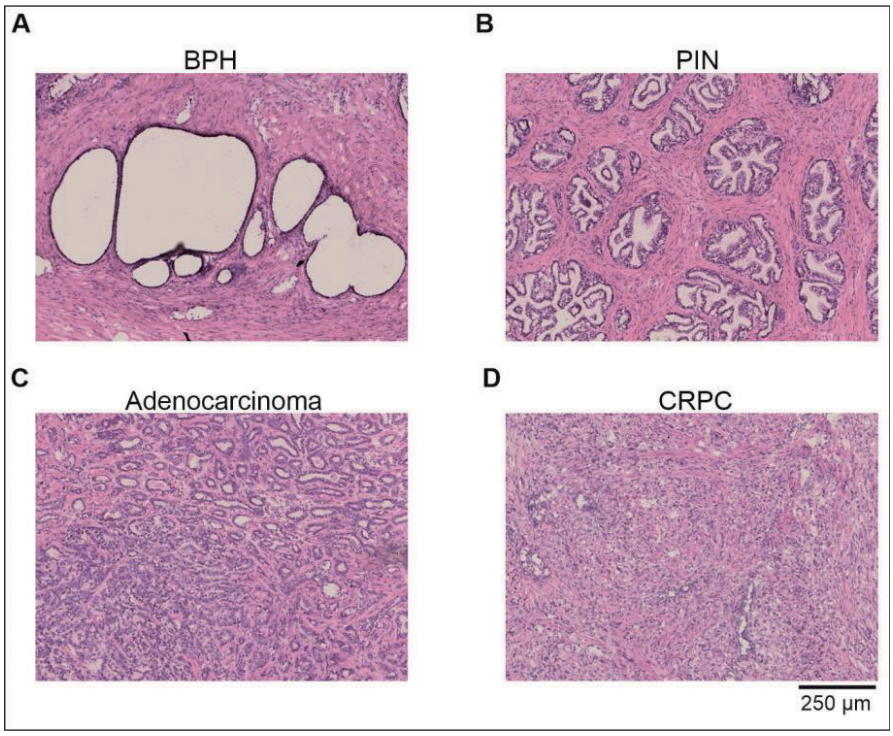

Figure 3. Hematoxylin & eosin-stained frozen section samples of the prostate.

A benign prostatic hyperplasia (BPH), **B** prostatic intraepithelial neoplasia (PIN), **C** adenocarcinoma and **D** castration-resistant prostate cancer (CRPC).

2.2.3 Histological grading of prostate cancer

Prostate adenocarcinomas are mostly graded according to the Gleason grading system by evaluating the pattern of glandular differentiation. Gleason scoring is a widely used grading system for prostate cancer due to its high prognostic value. Gleason grading system was published in 1966. Gleason grading is based on the glandular architecture of the cancerous epithelium. In prostatectomy samples the Gleason score is combined from two values of Gleason grades: predominant Gleason pattern 1 graded from 1 to 5 is summed to the second most common cancer pattern, Gleason pattern 2, together forming a Gleason score between 2 and 10 (Gleason 1966).

The first major revision of the Gleason grading system of needle biopsies took place (Epstein et al. 2005) at the International Society of Urological Pathology (ISUP)

Consensus Conference 2005, after which the most aggressive Gleason pattern was included next to the most predominant pattern as part of the Gleason scoring. Moreover, Gleason score 1 + 1=2 was no longer used, and Gleason score 2-4 carcinomas should never or rarely be diagnosed from the needle biopsy. Improved reproducibility of the scoring was also required, as depending on the sample source (needle biopsy or radical prostatectomy), the results often varied. Hence, there was a need to standardize the scoring, and a prognostic cutoff was also needed between low-grade and high-grade tumors from Gleason scores 6 versus 7 to Gleason scores 3+4 versus 4+3 (Figure 4, Table 1) (Epstein et al. 2005, Epstein 2010).

The major changes to the contemporary Gleason grading system have been introduced in 2005 and 2010 and approved in the ISUP consensus meeting in 2014 where also more distinct prognostic groups were introduced (Epstein et al. 2016). Gleason grades and the new grade groups were updated from Gleason scores 2 to 10 into ISUP Grade Groups 1-5. This new grading system has been approved by the World Health Organization for the 2016 edition of Pathology and Genetics: Tumours of the Urinary System and Male Genital Organs.

Table 1. Gleason grading renewal 2005

GLEASON PATTERN	GENERAL DESCRIPTION OF THE PATTERN
Gleason pattern 1	Circumscribed nodule of closely packed but separate, uniform, rounded to oval, medium-size acini (larger glands than pattern 3)
Gleason pattern 2	Similar to pattern 1, minimal infiltration may occur at the edge of the tumor nodule, glands more loosely arranged and not as uniform as Gleason pattern 1
Gleason pattern 3	Glands have a small round contour of nodules of tumor, usually smaller glands than in Gleason pattern 1 or 2
Gleason pattern 4	A fusion of the glands, poorly formed glands, large cribriform glands without regular border, hypernephromatoid
Gleason pattern 5	Infiltrating single cells and strands of cells, no glandular differentiation, solid pattern with or without comedonecrosis

Gleason grading patterns according to Epstein et al. 2005 and Epstein 2010.

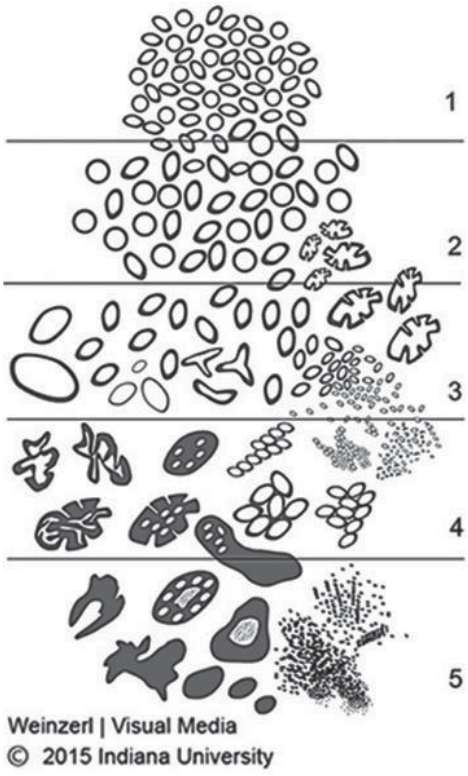

Figure 4. Prostatic adenocarcinoma Gleason patterns visualized based on 2015 modified ISUP Gleason schematic diagrams.

(Reprinted by permission of Wolters Kluwer Health, Inc. Epstein et al. 2016, copyright (2021)).

2.2.4 Pathological staging of prostate cancer

The TNM classification of malignant tumors was developed together by the Union for International Cancer Control (UICC), and the American Joint Commission on Cancer (AJCC). The TNM classification categorizes the anatomical appearance of tumors based on the size and extent of the primary tumor (T category), regional lymph node involvement (N category) and the presence of distant metastases (M category) (Cheng et al. 2012). Pathological TNM (pTNM) determines the appearance, location, and invasiveness of the tumor. The rules applying to TNM classification of malignant tumors from radical prostatectomy specimens provide a tool for prognostic assessments and treatment allocation of patients with prostate cancer as well as information for data collection by cancer registries worldwide.

2.2.5 Prostate cancer therapy

The prognosis and treatment options depend principally on the stage of the cancer including level of PSA, Gleason score/Grade group, and whether the cancer has spread to other compartments in the body. Comorbidity, age, and personal preferences of the patient also effects the treatment selection (Siegel et al. 2012). Patients with prostate cancer are divided into different risk categories by D'Amico risk classification for prostate cancer: low-risk, intermediate-risk, and high-risk disease of biochemical recurrence after surgery according to Gleason score, the clinical TNM stage, and preoperative PSA level. (D'Amico et al. 1998, EAU Guidelines 2021: https://uroweb.org/guideline/prostate-cancer/). Active surveillance may be suitable for men with low-risk prostate cancer and for some selected patients with intermediate-risk disease (Rodrigues et al. 2012, Sandhu et al. 2021). These patients are under regular monitoring of serum PSA, findings from digital rectal examinations, biopsies, and diagnostic imaging of the prostate by MRI or positron emission tomography–computed tomography (PET-CT). For patients with a risk of metastasis, bone scans are also performed (EAU Guidelines 2021: https://uroweb.org/guideline/prostate-cancer/).

After the patient is diagnosed with prostate cancer, two of the main treatment options for organ-confined prostate cancer are surgery and radiation therapy. In prostatectomy the prostate is removed. This is usually performed in patients with localized cancer. Currently, surgery is mostly performed by robotic-assisted laparoscopic radical prostatectomy (RALP). Radiation can be given as external beam radiation therapy or with either internal low dose-rate (LDR) or high dose-rate (HDR) brachytherapy (Fischer-Valuck et al. 2019). Patients in the low-intermediate-risk category are treated with radiation therapy or radical prostatectomy. Hormonal therapy may also be an option or additionally included for treatment. The growth of prostate cancer is dependent on androgens, and hence androgen deprivation (ADT) is an effective therapeutic strategy (Teo et al. 2019). ADT is usually used for the treatment of advanced disease to slow cancer progression and reduce symptoms. Most often, medical castration is used to block the synthesis of testosterone or activation of AR. Recurrent or metastatic, castration-sensitive or castration-resistant tumors can be treated with chemotherapy or antiandrogens (Evans 2018).

For CRPC, there is no curative treatment available even though numerous therapeutic agents have been developed and FDA-approved in recent years to

improve the survival of patients. Moreover, secondary hormonal ablation therapy, including antiandrogens such as enzalutamide, has demonstrated survival benefits (Teo et al. 2019). Abiraterone, which is a small-molecule inhibitor of cytochrome P450 17 (CYP17), is a main enzyme in both adrenal and intratumoral synthesis of androgens. Enzalutamide (Davis et al. 2019), apalutamide (Chi et al. 2019), and darolutamide (Moilanen et al. 2015, Fizazi et al. 2020) are the second-generation antiandrogens that inhibit androgen receptor (AR). They bind competitively to the ligand-binding domain of AR and thereby prevent AR translocation to the nucleus and binding to DNA. Although these drugs have shown promise for increasing the survival of patients with CRPC, several resistance mechanisms have been described for these agents (Hoang et al. 2017, Teo et al. 2019). Besides the AR antagonists there are several chemotherapeutic agents used for prostate cancer therapeutics. Docetaxel disrupts the normal function of microtubules and thereby stops cell division. Moreover, it was the first systemic therapy to demonstrate survival benefit in metastatic CRPC (mCRPC) (Teo et al. 2019). Cabazitaxel, which is a second-generation chemotherapeutic of the taxane class, binds to tubulins with the indicated activity in docetaxel-resistant cancers (Sandhu et al. 2021). Approximately 23% of metastatic castration-resistant prostate cancer patients have somatic or germline loss-of-function alterations in DNA damage responsive genes (DDR) including *BRCA2*, *BRCA1*, *ATM*, and *CHEK2*. These DDR gene pathways are responsive to Poly(ADP-ribose) polymerase (PARP) inhibitors e.g. olaparib and talazoparib which have indicated effectiveness in mCRPC (Sandhu et al. 2021). Bone metastasis-targeting treatments are relevant for most patients as bone metastasis are common in metastatic prostate cancer. Most common option is radiotherapy, the α-emitting radionuclide radium-223 (^{223}Ra), which mimics calcium and is hence uptaken by the osteoblastic bone metastasis (Sandhu et al. 2021). The clinical pathway of prostate cancer patient is given in a broad outline on Figure 5.

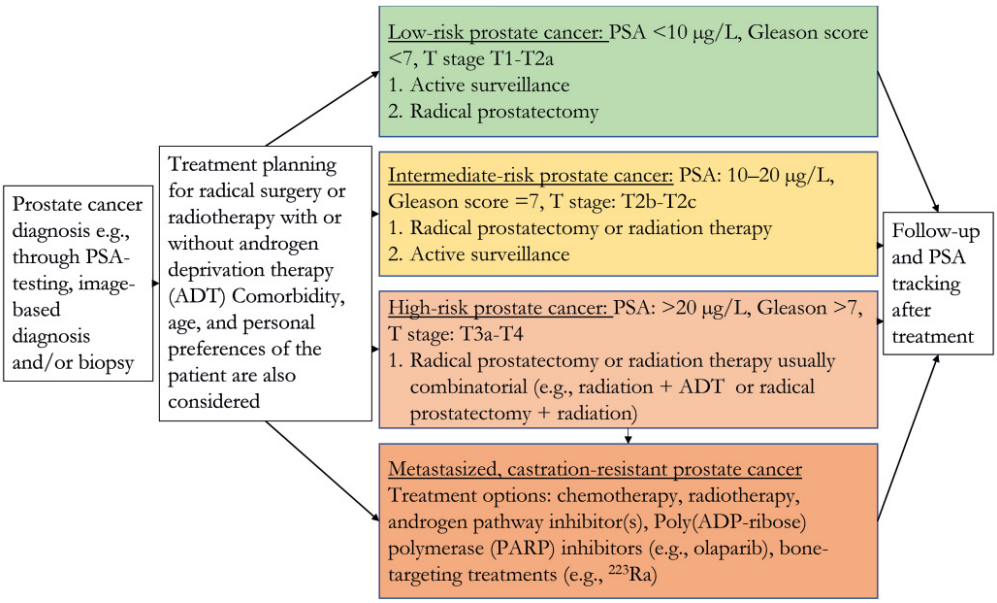

Figure 5. Clinical pathway of prostate cancer treatment

Information based on Sandhu et al. 2021 and Gosein et al. 2020.

2.2.6 Metastatic properties of prostate cancer cells

Prostate cancer cells can metastasize from the primary site to other parts of the body, especially to bones and local lymph nodes. Less commonly, prostate cancer cells spread to the lungs, liver, or brain (Wang et al. 2018). The metastatic process consists of multiple steps, including detachment of cancer cells from the primary tumor, migration, adhesion, invasion and intravasation into the vasculature and extravasation into the secondary site to colonize distal organs. Epithelial-mesenchymal transition (EMT) enables cancer cells to suppress their epithelial features. Epithelial cells are nonmotile and embedded via cell-cell and cell-extracellular matrix (ECM) junctions. During EMT, cells lose their polarity and junctions, and thereby acquiring mesenchymal traits. This transition allows cancer cell mobility and the possibility to migrate from the primary site to secondary sites (Lamouille et al. 2014, Winkler et al. 2020). With most solid tumors of epithelial origin, the metastatic cascade begins with cancer cells penetrating through the basement membrane. From invasive tumors, single cells or clusters of cells infiltrate the stroma and migrate into the distal organs by different integrin-dependent mechanisms (Hamidi and Ivaska 2018, Winkler et al. 2020). Proteolytic activity is

considered to play a role in this process. Integrins participate by upregulating the expression of matrix metalloproteinases (MMPs) and by promoting their activation. The MMP family of secreted and membrane proteinases are enzymes that degrade ECM and cell surface proteins (Das et al. 2017).

Integrins are the main cell adhesion receptors for components of the ECM. Integrins are a family of transmembrane heterodimers formed from 18 different alpha and eight different beta integrin subunits. When integrin is in a bent (closed) position, it is inactive, with low affinity for ECM ligand proteins. However, fully extended (open) integrin is active and able to produce downstream signaling and cellular responses after it is attached to an appropriate ligand. As a result, integrin engages to its ligand in a process called adhesion (Hamidi and Ivaska 2018, Xiong et al. 2021).

Adhesion of integrins to the ECM provides the gravity required for cancer cell invasion. Integrins ligated to the ECM mediate survival signals, and integrins that are not ligated to the ECM can enhance pro-apoptotic cascades (Desgrosellier and Cheresh, 2010). Accordingly, dysregulated integrin-mediated adhesion and signaling can also give rise to the initiation of several cancers by inducing oncogenic properties in cells (Hamidi and Ivaska 2018, Xiong et al. 2021).

Several studies have demonstrated a positive correlation between the malignant properties of prostate cancer and increased expression or activity of MMPs, especially MMP2 and MMP9 (Wood et al. 1997, Castellano et al. 2008, Zhong et al. 2008, Littlepage et al. 2010). Both MMP2 (gelatinase A) and MMP9 (gelatinase B) are members of the gelatinase subfamily. Progression of prostate cancer can be promoted by elevated MMP activity, which impacts multiple steps of metastasis formation by promoting cell proliferation, apoptosis, angiogenesis and EMT. MMPs are more active in advanced stages of prostate cancer, as tumors with high Gleason scores mostly display higher MMP expression levels. (Gong et al. 2014) However, cancer therapeutics designed to target adhesion receptors or MMPs have thus far not been shown to be efficient in the clinic (Hamidi and Ivaska 2018).

2.2.7 Genomic alterations of prostate cancer

Understanding the genetic mechanisms of cancer may provide ways to develop better tools for diagnostics, prognostics and targeted treatment options. Somatic aberrations in several genes, including the breast cancer 1 or 2 gene *(BRCA1,*

BRCA2), serine/threonine kinase *(ATM*), checkpoint kinase 2 (*CHEK2*), cyclin-dependent kinase 12 (*CDK12*), and partner and localizer of *BRCA2* (*PALB2*), are found in approximately 23% of metastatic prostate cancers (Sandhu et al. 2021). The most frequently mutated genes in primary prostate cancers are genes coding for speckle-type POZ protein (*SPOP*), *TP53*, forkhead box protein A1 (*FOXA1)*, and phosphatase and tensin homolog (*PTEN)* (Barbieri et al. 2012). Early genomic aberrations include loss-of-function mutations in *SPOP* in 5–15% of patients and gain-of-function mutations in *FOXA1* in 3–5% of patients (Sandhu et al. 2021). P53 plays a major role in controlling the death of tumor cells and works as a tumor suppressor. P53 arrests the cell cycle in the G1 phase in response to damaged DNA and is required for cell apoptosis. *TP53* is inactivated by mutation in most cancers, thereby increasing tumor formation. Moreover, *TP53* is commonly deleted during the later stages of prostate cancer (Aubrey et al. 2016). *PTEN* is a tumor suppressor, and homozygous deletions of *PTEN* and loss-of-function mutations of *TP53* occur in 10–20% of cases of localized prostate cancer (Sandhu et al. 2021). Whereas the frequency of homozygous deletions in *PTEN* occurs in more than 40% of mCRPC patients. Alterations in *TP53* are found in approximately 50% of mCRPC patients (Sandhu et al. 2021). In addition, *TMPRSS2:ERG* gene fusion is the most common chromosomal aberration in more than 40% of prostate cancer patients. *MYC* oncogene is also frequently upregulated by gain-of-function mutation in prostate cancer and increased activation is present in up to 30% of mCRPC (Table 2).

In prostate cancer, some mutations may also be inherited and lead to a higher tendency to malignancies. Men with germline *BRCA1* or *BRCA2* mutations are found in families with high ratios of breast and ovarian cancer and have a three- to eightfold higher risk of prostate cancer. Moreover, patients with germline *BRCA2* mutations may have more aggressive tumors and worse prognosis (Sandhu et al. 2021).

Table 2. Somatic mutations give rise to high intratumoral heterogeneity in prostate cancer

Somatic mutations	Localized	Metastatic and CRPC
BRCA1 mutation or deletion *BRCA2 mutation or deletion* *CDK12* mutation *ATM mutation* *CHEK2 mutation*		~23% in metastatic
SPOP mutation	~11%	
FOXA1 mutation	~4%	9% and 19%
PTEN deletion (homozygous)	10–20%	~30% and 45%
TP53 mutation or deletion	10–20%	40% and 57%
MYC gain-of-function		~20% and ~30%
AR amplification or mutation		~60% and 70%
TMPRSS2-ERG fusion	46 %	41% and 43%

Modified from Sandhu et al. 2021.

2.2.7.1 MYC oncogene

MYC (v-myc avian myelocytomatosis viral oncogene homolog) is a transcription factor involved in cell cycle progression, apoptosis and cellular transformation. The *MYC* oncogene is constitutively and aberrantly expressed and contributes to the genesis of several human cancers (Dang 2012, Madden et al. 2021). *MYC* gene expression has been found to be dysregulated and upregulated due to amplification or translocation in most human cancers (Chen et al. 2018, Madden et al. 2021). Moreover, overexpression of the *MYC* oncogene is one of the most typical alterations in prostate cancer (Gurel et al. 2008). The *MYC* oncogene is upregulated in 20–30% of mCRPC patients (Quigley et al. 2018, Sandhu et al. 2021). MYC transcription factors form heterodimers with MYC-associated factor X (MAX). Heterodimerization with MAX is compulsory for MYC to fold and become transcriptionally active. Dimerized MYC-MAX complexes bind to specific regulatory sequences (E-boxes; CACGTG) that are in the promoter regions of their specific target genes (Dang 2012, Madden et al. 2021).

In cancer, the overexpressed *MYC* oncogene acts as a cell proliferation promoting transcription factor by regulating target genes required for cell cycle regulation, such as cyclins and cyclin-dependent kinase 4 (CDK4). In contrast, *MYC* decreases and

interferes with the function of genes reducing cell proliferation e.g., *p21* and *p27,* which are inhibitors of CDK (Dang 2012, Madden et al. 2021).

2.2.7.2 ERG oncogene

The E26 transformation-specific (ETS) family of transcription factors is often excessively overexpressed in prostate cancer. One of the members of the ETS family is the *ERG* (ETS transcription factor 1/*ETS*-related gene 1) gene, which is often fused with the prostate-specific and androgen-responsive *TMPRSS2* (transmembrane protease, serine 2) gene, resulting in ERG overexpression. *TMPRSS2:ERG* fusion is the most frequent chromosomal aberration in prostate cancer and promotes tumorigenesis in more than 50% of patients. (Tomlins et al. 2005) *ERG* is translocated by forming a fusion of its 3'-segment with the 5'-end of *TMPRSS2*. *TMPRSS2* is a membrane-bound serine protease (Lin et al. 1999). In prostate cancer *TMPRSS2* is also overexpressed compared to normal adjacent tissue (Vaarala et al. 2001). In addition, two more rare *ERG* gene fusions can contribute to its increased expression, *SLC45A3:ERG* (solute carrier family 45, member 3) and *NDRG1:ERG* (N-myc downstream regulated gene 1). However, these fusions occur in less than 5% of prostate cancer cases (Pflueger et al. 2009).

In prostate cancer, elevated ERG expression levels have been associated with more aggressive phenotype and lower survival rates (Hägglöf et al. 2014). However, in some other reports ERG positivity has been combined with a more positive prognosis and without association to Gleason scores (Saramäki et al. 2008, Leinonen et al. 2013). Therefore, there is no clear prognostic value indicated with ERG expression in prostate cancer. However, elevated expression levels of ERG promote cell invasion by activating MMPs and upregulating CXCR4 (Klezovitch et al. 2008, Singareddy et al. 2013, Adamo & Ladomery 2016). CXCR4 is a chemokine receptor that mediates invasion and metastasis. CXCL12 ligand and its receptor CXCR4 increases tumor malignancy by increasing adhesion of tumor cells to extracellular matrix components and endothelial cells (Sun et al. 2007). CXCR4 is upregulated by ERG in most primary prostate cancers (80%) and promotes the formation of metastases into bones (Singareddy et al. 2013, Adamo & Ladomery 2016).

2.2.7.3 Androgen receptor activation

Androgens, especially testosterone and dihydrotestosterone (DHT) are essential for the growth and development of the prostate, and they play a key role as survival factors for epithelial cells of the prostate (Heinlein & Chan, 2004). Androgens act through the androgen receptor (AR) molecule, which is a transcription factor. The signaling pathway of AR is essential in the development and progression of prostate cancer. Testosterone and DHT bind to the ligand binding domain (LBD) of AR, upon which the conformation of the protein changes. After ligand binding in the cytoplasm, AR translocates into the nucleus where the dimerized receptor complex binds to the androgen-response element (ARE) on promoters and/or enhancers of targeted genes, thus influencing their expression. ADT inhibits AR activity and suppresses hormone-naïve prostate cancer. Eventually, however, AR can adapt to survive under castration levels of androgens. AR is altered in approximately 60-70% of mCRPC cases, making it one of the most significant oncogenes in CRPC (Robinson et al. 2015, Sandhu et al. 2021).

In addition to AR gene amplification, AR alteration mechanisms include point mutations, upregulation, constitutively active AR splice variants, and alterations in androgen biosynthesis as well as in androgen cofactors (Fujita & Nonomura 2019). AR alterations are rare in the early stage of prostate cancer, but they are the major drivers of CRPC and mCRPC (Sandhu et al. 2021). Point mutations in the AR gene are found in approximately 15-30% of CRPC patients (Waltering et al. 2012, Grasso et al. 2012). Through point mutations, AR can lose its specificity to the ligand and hence become activated without the presence of androgens.

AR has several known splicing variants such as AR-V7, which are functionally active without androgens (Dehm et al. 2008). Most AR splice variants do not contain a ligand-binding domain and hence cause activation of AR signaling even in the absence of ligands. Prostate cancer cells express full-length AR and AR variants that are androgen independent and resistant to several AR inhibitors and antagonists (Paschalis et al. 2018).

Changes in the biosynthesis of androgens can cause the progression of prostate cancer. The cytochrome P450 enzymes CYP11A1 and CYP17A1 synthesize dehydroepiandrosterone (DHEA) and androstenedione in the adrenal glands. Normal prostate cells can convert these weak adrenal androgens into testosterone and DHT. In CRPC, enzymes converting weak androgens into androgens can be

overexpressed. In addition, expression of a gain-of-stability mutation leading to a gain-of-function mutation catalyzes a rate-limiting step for DHT synthesis from adrenal DHEA and thereby increases the expression of androgens and hence activates AR. In CRPC, cholesterol can also be used for androgen synthesis by cancer cells and cancer can become independent from circulating adrenal androgens (Fujita & Nonomura 2019).

Multiple AR coactivators interact with AR and stimulate its transcriptional activity by enhancing the opening of the chromatin structure at AR-binding sites, after which the transcriptional machinery is recruited to initiate gene transcription. One example is the family of nuclear receptor coactivators (NCOAs) that contains three transcriptional coregulators: NCOA1, NCOA2, and NCOA3 (Fujita & Nonomura 2019). NCOA1 expression is related to the aggressiveness of prostate cancer. NCOA2 is amplified in primary and metastatic prostate cancer (Taylor et al. 2010). NCOA2 is induced by androgen deprivation, which activates PI3K signaling, promoting the formation of prostate cancer metastases and the development of CRPC. Furthermore, NCOA3 expression is enhanced in advanced prostate cancer and in CRPC (Fujita & Nonomura 2019).

2.3 Protein phosphorylation and protein kinases

Protein phosphorylation is an important and common post-translational mechanism that regulates the biological activity of proteins, especially in eukaryotic organisms (Huang et al. 2020). Moreover, the eukaryotic protein kinase family forms one of the largest protein subfamilies (Hanks & Hunter 1995). Phosphorylation can lead to a significant change in protein structure, which may further affect the stability, activity, and subcellular localization of the protein to regulate cellular processes. Additionally, phosphorylation can affect interactions between proteins (Nishi et al. 2011). Phosphorylation is mediated by protein kinases, ATP-dependent phosphotransferases, which add the γ-phosphate of ATP to a hydroxyl group of serine, threonine, or tyrosine residues of the substrate protein (Huang et al. 2020). Substrate proteins can be phosphorylated at one or multiple sites. A necessity for the reaction is a bivalent cation, most commonly magnesium (Mg^{2+}) or manganese (Mn^{2+}), which catalyzes the kinase reaction and the binding of the phosphate (Adams 2001).

One protein kinase is able to phosphorylate several substrate molecules, which can remarkably amplify the activation signal. Phosphorylation is a reversible reaction, and through dephosphorylation, protein phosphatases remove the phosphate group and restore the original state of the target protein (Lewin 2004). Since protein kinases have important roles in regulating cellular signaling pathways, they are often abnormally activated in cancer cells due to mutations. As a consequence of loss-of-function mutations, kinases are transformed, or become defective. Gain-of-function mutations have opposite effects, and possibly transform protein kinases to uncontrolled activators of cell growth and division (Cohen 2002).

2.4 PIM kinases

2.4.1 Structure and function of PIM kinases

The *PIM1* gene was originally discovered as a proviral integration site for Moloney murine leukemia virus, and it was found to act as a proto-oncogene and to promote lymphatic tumor progression upon oncogenic activation (Cuypers et al. 1984). Studies with transgenic mice have proven that *PIM1* acts as an oncogene and affects cancer formation together with other oncogenes, such as *MYC* (van Lohuizen et al. 1989). *PIM1* orthologs have been found in a variety of eukaryotic organisms, including human, mouse and zebrafish (Kalichamy et al. 2019). In human and mouse, two other PIM family members have also been identified: the *PIM2* and *PIM3* genes, whose protein products have highly overlapping functions with the PIM1 protein (Bachmann & Möröy 2004). The *PIM1* gene encodes for two proteins whose translation starts at alternative translation initiation regions. A smaller 34 kDa PIM1S (short) isoform is produced from an ATG codon, and a larger 44 kDa PIML (long) amino-terminal variation is produced from an alternative upstream translation initiation region, with a CTG codon (Saris et al. 1991, Nawijn et al. 2011). *PIM2* has three alternative translation initiation sites forming three isoforms. Only one translation initiation site has been described for *PIM3*. All human *PIM* genes consist of six exons and five introns (Figure 6). The smaller PIM1 protein isoform in human, mouse, and rat consists of 313 amino acids with 94% identical sequences (Zakut-Houri et al. 1987, Nawijn et al. 2011). The PIM2 protein is 61% identical at the amino acid level to the PIM1 protein. The greatest differences exist in the amino and carboxyl ends of the coding proteins. Additionally, the PIM3 protein is 71%

homologous with the PIM1 protein (Mikkers et al. 2004, Peng et al. 2007, Nawijn et al. 2011).

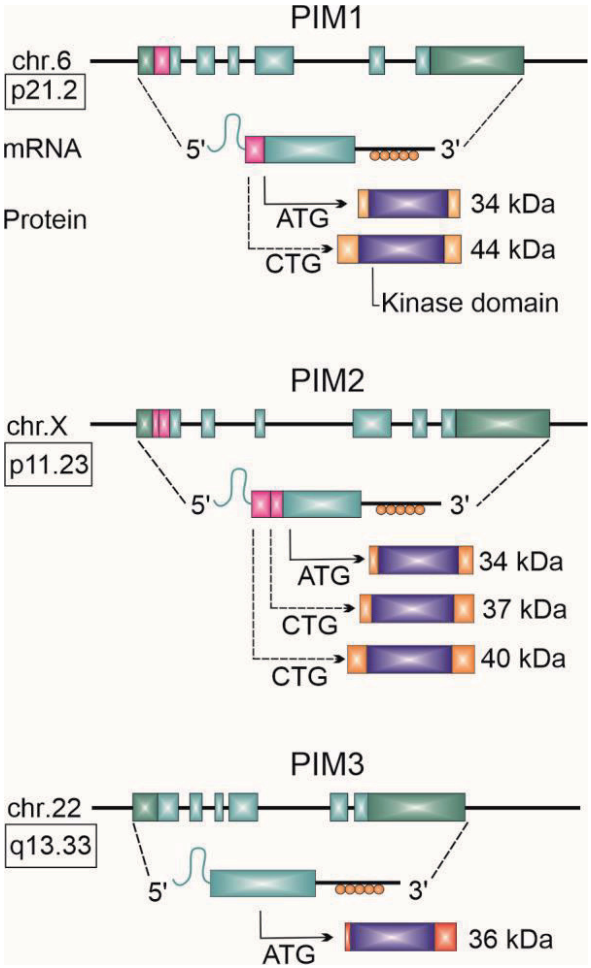

Figure 6. Structures of PIM protein-encoding genes and proteins.

In the genome, *PIM* genes are located on different chromosomes. *PIM* mRNA transcripts are encoded by 6 exons (turquoise boxes) and their 5' and 3' untranslated regions (UTRs; dark green boxes) are large, incorporating a G/C-rich region in the 5' UTRs (light blue variant). Moreover, mRNAs include five copies of AUUUA-destabilizing motifs (orange circles) in the 3' UTRs that are responsible for the short half-life of *PIM* transcripts. While synthesis starts at alternative translation initiation sites (solid and dashed arrows) different protein isoforms are formed. (Additional codons are presented at the 5' of these mRNAs as pink boxes). PIM protein isoforms differ in molecular mass but retain their serine/threonine kinase activity. PIM kinases are not known to contain any regulatory domains and they have significantly conserved kinase domains (purple boxes) (Nawijn et al. 2011).

PIM kinases are serine/threonine kinases, so they phosphorylate serine (S) and threonine (T) residues of their substrates (Saris et al. 1991). The PIM1 kinase recognizes and phosphorylates amino acid sequence containing K/RK/RRK/RLS/TX, where K is lysine, R is arginine, L is leucine, and X represents an amino acid residue with a small side chain (Palaty et al. 1997). The consensus sequence RXRHXS was determined for PIM1 and PIM2, and in this sequence, X is a variable amino acid, S is serine and H is histidine (Peng et al. 2007). Through phosphorylation, PIM kinases stimulate or repress the biological activities of their substrates. In addition, phosphorylation can lead to degradation or stabilization of phosphorylated proteins.

If one of the three PIM family members is knocked out in mice, the mice grow and develop normally (te Riele et al. 1991). This is possible because *PIM* gene products have overlapping functions and thus can compensate for each other. Mice in which all three PIM family members have been knocked out (*Pim1-/-, Pim2-/- and Pim3-/-*) are viable and fertile but division of lymphocytic and T cells and growth factor responses are decreased. *Pim* knockout mice are approximately 30% smaller than their wild-type littermates or mice with only one or two *Pim* family member knockouts (*Pim1*$^{+/-}$, *Pim2*$^{-/-}$, *Pim3*$^{-/-}$ *or Pim1*$^{-/-}$, *Pim2*$^{-/-}$, *Pim3*$^{+/-}$ *or Pim1*$^{+/-}$, *Pim2*$^{-/-}$, *Pim3*$^{+/-}$) (Mikkers et al. 2004) (Figure 7). Mice, from which *Pim1* gene has been deleted, have only small changes in cytokine signaling. These mice have disordered IL3/IL7-dependent proliferation of mast cells and B cell precursors in the bone marrow (Domen et al. 1993).

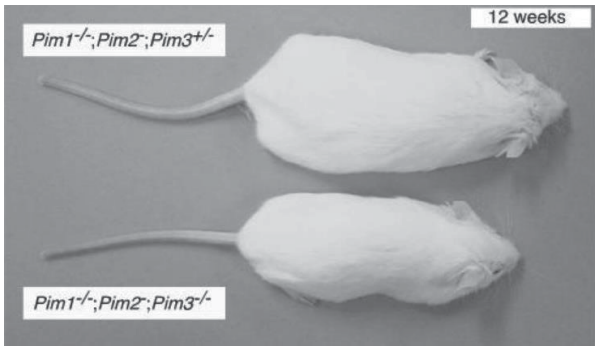

Figure 7. *Pim* knockout mice

A *Pim* triple knockout mouse next to a mouse with *Pim1* and *Pim2* double knockout combined with *Pim3* single knockout (Mikkers et al. 2004) Creative Commons, Attribution license, Version 4.0 (CC-BY).

2.4.2 Regulation of PIM kinases

The activity of PIM kinases is mainly regulated by transcription, translation and proteasomal degradation (Amaravadi & Thompson, 2005, Liang & Li, 2014). *PIM* gene expression is induced by several cytokines, mitogens, and growth factors (Zhu et al. 2002, Kisseleva et al. 2002). The main signaling pathway affecting *PIM* gene expression is the JAK/STAT pathway of Janus kinases with signal transducers and activators of transcription affecting *PIM* gene expression. This pathway is activated when cell surface receptors are bound by cytokines, interferons (IFNs) such as IFNα and interleukins (IL) such as IL2, resulting in activation of JAK kinases, which phosphorylate and activate STAT family members. Phosphorylated STAT proteins dimerize and translocate to the nucleus, where they activate transcription of their target genes (Kisseleva et al. 2002). STAT1, STAT3, STAT4 and STAT5 are able to bind directly to gamma interferon activation sequences (IGFR/GAS) on the *PIM1* promoter and enhance *PIM1* expression (Matikainen et al. 1999, Bachmann & Möröy 2004). However, PIM1 phosphorylates and stabilizes the suppressor of cytokine signaling, SOCS1, producing negative feedback regulation of the JAK/STAT pathway (Peltola et al. 2004). In addition, transcription factor nuclear factor kappa-B (NF-κB) induces PIM1 expression by CD40 signaling (Zhu et al. 2002), and krüppel-like factor 5 (KLF5) binds directly to the PIM1 promoter and activates its expression (Zhao et al. 2008). Moreover, ERG transcription factor plays a role in the enhancement of *PIM1* expression by increasing *PIM1* transcription especially in the initial phases of prostate tumorigenesis (Magistroni et al. 2011). Furthermore, hypoxic conditions induce PIM1 protein levels in response and PIM inhibitors selectively kill hypoxic cancer cells indicating that PIM kinases have a role in tumor growth under hypoxia (Casillas et al. 2018). Multiple copies of AUUU(A) motifs in the 3'UTR and GC-rich regions in the 5'UTR shorten the half-life of *PIM* mRNA transcripts (Wang et al. 2005). Moreover, multiple microRNAs, such as miR-210 (Huang et al. 2009), miR-33a (Thomas et al. 2012), and miR-328 (Eiring et al. 2010) regulate the expression of *PIM* genes.

The crystal structure of PIM1 kinase revealed that it constitutively resides in a catalytically active form (Kumar et al. 2005, Jacobs et al. 2005). This finding correlates well with the absence of a known regulatory domain. Unlike other kinases that are regulated by phosphorylation, no phosphorylation sites for PIM activation have been found (Amaravadi & Thompson, 2005). Moreover, it is notable that phosphorylation of PIM1 is not necessary for its kinase activity but rather enhances

the stability of the enzyme (Qian et al. 2005). The half-lives of PIM kinases are relatively short, approximately ten to 180 minutes, and are primarily regulated at the post-translational level by proteasomal degradation. Binding to heat shock protein 90 (HSP90) stabilizes the PIM1 protein and its kinase activity. Moreover, HSP90 also prevents PIM1 degradation under hypoxic conditions that are common in many cancers (Mizuno et al. 2001). Binding to HSP70, conversely, leads to degradation of PIM1 (Petersen et al. 2005). Moreover, serine/threonine-specific protein phosphatase 2A (PP2A) negatively regulates PIM stability and function through dephosphorylation (Losman et al. 2003). Dephosphorylation by PP2A in turn leads to ubiquitinylation and proteasomal degradation of the PIM1 protein (Ma et al. 2007). However, PIM kinases are able to autophosphorylate themselves and hence may stabilize their own functions (Bullock et al. 2005).

2.5 PIM kinases in cancer formation

Cancer formation can result from uncontrolled activation of survival kinases. Upregulated expression of PIM family members has been detected both in malignancies of hematological origin and in multiple solid tumors (Bachmann & Möröy 2005, Nawijn et al. 2011, Santio & Koskinen 2017). Moreover, they affect tumor progression by interacting with and phosphorylating multiple cellular substrates and thereby regulating many different cellular processes such as progression of the cell cycle, cellular division, differentiation, and apoptosis.

PIM kinases function in close interaction and often with similar or overlapping mechanisms of action as other oncogenic pathways, such as the phosphatidylinositol-3-kinase (PI3K)/protein kinase B (AKT) and mammalian target of rapamycin (mTOR) pathways (Warfel & Kraft 2015). Among the PIM phosphorylation targets, there are several well-known factors affecting cancer formation. PIM kinases can promote cancer progression by blocking apoptotic cell death through regulation of pro- and anti-apoptotic members of the B-cell lymphoma (BCL) 2 protein family and thereby act as survival factors (Lilly et al. 1999). PIM kinases inactivate the pro-apoptotic protein BAD through phosphorylation of Ser112 and possibly two other residues, Ser136 and Ser155, and hence increase the survival of several cell types by prohibiting apoptosis (Yan et al. 2003, Aho et al. 2004, Macdonald 2006).

Several studies have demonstrated that PIM1 upregulation may cause resistance to chemotherapy, and radiotherapy. PIM1 upregulation has been indicated to play a role in the development of acquired resistance to chemotherapeutic agents in multiple malignancies, including prostate cancer (Zemskova et al. 2008), hematopoietic malignancies (Pircher et al. 2000) and non-small-cell lung cancer (Henry et al. 2016). Similar to radiation therapy, chemotherapeutic tubulin-binding drugs such as docetaxel induce PIM upregulation in prostate cancer cells leading to increased survival of the cells (Zemskova et al. 2008). PIM knockout and inhibition with the PIM inhibitor quercetin increase apoptotic cell death of prostate cancer cells. Moreover, PIM inhibition combined with the chemotherapeutic tubulin-binding agent paclitaxel increases DNA damage and induces apoptosis (Hsu et al. 2012). When PIM1 inhibitors were combined with paclitaxel in prostate cancer, cell viability was reduced, and apoptosis was induced (Mori et al. 2013). Experiments with multiple cell lines from solid cancers have indicated that cancer-associated hypoxia increases PIM expression which in turn supports chemoresistance (Chen et al. 2009).

Several studies have also demonstrated that enhanced expression of PIM kinases contributes to tumor radioresistance in head and neck cancer (Peltola et al. 2009), lung (Kim, et al. 2013), pancreatic (Chen et al. 2016), prostate (Gu et al. 2016), and non-small-cell lung cancer (Kim et al. 2011). Both hypoxia and radiation induce PIM1 expression in prostate cancer cells, and PIM inhibitor sensitizes cancer cells to radiation (Kirschner et al. 2014). PIM-specific inhibitors could therefore play a role as novel radiosensitizers to enhance the efficacy of radiotherapy by inhibiting irradiation-induced signaling pathways that are associated with resistance against radiotherapy.

The PI3K pathway is dysregulated in several human cancers and controls cellular processes promoting cancer initiation and maintenance. AKT is a serine/threonine kinase acting downstream of PI3K (Vivanco & Sawyers, 2002). Several drugs inhibiting the PI3K pathway have been under clinical development for targeting multiple cancers. However, they have displayed difficulties with resistance due to substitutive mechanisms or feedback loops (Heavey et al. 2014, Yang et al. 2019, Luszczak et al. 2020a). The AKT kinase has mechanistic similarities to PIM kinases, and they have several common substrates. Both PIM1 and AKT phosphorylate and thereby inactivate the pro-apoptotic protein BAD (Aho et al. 2004, Datta et al. 1997). Moreover, PIM and AKT phosphorylate the proline-rich Akt substrate of 40 kDa

(PRAS40) at Thr246, which increases the activity of mTOR (Zhang et al. 2009). Glycogen synthase kinase-3β (GSK3β) is also a direct target of PIM and AKT, which phosphorylate GSK3β at Ser9, inhibiting its activity (Cross et al. 1995, Santio et al. 2016). The presence of common targets of PIM and AKT suggests that PIM kinases may partially mediate resistance to PI3K/AKT inhibitors, and that co-targeted therapy options may show clinical benefits (Song et al. 2018, Luszczak et al. 2020a). Indeed, the results from several studies have already supported this hypothesis. First, in *in vitro* experiments and mouse models, co-targeted therapy against PIM and PI3K, inhibited the growth and survival of cancer cells as well as the size of tumors in mice more effectively (Song et al. 2018). Moreover, IBL-302 (AUM302), a novel triple inhibitor against PIM/PI3K/mTOR kinases, has recently been shown to significantly reduce cancer cell viability and growth in patient-derived xenograft neuroblastoma models (Mohlin et al. 2019). In addition, IBL-302 decreased the proliferation of prostate cancer cells (Luszczak et al. 2020b). Furthermore, IBL-302 demonstrated efficacy against the proliferation of breast cancer cells (Kennedy et al. 2020). Another, structurally related PI3K/mTOR/PIM kinase inhibitor (IBL-301) was tested in non-small-cell lung carcinoma cell lines and patient-derived tumor tissue explants. The results indicated inhibition of the PI3K-Akt and JAK/STAT pathways *in vitro* and in NSCLC tumor tissue explants. Moreover, IBL-301 decreased the amount of the secreted pro-inflammatory chemokine MCP1 (Moore et al. 2021). These results provide potential treatment options for several cancer types and suggest that combinatorial treatments should be considered for clinical investigations (Malone et al. 2020).

Chemokine (C-X-C motif) receptor 4 (CXCR4) is a member of the CXC chemokine subfamily and is expressed in a variety of cancer cells. Chemokine 12 (CXCL12) is a ligand of the CXCR4 receptor. Aberrant overexpression of CXCR4 is critical for tumor survival, proliferation, angiogenesis, cancer cell homing and the formation of metastasis (Furusato et al. 2010, Mukherjee & Zhao 2013). To date, it has been shown that PIM1 kinase regulates the CXCR4/CXCL12 chemokine pathway by phosphorylating CXCR4 on serine 339, thereby enhancing cell survival in acute myeloid leukemia, diffuse large B-cell lymphoma, and chronic lymphocytic leukemia. In addition, PIM1 activity has an impact on the homing and migration of hematopoietic cells through modification of CXCR4 (Grundler et al. 2009, Brault et al. 2012, Decker et al. 2014). In prostate cancer, CXCR4 and CXCL12 protein expression is remarkably elevated in localized and especially metastatic cancers (Sun et al. 2003). Additionally, the CXCR4/CXCL12 pathway leads to increased tumor

growth, vascularization, and metastasis (Darash-Yahana et al. 2004), and it increases migration of prostate cancer cells (Kukreja et al. 2005). Moreover, in prostate cancer, the CXCR4 pathway drives metastatic formation notably into bones (Taichman et al. 2002). Interestingly, PIM1 activity has been shown to be essential for CXCR4 surface expression and cell migration toward higher levels of CXCL12 (Grundler et al. 2015), suggesting PIM inhibition as a therapeutic option to prevent cancer cell migration and the formation of metastases.

2.5.1 PIM kinases in prostate cancer

PIM kinases are rather weak oncogenes promoting cancer initiation and progression, mainly in collaboration with other oncogenes. Several *in vitro* studies have indicated that PIM kinases enhance the tumorigenic properties of cells. Elevated expression of PIM1 has been implicated in the pro-invasive and pro-migratory behavior of prostate cancer cells (Santio et al. 2010). In clinical prostate cancer samples, PIM1 protein levels are elevated compared to benign prostatic lesions (Dhanasekaran et al. 2001, Valdman et al. 2004, Xu et al. 2005, Cibull et al. 2006). Whether upregulation of PIM1 is associated with prostate tumor aggressiveness is not as clear (Dhanasekaran et al. 2001, van der Poel et al. 2010, Valdman et al. 2004, Xu et al. 2005). Enhanced PIM2 gene and protein levels in prostate cancer have been shown to correlate with increased proliferation and a decreased rate of apoptosis (Dai et al. 2005, Ren et al. 2019). Both PIM1 isoforms PIM1S and PIM1L phosphorylates AR at Ser213 which promotes alteration in AR-mediated transcription. As PIM1 phosphorylates both AR and its co-activator 14-3-3 ζ, PIM1 induces co-activation of AR, which increases transcription of several cell migration and invasion promoting genes, such as MMP7 and MMP10. AR phosphorylation on Ser213 is also associated with higher-grade tumors and castration-resistant prostate cancer (Linn et al. 2012, Ha et al. 2013, McAllister et al. 2020, Ruff et al. 2021) (Figure 8A). However only PIM1L phosphorylates AR at Thr850 and thereby stabilizes AR and promotes AR-mediated transcription (Linn et al. 2012). Moreover, Ren and others have proposed that PIM2 affects prostate tumorigenesis via phosphorylation of eukaryotic translation initiation factor 4E (eIF4B) (Ren et al. 2013). In addition, *PIM3* gene expression levels have been positively correlated with Gleason scores and patient survival (Qu et al. 2016), although this observation was based only on mRNA data. In addition, comprehensive expression level studies of all PIM kinases have not been conducted in parallel in prostate samples partly due to high interest towards

PIM1 protein expression in prostate cancer patients. The role of PIM2, and especially PIM3 in prostate cancer progression, have been cleared out later (Ren et al. 2013, Qu et al. 2016). Furthermore, PIM expression levels in aggressive and more malignant CRPC samples have not been previously determined.

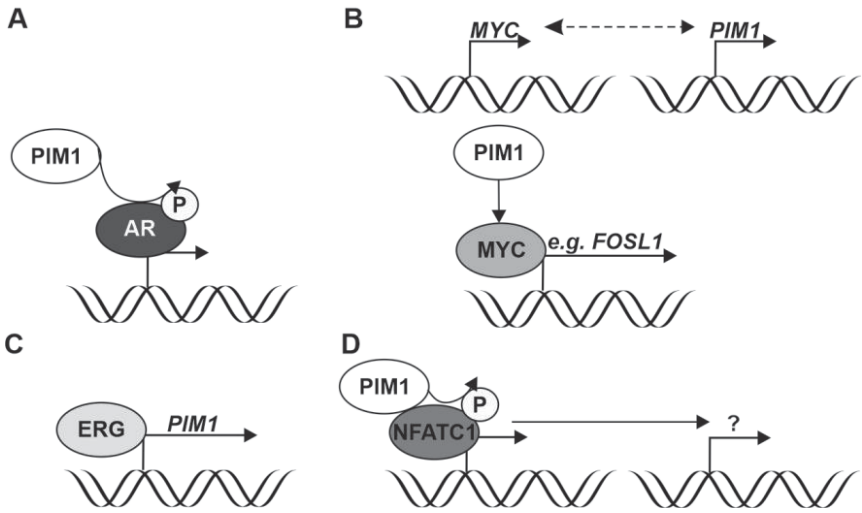

Figure 8. PIM kinase pathways promoting prostate cancer progression

A PIM1 phosphorylates AR at Ser213 and at Thr850 and alters AR-mediated transactivation especially under androgen ablative circumstances. **B** *MYC* and *PIM1* have shown to associate in prostate cancer. PIM1 bind MYC and MAX, resulting in a MYC-MAX-PIM1 complex which recruits PIM1 to chromatin, where it phosphorylates Ser10 on histone H3, thereby stimulating the binding of RNA polymerase II, which contributes to transactivation of several MYC target genes including FOS Like 1, AP-1 transcription factor subunit (*FOSL1*) **C** ERG directly binds to the *PIM1* promoter inducing *PIM1* expression. **D** PIM1 kinase phosphorylate NFATC1 and thereby increasing its transcriptional activity and stabilizing it. However, the targets of this PIM1/NFATC1 axis are not yet known.

2.5.2 Novel PIM kinase inhibitors to restrict cancer progression

The emerging role of PIM kinases as cancer-promoting factors has gained attention as potential therapeutic targets. The discovery of the PIM1 crystal structure in 2005 provided more information on the model of PIM function (Jacobs et al. 2005, Kumar et al. 2005). The PIM1 protein contains two subunits connected by a hinge region. The smaller amino (N)-terminal domain contains mainly β-sheets and one α-helix. The larger carboxy (C)-terminal domain is mainly formed by α-helixes (Jacobs et al. 2005). PIM kinases are constitutively active since the hinge region of PIM kinases forces the activation loop into an open form. (Kumar et al. 2005). The hinge

region in PIM kinases contains an ATP binding site that is unusual in both its sequence and shape due to a proline-123 amino acid residue. Corresponding amino acids have not been found in the ATP binding sites in any other protein kinases. The proline residue prevents the formation of hydrogen bonds with ATP. This structural feature is a key player in the selective binding of PIM inhibitors (Jacobs et al. 2005) (Figure 9). Based on the PIM1 crystal structure, it was determined that staurosporine, which is a generally known kinase inhibitor, also binds to the PIM1 ATP binding area and prevents the binding of ATP and thus kinase activity (Bregman & Meggers 2006). Staurosporine derivatives and flavonoids, however, inhibit many different protein kinases. Thus, usage of these inhibitors is not recommended (Bregman & Meggers 2006).

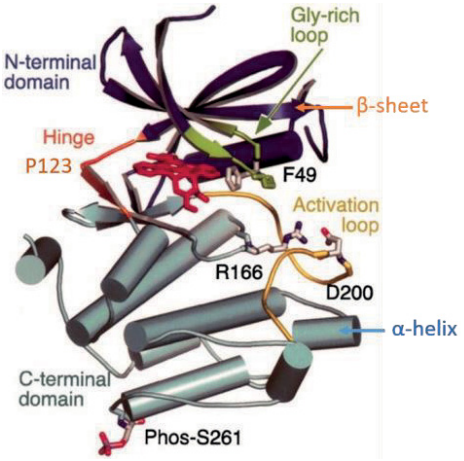

Figure 9. PIM1 crystal structure

Unique structural details within the hinge region connecting the N- and C-terminal lobes around the ATP-binding site render the PIM kinases constitutively active and enable engineering of selective inhibitors (Proline-123, P123) (modified from Jacobs et al. 2005). Attribution 4.0 International (CC BY 4.0).

A French group tested pyrrolo[2,3-a]carbazole derivatives and found potential PIM kinase inhibitors. One of these derivatives, DHPCC-9 (dihydropyrrolocarbazole compound 9), proved to have very selective inhibitory potential toward all three PIM family members. In addition, other specific PIM inhibitors were found. Two of the derivatives were tested *in vitro* in cell lines derived from human solid tumors and were shown to diminish cell proliferation. The selectivity of the pyrrolo[2,3-a]carbazole derivatives for PIM kinases was explained by a non-ATP mimetic binding mode without hydrogen bond formation with the kinase hinge region. Indeed, DHPCC-9

inhibitor competes with ATP and hence prevents PIM kinases from phosphorylating their targets (Akuè-Gèdu et al. 2009, Akuè-Gèdu et al. 2010).

The PIM inhibitor DHPCC-9 has been shown to inhibit cellular PIM kinase activity in cell culture. DHPCC-9 also diminishes the anti-apoptotic effects of PIM1 and the migration of prostate cancer cells. PIM inhibition also prevents the migration of prostate cancer cells, which overexpress the nuclear factor of activated T-cells (NFATC1), indicating that NFATC1 may act as a mediator of the pro-motility effects of PIM kinases (Santio et al. 2010).

Table 3. PIM inhibitors in cancer and their clinical trials

Drug Name	Target	Tested in cancer	Phase studies	Status	Trial
SGI-1776	pan-PIM	Prostate cancer and Non Hodgkin's lymphoma	I	Terminated	NCT00848601
AZD1208	pan-PIM	Acute myelogenous leukemia	I	Terminated	NCT01489722
AZD1208	pan-PIM	Advanced solid tumors and malignant lymphoma	I	Completed	NCT01588548
PIM447 (LGH447)	pan-PIM	Myelofibrosis	I	Completed	NCT02370706
PIM447 (LGH447)	pan-PIM	Relapsed and refractory multiple myeloma	I	Completed	NCT02144038
PIM447 (LGH447)	pan-PIM	Acute myeloid leukemia	I	Completed	NCT02078609
TP-3654 (SGI-9481)	pan-PIM (greater efficacy for PIM1)	Advanced solid tumors	I	Completed	NCT03715504
TP-3654 (SGI-9481)	pan-PIM (greater efficacy for PIM1)	Myelofibrosis	I	Active	NCT04176198
SEL24	pan-PIM & FLT3	Acute myeloid leukemia	I/II	Recruiting	NCT03008187

Several PIM inhibitors have undergone clinical trials to investigate their potential in cancer therapies. SGI-1776, a pan-PIM inhibitor (Chen et al. 2011) was under phase I clinical trials to determine escalation of the dosage in prostate cancer and non-Hodgkin lymphoma. However, both of these trials were terminated due to their off target cardiotoxic effects (Zhang et al. 2018). Another small molecule pan-PIM inhibitor is AZD1208, which has been studied in cells of acute myeloid leukemias (Keeton et al. 2014), prostate cancer (Kirschner et al. 2015), and liposarcoma (Yadav et al. 2019). Moreover, phase I dose-escalation studies of AZD1208 inhibitor in acute myeloid leukemia and advanced solid tumors were performed. With refractory acute myeloid leukemia AZD1208 treatment showed a reduction in the phosphorylation of PIM targets, indicating preliminary evidence for the biological activity of AZD1208 in patients (Cortes et al. 2018) (Table 3).

PIM447 (alternatively LGH447) is a small molecule pan-PIM inhibitor that interrupts the cell cycle and affects the expression of different pro-apoptotic proteins, such as BCL2 (Burger et al. 2015). A clinical phase I dose-escalation study of PIM447, with relapsed or refractory multiple myeloma was well-tolerated (NCT02144038) (Raab et al. 2019). Another phase I study (NCT02370706) was conducted in 2020 with PIM447 in combination with other supplements, the FDA-approved JAK1/JAK2 inhibitor ruxolitinib, and the CDK4/6 inhibitor LEE011 in patients with myelofibrosis. GDC-0339 is a pan-PIM inhibitor and a clinical candidate for the treatment of multiple myeloma, as it showed efficacy in human multiple myeloma xenograft mouse models, and it was well tolerated in phase I safety studies (Wang et al. 2019). TP-3654 (SGI-9481) is a second-generation small molecule pan-PIM inhibitor that reduces the expression of phospho-BAD, has no toxic side effects and reduces tumor cell growth (Foulks et al. 2014, Luszczak et al. 2020a). One clinical phase I trial (NCT03715504) with this inhibitor in advanced solid tumors is completed and another phase I (NCT04176198) trial in myelofibrosis is ongoing. Clinical phase I/II trial (NCT03008187) with SEL24, a dual inhibitor of PIM and FLT3 kinases, in acute myeloid leukemia, is recruiting patients (Table 3).

2.5.3 PIM and MYC

Cooperation between *PIM1* and *MYC* oncogenes was demonstrated for the first time by the finding that *Pim1* transgenic mice cooperate with *Myc* family members in lymphomagenesis (van Lohuizen 1989). The cooperation of PIM kinases with MYC was further supported by cellular experiments, where PIM-mediated phosphorylation of histone H3 selectively affected the expression of several MYC targets including FOS Like 1, AP-1 transcription factor subunit (*FOSL1*) and inhibitor of DNA binding 2 (*ID2*) genes. Moreover, PIM1 was shown to bind MYC and MAX, resulting in a MYC-MAX-PIM1 complex in the nucleus. This complex recruits PIM1 to chromatin, where it phosphorylates Ser10 on histone H3, thereby stimulating the binding of RNA polymerase II, which contributes to transcriptional activation of several MYC target genes (Figure 8B) (Zippo et al. 2007). Moreover, based on one study, MYC phosphorylation on Ser329 by PIM1 and PIM2 and on Ser62 by PIM1 may increase the stability of the MYC protein and enhance its transcriptional activity (Zhang et al. 2008).

Several experiments with transgenic mouse models have indicated that PIM1 cooperates with MYC family members during the progression of T cell lymphomas

(van Lohuizen et al. 1989). It has also been found that 10-20% of mice expressing PIM2- or MYC-transgenes develop lymphomas within six months of age. Mice expressing both of these transgenes developed aggressive leukemias and died between 3 and 4 weeks of age (Allen et al. 1997). Molecular analysis of the lymphomas indicated cooperation between *PIM1* and *MYC* oncogenes (Zhang et al. 2018). Moreover, the *PIM1* and *MYC* genes synergize in triple-negative breast cancer with a poor prognosis (Brasó-Maristany et al. 2016, Horiuchi et al. 2016). PIM1 kinase is co-expressed with MYC protein and enhances MYC-induced tumorigenicity in human prostate cancers (Wang et al. 2010). Interestingly, co-expression of PIM1 and MYC in human prostate tumors has been associated with higher Gleason grades, suggesting that these oncoproteins synergize to induce advanced prostate carcinoma. Cells expressing both MYC and PIM correlated with enhanced tumor progression in mice. In contrast, silencing PIM1 led to MYC-related tumor inactivation, indicating that PIM1 may be essential to maintain MYC-driven aggressive prostate cancer. (Wang et al. 2010, Wang et al. 2012) However, no evidence of PIM3 and MYC cooperation in prostate cancer has been reported thus far.

2.5.4 ERG interaction with PIM kinases in prostate cancer

Based on recent studies, the transcription factor ERG and PIM1 are co-expressed in clinical prostate cancer specimens. ERG directly binds to the *PIM1* promoter inducing *PIM1* expression (Figure 8C) (Magistroni et al. 2011). Moreover, fusion of *TMPRSS2:ERG* promotes tumorigenesis in more than 50% of patients leading to ERG overexpression (Tomlins et al. 2005). Indeed, Mologni and others have indicated that inhibition of PIM1 (NMS-P645) together with PI3K inhibitor (GDC-0941) reduces the survival and proliferation of TMPRSS2:ERG-positive prostate cancer cells (Mologni et al. 2017). Similar information on PIM2 and PIM3 kinases is still lacking.

2.6 Nuclear Factor of Activated T-cells

Nuclear factor of activated T cells (NFAT) is an inducible nuclear factor that binds to interleukin 2 (IL2) antigen receptor response element (ARRE2) (Shaw et al. 1988). NFAT transcription factors are ubiquitously expressed in human tissues and regulate

various cellular processes, such as immune responses including development and activation of lymphocytes and the differentiation of cardiac muscle cells (Crabtree & Olson 2002, Hogan et al. 2003). NFAT transcription factors belong to a family of five different members (Table 4). NFAT5 is more distant to other family members and unlike all the other members it is not regulated by calcium signaling as it is constitutively located in the nucleus (López-Rodríguez et al. 1999). The activation and localization of NFATs are regulated by calcineurin-mediated dephosphorylation. Expression of NFAT protein in the nuclei of T-cells requires activation through the T-cell antigen receptor.

Table 4. NFAT family members

NAME	OTHER NAMES	REFERENCE
NFATC1	NFATC, NFAT2	Northrop et al. 1994
NFATC2	NFATP, NFAT1	McCaffrey et al. 1993
NFATC3	NFATX, NFAT4	Hoey et al. 1995, Masuda et al. 1995
NFATC4	NFAT3	Hoey et al. 1995
NFAT5	TonEBP	López-Rodríguez et al. 1999, Miyakawa et al. 1999

2.6.1 Structure of NFATC transcription factors

Common to all NFAT proteins is a conserved amino-terminal regulatory domain, also known as the NFAT homology region (NHR). The NHR domain contains the transactivation region of NFAT isoforms, which binds promoter elements and hence initiates transcription of NFAT target genes. The regulatory domain contains several serine-rich regions (SRR1, SRR2, and KTS) that are phosphorylated and inactivated by multiple kinases, including protein kinase A (PKA), glycogen synthase kinase 3 (GSK3) and casein kinase 1 (CK1). NHR contains three serine-proline-x-x (SP) repeats (SP1, SP2 and SP3). In addition, the NHR contains an amino-terminal transactivation domain (TAD), and a nuclear localization sequence (NLS), which controls shuttling of NFAT protein between cytoplasm and nucleus and thereby also transcriptional activation. In addition to the nuclear localization signal, the NFAT protein contains a nuclear export signal (NES), which also controls subcellular localization. Furthermore, the NHR contains binding sites for calcineurin (SPRIEIT) and different NFAT phosphorylating kinases, such as CK1 (FSILF), which control NFAT activation by regulating the phosphorylation status of the SRR1 region. NFAT proteins also contain a carboxy-terminal domain and a highly conserved

DNA binding domain (DBD), which is similar to REL/NF-κB- transcription factors and thus called the REL homology domain (RHD) (Figure 10) (Rao et al. 1997, Müller & Rao 2010).

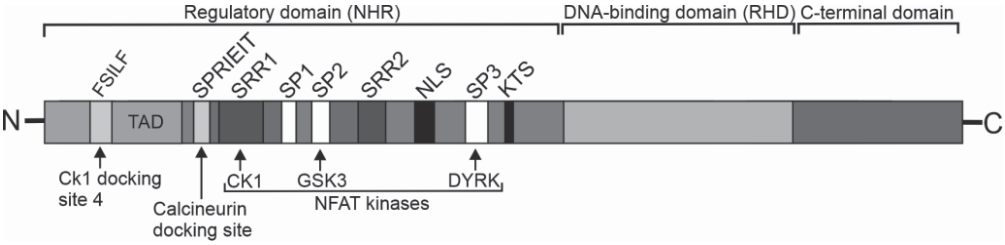

Figure 10. Structure of NFATC1 protein

The NFATC1 protein consists of an amino-terminal regulatory domain (NHR), and a DNA-binding domain (RHD). The regulatory domain contains transactivation domain (TAD), a casein kinase 1 (CK1) docking site called FSILF, and a docking site for calcineurin, called SPRIEIT. It also includes multiple serine-rich motifs (SRR1, SP1, SP2, SRR2, SP3 and KTS) and a nuclear localization sequence (NLS) (based on Müller & Rao 2010).

2.6.2 NFAT activation

In resting cells, NFAT proteins are hyperphosphorylated and located in the cytoplasm. Translocation of NFATC proteins between the cytoplasm and nucleus is an outcome of the calcium and calcium/calcineurin–NFAT signaling pathway. NFAT proteins are activated when the amount of free intra-cellular calcium increases from stores of the endoplasmic reticulum and from the extracellular space through the activation of calcium channels in the plasma membrane (Macini & Toker 2009). Calcium binds to the calcium sensor protein calmodulin, which in turn activates calcineurin. Calcineurin is a phosphatase that dephosphorylates and activates NFAT transcription factors, which then translocate to the nucleus, where they interact with multiple transcriptional partners and hence regulate gene expression (Macian 2005). Activation of calcineurin can be prevented by immunosuppressors, cyclosporin A (CsA) and FK506, which are pharmaceutical inhibitors of calcineurin calcium/calmodulin-dependent activity (Clipstone et al. 1994, Sieber et al. 2007).

Calcineurin controls the translocation of NFAT proteins from the cytoplasm to nucleus by interacting with the NFAT regulatory domain in an amino(N)-terminal site. Calcineurin dephosphorylates SRR and SP repeats in the NFAT regulatory

domain, revealing the nuclear localization domain. This leads to translocation of NFAT from cytoplasm into nucleus, where it becomes transcriptionally active. In the nucleus, the DNA binding domains of NFAT bind to certain cytokine-responsive units.

In the nucleus, after binding with DNA, NFAT proteins intensify the induction of NFAT-mediated gene transcription. NFAT proteins can bind to DNA as homo- or heterodimers or they can cooperate with other transcription factors and bind together e.g. with AP1 transcription factors (heterodimer of Fos and Jun) into specific NFAT/AP1 binding sites of several gene regulatory elements (Rao et al. 1997, Hogan et al. 2003, Müller & Rao 2010). Moreover, NFAT proteins cooperate and bind to DNA with forkhead box P3 (FOXP3). These transcriptional complexes can then induce the expression of a wide number of genes, including interleukin 2 (IL2), gene related to anergy in lymphocytes (GRAIL), caspase 3 protease, and transcriptional activator early growth response 2 (EGR2) (Müller & Rao 2010). These DNA-binding protein complexes are significantly more stable, and have a stronger affinity for DNA than proteins of the same complex alone. (Jain et al. 1995) MAP kinases (MAPKs) and other signaling pathways such as protein tyrosine kinases (PTKs), Ras, and PI3K, regulate the activation of NFAT transcriptional partners. Their activation leads to the synthesis and activation of the heterodimeric transcription factor AP-1 components Fos and Jun, which bind with NFAT to form the NFAT:AP-1 complex (Hogan et al. 2003).

Several kinases phosphorylate serine residues of NFAT proteins and thereby affect their activity and intra-cellular location (Figure 11). NFAT transcription factors are located in the cytoplasm when so-called maintenance kinases act to keep NFAT proteins phosphorylated and prevent their nuclear translocation in resting cells. These maintenance kinases include dual specificity tyrosine phosphorylation-regulated kinase 2 (DYRK2) and casein kinase 1 (CK1). In the cytoplasm, the NFATC1 NLS is hidden since it is bound to phosphorylated SP repeats and SRR regions (Beals et al. 1997, Okamura et al. 2000).

Furthermore, there are also nuclear export kinases that rephosphorylate activated NFAT proteins in the nucleus, which masks the NLS and exposes the NES and shuttles the NFAT proteins out of the nucleus and inactivates them. These export kinases include glycogen synthase kinase 3 (GSK3) and protein kinase A (PKA) (Müller & Rao 2010). In addition, IkB kinase epsilon (IKKε) has been shown to

inhibit NFATC1 activity and promote NFATC1 translocation back to the cytoplasm (Zhang et al. 2016). The role of these kinases is to end NFAT-mediated transcription, after T cell stimulation has ended and the activity of calcineurin has declined. (Macian 2005). However, the third type of NFAT kinase has been described to activate the transcriptional activity of NFAT proteins. PIM1 and DYRK1A kinases have been shown to phosphorylate NFATC1 in a positive manner by increasing its transcriptional activity and stabilizing it (Figure 8D) (Rainio et al. 2002, Liu et al. 2017, Liu et al. 2021). If all the serines in NFATC1 are replaced by alanines, the protein is permanently located in the nucleus. Amino acids 263-271 and 681-685 are essential for nuclear entrance (Beals et al. 1997).

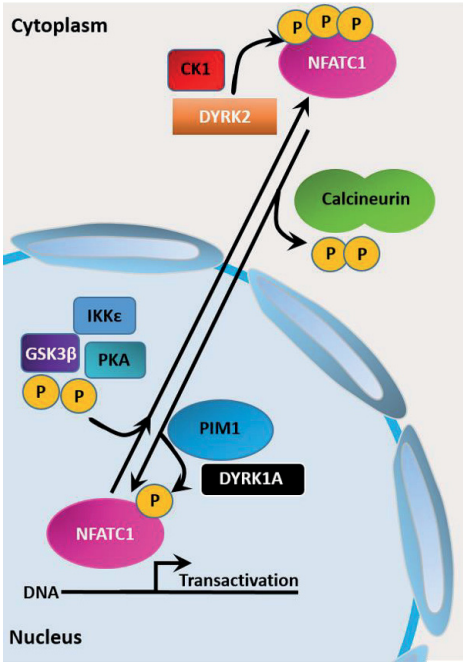

Figure 11. NFATC1 activation.

NFATC1 localization and activation are regulated by phosphorylation. (Modified from Kuhn et al. 2009.)

2.7 NFAT family members in cancer

Overexpression and increased transcriptional activity of NFAT isoforms has been detected in hematological malignancies as well as in various human solid tumors and cell lines. This may lead to the induction of genes that promote cell proliferation,

survival, migration, and invasion that are all associated with tumor progression and the formation of metastases. NFAT family members are evidently overexpressed in multiple human solid tumors including breast and prostate cancer, and hematological malignancies (Medyouf et al. 2007, Macini & Toker 2009, Kawahara et al. 2015, Manda et al. 2016). NFATC1 protein expression levels are induced in prostate cancer and NFATC1 enhances prostate cancer cell motility (Kawahara et al. 2015, Liu et al. 2019). In addition, NFAT isoforms promote tumor angiogenesis by inducing pro-angiogenic genes including cyclooxygenase 2 and E-selectin in endothelial cells (Hernández et al. 2001, Johnson et al. 2003, Ryeom et al. 2008). In contrast, inactivation of NFAT family members decreases cancer progression even though the long-term inhibition of the NFAT-signaling pathway has rather increased tumor incidence (Durnian et al. 2007). NFATC2 and NFAT5 isoforms are expressed in invasive human ductal breast carcinomas and promote the migration and invasion of human breast and colon cancer cells. Moreover, they have also been combined with integrin signaling as NFATC2 and NFAT5 colocalized with α6β4 integrin in breast carcinoma. Additionally, the transcriptional activity of NFAT5 was induced in an α6β4 integrin-dependent manner, indicating that NFAT transcription factors may play a role together with α6β4 integrin in the pro-invasive actions of cancer cells (Jauliac et al. 2002).

Mice lacking individual NFAT proteins do not display any significant phenotypic abnormalities. Apart from a few exceptions, deletion of NFATC1 leads to defective cardiac valve formation, causing embryonic lethality (De La Pompa et al. 1998, Qin et al. 2014). However, pronounced physiological defects occur only when at least two NFAT proteins are knocked down. For instance, concurrent deletion of both NFATC1 and NFATC2 effectively eliminates cytokine production and cytolytic activity in T cells (Peng et al. 2001). Because of the increasing evidence of NFAT contributing to cancer progression, there is also growing development and testing of safe and efficient treatment options targeting the NFAT pathway in cancer. Targeting NFAT signaling in cancers with various inhibitors, such as CsA and tacrolimus, has been performed and shown to have anticancer activity (Qin et al. 2014).

2.8 Interactions of PIM1 and NFATC1

PIM kinases and NFATC1 proteins are important for cancer progression events such as enhanced cell migration, invasion, and angiogenesis (Mancini and Toker, 2009, Santio et al. 2010, Kawahara et al. 2015, Liu et al. 2019). Moreover, PIM1 directly binds NFATC1, phosphorylates it *in vitro* on several serine residues, and thereby enhances NFATC-dependent transactivation in both immune and neuronal cells (Rainio et al. 2002, Glazova et al. 2005). These studies have revealed a new NFATC1-dependent regulatory mechanism in which PIM1 acts by enhancing IL2-dependent proliferation and/or survival. NFATC1 factors can mediate the pro-migratory effects of PIM kinases, as indicated by decreased NFATC1-dependent migration of prostate cancer cells treated with PIM inhibitors (Santio et al. 2010). However, the exact PIM1 phosphorylation target sites that cause an increase in NFATC1 activity and whether they have an impact on the malignant properties of prostate cancer cells are not fully understood.

3 AIMS OF THE STUDY

The aim of this thesis was to determine how and where PIM kinases mediate their effects on prostate cancer. The goal was also to elucidate the role of all three PIM family members in prostate cancer progression and identify the other oncogenic molecules with which they cooperate. Moreover, the aim was to assess the different methods of inhibiting the development of prostate cancer through inhibition of PIM kinases and their possible counterparts. One objective was also to survey novel PIM downstream targets in prostate cancer and assess new approaches for the targeted treatment of prostate cancer.

The detailed questions were:

1. Do novel PIM kinase inhibitors restrict cancer cell proliferation and migration *in vivo*?

2. Do PIM kinases promote the migration and invasion of prostate cancer cells via phosphorylation of its substrate NFATC1, and if so, which PIM mediated NFATC1 target genes are essential for the pro-migratory and invasive effects?

3. How are different PIM family members expressed in prostate cancer and how do other genes regulate their expression? Is MYC or ERG co-expressed in PIM-overexpressing prostate tumors?

4 MATERIALS AND METHODS

4.1 Cell lines (I, II, II)

Multiple eukaryotic cell lines were used in different experiments of the study (Table 5). Cells were cultured under recommended conditions specifically modified for each cell line. All the cell lines were also tested for mycoplasma contamination prior to use and frequently during the studies.

Table 5. All eukaryotic cell lines used for the experiments

Xenograft cell line	Origin	Androgen sensitivity	Medium	Used in publication
DU145	human, prostate adenocarcinoma, brain metastasis	-	EMEM, 10 % FBS, 1% L-glutamine, 1 % penicillin/streptomycin	II
LNCaP	human, prostate carcinoma, lymph node metastasis	+	RPMI-1640, 10 % FBS, 1% L-glutamine, 1 % penicillin/streptomycin	II
MG-63	human, bone osteosarcoma	-	DMEM (conditioned medium: 0,5 µg/ml of ascorbic acid for 10 days, and 0,1 % BSA + ascorbic acid for two days) → used for invasion assay	II
PC-3	human, prostate adenocarcinoma, skull metastasis	-	RPMI-1640, 10 % FBS, 1% L-glutamine, 1 % penicillin/streptomycin	I, II
PC-3/ Mock/ Tomato (stable cell line)			RPMI-1640, 10 % FBS, 1% L-glutamine, 1 % penicillin/streptomycin, selection by 200 µg/ml of G418	I, II
PC-3/ PIM1/ Tomato (stable cell line)			RPMI-1640, 10 % FBS, 1% L-glutamine, 1 % penicillin/streptomycin, selection by 200 µg/ml of G418	I, II
PC-3/ PIM3/ Tomato (stable cell line)			RPMI-1640, 10 % FBS, 1% L-glutamine, 1 % penicillin/streptomycin, selection by 200 µg/ml of G418	I
VCaP	human, prostate cancer metastasis from vertebrae	+	RPMI-1640, 10 % FBS, 1% L-glutamine, 1 % penicillin/streptomycin	III

4.2 Zebrafish embryos (I)

Wild-type zebrafish (Danio rerio) embryos were used to test the severe side effects of PIM inhibitors. Housing and experiments were performed according to the European Convention for the Protection of Vertebrate Animals used for Experimental and other Scientific Purposes and Statutes 1076/85 and 62/2006 of The Animal Protection Law in Finland and EU Directive 86/609.

4.3 Xenograft models (I)

Two batches of mice from Harlan Laboratories (Horst, the Netherlands) were used for toxicity tests, males (FVB/NhanHsd) and females (BALB/cOlaHsd). Subcutaneous and orthotopic tumor experiments were performed with athymic nude male mice (Balb/cOlaHsd-Foxn1nu/nu, Harlan Laboratories, Horst, the Netherlands).

All mouse experiments were carried out according to the European Convention for the Protection of Vertebrate Animals used for Experimental and other Scientific Purposes, Statutes 1076/85 and 1360/90 of The Animal Protection Law in Finland and EU Directive 86/609. The experimental procedures were reviewed by the local Ethics Committee on Animal Experimentation of the University of Turku and approved by the Provincial State Office of Western Finland with the license IDs ESAVI/2008-05531 and ESAVI/3937/04.10.03/2011.

4.4 Patient samples (III)

A total of 254 prostate tissue microarray (TMA) samples, including benign samples (n=23) from adjacent tissue of untreated primary prostate cancer prostatectomy samples, untreated primary prostate cancers (n=186) and locally recurrent CRPCs (n=45), were obtained from Tampere University Hospital (TAUH, Tampere, Finland). The mean age of patients at diagnosis was 63.5 years (range: 49–72), and the mean prostate-specific antigen (PSA) concentration was 14.3 ng/ml (range: 1.5–78.2). Biochemical progression was defined as two consecutive samples with PSA $\geq$ 0.5 ng/ml. The use of clinical material was approved by the Ethics Committee of the Tampere University Hospital and the National Authority for

Medicolegal Affairs. For prospective sample collection, informed consent was obtained from all the subjects.

4.5 Cell viability assay (I, II)

The viability of cells was analyzed by two different assays: the MTT assay and the AlamarBlue® cell viability assay (Thermo Fisher Scientific, Waltham, MA, USA).

PC-3 or DU-145 cells (either ectopically transfected with empty vector or NFATC1 MM, DM or WT) were plated on 96-well plates, and one day later, they were either treated with 10 μM DHPCC-9 or BA-1a inhibitors or control-treated with DMSO/DMA (0.1%). Cell viability was measured with a spectrophotometer by absorbance in the MTT assay or by fluorescence in the Almar blue assay with the EnVision 2104 Multilabel Reader.

4.6 Cell transfections (I, II, III)

Transfections of eukaryotic cells were performed with Fugene 6 or Fugene HD (Promega, Madison, WI, USA) transfection reagents in a 2:1 or 3:1 ratio to DNA according to the manufacturer's instructions.

For gene knockdown, transfections of the cells were performed with Lipofectamine RNAiMAX (Invitrogen, Carlsbad, CA, USA) transfection reagent by transfecting siRNAs targeting ERG or a negative control siRNA (Table 6). Reverse transfection with 25 nM siRNA was used for VCaP prostate cancer cells, after which cells were grown for 72 hours before RNA and protein extraction.

Table 6. siRNA oligos

Target	Sequence and details	Company	Used in publication
ERG	5´ – UGAUGUUGAUAAAGCCUAUU – 3' 5' – UAGGCUUUAUCAACAUCAUU – 3'	Sigma-Aldrich	III
non-targeting	MISSION siRNA Universal negative Control #2	Sigma-Aldrich	III

4.7 Cloning (II)

Full-length NFATC1 was amplified by PCR from pBJ5-NFATC1-Flag by using the primers presented in Table 7, digested with KpnI and BamHI, and ligated into the pFlag-CMV-2 vector (Sigma–Aldrich), from which it was transferred to pEGFP-C3 (Clontech) by BglI and BamHI digestion and ligation. Truncated NFATC1 was digested from pGEX-3X with PflMI and ligated to pEYFP-C2 (Clontech Laboratories, Mountain View, CA, USA).

Table 7. Cloning primers

Target	Forward (F) sequence Reverse (R) sequence	Used in publication
NFATC1	F: 5' GCG GTA CCG CCA CCA TGG ACT ACA AGG CA 3' R: 3' CCC GGA TCC CTG CGT CTT TAG 5'	II

To prepare stably PIM-overexpressing human PC-3-derived cell lines, PC-3 cells were transfected with pcDNA3.1/V5-His-C-based expression vectors for PIM1 or PIM3 (kindly provided by Markku Varjosalo, University of Helsinki, Finland) or transfected with the empty vector (Thermo Fisher Scientific, Waltham, MA, USA) to produce the control cells. Moreover, the fluorescent follow-up marker Tomato was used for all the stable cell lines and thus all cells were co-transfected with the pCMV-Td-Tomato plasmid (Clontech Laboratories Inc., Mountain View, CA, USA) (Table 8.)

The pcDNA3.1/V5-HisC, pGEX-6P-1 and pTag-RFP vectors expressing wild-type (WT) or kinase-deficient (KD) human PIM1-3 or mouse Pim3 are presented in Table 8. The NFAT-luciferase reporter plasmids as well as WT, N-terminally truncated (amino acids 1–418), dominant negative (DN, amino acids 410–680) and constitutively active SRR mutant (mSRR) human NFATC1 expression vectors based on pGEX-3X or pBJ5-Flag were kindly provided by the G.R. Crabtree (Stanford University, CA, USA) (Table 8).

Table 8. DNA plasmids

Tag	Plasmid	Insert	Used in publication
Flag	pBJ5	NFATC1 N-terminally truncated (amino acids 1–418)	II
		NFATC1 dominant negative (DN) (amino acids 410–680)	
		NFATC1 constitutively active SRR mutant (mSRR)	
	pCMV-2	NFATC1 (full-length)	
		NFATC1 multi mutant (MM)	
		NFATC1 triple mutant ™	
		NFATC1 double mutant (DM)	
Firefly luciferase	pGL3	IL-2	II
		NFAT	
GFP	pEGFP-C3	NFATC1 (full-length)	II
GST	pGEX-6P-1	PIM1	I
		PIM2	I
		PIM3	I
	pGEX-3X	NFATC1	II
Renilla luciferase	pRLT	-	II
RFP	pTag-RFP-N	PIM1 WT	I, II
		PIM1 KD	I
		PIM2	I
		PIM3	I
		Pim3 (mouse)	I
Tomato	pCMV-Td	-	I, II
V5	pcDNA3.1. /V5-His-C	PIM1	I, II
		PIM2	I
		PIM3	I
YFP	pEYFP-C2	NFATC1 (N-terminally truncated aa 1-418)	II

4.8 Kinase inhibitors (I, II)

Three validated PIM-selective inhibitors were utilized in the studies: the pyrrolozarbazole DHPCC-9 (1,10-dihydropyrrolo[2,3-a]carbazole-3-carbaldehyde) (Santio et al. 2010, Akué-Gédu et al. 2009) and the benzo[cd]azulenes BA-1a and BA-2c (Aumüller & Yli-Kauhaluoma 2009, Kiriazis et al. 2013).

4.9 Cell migration assays (II)

PC-3 or DU-145 cells were first plated on cell plates and after 24 or 48 hours, confluent cell layers were scratched with 10 µl pipette tips or alternatively after 24 hours first ectopically transfected with WT or mutant NFATC1 (mSRR, DM, MM) expression vectors, and then after 24 hours, the cell layers were scratched with 10 µl pipette tips. Wounded cells were treated with 10 µM DHPCC-9 or BA-1a or control-treated with vehicle DMSO/DMA (0.1%). The anti-proliferative agent mitomycin C (15 µg/ml, Sigma–Aldrich) was used to confirm that cell proliferation caused no changes in cell migration.

Imaging was performed with a Zeiss Stereo Lumar-V12 microscope with AxioVision Rel.4.8 software after 0- and 24-hours' time-points by 20× magnification. The width of the wound in PC-3 cells was analyzed by ImageJ software (1.37v, Wayne Rasband, National Institute of Health, Bethesda, MD, USA) by manually drawing the lines of the wounds and analyzing the wound area in square pixels. DU-145 cells were imaged with CM Technologies Cell-IQ (D.I. Biotech, Korea) by using a 4× objective and image analysis with the Cell-IQ software 4.3 by the scratch wound measurement tool.

4.10 Toxicity assays with zebrafish embryos (I)

The zebrafish embryos were maintained at 26 °C according to standard procedures (Kimmel et al. 1995). Embryos were collected after spawning, cultured in E3 medium (5 mM NaCl, 0.17 mM KCl, 0.33 mM CaCl2, 0.33 mM MgSO4, 0.01% methylene blue) at 28 °C and treated for 6-50 hours after fertilization with the PIM-inhibitor DHPCC-9 or 0.1% DMSO used as a vehicle. Toxicity was assessed by scoring embryos as live or dead, and further detailed morphological analysis of the length, developmental stage, body curvature and possible pericardiac edema were assessed with stereomicroscopy imaging (ZeissStereoLumar V.12, Carl Zeiss Microscopy GmBH, Jena Germany). All image analyses were performed using ImageJ software (1.48s, Fiji, Wayne Rasband, National Institutes of Health, Bethesda, MD, USA).

4.11 Toxicity assays with mice (I)

Two lots of mice from Harlan Laboratories (Horst, the Netherlands) were used, males (FVB/NhanHsd) and females (BALB/cOlaHsd). All mouse experiments were carried out by first treating the mice with PIM-inhibitor (DHPCC-9/BA-1a) or vehicle and monitored daily for 6-17 days, after which the mice were sacrificed, and tissues were collected and stained immunohistochemically to detect possible abnormalities.

DHPCC-9 was dissolved in DMSO and intraperitoneally injected in 20 µl total volume of DMSO into FVB/NHanHsd male mice at a concentration of 100 mg/kg/day for two days and thereafter at 50 mg/kg/day for 8 days. BA-1a was dissolved in DMA and intraperitoneally injected into BALB/cOlaHsd female mice, either 25 mg/kg/day in 25 µl of total volume of DMA for 6 days or 10–20 mg/kg/day in 10 µl of total volume of DMA for 17 days.

Accordingly, the clinical signs of the mice were recorded daily, and if the criteria of humane endpoints were met, the animal was sacrificed. Humane endpoints were considered rapid or gradual weight loss, abnormal changes in behavior and motion (social and eating behavior), subcutaneous tumor size greater than 1.5 cm in diameter or skin problems (wounds or signs of inflammation). Animal welfare and weight were also monitored daily until the mice were sacrificed. Tissue samples from the liver, spleen and kidneys were collected to determine possible abnormalities.

4.12 Subcutaneous tumor experiments (I)

For subcutaneous inoculations, PC-3 cells stably transfected with PIM1, PIM3 or the empty vector were collected, while cells were growing in a logarithmic phase. The cells were suspended in sterile PBS (4.5× 106 cells in 100 µl) and injected into both flanks of athymic nude male mice (Balb/cOlaHsd-Foxn1nu/nu, Harlan Laboratories, Horst, the Netherlands). Animal welfare was monitored daily, animals were weighed, and tumors were palpated every other day. Tumor volume was calculated according to the Formula $V = (\pi/6)(d1 \times d2)3/2$ (20), where d1 and d2 are perpendicular tumor diameters (width, length). The fluorescently labeled tumor cells were imaged by IVIS Lumina II (Xenogen corp./Caliper Life Sciences, Inc., Hopkinton, MA, USA) at different time points during the experiment, after which

tumor areas (square pixels) and average signal intensities were measured by ImageJ. After three weeks, mice were sacrificed, and tumors as well as selected tissues (kidneys, spleen, liver, lungs, and prostate-draining lymph nodes) were collected.

4.13 Immunoblotting (I, II, III)

Sample preparation began by washing cells with PBS and resuspending in 2x Laemmli Sample Buffer. Samples were vortexed for 5 s and heated at 95 °C for 5 min. After gene knockdown experiments, cells were lysed in Triton-X lysis buffer containing 50 mM Tris-HCl, 150 mM NaCl, 0.5% Triton X-100, 1 mM PMSF, 1 mM DTT and 1× Halt protease inhibitor cocktail (Thermo Fisher Scientific), after which the lysates were sonicated four times for 30 s at medium power with Bioruptor equipment (Diagenode Inc.). Protein samples were separated by SDS–PAGE or Mini-PROTEAN TGX Precast Gel (Bio–Rad) immobilized onto PVDF-membrane (Merck Millipore, Billerica, MA, USA) and incubated with primary and secondary antibodies (Tables 7 and 8). Chemiluminescence reagents Amersham™ ECL Plus or ECL Prime (GE Healthcare) or Pierce ECL (Thermo Fisher Scientific Inc.) were used to detect the signal.

4.14 Orthotopic tumor experiments (I)

For orthotopic inoculations, cells were suspended in sterile PBS (Biochrom AG, Berlin, Germany; 106 cells in 20 µl) containing green food color 33022 (5 µg/ml; Roberts Oy, Turku, Finland). Cells were inoculated into the ventral prostates of anesthetized mice as previously described (Tuomela et al. 2008). The analgesic drug temgesic (Reckitt Benckiser Healthcare Ltd, Hull, UK) was given to mice prior to and 24 h and 48 h after the operation and during the three-week follow-up period if needed.

Two separate orthotopic sets of experiments were performed. In the second set, some of the mice inoculated with PIM3-overexpressing cells were treated daily with intraperitoneal injections of either 50 mg/kg DHPCC-9 in 20 µl DMSO or 20 mg/kg BA-1a in 10 µl DMA or equal amounts of the dissolvents as controls. All treatments were initiated one day after the orthotopic inoculations. Animal welfare and weight were monitored daily until the mice were sacrificed. All the tumors and tissue

samples were imaged by IVIS Lumina II (Xenogen corp./Caliper Life Sciences, Inc., Hopkinton, MA, USA) and then stored for further analysis. Tumor volume was calculated according to the Formula V = (π/6)(d1 × d2× d3), where d1—d3 are perpendicular tumor diameters (width, length, height) (Ruohola et al., 1999).

4.15 Histology and immunohistochemistry (I, III)

Formalin-fixed paraffin-embedded (FFPE) mouse tumor samples or TMA samples from prostate cancer patients were deparaffinized, stained and rehydrated and mounted into sample slides. All tumor and tissue samples were first stained with Mayer's hematoxylin and eosin (H&E).

Additional immunohistochemical staining was performed for mouse tumor samples to visualize mitotic cells, expression of V5-tagged constructs, blood vessels, lymphatic vessels, and phosphorylation of CXCR4 (Tables 9 and 10). For the negative staining control, the primary antibody was replaced by PBS or TBS in each sample. Stable PC-3/pcDNA3.1-VEGF-C tumor tissue (Tuomela et al. 2009) was used as a negative control for V5 staining.

To analyze the mouse tumor samples, representative images were taken by a Leica DMRXA microscope (Leica Microsystems CMS GmbH, Mannheim, Germany) and ISCapture V2.6. software (Xintu Photonics Co., Ltd, Tucsen, Fuzhou, China), while whole tumor scans were performed either by an Olympus BX51 microscope with DotSlide software (Olympus Corporation, Tokyo, Japan) or a Pannoramic 250 slide scanner with Pannoramic Viewer (3DHistech Ltd., Budapest, Hungary). Images were analyzed by ImageJ. For analysis of signal intensities and stained areas, color deconvolution by H&E DAB was performed. Then images were converted to grayscale, colors were inverted, background was subtracted, and threshold levels were adjusted. Thereafter particles were analyzed. For other than vessel analyses, necrotic areas were avoided. In addition, fully necrotic tumors were excluded from analyses.

PIM protein expression levels in prostate carcinomas were validated by IHC staining of formalin-fixed paraffin-embedded (FFPE) TMA samples. TMA sections were deparaffinized, and antigen retrieval was performed by heat-induced epitope retrieval in TE buffer (pH 9) at 98 °C for 15 minutes. Primary antibodies (Table 9) were

diluted in Antibody Diluent (ImmunoLogic, Duiven, The Netherlands). Staining was performed using a Lab Vision Autostainer 480S (Thermo Fisher Scientific, Waltham, MA, USA). Sections were counterstained with Mayer's hematoxylin (Histolab AB, Gothenburg, Sweden) for 2 minutes and mounted with Neo-Mount (Merck KGaA, Darmstadt, Germany).

For negative controls, the primary antibody was omitted, and for positive controls, FFPE samples of tonsil, glioma and/or colon tissues were used. Slides were scanned with an Olympus BX51 scanner with a 20x objective and Slide Strider software (Jilab Inc., Tampere, Finland) or with a NanoZoomer S60 Digital slide scanner (C13210-01, Hamamatsu Photonics, K. K., Japan) with a 20x objective. Nuclear and cytoplasmic scoring of the figures was performed with ImageJ® software (Wayne Rasband, NIH, USA).

Nuclear and cytoplasmic staining intensities of PIM protein expression were classified from 0 to 3 with negative (0), weak (1), moderate (2) or strong (3) staining in proportion to the stained cancerous area. In the case of nuclear staining, if possible, a minimum of 200 cells were calculated from carcinogenic areas. The Histo score (H-score/HS) was calculated by a semiquantitative assessment of both the intensity of staining with the 0 to 3 scale and the percentage of positive prostate cancer cells/area. The range of possible scores was from 0 to 300 or from 0 to 600 when both the cytoplasmic and nuclear scores were combined or summed. Samples stained against ERG antibody were categorized into ERG-positive and ERG-negative. The results from 85 ERG-stained samples were published previously in Leinonen et al. 2013, while 38 additional samples were stained and analyzed for these studies.

Table 9. Primary antibodies used in experiments

Target of the antibody	Product number and Company	Dilution	Used in publication
ACTB	13E5; Cell signaling Technology	1:1000 (WB)	I, II
	D13K4803; Sigma-Aldrich	1:20000 (WB)	I
CD34 (blood vessels)	ME 14.7, sc-18917; Santa Cruz	1:50 (IHC)	I
CXCR4	ab2074; Abcam	1:1000 (WB) 1:1000 (IF) 1:200 (IHC)	I
ERG	EPR3864; Epitomics, Inc.	1:200 (IHC) 1:5000 (WB)	III
Fibrillarin	Cell Signaling Technology	1:1000 (WB)	II, III
Flag	F1804; Sigma-Aldrich	1:500 (WB) 1:500 (IF)	II
GAPDH	G8795; Sigma-Aldrich	1:20 000-50 0000 (WB)	II
NFATC1	F1804; Sigma-Aldrich	1:500 (WB)	II
m-LYVE1 (lymphatic vessels)	Dr. Jackson, WIMM	1:200 (IHC)	I
Phospho-histone H3 (pH3F3) (mitosis)	Cell Signaling Technology #9701	1:200 (IHC)	I
Phospho(Ser339)-CXCR4	ab74012, Abcam	1:1000 (WB) 1:1000 (IF) 1:500 (IHC)	I
PIM1	ab224772; Abcam	1:200 (IHC) 1:2000 (WB)	III
	12H8; Santa Cruz Biotechnology, Santa Cruz	1:500 (WB)	I, II
PIM2	D1D2; Cell Signaling Technology	1:1000 (WB)	I, II
	TA501166; OriGene Technologies Inc.	1:50 (IHC) 1:2000 (WB)	III
PIM3	D17C9; Cell Signaling Technology	1:1000 (WB)	II
	TA351349; OriGene	1:200 (IHC) 1:10000 (WB)	III
β-Tubulin	Sigma-Aldrich	1:40 000 (WB)	III
V5	ab95038; Abcam	1:500 (IHC)	I
	Invitrogen	1:500 (WB)	II

Table 10. Secondary antibodies used in experiments

Antibody	Product number and Company	Dilution	Used in publication
anti-mouse Alexa Fluor® 488	Thermo Fisher Scientific	1:1000 (IF)	II
chicken anti-rabbit Alexa Fluor® 488	A21441; Life Technologies	1:1000 (IF)	I
Histofine Simple Stain MAX PO multi, Universal Immunoperoxidase Polymer Anti-Mouse and Anti-Rabbit	Nichirei Biosciences Inc.	no dilution (IHC)	III
goat anti-rabbit IgG	BA-1000, Vector	1:200 (IHC)	I
	#7074; Cell Signaling Technology	1:5000 (WB)	I
horse anti-goat IgG	BA-9500; Vector	1:200 (IHC)	I
horse anti-mouse	#7076; Cell Signaling Technology	1:5000 (WB)	I
rabbit anti-mouse HRP-conjugated antibody	DAKO	1:10 000 (WB)	III
swine anti-rabbit HRP-conjugated antibody	DAKO	1:5000 (WB)	III
rabbit anti-rat	097(101)E0468; DAKO	1:200 (IHC)	I
anti-mouse HRP-conjugated antibody	#7076, Cell Signaling Technology	1:5000 (WB)	I
anti-rabbit HRP-conjugated antibody	#7074, Cell Signaling Technology	1:5000 (WB)	I

4.16 Immunofluorescence (I, II)

To determine the subcellular localizations and signal intensities of phosphorylated versus overall CXCR4 expression, immunofluorescent (IF) staining of stably PIM1- and PIM3-overexpressing PC-3 cells treated with either 0.1% DMSO or 10 μM PIM inhibitor DHPCC-9 was performed. After 24 h incubation with PIM inhibitor, samples were fixed, permeabilized, and stained with anti-phospho(Ser339)-CXCR4 or anti-CXCR4 (1:1000) and relevant secondary IF antibodies (Tables 9 and 10). Cells were imaged by a Leica DMRXA TCS SP5 Matrix confocal microscope with LAS AF Application (Leica Microsystems CMS GmbH, Mannheim, Germany). Signal intensities were analyzed by ImageJ.

To diagnose the subcellular localizations of wild-type and mutant NFATC1 proteins, PC-3 cells were ectopically transfected with Flag-tagged expression vectors (NFATC1, WT and MM). Staining was performed as described above; however sample imaging was performed and analyzed with a Zeiss ApoTome.2 fluorescence microscope and Zen lite 2012 software. Approximately 15 images were taken from each sample.

4.17 Fluorescence-lifetime imaging method (FLIM) (II)

Localization and signal intensity of phosphorylated versus overall CXCR4 expression were analyzed by immunofluorescent (IF) staining of stably transfected cells treated with either 0.1% DMSO or 10 μM DHPCC-9. The experiment was controlled by parallel samples in which the primary antibody was omitted. Staining was repeated twice, and stacks of images were taken by confocal microscopy from a minimum of 30 cells from each sample per experiment. Shown are the signal intensities of phospho-CXCR4 staining compared to overall CXCR4 levels along with representative images from phospho-CXCR4 and CXCR4 staining.

To visualize interactions between RFP-tagged PIM1 and GFP-tagged NFATC1, PC-3 cells plated on coverslips were ectopically transfected with the corresponding expression vectors and/or their empty controls. Some of the samples were treated overnight with DMSO or 10 μM DHPCC-9. Forty-eight hours after transfection, cell samples were fixed with 4% PFA and mounted with Mowiol. First, physical interactions between tagged proteins were measured by analyzing the GFP lifetime with Lambert Instruments Fluorescence Lifetime Attachment (LIFA) and LI-FLIM software as previously described (Santio et al. 2016). Then, co-localization of proteins was imaged by a Zeiss LSM 780 confocal microscope and by sequential scanning with ZEN lite 2012 software. Excitation wavelengths were 488 nm (GFP) and 561 nm (RFP), and emission wavelengths were 500–535 nm (GFP) and 599–651 nm (RFP). Image analyses were performed with ImageJ® software (Wayne Rasband, NIH, USA).

4.18 *In vitro* kinase assays (II)

The E. coli BL21 strain was used to produce GST fusion proteins. Protein production was induced with 0.5 mM IPTG, and protease activity was inhibited by aprotinin (1:200; Sigma–Aldrich) during cell lysis. Proteins were either eluted as GST fusion proteins or cleaved by the PreScission protease according to the manufacturer's protocol (GE Healthcare Life Sciences, Little Chalfont, UK). For *in vitro* kinase assays, cleaved PIM kinase (0.5 μg) and GST-tagged NFATC1 (amino acids 1–418) fusion protein (1 μg) were mixed prior to addition of the 2x kinase buffer (20 mM pipes, pH 7.0, 5 mM MnCl2, 0.25 mM β-glycerophophate, 0.4 mM spermine, 10 μM ATP) with 0.5 MBq of [32P] adenosine triphosphate. Samples were

pretreated for 15 min with 10 μM DHPCC-9 to inhibit PIM kinase activity or in 0.1% DMSO used as the solvent. After 15 to 30 min kinase reactions at 30 °C, samples were dissolved in 2x Laemmli sample buffer (LSB) and denatured for 5 min at 95 °C. Phosphorylated proteins were resolved by SDS–PAGE, stained with Page Blue solution (Thermo Fisher Scientific) and detected by autoradiography.

GST-tagged constructs expressing human CXCR4 C46-WT and C46-S339A fragments (Grundler et al. 2009) as well as full-length human PIM1, human PIM2 and mouse PIM3 proteins were analyzed by *in vitro* phosphorylation assays as described above except that no radioactively labelled ATP was used. Samples were separated by SDS–PAGE, after which Western blotting with anti-phospho(Ser339)-CXCR4 was used to detect CXCR4 phosphorylation. Protein loading was analyzed from PVDF-membrane by staining with Ponceau S solution (Sigma, St.Louis, MO, USA). In addition, to analyze the phospho-CXCR4 levels, the signal intensities were calculated by a ChemiDoc MP System with Image Lab software (Bio–Rad Laboratories, Inc., Hercules, CA, USA). Thereafter the phospho-CXCR4 signal values were compared to the overall CXCR4 values.

4.19 Mutant constructs and NFATC1 mutagenesis (II)

The QuikChange™ site-directed mutagenesis kit (Stratagene, Agilent Technologies, Santa Clara, CA, USA) was used to prepare phosphodeficient mutants of NFATC1 (Table 11). Other mutant constructs provided ready to use are also shown in Table 9. Mutations to replace serines or threonines with alanine residues were introduced into ten PIM1 target sites with the use of five different primer pairs (Additional Table S1), resulting in the production of double mutant (DM, two primer pairs, 1–2), triple mutant (TM, three primer pairs, 3–5) or multimutant (MM, all primer pairs) NFATC1.

Table 11. Mutagenesis

Mutated amino acids (aa): S=serine, T=threonine were generated by mutagenesis into A=alanine. K=Lysine was mutated into M=Methionine

Gene	Mutation	Name of the mutant	Used in publication
CXCR4	S339>A	SA	I
NFATC1	S245>A, → 2. residue S269>A → 5. residue	Double mutant (DM)	II
NFATC1	S151>A, S153>A, T154>A, (1. residue) S256>A, S257>A, (3. residue) S335>A, T338>A, T339>A (5. residue)	Triple mutant (TM)	II
NFATC1	S151>A, S153>A, T154>A, (1. residue) S245>A, (2. residue) S256>A, S257>A, (3. residue) S269>A, (4. residue) S335>A, T338>A, T339>A (5. residue)	Multimutant (MM)	II
NFATC1	all 11 serines mutated to alanines in the SRR (172–194)	constitutively active SRR mutant (mSRR)	II
NFATC1	aa: 410-680	dominant negative (DN)	II
PIM1	K67>M	kinase-deficient (KD)	II

4.20 Identification of NFATC1 *in vivo* phosphorylation sites by mass spectrometry (II)

PC-3 prostate cancer cells were ectopically transfected with the pEYFP-NFATC1 expression vector. After 48 h, cells were stimulated with TPA and IM for 1 h prior to cell lysis in RIPA buffer supplemented with complete mini EDTA-free protease inhibitors (Roche, Basel, Switzerland). One milligram aliquots of proteins were

mixed with Chromotek-GFP-Trap® Magnetic beads (Allele Biotechnology, San Diego, CA, USA), after which GFP-tagged proteins were immunoprecipitated according to manufacturer's protocol, dissolved in 2x LSB, denatured, resolved in Bis-Tris gel (Bio-Rad) and stained with colloidal Coomassie blue solution (Thermo Fisher Scientific). NFATC1 protein isolation, trypsin digestion and titanium dioxide enrichment without salt extraction were performed as previously described (Imanishi et al. 2007, Kouvonen et al. 2011). Samples were analyzed by an LTQ Orbitrap Velos mass spectrometer (Thermo Fisher Scientific), using the HCD Top 10 method with a 10 min gradient and mass value of 300 to 2000.

4.21 Luciferase assays (II)

To measure NFAT-dependent transcriptional activity, PC-3 cells were ectopically transfected with the pGL3-IL-2-luciferase reporter and either pBJ5-NFATC1-Flag or an empty control vector. To stimulate NFATC1 activity and nuclear translocation, cells were treated for 7 h with 15 ng/ml of 12–0-tetradecanoyl-phorbol-13-asetate (TPA; Sigma–Aldrich, St. Louis, MO, USA) in DMSO and 1 μM ionomycin (IM; Merck KGaA, Darmstadt, Germany) in EtOH. To inhibit PIM kinase activity, cells were treated for 24 h with 10 μM DHPCC-9 in 0.1% DMSO. For all chemical compounds, their solvents were used as controls. Twenty-four or 48 hours after transfections, cells were collected, lysed in 1% NP-40 buffer by repeated freezing and thawing, and analyzed for luciferase activity using a Luminoscan Ascent luminometer (Thermo Fisher Scientific).

To compare the activities of WT and MM NFATC1 in PC-3, DU-145 and LNCaP prostate cancer cell lines, cells were ectopically transfected with the pGL3-NFAT-luciferase reporter and either WT or MM pCMV-NFATC1-Flag or an empty control vector. As an internal transfection efficiency control, Renilla luciferase (pRLTk; Promega) was co-transfected into the cells. Some of the cells were treated with TPA and IM and/or DHPCC-9 as described above. Luciferase assays with four parallel samples were performed on 96-well plates using the Dual-Glo® Luciferase Assay System (Promega) according to the manufacturer's protocol. Luciferase activities were measured with an EnVision 2104 Multilabel Reader (Perkin Elmer, Waltham, MA, USA). The results are presented as relative luciferase activity (RLU) corresponding to the firefly luciferase light emission values normalized against Renilla luciferase light emission values.

4.22 Boyden chamber invasion assays (II)

The invasiveness of PC-3 cells was analyzed one day after ectopic cell transfection (control, NFATC1 WT or MM), using cell culture invasion inserts of 8 μm pore size (Corning BioCoat™ Matrigel® Invasion Chamber, Bedford, MA, USA) according to the manufacturer's instructions. For this purpose, cells were suspended in DMEM supplemented with 1% BSA (20,000 cells/ chamber) and either DMSO or 10 μM DHPCC-9. Conditioned medium from confluent MG-63 human osteosarcoma cells was used as a chemoattractant (Virtanen et al. 2002). Cells were incubated for 48 h, after which insert membranes were fixed in methanol for 2 minutes and stained for 10 minutes with 0.2 % crystal violet in methanol. Then, membranes were cut out from the inserts and mounted with immersion oil. Invaded cells on the membranes were scanned by an Olympus BX51 scanner with Surveyor software and analyzed by automated image analysis. The results were verified by manual counting with ImageJ® software from 5 random fields or 200 cells of each membrane.

4.23 Gelatinase activity assay (II)

A gelatinase activity assay was performed with an InnoZyme™ gelatinase (MMP2/MMP9) fluorogenic activity assay kit (Merck) according to the manufacturer's instructions. Medium samples were collected from the upper chambers of invasion inserts after the invasion assays described above and used for the assay. Samples were incubated at + 37 °C for 3 h protected from light. Fluorescence measurements were analyzed by an Envision plate reader (Perkin Elmer) with an excitation wavelength of 320 nm and an emission wavelength of 405 nm.

4.24 Microarray analyses (II)

For microarray analyses, PC-3 cells with stable PIM1 overexpression were ectopically transfected with WT or MM NFATC1 expression vectors and compared to cells without stable PIM1 overexpression. On the following day, total RNA was extracted using TRIzol reagent (Invitrogen, Carlsbad, CA, USA) according to the manufacturer's protocol. The samples were then labeled and hybridized using Agilent whole genome oligo microarray platform on Human Gene Expression v2

4x44K Microarray slides (G4845A; Agilent Technologies, Palo Alto, CA, USA). An Agilent C-Scanner was used to scan the slides and the mRNA expression values were extracted using Agilent Feature Extraction software v. 11.0.1.1. The mRNA expression values were imported using the limma read.maimages function. Probes with low quality were filtered using the distribution of negative control probes as a reference. Only probes with expression values higher than the 90th percentile of negative control probes were retained for successive analysis. Expression values were log2 transformed, quantile normalized between samples and median aggregated at the gene symbol level using Agilent annotation. A limma-based approach (Ritchie et al. 2015) was applied to estimate the difference in average expression in each comparison. A fold-change cutoff (≥ 0.1) and p-value of (< 0.05) were used to determine differential gene expression.

4.25 Canonical pathway analysis (II)

IPA (Ingenuity Pathway Analysis, Ingenuity Systems) was used for functional enrichment and detection of pathways with significant alterations based on microarray gene expression. In canonical pathway analysis -log(p-values) over threshold 2.5 were considered significant.

4.26 Quantitative reverse transcription PCR (qRT–PCR) (II, III)

PIM, NFATC1, ITGA5 and *ERG* mRNA expression levels were determined from total RNAs isolated from PC-3 or VCaP cells according to the manufacturer's protocol. qRT–PCR was performed using random hexamer primers, Maxima reverse transcriptase, Maxima SYBR Green qPCR Master Mix (all from Thermo Fischer Scientific, Waltham, MA, USA) and the CFX96™ Real-Time PCR Detection System (Bio–Rad Laboratories, Inc. Hercules, CA, USA). The expression levels were measured from three biological and technical replicates and normalized against mRNA of the TATA-binding protein (*TBP*).

4.27 Gene correlation analyses (II, III)

Gene correlation analysis was performed within three different publicly available datasets. The Cancer Genome Atlas (TCGA) - Prostate adenocarcinoma RNA-seq data (Table 12) was used to determine the correlation between *ITGA5* and *NFATC1* mRNA expressions. Second, the Integrative Genomic Profiling of Human Prostate Cancer microarray data (Table 12) was used to assess correlations between ITGA5 and *PIM1* or *NFATC1* genes in clinical prostate cancer patient samples and correlations between all *PIM* genes and *ERG* or *MYC*. The Tampere PC RNA-seq dataset was used to determine correlations between *ITGA5* and *PIM1* or *NFATC1* genes in clinical prostate cancer patient samples and correlations between all *PIM* genes and *ERG* or *MYC* (Table 12).

Table 12. Publicly available datasets utilized in the study

Dataset	Explore	Reference	Used in publication
The Cancer Genome Atlas (TCGA) - Prostate adenocarcinoma RNA-seq data	To assess correlations between *ITGA5* and *NFATC1* genes in clinical prostate cancer patient samples	TCGA Research Network, 2015	II
Integrative Genomic Profiling of Human Prostate Cancer microarray data	To assess correlations between *ITGA5* and *PIM1* or *NFATC1* genes in clinical prostate cancer patient samples	Taylor et al. 2010	II
	To assess correlations between all PIM genes and *ERG* or *MYC*		III
Tampere PC RNA-seq cohort	To assess correlations between *ITGA5* and *PIM1* or *NFATC1* genes in clinical prostate cancer patient samples	Annala et al. 2015	II
	To assess correlations between all *PIM* genes and *ERG* or *MYC* .		III
RNA-seq dataset	To assess expression levels of *PIM1* and *NFATC1* mRNAs from PC-3, DU-145 and LNCaP cells.	Ylipää et al. 2015	II
TMPRSS2-ERG gene fusion dataset (GSM353647)	To investigate the binding sites of ERG in all *PIM* promoter areas with Integrative Genomics Viewer (IGV) version 2.5.0 to observe ERG ChIP-seq peaks compared to *PIM* regulatory regions in VCaP prostate cancer cells.	Yu et al. 2010	III

4.28 ChIP-seq analysis (III)

To investigate the binding sites of ERG in all *PIM* promoter areas Integrative Genomics Viewer (IGV) version 2.5.0 was used to observe ERG ChIP-seq peaks in a publicly available TMPRSS-ERG gene fusion dataset (Table 12) and they were compared to *PIM* regulatory regions in VCaP prostate cancer cells.

4.29 Statistical analyses (I, II, III)

Table 13. Statistical analysis used in the experiments

Statistical analysis	Used analysis of the experiment	Used in publication
one-way ANOVA variance analyses with LSD post hoc multiple comparison test		I
Grubbs' test, also called the extreme studentized deviate (ESD) method	To analyze possible outliers from the PIM-MYC gene correlation dataset. p-value of 0.05 was used as a cutoff for the significance of the outliers.	III
Kaplan–Meier survival analysis and the log-rank (Mantel-Cox) test	To estimate the progression-free (PSA-free) time (survival) between PIM stained IHC samples divided by their median expression into PIM low and PIM high expression groups.	III
Mann-Whitney U-test	RT-qPCR	II, III
	IHC protein expression levels were divided into three groups based on progression: (BPH, PCa, CRPC) and Gleason scores: low (scores <7), intermediate (scores equal to 7), and high (scores >7 (from 8 to 10)).	III
	Associations between all *PIM* gene expressions with *ERG*	III
Pearson's correlation coefficient	Gene correlation analyses	II, III
Unpaired two-sided t-test	FLIM	II
	Cell viability assay	I, II
	Luciferase transactivation assay	II
	Migration assay	I, II
	Cell invasion assay	II
	Gelatinase activity data	II
Wilcoxon matched pairs test	Cell invasion assay	II
	Gelatinase activity data	
Chi-square or Fisher's exact test	Associations between protein expression levels of PIM1/PIM2 or PIM3 and ERG	III

In publication I, statistical analyses were performed by one-way ANOVA with LSD post hoc multiple comparison tests (IBM SPSS Statistics 22, Chicago, Illinois, USA). Microsoft Excel data analysis tool t-test: Two-Sample Assuming Unequal Variances was used in the supplementary assays and the graphs were produced by Microsoft Excel. All the statistical analyses and graphs used in publications II and III were performed using GraphPad Prism version 5.02 (GraphPad Software Inc, La Jolla, CA, USA).

P-values < 0.05 (*), p-values < 0.01 (**) and p-values < 0.001 (***) were considered statistically significant. Error bars represent standard deviation (SD), or min to max range values in each graph.

5 RESULTS

5.1 PIM upregulation induces prostate cancer progression (I, III)

5.1.1 Upregulation of PIM3 enhances tumor growth *in vivo*

To test the tumorigenic potential of PIM3 overexpression *in vivo*, a PC-3 prostate cancer cell line stably overexpressing human PIM3 or a control vector along with the fluorescent follow-up marker Tomato was inoculated subcutaneously into athymic nude male mice. Progression of the tumors was followed for approximately three weeks, and tumor volumes were measured by manual palpation and fluorescence-based imaging. Based on the analysis, xenografts overexpressing PIM3 had increased tumor volumes compared to the control-transfected cells. (I: Figure 1A-B). The results from manually determined tumor sizes correlated with those of fluorescence-based imaging (I: Supplementary Figure S1A). IHC staining with phospho-histone H3 antibody used for mitotic cell analysis was performed to determine the growth properties of the tumors. Consistent with the tumor volumes, the proportion of mitotic cells was higher in the PIM3-overexpressing tumors than in the controls (I: Figure 1C, Supplementary Figure S1B). Whole tumor scanning by the Pannoramic 250 slide scanner indicated that PIM3-overexpressing PC-3 cells formed larger tumors than control cells (I: Supplementary Figure S1C). Overexpression of PIM3 remained stable during the whole follow-up period of the animals, as measured by Western blotting (I: Supplementary Figure S1D). Collectively, these results confirmed the hypothesis that PIM3 supports the prostate tumorigenic potential.

5.1.2 Stable upregulation of PIM3 induces the formation of prostate cancer metastasis *in vivo*

Subcutaneous xenografts did not form metastases; hence, studies were continued with an orthotopic prostate cancer model, which has been shown to better support metastatic growth (Stephenson et al. 1992). Preliminary orthotopic inoculations of control or PIM3-overexpressing PC-3 cells into the prostates of nude male mice were conducted. The growth of the tumors was assessed for three weeks, after which tumor volumes were analyzed, and selected organs were utilized for IHC staining. As no significant changes in tumor volumes were observed, mitotic potential was analyzed, and the numbers of mitotic cells were assessed in PIM3-overexpressing tumors, from which nearly two-fold increase of mitotic cells was detected compared to control tumors (I: Figure 1D). According to our results, control cells invaded prostate-draining lymph nodes but did not further invade more distant organs. These observations were supported by former findings on the inability of parental PC-3 cells to form distant metastases (Tuomela et al. 2008, Tuomela et al. 2009). Strikingly, PIM3-overexpressing cells also invaded the lungs (I: Figure 1E). These results indicate that PIM3 upregulation promotes the metastatic potential of prostate cancer *in vivo*.

5.1.3 *PIM1* and *PIM3* genes are upregulated in prostate cancer

The RNA-seq-based gene expression Tampere prostate cancer (PC) dataset (Annala et al. 2015) and a microarray dataset (Taylor et al. 2010) of prostate cancer patient samples were used to study the expression of all *PIM* family members in prostate cancer. In the Tampere PC dataset, the overall expression of *PIM3* was the highest, and *PIM2* expression was the lowest (III: Supplementary Figure S2A). Similar results were observed in the microarray dataset (III: Supplementary Figure S2B). Transcriptional expression levels of the tumor samples were also analyzed based on pathological stage (BPH, PCa and CRPC). In the Tampere PC dataset, *PIM1* and *PIM3* but not *PIM2* gene expression increased significantly in prostate cancer compared to BPH patient samples (III: Figure 1A-C and Figure 12A-C). Primary tumors were also categorized according to Gleason scores (GS<7, GS=7 and GS>7), and a minor increase was assessed for *PIM2* in samples with Gleason scores >7 when samples were compared to lower Gleason score samples (III: Figure 1E and Figure 12E). However, *PIM1* or *PIM3* expression levels were not associated with

Gleason scores (III: Figure 1D and F and Figure 12D and F). The microarray dataset from Taylor and others provided parallel results with the Tampere PC cohort but remained statistically non-significant (III: Supplementary Figure S3).

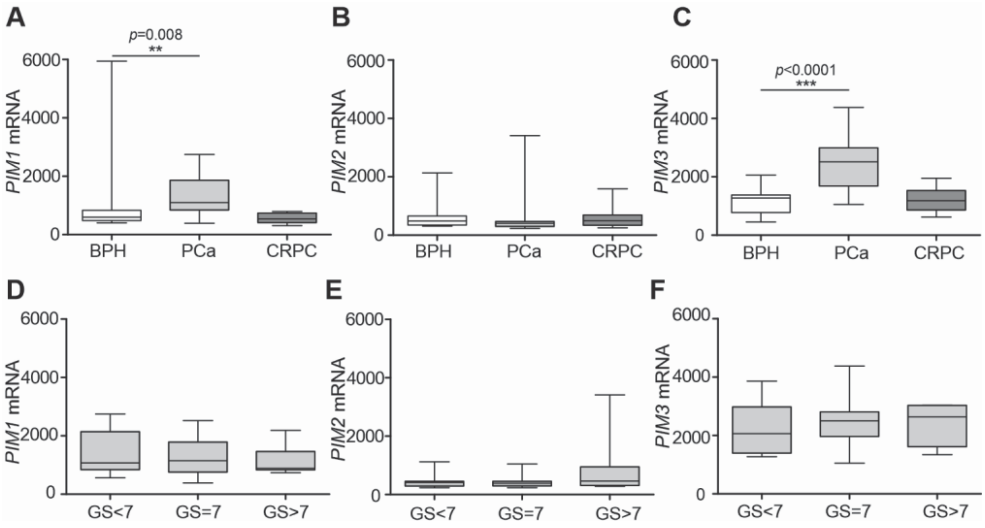

Figure 12. *PIM1* and *PIM3* expression levels are elevated in primary prostate cancer.

PIM1 (**A**, **D**), *PIM2* (**B**, **E**), and *PIM3* (**C**, **F**) mRNA expression levels were determined by the Tampere PC sequencing dataset. The results were categorized into BPH (n = 12), primary prostate cancer (PCa) (n = 30), and CRPC (n = 13) samples (**A**–**C**). Primary PCa samples were further divided based on Gleason scores GS<7 (n = 7), GS = 7 (n = 7), and GS>7 (n = 15) (**D**–**F**). (Modified from Publication III: Figure 1, Creative Commons, Attribution license, (CC-BY)).

5.1.4 PIM protein levels are elevated during prostate cancer progression

To further evaluate the expression of all PIM proteins in prostate cancer patient data, we used a sample cohort of 23 benign adjacent tissue samples from primary prostate cancer samples, 186 primary prostate cancer samples and 45 CRPC samples. Samples were analyzed by IHC staining, and our results revealed significantly upregulated protein levels for all three PIM kinases in primary prostate cancer compared to benign prostate samples (III: Figure 2A-C and Figure 13A-C). We compared the PIM expression levels with progression-free survival, but no association was observed (III: Supplementary Figure S4A-C). Similar to the primary prostate cancer sample cohort of PIM mRNA, PIM protein expression data were categorized into different Gleason score groups. Indeed, PIM1 protein expression with Gleason scores >7 indicated a significant increase compared to samples with Gleason scores

<7 (III: Figure 2D and Figure 13D). However, PIM2 and PIM3 protein expression levels were not different between the different Gleason score groups (III: Figure 2E-F and Figure 13E-F). The expression levels of both PIM1 and PIM2 were significantly higher in CRPC samples than in primary prostate cancer patient samples (III: Figure 2A-B and Figure 13A-B). Moreover, the expression level of PIM3 was significantly higher in both primary prostate cancer and CRPC samples compared to BPH samples (III: Figure 2C and Figure 13C). Altogether, our data indicate that the expression of all PIM kinases, especially PIM1 and PIM2, increases during prostate cancer progression.

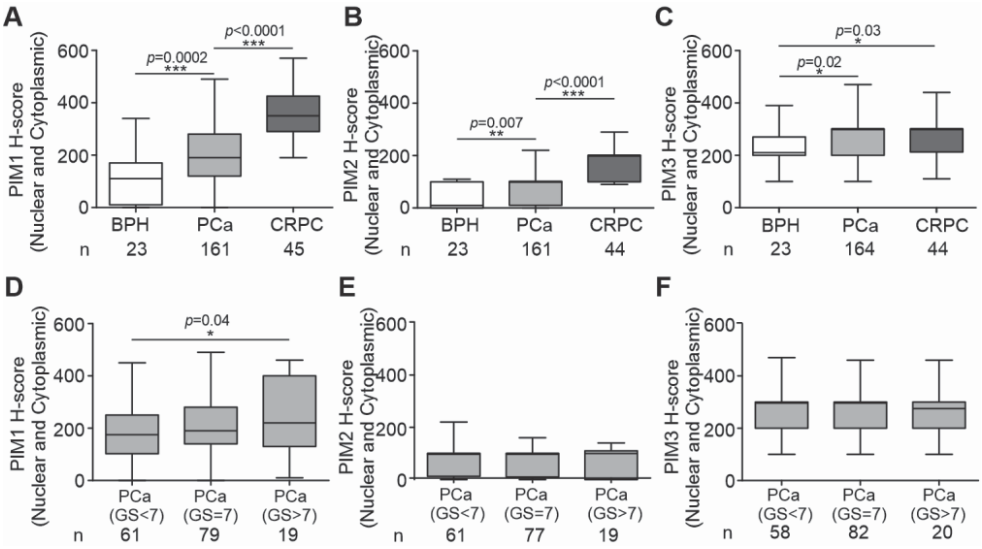

Figure 13. PIM protein expression levels are induced during prostate cancer progression.

IHC staining was performed for FFPE TMA samples of 23 benign prostate, 186 primary prostate cancer, and 45 CRPC samples, which were stained with PIM1 (**A**), PIM2 (**B**), and PIM3 (**C**) antibodies. Boxplots representing IHC staining results by combined Histoscore numbers of nuclear and cytoplasmic staining of the samples. Primary prostate cancer samples were categorized by Gleason scores (GS<7, GS = 7, and GS>7) and PIM1 (**D**), PIM2 (**E**), and PIM3 (**F**) protein expression levels. (Modified from III: Figure 2, Creative Commons, Attribution license, (CC-BY)).

5.2 PIM upregulation promotes, and PIM inhibitors repress the formation of prostate cancer metastasis (I)

5.2.1 PIM1 and PIM3 promote cell migration, while PIM inhibitors decrease the effect

To study the effects of PIM1 and PIM3 on cell viability and migration, we utilized overexpression and PIM inhibitor assays in cultured prostate cancer cells. The cell migration of PC-3 cells overexpressing either PIM1 or PIM3 was studied by wound healing assays. Cells were also treated with previously validated small molecule PIM inhibitors, the pan-PIM inhibitor DHPCC-9 (Akué-Gédu et al. 2009) or BA-1a, which targets PIM1 and PIM3 more efficiently than PIM2 (Kiriazis et al. 2013). The results indicated that stable overexpression of both PIM1 and PIM3 significantly increases the migration of PC-3 cells in wound healing assays, while PIM inhibitors impair migration (I: Supplementary Figure S2A-B).

Cell viability was studied with stable PIM1- and PIM3-overexpressing cell lines, where no significant effects of either PIM1 or PIM3 overexpression were observed (I: Supplementary Figure S2C and Figure 14). However, both PIM inhibitors reduced cell viability, especially at the later time point (I: Supplementary Figure S2C and Figure 14). These results indicated the impact of PIM kinase activity in promoting both cell motility and cell survival.

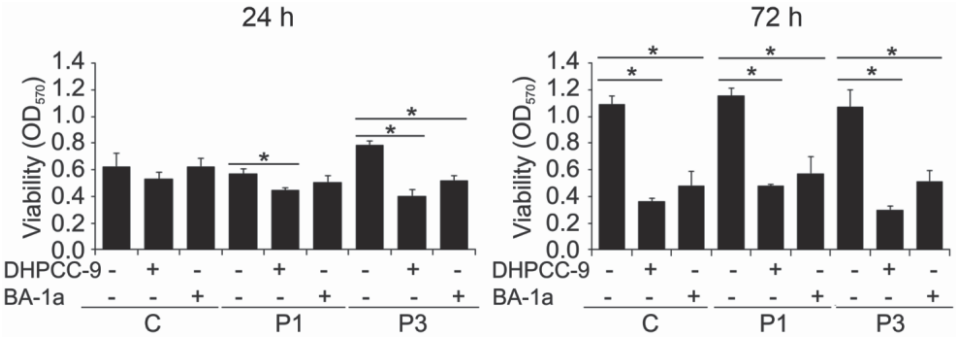

Figure 14. DHPCC-9 and BA-1a PIM inhibitors decrease viability of stable PIM-overexpressing PC-3 cells.

Cell viability assay from stable PIM1 and PIM3 overexpressing cells treated with DHPCC-9, BA-1a, or control vehicles in 24-hour and 72-hour time points (modified from Publication I: Figure S2C, Creative Commons, Attribution license, (CC-BY)).

5.2.2 PIM inhibitors DHPCC-9 and BA-1a are nontoxic *in vivo*

Before starting *in vivo* experiments, the toxicity of the compounds was tested. First, zebrafish embryos were treated with the PIM inhibitors DHPCC-9 and BA-1a from 6 to 50 hours post fertilization. Neither inhibitor, caused major impairment in the survival, body size or structure of the embryos, while a cytotoxic control compound, BA-2c, inhibitor decreased their survival and caused major developmental defects (I: Supplementary Table S1, Supplementary Figure S3A-B). However, slight changes in body curvature were detected after DHPCC-9 treatment, which also caused enlargement of the pericardiac sac (I: Supplementary Figure S3C-D), indicating a possible role for PIM kinase activity during the development of zebrafish embryos.

Thereafter, PIM inhibitors were tested intraperitoneally in both male and female mice. The DHPCC-9 inhibitor diluted in 20 µl of DMSO was tested in two male mice, first at 100 mg/kg for two days and then 50 mg/kg for eight additional days. During this time, no signs of toxicity were detected (I: Supplementary Figure S4A). The BA-1a inhibitor was first tested in two female mice at 25 mg/kg dissolved in 25 µl of DMA. However, 25 µl of DMA caused irritation in the injection area and restless behavior as well as a slight reduction in body weight (I: Supplementary Figure S4B). Therefore, the amount of DMA was reduced, and a second toxicity test was performed including control mice without treatment, with vehicle only, at 10 and 20 mg/kg of BA-1a inhibitor diluted in 10 µl of DMA for 17 days. The results showed no side effects nor changes in body weight (I: Supplementary Figure S4C).

5.2.3 PIM inhibition by DHPCC-9 prevents PIM-induced metastatic growth of prostate cancer cells

After confirmation of no severe side effects, these compounds were utilized in the orthotopic prostate cancer model to determine their possible impact on prostate cancer progression and the formation of metastasis. For this purpose, PIM1- and PIM3-overexpressing PC-3 prostate cancer cells were inoculated into the prostates of athymic nude mice. Mice with both PIM1 and PIM3 overexpression developed significantly larger tumors than control mice (I: Figure 2A and 2D). Mice with stable PIM3 overexpression were treated daily with 50 mg/ml DHPCC-9 in DMSO or 20 mg/kg BA-1a in DMA or with vehicle DMSO or DMA only. The health of the mice was followed daily by observing weight gain and behavioral differences, and no

effects related to inhibitor treatments were shown (Supplementary Figure S5). The results indicated that DHPCC-9 significantly decreased the tumor volumes of PIM3-overexpressing tumors (I: Figure 2B and 2D). However, no reduction in tumor size was detected with the BA-1a inhibitor (I: Figure 2C-D). Tumor volumes correlated with fluorescence-based imaging and manual evaluation of the samples (I: Supplementary Figure S6A). IHC staining analyses were also performed for the collected tumors and assessed by phospho-histone H3 staining. The number of mitotic cells was higher in PIM3-overexpressing tumors than in DHPCC-9-treated PIM3-overexpressing tumors (I: Figure 2E).

In addition to the actual tumors, other organs were collected for further analyses. Strikingly, metastases were found not only in the prostate-draining lymph nodes but also in the lungs of PIM1- and PIM3-overexpressing mice. In contrast, only lymph node metastases but no lung metastases were found in control cell-inoculated mice (I: Figure 3A). The PIM inhibitor DHPCC-9 diminished the percentage of metastases both in lymph nodes and in lungs (I: Figure 3B-C, and Supplementary Figure S6B). However, the sizes of necrotic areas were not connected to PIM activities between the metastases (I: Supplementary Figure S6B). Stable PIM1 and PIM3 overexpression of the tumors and metastases was ensured by IHC analysis with V5 antibody, as V5 was used as a tag in the expression vector (I: Supplementary Figure S7). These results indicated that PIM1 and PIM3 induce metastatic growth of prostate cancer, while PIM inhibition by DHPCC-9 impairs this effect.

5.2.4 PIM upregulation promotes vascularization of prostate xenografts

Vasculature assessments were performed to further analyze the formation of metastases. Vasculature was stained from the orthotopic xenografts by specific antibodies to blood vessels (anti-CD-32 ab) and lymphatic vessels (anti-m-LYVE1). The results demonstrated significantly increased amounts of blood vessels in both PIM1- and PIM3-overexpressing tumors. After treatment of PIM3 overexpressing orthotopic xenografts with DHPCC-9, blood vessel formation decreased significantly (I: Figure 4A and C). A similar increase in the number of lymphatic vessels was not established in PIM1- or PIM3-upregulated tumors, but treatment with DHPCC-9 resulted in a major reduction in lymphatic vessel formation (I: Figure 4B and D). Taken together, the increase in vascularization promoted by PIM kinase activity may account for the enhancement of metastatic activity.

5.2.5 PIM-upregulation leading to the formation of metastasis may be supported by CXCR4

The CXCL12 ligand and its receptor CXCR4 enhance the adhesion of tumor cells to extracellular matrix components and endothelial cells and thereby increase tumor aggressiveness. Previous studies have shown that the CXCR4/CXCL12 chemokine pathway influences the migration and invasion of cancer cells, including prostate cancer cells (Kukreja et al. 2005). PIM1 phosphorylates CXCR4, causing enhanced expression of CXCR4 on the cell surface (Grundler et al. 2009). CXCR4 phosphorylation analysis was therefore performed both in the stable and ectopically PIM1- and PIM3-transfected cells as well as in parental PC-3 cells. Overexpression of PIM1 and PIM3 enhanced the phosphorylation of CXCR4, while the PIM inhibitor DHPCC-9 diminished CXCR4 phosphorylation (I: Figure 5A-B, Supplementary Figure S8). An *in vitro* kinase assay also confirmed that human PIM1 and murine Pim3 but not human PIM2 directly phosphorylate CXCR4 (I: Figure 5C). The localization and signal intensity of phosphorylated CXCR4 were analyzed in stable PIM1- and PIM3-overexpressing PC-3 cells and in control cells. In all of them, positive phosphorylation was detected on the cell membranes. After treatment with DHPCC-9, the phosphorylation intensity of CXCR4 was significantly weaker, and the signal was fragmented (I: Figure 5D-E). After DHPCC-9 treatment, the nuclear CXCR4 signal was also slightly increased compared to that of control-treated cells (I: Figure 5E). IHC analyses were also performed to analyze phosphorylation in orthotopic xenografts. The results demonstrated that PIM1- and PIM3-upregulated tumors had increased levels of CXCR4 phosphorylation compared to control tumors. Moreover, DHPCC-9 diminished the phosphorylation of CXCR4 (I: Figure 5F).

5.3 Prostate cancer cell motility is reduced after prevention of PIM1-targeted phosphorylation of NFATC1 (II)

5.3.1 NFATC1 is constitutively active in PC-3 prostate cancer cells

To determine the expression status and activation of NFATC1 in prostate cancer cells, expression, transactivation, and localization studies were performed. First, the basal expression and transcriptional activity of NFATC1 were analyzed in PC-3 cells,

from which both endogenously expressed and ectopically transfected NFATC1 proteins were detected by Western blotting (II: Figure 1A). NFAT-dependent transcriptional activity assays indicated endogenous NFAT activity in PC-3 cells, which was detected by luciferase assays. PC-3 cells with a luciferase reporter with WT NFAT binding sites showed stronger transcriptional activity when compared to activity of a reporter with mutated (M) NFAT binding sites (II: Figure 1B). Transcriptional activity was further enhanced by ectopic upregulation of NFATC1, but surprisingly, stimulation of cells with TPA and the calcium ionophore ionomycin (IM) resulted in no major increase in activity (II: Figure 1C). With ectopic overexpression of WT or mutant NFATC1 proteins (Table 11), the intracellular localization of NFATC1 in PC-3 cells was determined. The constitutively active (mSRR) mutant, in which 11 regulatory serines are mutated into non-phosphorylatable alanines, was detected only in the nucleus. On the contrary, the dominant negative (DN) mutant, which lacks the NFAT regulatory domain, was located nearly 80% of the times in the cytoplasm. However, WT protein with intact phosphorylation sites could be detected in more than 60% of the times in both cellular compartments (II: Figure 1D, Additional Figure S1A). These findings indicated that WT NFATC1 can shuttle between the compartments of PC-3 cells. Wound healing assays were performed to compare the effects of NFATC1 WT and mSRR on cell motility, and both of them improved cell migration compared with control cells (II: Figure 1E). In cell viability assays, constitutively active mSRR mutant caused significant increase in cell viability compared to control cells and WT NFAC1 expressing cells (II: Additional Figure S1B).

5.3.2 NFATC1 is phosphorylated by PIM kinases at several amino acid residues

To identify the PIM target sites in NFATC1, a mass spectrometry-based analysis was performed with PC-3 prostate cancer cells. Together, eight phosphopeptides were found in the PC-3-derived cell samples. Based on the *in vitro* analysis, two other phosphopeptides were also found and considered likely PIM1-targeted phosphorylation sites (II: Figure 2A and Additional Table S3, Figure 15). As more phosphorylation sites were found from the prostate cancer cell-derived mass spectrometry analysis compared to *in vitro* target sites, it seemed likely that some sites were targeted by other kinases. The functional impact of different PIM1 phosphorylation sites was analyzed by making mutant versions of NFATC1 from

which different putative PIM-targeted serine and threonine residues were mutated into alanines (Figure 15) (II: Table 1 and Additional Table S3).

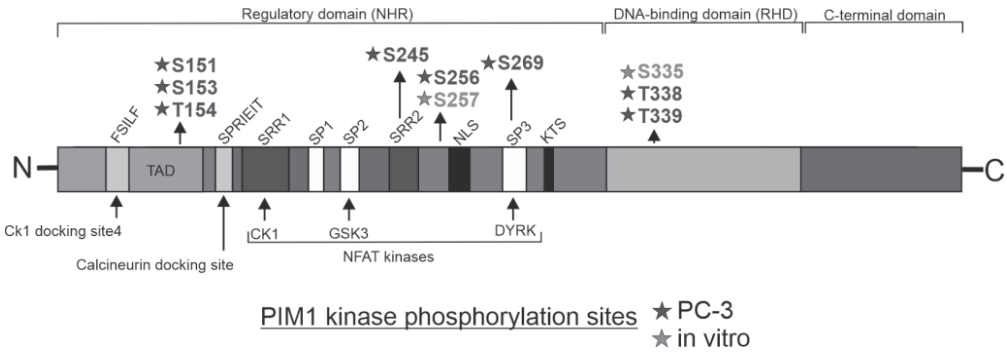

Figure 15. PIM1 phosphorylation sites in NFATC1 protein

PIM1 phosphorylation sites in NFATC1 containing serine and threonine amino acids were detected *in vivo* in PC-3 prostate cancer cells (dark gray stars) and *in vitro* kinase assays (light gray stars) (modified from publication II: Figure 2A).

Double mutant (DM) NFATC1, in which two amino acid residues, Ser245 and Ser265, were mutated, demonstrated only an approximately 50 % phosphorylation efficacy compared to WT NFATC1. Moreover, MM NFATC1, in which all the detected PIM1 phosphorylation sites were mutated, demonstrated an approximately 90 % reduction in phosphorylation capacity (II: Figure 2B). The PIM inhibitor DHPCC-9 prevented both autophosphorylation of PIM1 and PIM1-mediated phosphorylation of NFATC1 (II: Figure 2B). In addition to PIM1, WT NFATC1 was also phosphorylated by PIM2 and PIM3; however, they were unable to phosphorylate NFATC1 mutated at multiple sites (MM) *in vitro* (II: Figure 2C). These results indicated that the identified PIM1 phosphorylation sites of NFATC1 are substantial for NFATC1 phosphorylation.

The identified phosphorylation sites were then mutated in different combinations to produce DM, TM and MM NFATC1. The results indicated that mutations of S245 and S269 phosphosites did not have a significant impact on cell migration, as supported by data on TM NFATC1, which had intact serines 245 and 269 but prevented cell migration, similar to MM with mutated serines. This result indicates that the pro-migratory effects of NFATC1 are mostly dependent on the phosphorylation of other PIM1 target sites (S151, S153, T154, S256, S257, S335, S338 and T339) (II: Additional Figure 3D).

5.3.3 NFATC1 physically interacts with PIM1 in PC-3 cells

After mutation of the PIM1 phosphorylation sites in NFATC1, the effect on physical interaction between these proteins was assessed. The hypothesis was that the PIM1-NFATC1 interaction could be disturbed by preventing PIM1 phosphorylation. Immunofluorescence analysis revealed that no effects on subcellular localization were observed after elimination of PIM1 target sites (II: Figure 3A, Additional Figure S1C). Colocalization and physical interaction of PIM1 and NFATC1 were analyzed by confocal microscopy and fluorescence-lifetime imaging (FLIM). FLIM is a key fluorescence microscopy technique to map interaction of proteins through Förster or fluorescence resonance energy transfer (FRET) process (Förster 1948). If two proteins tagged with fluorescent probes are physically interacting with each other, a donor chromophore, in its electronic excited state, may transfer energy to an acceptor chromophore and excite it. Therefore, emission wavelength of the acceptor excitation wavelength must be overlapping. The transfer or loss of energy of the donor chromophore decreases its fluorescent lifetime. Both WT and MM NFATC1 showed nuclear colocalization with PIM1 as assessed by merged confocal images (II: Figure 3B). The interaction of WT and MM NFATC1 together with PIM1 was evident from the reduced lifetimes of GFP signals (II: Figure 3C). Moreover, the PIM inhibitor DHPCC-9 had no major effects on the localizations or interactions (II: Figure 3B-C). No disruption of interactions between NFATC1 and PIM1 was detected by interaction assays even after mutation of the PIM1 phosphosites. These results indicated that NFATC1 and PIM1 could interact even if the phosphorylation reaction was prevented.

5.3.4 NFATC1 mutation reduces its transactivation ability

The effects of PIM-dependent phosphorylation on NFAT transcriptional activity were assessed in three different prostate cancer cell lines: in androgen-insensitive PC-3 and DU-145 cells and androgen-sensitive LNCaP cells. In these cell lines, the highest *PIM1* gene expression was detected in PC-3 cells, and the expression was lower in DU-145 cells and lowest in LNCaP cells (Figure 16). *NFATC1* was not highly expressed in any of these three cell lines based on our previously published RNA-seq dataset (Ylipää et al. 2015) (II: Figure 1A and 4A). Luciferase assays indicated that PC-3 cells had higher NFAT activity than DU-145 cells. However, in contrast to PC-3 cells, NFAT activity in DU-145 cells was increased after stimulation by TPA and calcium ionophore ionomycin (II: Figure 4B, Additional Figure S4A).

Cyclosporine was used to prevent NFAT activity, which however was diminished only in stimulated DU-145 cells (II: Figure 4C, Additional Figure S4B). Ectopically upregulated WT NFATC1 enhanced NFAT activity in all three cell lines. Phosphomutant NFATC1 targeted by PIM1 phosphorylation sites, or alternatively inhibition of PIM activity by DHPCC-9 treatment, disrupted NFAT activity in PC-3 and DU-145 cells but not in LNCaP cells (II: Figure 4B, Additional Figure S4). Altogether, these data suggested that in PC-3 and DU145 cells, the activity of NFATC1 is reliant on the phosphorylation of PIM target sites. However, in LNCaP cells, NFATC1 activation is PIM-independent, as only low *PIM* mRNA levels were observed in these cells (II: Figure 4A).

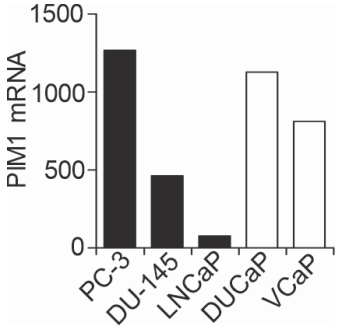

Figure 16. Relative *PIM1* mRNA expression in different prostate cancer cell lines.

Relative *PIM1* mRNA expression in PC-3, DU-145, LNCaP that were used in the studies and additionally also expression levels in DuCaP, and VCaP prostate cancer cells (modified from Publication II: Figure 4, Creative Commons, Attribution license, (CC-BY)).

NFATC1 nuclear translocation and activation is usually strongly regulated in a calcium- and calcineurin-dependent fashion (Rao et al. 1997, Müller & Rao 2010). However, our results indicated that stimulation of calcium signaling with TPA and IM had no effect on NFATC1 activity in PC-3 and LNCaP prostate cancer cells. Indeed, dysregulation of the calcium–NFAT signaling pathway has been observed in several cancer types, including hematological malignancies, breast cancer and pancreatic adenocarcinomas (Müller & Rao 2010). Hence, there might also be calcium signaling dysregulation in PC-3 and LNCaP cells. However, another prostate cancer cell line, DU-145 was affected by calcium channel activation (II: Figure 4B, Additional Figure S4A). These results suggest that nuclear translocation and activation of NFAT are normally regulated by calcium and calcineurin in DU-145 cells unlike in PC-3 and LNCaP cells. Taken together, these results indicated that phosphorylation sites of PIM1 are important for NFATC1 transcriptional activation.

5.3.5 Prevention of PIM-targeted phosphorylation of NFATC1 decreases prostate cancer cell migration and invasion

Santio and colleagues showed previously that inhibition of PIM blocks the migration of NFATC1 in PC-3 prostate cancer cells. The roles of PIM1-targeted phosphorylation sites of NFATC1 for cell motility were analyzed in PC-3 and DU-145 cells. Wound healing assays demonstrated that mutations in the PIM target sites or inhibition of PIM1 by the PIM inhibitor DHPCC-9 significantly impaired the ability of NFATC1 to promote cell migration (II: Figure 5A-B). The effects of different phosphosites were also determined by comparing the migration of WT, DM and MM NFATC1 in PC-3 cells. The results indicated that MM contains substantial phosphosites for cell motility when compared to WT and DM NFATC1 (II: Figure 5A). Equivalent protein levels of NFATC1 and PIM family members were confirmed by Western blotting in wound healing samples of PC-3 cells (II: Additional Figure S3A). The PIM inhibitor DHPCC-9 did not have significant effects on cell viability even though it slightly decreased the amount of proteins (II: Additional Figure S3A-B). Cell viability and protein expression analyses were performed similarly to DU-145 cells where a decrease in cell viability was observed after DHPCC-9 treatment, but it was not statistically significant (II: Additional Figure S3C). Additionally, mitomycin C was used to exclude the effects of cell proliferation on cell migration in wound healing assays in PC-3 cells (II: Additional Figure S3D); nevertheless, similar results were obtained as in the previous experiments without mitomycin C (II: Figure 5A). Strikingly, TM NFATC1 with intact S245 and S269 phosphosites prevented cell migration, similar to MM NFATC1 which lacked these sites.

The role of NFATC1 phosphorylation in cell invasion was also investigated. PC-3 cells transiently transfected with WT NFATC1 exhibited enhanced invasion, while it was decreased when PIM target sites were mutated in MM NFATC1 or cells were treated with DHPCC-9 (II: Figure 6A). In the invasion experiments, NFATC1 protein levels were examined by Western blotting (II: Additional Figure S3E). No significant alterations were observed in the viability of the cells. However, MM NFATC1 cell viability was slightly increased after 72 hours (II: Additional Figure S3F). Since the activities of MMPs, such as MMP2 and MMP9, take part in the initiation of cell invasion and because their expression may be regulated through the activity of NFAT in prostate cancer (Macini & Toker 2009), the effects of NFATC1 phosphorylation on the expression of MMPs were assessed by gelatinase activity

assays. After mutation of PIM phosphosites in NFATC1, the relative MMP expression levels decreased, although the decrease was not significant. However, the reduction in MMP activities was more remarkable with the PIM inhibitor DHPCC-9 (II: Figure 6B). Altogether, MMP enzymatic activities correlated with our results from the invasion assays, suggesting that MMPs are relevant NFATC1 targets, whose activities can be indirectly regulated through phosphorylation by PIM kinases.

5.3.6 ITGA5 is a putative target for PIM1-phosphorylated NFATC1

Microarray experiments were designed to identify additional targets of PIM1 and NFATC1. Upregulation of *PIM1* and/or *NFATC1* genes in PC-3 cells was first confirmed by RT qPCR (II: Additional Figure S4A-B). Microarray analyses of parental PC-3 cells was compared to their PIM1 expressing derivatives, to identify genes that were up- or down-regulated as a result of stable PIM1 overexpression. Moreover, to identify genes that are regulated by the levels of NFATC1 activity, PC-3 cells transiently overexpressing WT or MM NFATC1 were compared. Finally, to discover genes regulated by PIM1-dependent phosphorylation of NFATC1, PIM1, and PC-3 cells with upregulated WT or MM NFATC1 were compared. Altered gene expression profiles of the comparisons are listed in Additional Table S4: II.

Gene clustering analyses indicated different expression profiles for PC-3 cells overexpressing both PIM1 and WT NFATC1 when compared to the other samples (II: Additional Figure S4C). PC-3 cells with stable PIM1 and ectopic WT NFATC1 overexpression induced the expression of multiple genes, while the expression of these same genes was reduced in cells with stable PIM1 but ectopic MM NFATC1 upregulation (II: Figure 7A and Additional Table S4). Moreover, the same genes were expressed at lower levels in the other control samples (II: Additional Figure S4C). A canonical pathway analysis was performed for the detected gene expression profiles to assess those cellular functions that are influenced by the PIM1-dependent phosphorylation of NFATC1. Altogether, five pathways were significantly enriched, many of which regulate cell adhesion and motility-related functions, including integrin, paxillin and FAK signaling pathways (II: Additional Figure S5).

For validation of microarray data, integrin alpha 5 (ITGA5) was selected for gene expression analyses. Based on previous publications, ITGA5 is a potent target of NFATC1 in prostate cancer as it is involved in the cancer cell invasion process by regulating cell adhesion to matrices such as fibronectin (Desgrosellier & Cheresh

2010, Cai et al. 2018). Previously, PIM inhibition has also been associated with decreased adhesion to fibronectin (Santio et al. 2016). The gene expression levels of *ITGA5* were compared in one independent dataset (24 h after transfections) and in microarray samples (48 h after transfections). The expression of ITGA5 decreased in PC-3 cells ectopically expressing MM NFATC1, where PIM1-targeted phosphorylation was prevented compared to control cells or cells with WT NFATC1 upregulation (II: Figure 7B). These differences correlated with the results of MMP enzymatic activities experiments (II: Figure 6B), indicating that PIM1-mediated phosphorylation and activation of NFATC1 are involved in regulating *ITGA5* gene expression levels.

Three independent patient-derived datasets (Annala et al. 2015, Taylor et al. 2010 and TCGA Research Network, 2015) were utilized to examine the correlation between *PIM1* or *NFATC1* and *ITGA5* gene expression in prostate cancer. Pairwise comparisons of the expression levels of these genes were performed, and *PIM1* and *ITGA5* as well as *NFATC1* and *ITGA5* were positively correlated in these datasets (II: Additional Figure S6). Strikingly, the positive correlation between *NFATC1* and *ITGA5* expression was enhanced together with the Gleason score, and the strongest correlation was detected within prostate cancer patients with Gleason ≥8.

5.4 PIM kinases cooperate with ERG in prostate cancer (III)

5.4.1 PIM kinases associate with ERG oncogenes in prostate cancer

PIM associations were first assessed with *ERG* at the transcriptional level in primary tumors. However, *PIM1* and *ERG* had no significant association at the transcriptional level in our Tampere PC dataset (III: Figure 4A); moreover, the association between PIM2 and ERG was significantly negative (III: Figure 4B). Strikingly, the association between *PIM3* and *ERG* was significantly positive (III: Figure 4C). In contrast, in the larger Taylor et al. dataset, *ERG* expression was positively associated with *PIM1* but not with *PIM2* or *PIM3* gene expression in primary untreated prostate cancer samples (III: Supplementary Figure S6A-C).

Associations between PIM and ERG were also investigated at the protein level. In our cohort, all PIM family members demonstrated a positive association with ERG in prostate cancer patient samples based on IHC staining results. Higher PIM1

expression in the nuclei, cytoplasm or both nuclei and cytoplasm was associated with ERG positivity (Figure 5A). Elevated PIM2 expression in both the cytoplasm and nuclei was associated with the expression of ERG (III: Figure 5B). Moreover, upregulated PIM3 expression in the cytoplasm and combined expression in the cytoplasm and nuclei were associated with ERG expression (III: Figure 5C), while for nuclear PIM2 and PIM3 expression, no association was detected with ERG positivity (III: Figure 5B, C). In summary, these results at both the mRNA and protein level demonstrate that higher expression levels of all PIM family members are associated with ERG positivity in prostate cancer.

5.4.2 *PIM* gene expression is regulated by the *ERG* oncogene

The associations between the expression of ERG oncoprotein and PIM kinases prompted us to examine the nature of the possible interaction between them. Previously, Magistroni and others demonstrated that the TMRSS2:ERG fusion protein directly binds to the *PIM1* promoter, permitting ERG-mediated regulation of PIM1 expression in benign RWPE-1 prostate cells. We utilized a public ERG ChIP-seq cohort from VCaP prostate cancer cells (Yu et al. 2010) to examine the potential ERG binding sites at the *PIM1*, *PIM2* and *PIM3* loci. As expected, our analysis exposed several ERG binding sites at the *PIM1* promoter but more interestingly also at the *PIM2* and *PIM3* promoter regions (III: Figure 6A-C).

qRT–PCR assays were performed to examine the role of ERG in the transcriptional regulation of *PIM* genes by silencing ERG with siRNA (siERG) in VCaP prostate cancer cells. The results indicated significant transcriptional downregulation of all *PIM* mRNAs in ERG-silenced samples compared to control samples transfected with scrambled negative control (NC) siRNA (III: Figure 6D). Furthermore, PIM downregulation was also examined at the protein level in immunoblotted samples (III: Figure 6E). In summary, these results indicate that not only the expression of PIM1 but also PIM2 and PIM3 is regulated in an ERG-dependent manner.

5.4.3 Expression of PIM and MYC oncogenes is correlated in prostate cancer (III)

PIM1 kinase cooperates with the MYC oncoprotein to induce advanced prostate cancer (Wang et al. 2012). Correlation analyses were performed to investigate the possible associations between the expression of different *PIM* family genes and the *MYC* oncogene. Correlations were observed between *PIM1* (III: Figure 3A), *PIM2* (III: Figure 3B) or *PIM3* (III: Figure 3C) and *MYC* gene expression in the Taylor et al. microarray dataset. Moreover, the correlation of *PIM3* and *MYC* was verified in our Tampere PC cohort, but it was not observed for *PIM1* or *PIM2* and *MYC* (III: Supplementary Figure S5A-C). Altogether, these data suggest that not only *PIM1*, but also *PIM3* may cooperate with *MYC* to promote prostate tumorigenesis.

6 DISCUSSION

The role of PIM kinases in the development of multiple cancers, including prostate cancer has been broadly investigated. Several studies have demonstrated the efficiency of PIM overexpression to enhance tumor progression even though other often more robust oncogenes or oncogenic pathways affect the process in parallel or with overlapping activities. PIM kinases affect their targets through phosphorylation, and various PIM substrates have been identified over the past few decades such as NFATC1 (Rainio et al. 2002), BAD (Aho et al. 2004), and AR (Ha et al. 2013, Linn et al. 2012). Some phosphotargets have been shown to have strong roles in cancer progression while others are still under investigations and continuously provide new information on the PIM kinase pathway.

Gene mutations and amplifications are the most common cancer driving factors. However, it seems that these gene alterations do not commonly play a role in dysregulated expression of PIM kinases. Enhancement of the expression levels happens mainly at the transcriptional and protein stabilization level, and increased expression promotes tumor progression. In hematological malignancies, PIM expression can be induced by several cytokines, growth factors, and mitogens (Santio & Koskinen 2017). In solid tumors, PIM expression may also be induced, for instance, by hypoxia (Casillas et al. 2018), DNA damage (Zhao et al. 2008), and estrogen (Malinen et al. 2013). Mostly, different PIM kinase family members have been examined separately and no comprehensive studies on all of them in parallel have been conducted. Due to their role in carcinogenesis, PIM kinases have been of clinical and pharmacological interest, as indicated by several recent clinical trials. However, there is growing evidence of synergistic oncogenic pathways that must be considered when therapeutic strategies are evaluated.

6.1 The role of PIM upregulation in prostate cancer

The impact of PIM kinases on cancer progression has been indicated in several *in vitro* and *in vivo* studies. In particular, the role of PIM1 and PIM2 in cancer

progression has been well established. For example, PIM1 and PIM2 have been shown to improve the tumor growth of PC-3 cell-derived subcutaneous prostate cancer xenografts (Chen et al. 2005). In this thesis, we demonstrated that in addition to PIM1, PIM3 supports prostate tumorigenesis *in vivo* in both subcutaneous and orthotopic xenograft mouse models. Consistent with previous observations in transgenic mouse models, elevated expression of PIM1 and PIM2 in mice and human prostate tumors correlated with inflammatory responses and markers of stemness, emphasizing their significance in aggressive, drug-resistant, advanced disease (Jiménez-García et al. 2016). Moreover, in our studies, overexpression of PIM1 or PIM3 in human PC-3 cells that were orthotopically inoculated into mouse prostates resulted in an increased capacity to form metastases into the adjacent lymph nodes and lungs. The orthotopic cancer model recapitulates the original microenvironment of prostate cancer, facilitating local invasion and metastases. Orthotopically inoculated PC-3 cells have also previously been observed to migrate from the prostate to the local prostate-draining sacral and iliac lymph nodes, but metastases have rarely been detected in the lungs (Stephenson et al. 1992, Tuomela et al. 2008, Tuomela et al. 2009). This suggests that PIM1 and PIM3 upregulation has a significant impact on cancer cell migration, invasion and metastasis. However, the presence of bone metastases, which are one of the most common forms of prostate cancer metastasis, was not determined and warrants further investigation.

One of our major goals was to determine the levels of all PIM kinase family members in tumors of prostate cancer patients to evaluate their potential role in different progression levels of the malignancy. It is also important to keep in mind that mRNA datasets are analyzed from the total collection of tumor tissue, which includes also surrounding stroma and immune cells, and thus gives information from the total collection of the area. Whereas immunohistochemically stained tumor samples are rather specific, as tumor cells are stained and analyzed from a small region of interest, providing more specifical information about expression of certain proteins analyzed from that region. Therefore, the datasets from these different sample types are not directly comparable. However, data from prostate cancer patient samples supported our own observations from *in vivo* studies and were consistent with previous findings, where PIM expression was upregulated in primary tumors compared to benign samples (Dhanasekaran et al. 2001, Valdman et al. 2004, Xu et al. 2005, Dai et al. 2005, Cibull et al. 2006, Qu et al. 2016, Ren et al. 2019). Consistent with our *in vivo* results, *PIM1* and *PIM3* mRNA expression levels were increased in prostate cancer compared to benign prostate samples, however, no similar increase was observed

with *PIM2*. High *PIM3* gene expression levels have been shown to positively correlate with Gleason scores and patient survival (Qu et al. 2016). However, no association of higher *PIM1* or *PIM3* expression levels with higher Gleason scores was observed in the cohorts examined here (Taylor et al. 2010, Annala et al. 2015). As hypothesized, PIM1 protein expression increased with the progression of the disease. PIM2 has previously been shown to have a stronger role in lymphatic malignancies (Mondello et al. 2014); however, in this work, we demonstrated a clear increase in PIM2 expression levels during the progression of cancer from benign prostate to primary tumor and further to CRPC. PIM3 protein expression levels are high in all progression phases; however, expression increased in cancer compared to normal prostate or benign lesions. Based on our findings, PIM kinases do not seem to compensate for their expression levels between different family members, making prostate tumors highly heterogeneous with respect to PIM expression. Although it was not the main objective of this thesis, our results do not support an independent prognostic role for PIM-kinase expression. The importance of PIM-expression as a prognostic biomarker in addition to the known clinicopathological factors warrants further investigation.

6.1.1 PIM upregulation enhances the metastatic properties of prostate cancer cells by regulating the CXCL12/CXCR4 chemokine pathway

To further validate the formation of metastases mediated by PIM kinases, we analyzed IHC markers of mitotic activity, angiogenicity and invasiveness. The number of mitotic cells was only slightly higher in PIM-overexpressing tumors; however, an increase in vascularization promoted by PIM kinase activity may contribute to enhancement of metastatic activity. Significant PIM-dependent upregulation was also detected in the phosphorylation and cell surface expression of CXCR4. PIM1 kinase regulates the CXCL12/CXCR4 chemokine pathway through phosphorylation of Ser339 (Grundler et al. 2009). This pathway has an important function in the migration and invasion of both leukemic (Teicher and Fricker 2010, Furusato et al. 2010) and prostate cancer cells (Kukreja et al. 2005, Singh et al. 2004, Taichman et al. 2002, Ye et al. 2018). CXCR4 expression is elevated in both localized and metastatic prostate cancer (Sun et al. 2003, Mochizuki et al. 2004) and is associated with poor survival of patients (Akashi et al. 2008). Supporting our own findings of distant metastasis in PIM-overexpressing prostate cancer cells, the expression of CXCR4 is significantly associated with local recurrence after therapy

and the formation of distant metastases (Jung et al. 2011). In this thesis, we observed that in addition to PIM1, PIM3 can also phosphorylate CXCR4 at Ser339. In contrast, PIM2 does not phosphorylate CXCR4 (Grundler et al. 2009). Tumor cells expressing CXCR4 metastasize to target organs expressing high levels of CXCL12. The function of CXCR4 is also based on cellular location, internalization and surface re-expression (Busillo & Benovic, 2007). PIM-dependent phosphorylation of CXCR4 causes enhanced cell surface expression of the receptor (Grundler et al. 2009), allowing these cells to migrate and invade to sites that secrete CXCL12, including lymph nodes, lungs, bone, and liver (Maroni et al. 2007). Hence, the PIM1/PIM3-CXCR4 interaction may have also improved the ability of PIM-overexpressing orthotopic PC-3 cancer cells to form metastases in the prostate-draining lymph nodes and the lungs (Figure 17D). However, the expression of CXCL12 in lymph nodes, lungs and bone was not examined in our orthotopic xenograft model, and hence warrants further studies. Taken together, our studies along with others emphasize the clinical significance of PIM kinases in activating the CXCL12/CXCR4 pathway, which in turn promotes metastatic progression of prostate tumors.

6.2 PIM kinases associate with MYC and ERG oncogenes

Aberrations in several signal transduction pathways affect the initiation and progression of prostate cancer. Several of these pathways also work together with PIM kinases. Upregulation of the MYC oncogene is one of the most common alterations in prostate cancer (Gurel et al. 2008). Moreover, in prostate cancer both PIM1 and MYC levels are elevated (Dhanasekaran et al. 2001, Valdman et al. 2004, Xu et al. 2005, Cibull et al. 2006, Ellwood-Yen et al. 2003, Gurel et al. 2008). PIM1 and PIM2 increase the stability and transcriptional activity of MYC (Zippo et al. 2007). Moreover, PIM1 and MYC synergize to promote the development of advanced prostate carcinoma, as concurrent overexpression of MYC and PIM1 is associated with higher Gleason grades. (Wang et al. 2012). Aligned with these previously published data, we observed a positive correlation of upregulated *PIM1* and *MYC* gene expression levels in prostate cancer. However, here we also show a positive correlation between *PIM3* and *MYC* gene expression in two independent prostate cancer patient cohorts, suggesting that PIM3 and MYC may also cooperate in prostate cancer progression (Figure 17A). However, additional functional studies

are needed. Most likely, PIM3 also cooperates with MYC, similar to PIM1 (Zippo et al. 2007, Wang et al. 2010), but this must also be studied in more detail.

The transcription factor ERG is also often co-expressed with PIM1 in prostate cancer. ERG binds directly to the PIM1 promoter and enhances its expression (Magistroni et al. 2011). In this thesis, we found a correlation between *ERG* and *PIM3* mRNA expression in prostate cancer and demonstrated that all PIM kinases are associated with ERG at the protein level. Furthermore, ERG binding sites exist on the regulatory regions of all PIM family members, and ERG regulates their expression at both the mRNA and protein levels (Figure 17B). This regulation in turn may be relevant for ERG-induced prostate tumorigenesis.

6.3 NFATC1 phosphorylation by PIM kinases affects prostate cancer cell motility

PIM kinases enhance prostate cancer cell migration and invasion (Santio et al. 2010), but PIM-regulated pathways stimulating cell motility have not been comprehensively characterized. One of the well-known substrates of PIM kinases is NFATC1 (Rainio et al. 2002), which has been shown to promote cancer cell migration (Seifert et al. 2009, Santio et al. 2010, Kawahara et al. 2015). In our studies, we determined the possible effect of PIM1 phosphorylation of NFATC1 on prostate cancer cell motility. Moreover, we determined the phosphosites that affected the transcriptional activity of NFATC1 and its pro-migratory and pro-invasive effects in prostate cancer cells. The transcriptional and cell motility-promoting activities of NFATC1 with mutated PIM target sites were correspondingly diminished in PC-3 and DU-145 prostate cancer cell lines. The endogenous expression level of *PIM1* mRNA was relatively low in LNCaP cells and thereby may explain the mild effect on NFATC1 transactivation ability. Moreover, *PIM1* expression levels were higher in DuCaP and VCaP prostate cancer cell lines, which therefore may have been more suitable and interesting options for implemented experiments. Additionally, we discovered that all PIM kinases phosphorylate NFATC1, making it a substrate shared by all PIM family members.

Besides PIM1, several other NFATC1 phosphorylating kinases have been indicated. Phosphorylation by dual-specificity tyrosine-phosphorylation regulated kinase 1A (DYRK1A) stabilizes NFATC1 by phosphorylation as it interferes with

ubiquitination and ubiquitin-proteasome degradation of NFATC1. Moreover, by phosphorylation DYRK1A increases NFATC1 transactivation, similar to PIM kinases. While NFAT transcription factors are located in the cytoplasm, DYRK2 and CK1 kinases act to keep NFAT proteins phosphorylated and constrain their cytoplasmic location in resting cells. Furthermore, nuclear export kinases including GSK3 and IkB kinase epsilon (IKKε), re-phosphorylate activated NFAT proteins in the nucleus and inactivate them (Müller & Rao 2010, Zhang et al. 2016). Moreover, phosphosites found in our studies, Ser245 and Ser269, are also phosphorylation sites for another NFATC1 phosphorylating kinase, protein kinase A (PKA) (Sheridan et al. 2002). Mutation of these sites did not suppress migration, supporting the role of PIM-dependent phosphorylation of NFATC1 in cell motility. Moreover, similar studies with glioblastoma cells indicated that phosphorylation of NFATC1 by DYRK1A induced transcriptional activity of NFATC1, and inhibition of both of them reduced migration of glioblastoma cells (Liu et al. 2021).

Increased activity of matrix metalloproteinases, such as MMP2 and MMP9, affects the initiation of cell invasion, and their expression may be regulated in an NFAT-dependent manner in prostate cancer (Macini & Toker 2009). Hence, the effects of NFATC1 phosphorylation on MMP expression and activity were assessed by gelatinase activity assays. The results indicated that MMPs are NFATC1 targets, whose activities can be indirectly regulated by PIM kinases. Therefore, phosphorylation of NFATC1 by PIM1 kinase may be a relevant target for MMP activity (Figure 17C).

6.3.1 Novel putative PIM1/NFATC1 target genes

After our observation that PIM1 affects cancer cell motility through phosphorylation of NFATC1, we investigated targets of this signaling axis by microarray analysis. Indeed, we identified novel putative PIM1/NFATC1 target genes whose expression may be upregulated by PIM1-dependent phosphorylation of NFATC1. One of these putative PIM1/NFATC1 target genes encodes the known PIM substrate nuclear mitotic apparatus protein 1 (NUMA1) (Bhattacharya, 2002). Other target genes included regulators of transcription, the cell cycle, cell survival, cell motility, cell adhesion, and intracellular trafficking. In addition, multiple genes were implicated in the NFAT signaling pathway (Belinky et al. 2015), including those encoding the catalytic subunit alpha of protein kinase A (PRKACA) and the FK506 immunosuppressant-binding immunophilin protein (FKBP8). FKBP8 functions as

a chaperone for the anti-apoptotic BCL2 protein, and PIM kinases are known to upregulate the expression levels of BCL2 (Lilly et al. 1999). Additionally, the BCL2 homolog BCL2L1 was one of the putative PIM1/NFATC1 target genes. Moreover, multiple genes encoded proteins that are associated with intracellular trafficking (RAB11B, STXBP2, AP2A1, ARF1). However, the most interesting genes were involved in cell motility and control of the cytoskeletal actin network (INF2, FHOD1, ACTN3, CORO1B) and cell adhesion (COL6A2, PXN, ITGA5).

Integrins promote metastatic actions. As signaling pathways involving them were extremely enriched in our canonical pathway analysis, we selected ITGA5 for further expression analyses. Integrins are cellular adhesion receptors that mediate the attachment of cells to the extracellular matrix, and they play an important role in carcinogenesis (Hamidi and Ivaska, 2018). ITGA5 plays a key role in cell adhesion, migration and tumor invasion (Qin et al. 2011, Wong et al. 2011, Deng et al. 2019). Interestingly, prior studies have combined both PIM and other NFAT family members to integrin-mediated cell adhesion and motility. NFAT transcription factors have previously been associated with integrins. NFATC1 binds to the ITGB3 promoter and regulates its expression in osteoclast precursor cells, while in breast cancer, NFATC2 and NFAT5 promote ITGA6/ITGB4-mediated cell invasion (Crotti et al. 2006, Jauliac et al. 2002). Moreover, PIM inhibition reduces cell adhesion to collagen and fibronectin matrices through different integrin subunits (Santio et al. 2016). PIM-dependent alterations in integrin activity or expression have not been presented before. In this thesis, we discovered correlations between *PIM1* or *NFATC1* mRNA expression levels with *ITGA5*, both in PC-3 cells and in prostate cancer patient-derived samples (Figure 17C). Most importantly, correlation between *NFATC1* and *ITGA5* increased within higher Gleason scores, suggesting that PIM1 regulation of NFATC1-ITGA5 axis may have more important role in advanced prostate cancer. More functional studies are needed to understand how *ITGA5*, or other genes found in our analyses, may mediate pro-motility effects through the PIM-NFATC1 axis.

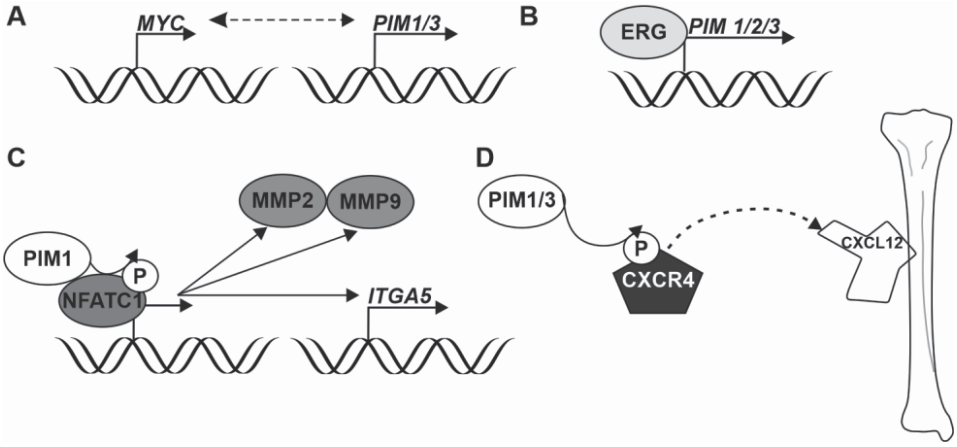

Figure 17. PIM signaling contributes to cancer progression and metastatic growth.

A mRNA **e**xpression levels of *MYC* and *PIM1/PIM3* are associated in prostate cancer. **B** ERG binds on the regulatory regions of all *PIM* family members, and ERG regulates their expression at both the mRNA and protein levels. **C** PIM1 affects cancer cell motility through phosphorylation of NFATC1 and thereby inducing NFATC1 transactivation ability. ITGA5 was assessed as one of the targets of this signaling axis. Moreover, gelatinase activity of MMP2 and MMP9 was induced which may play a role in tumor cell invasion. **D** PIM1/PIM3 phosphorylates and thereby upregulates cell surface expression of CXCR4. CXCR4 is well known chemokine receptor migrating towards organs expressing its ligand CXCL12, such as bones and lungs.

6.4 PIM inhibition in prostate cancer and targeted combinational therapy options

To address the tumorigenic mechanisms driven by PIM kinases, we investigated the effect of PIM inhibition on prostate cancer progression. We previously validated effective and selective PIM kinase inhibitors within two clusters of compounds that are structurally distinct, tetracyclic pyrrolocarbazoles (Akué-Gédu et al. 2009) and tricyclic benzo[cd]azulenes (Aumüller & Yli-Kauhaluoma 2009). DHPCC-9 diluted in DMSO acts as a pan-PIM inhibitor, while BA-1a diluted in DMA targets mostly PIM1 and PIM3 but less efficiently PIM2. Both the expression patterns and functions of different PIM kinase family members overlap; hence, pan-PIM inhibitors are the most reasonable option for therapy against malignancy. Previous functional validations were performed for these inhibitors both *in vitro* and in cell-based assays (Kiriazis et al. 2013, Santio et al. 2010). Here, our *in vitro* and *in vivo* studies demonstrated the efficacy of the PIM inhibitor DHPCC-9 against prostate cancer. Based on previous findings in *pim* knockout mice, deactivation of PIM

kinases is not presumed to induce serious side effects, as mice deficient in all three PIM family members are viable (Mikkers et al. 2004). Indeed, we did not observe any significant side effects, and DHPCC-9 was able to decrease PIM1/PIM3-dependent tumor growth and the formation of metastases. More accurate examinations of the effect of PIM inhibition with DHPCC-9 on metastatic properties demonstrated a decreased number of mitotic cells in PIM3 xenografts and efficient inhibition of the formation of metastases in lymph nodes and lungs. Moreover, treatment with the PIM inhibitor DHPCC-9 suppressed vascularization of both the blood and lymphatic vessels in PIM3 xenografts. Altogether, these findings suggested that this compound inactivated PIM kinases in tumor cells. DHPCC-9 is soluble only in DMSO, making it problematic in terms of clinical use, as DMSO can cause side effects. However, in 1978, FDA approved 50% dilution of DMSO (Rimso-50) for the treatment of interstitial cystitis (Capriotti and Capriotti, 2012). Several studies have used DMSO, for instance, in drug delivery purposes. However, based on multiple reports, the occurrence of adverse reactions to DMSO is dose-dependent and mainly transient and mild. Hence, it has been suggested that DMSO could be used in small amounts for human use (Kollerup Madsen et al. 2019). In the case of DHPCC-9, based on the current information, DMSO could be used for delivery of the compound. The other PIM inhibitor BA-1a is soluble only in DMA, which is also FDA-approved and used as a vehicle for several cancer drugs (Ghayor et al. 2017). However, DMA has low acute toxicity and thereby unsuitable for long-term chronic exposure and is inappropriate for oral intake. Although the PIM inhibitor DHPCC-9 is not proceeding to clinical trials, our results provide valuable information about the suitability of pan-PIM inhibitors for usage not only in cell and animal models but also in clinical trials.

Several PIM inhibitors are already under clinical trials including PIM447 and the orally available GDC-0339, and hopefully, some of them will be available for clinical use in the near future (Wang et al. 2019). TP-3654 (SGI-9481) is a second-generation small molecule pan-PIM inhibitor that is currently going through two clinical phase I and phase II trials with advanced solid tumors and myelofibrosis (Foulks et al. 2014, Luszczak et al. 2020a). Moreover, PIM inhibitors have already been tested both as monotherapy and in combination with other pathway inhibitors, including the PI3K-alpha inhibitor BYL719, JAK1/JAK2 inhibitor ruxolitinib, and CDK4/6 inhibitor LEE011 (Raab et al. 2019, Luszczak et al. 2020a). Based on the results of this thesis, several inhibitors against other molecules or signaling pathways should also be tested as co-targeted therapy. PIM inhibitors targeted together with other

oncogenic molecules might be beneficial in the clinical therapy of diverse cancers and could complement current cancer treatment therapies by blocking cancer cell survival and metastatic growth.

6.4.1 Co-targeting CXCL12/CXCR4 pathway and PIM kinases

CXCR4 is a chemokine receptor that regulates cell survival and proliferation and mediates the invasion and metastasis of cancer cells. CXCL12 ligand and its receptor CXCR4 act to enhance tumor aggressiveness by improving the adhesion of tumor cells to extracellular matrix components and endothelial cells (Sun et al. 2007). Due to its several cancer-promoting activities, the CXCL12/CXCR4 pathway is an appealing therapeutic target for cancer inhibitors. Multiple small molecule compounds have been produced to prevent the interaction between chemokines and their receptors or to inhibit signaling downstream from the receptor (Teicher and Fricker 2010, Furusato et al. 2010, Mollica Poeta et al. 2019). Based on our observations, inhibitors of the CXCL12/CXCR4 pathway may reduce the metastatic potential of prostate cancer, as PIM inhibition would block externalization of the CXCR4 receptor and hence prevent the cells from migrating and forming metastases into CXCL12-containing organs such as lungs, liver, bone marrow and brain (Zlotnik et al. 2011). A recent publication from Ye et al. 2018 indicated similar results with PIM1 kinase, as the malignant progression of prostate cancer cells was enhanced by PIM1 upregulation and the PIM1/CXCR4 interaction. However, these effects were effectively repressed by targeted therapy, with the flavonoid myricetin, which affected signaling pathways of both CXCR4 and PIM kinases. These results already indicate the benefits of combinatorial treatments both *in vitro* and *in vivo* in PC-3 xenograft mouse models (Ye et al. 2018). Indeed, the development and improvement of CXCL12/CXCR4 pathway inhibitors is ongoing. Several synthetic CXCR4 antagonists are under clinical phase I and II studies, and multiple currently studied flavonoid compounds have significant effects on the biological activity of CXCR4/CXCL12. Furthermore, one CXCR4 antagonist, Plerixafo, is already used in clinical cancer therapy (Zhou et al. 2018). In addition, CXCR4 is upregulated by ERG in most primary prostate cancers (80%) and hence promotes metastasis to bone tissue (Singareddy et al. 2013, Adamo & Ladomery 2016). If the patient has both PIM and ERG upregulated, the incidence of metastases is likely to increase, indicating the importance of co-targeted therapy options.

6.4.2 PIM/NFATC1-mediated therapy options

In our studies, we observed that the PIM-selective inhibitor DHPCC-9 decreased NFATC1 transactivation and prostate cancer cell migration and invasion. This PIM inhibitor prevented the activities of NFATC1 more efficiently compared to prevention of PIM1 targeted phosphorylation of NFATC1 alone, suggesting that it has an impact on additional downstream targets, only some of which are shared by PIM1 and NFATC1. Most of the targets may be regulated only by PIM1 phosphorylation, as indicated by the significant decrease in gene expression by the PIM inhibitor DHPCC-9. A similar effect was observed in case of MMP activities, which were more prominently decreased with the PIM inhibitor DHPCC-9 than with mutations of the PIM1 target sites in NFATC1. MMPs are more active in advanced stages of prostate cancer, as with high Gleason scores, most MMPs display higher expression levels (Gong et al. 2014). However, cancer therapeutics targeting adhesion receptors or MMPs have thus far not been shown to be efficient in clinical use (Hamidi and Ivaska 2018). More importantly, direct targeting of NFATC1 by calcineurin inhibitors does not have an impact on the PIM-targeted signaling pathway of NFATC1. Thus, inhibition targeted upstream of NFATC1, including PIM kinases and DYRK1A, is more justified. Nevertheless, a better understanding of the roles of NFATC1 in tumor progression may help establish efficacious therapeutics that target NFAT signaling in cancer progression and metastasis.

6.4.3 MYC and ERG as co-targeted therapy options

Due to their central role in prostate cancer initiation and progression, MYC and ERG oncogenes provide a strong rationale for targeted therapies. Inhibitor development directly targeting MYC, and ERG has been challenging as they are both transcription factors that lack a specific active site for small molecules, hence making them problematic for functionally diminishing their activity, similar to kinases (Duffy et al. 2021). However, several promising methods or compounds have been developed to inactivate MYC. Genetic knockout with lipid nanoparticle-based formulations (DCR-MYC) to transport siRNA into cancer cells has been successful in inhibiting MYC expression in *in vitro* and *in vivo* models. Moreover, this approach has already been tested in phase I clinical studies in patients with advanced solid tumors. However, it showed no therapeutic effects by other experiments, and the clinical study was terminated (Tolcher et al. 2015, Madden et al. 2021). Development of MYC inhibition by using antisense oligonucleotides is however ongoing and has

been shown to inhibit tumor growth in human liver cancer xenografts *in vivo* (Dhanasekaran et al. 2020). Although no compound directly targeting MYC has yet progressed to clinical testing, there are a few indirect MYC inhibitors. One of them is the intensively examined peptide/mini-protein called OmoMYC. OmoMYC prevents the binding of MYC to its target promoters, and it has anticancer activity against multiple preclinical models of malignancies, with minimal toxicity. Therefore, OmoMYC is currently under evaluation in clinical trials. APTO-253, which decreases MYC expression, is also now under a phase I clinical trial in patients with relapsed/refractory acute myeloid leukemia or myelodysplastic syndrome and several metastatic cancers (Duffy et al. 2021).

Oncogenic activation of *ERG* by recurrent TMPRSS2:ERG gene fusion is a well-established and frequent genomic alteration in prostate cancer. For this reason, it is also a potential therapeutic target. Based on our findings, the ERG oncogene cooperates and regulates all PIM kinases. Therefore, blocking ERG activity is also relevant. ERG inhibition strategies involve both direct and indirect targeting (Sedarsky et al. 2018). ERG-targeted therapies include small molecule inhibitors of ERG transcripts, suppression of the DNA-binding and transcription activator function of ERG, destabilization of ERG protein, inhibition of prostate cancer-associated *ERG* mRNA, direct prevention of ERG interacting coactivators, or downstream signaling events (Sedarsky et al. 2018). As an example, one small-molecule inhibitor, ERGi-USU, selectively inhibited the growth of ERG-positive cancer cell lines (Mohamed et al. 2018). Moreover, an interesting therapy option is the collective inhibition of the androgen axis with cooperating oncogenic factors downstream of ERG. This option of indirect ERG inhibition would also evade inhibition of wild-type ERG which is expressed in vascular endothelial cells and participating in endothelial differentiation. In this pipeline, PIM kinases may have a role as AR activity modulating agents and as ERG-regulated factors. PIM1 is known to phosphorylate AR at various sites, which leads to modification of AR stability and transcriptional activity (Ha et al. 2013, Linn et al. 2012, Ruff et al. 2021). Interestingly, elevated expression levels of ERG promote cell invasion by activating MMPs (Tomlins et al. 2008, Klezovitch et al. 2008). This thesis, together with other findings, indicates that ERG regulates PIM kinases, and both oncogenes induce cell invasion by activating MMPs, hence supporting co-targeted therapy. Indeed, there are already studies on combinatorial therapy against PIM and PI3K in PIM-upregulated and TMPRSS:ERG-fusion-positive prostate cancer cells, showing promising results

(Mologni et al. 2017). Based on our findings, these co-targeted treatments against the PIM, ERG, and MYC signaling pathways may be beneficial.

6.4.4 Challenges and benefits of targeted therapy options

Several drugs targeting carcinogenic pathways have lost their efficacy due to resistance mechanisms caused by substitutive mechanisms or feedback loops with closely related signaling pathways. This may also raise difficulties in the case of PIM inhibitors. PI3K/ATK pathway inhibition has already been proven to cause resistance, at least partly through the PIM kinase pathway; therefore, this feedback loop is very likely to play a role in PIM inhibition, hence underlining the need for co-targeted therapy options.

On the other hand, there are also several benefits in PIM-targeted inhibition of treatment resistance, including the common therapy options for prostate cancer, radiotherapy, and chemotherapy. Upregulation of PIM kinases especially PIM1 plays a role in tumor radioresistance, and a clear treatment benefit has been shown on combining both PIM inhibition and radiotherapy (Kim et al. 2011, Kim et al. 2013). The mechanism of PI3K inhibitor resistance has not been fully understood, but previous studies in breast cancer acknowledged PIM kinase as an additional therapeutic target in the PI3K pathway. PIM upregulation confers resistance to PI3K inhibitors, and therefore combinatorial inhibition of PIM and PI3K may be reasonable for relevant cancer patients (Le et al. 2016). Similar to radioresistance, PIM1 upregulation defends cancer cells from chemotherapy-induced apoptosis, while PIM inhibition leads to increased sensitivity to chemotherapy (Zemskova et al. 2008). These results suggest the possible benefits of PIM inhibition as adjuvant therapy for patients who have upregulated PIM expression and would hence develop resistance against various therapeutics.

7 CONCLUSIONS

The role of PIM kinases in prostate cancer progression is evident based on several studies. Moreover, PIM kinases work in close interaction or have cross-reactivities with other tumor-promoting genes and oncogenic molecular pathways. PIM kinases are constitutionally active as they lack a regulatory domain; hence, their activity correlates with their expression levels. Of the PIM family members, PIM1 is the most vastly studied, and its oncogenic role has been indicated both *in vitro* and *in vivo*. In our studies, we provide novel evidence for the role of PIM3 as a prostate cancer-promoting factor that cooperates with other oncogenes. In this thesis, we examined different pathways through which PIM kinases enhance metastatic formation by stimulating cancer cell migration and invasion as well as angiogenesis. For example, PIM kinases promote metastatic prostate cancer growth by employing the CXCL12/CXCR4 chemokine pathway.

Here, the aim was also to clarify the possible role of PIM phosphorylation of NFATC1 in the metastatic properties of prostate cancer cells. In summary, we showed that phosphorylation of PIM1 target sites increases the transcriptional activity of NFATC1 and improves its capacity to promote prostate cancer cell motility. Moreover, we shed further light on the PIM1-NFATC1 signaling axis, as we found putative novel target genes, including *ITGA5*, which may play a role in the metastatic properties of prostate cancer cells. This observation needs more investigation and functional studies. However, it is already clear that signaling through NFATC1-targeted phosphorylation by PIM kinases, may also offer opportunities for therapeutic interventions through combinatory approaches involving PIM-selective kinase inhibitors.

In this thesis, we indicated that the gene and protein expression levels of all three PIM family kinases may be enhanced during prostate cancer progression, especially in cooperation with other co-overexpressed oncoproteins, including MYC and ERG. Upregulation of PIM expression levels may be partly elucidated by our finding that ERG can enhance the expression of all PIM family members. As ERG itself is often upregulated in prostate cancer due to oncogenic gene fusions, our data indicate the

importance of detecting patients who express elevated levels of any PIM kinase at the same time with other oncoproteins, such as MYC or ERG. These patients may benefit the most from targeted and combinatorial therapies.

In summary, the results of this thesis show that PIM kinases impact prostate cancer migration, invasion, and the formation of metastases (Figure 18). Moreover, the expression levels of PIM kinases increase during prostate cancer progression from benign prostate cancer to CRPC. Furthermore, the results support an oncogenic role for PIM1 and PIM3 kinase in prostate cancer progression, especially in collaboration with MYC. We demonstrate a clear cooperative and regulatory role of ERG and all PIM kinases. We also demonstrate the efficacy, selectivity, and safety of the PIM inhibitor DHPCC-9, both in cell experiments and in *in vivo* mouse models.

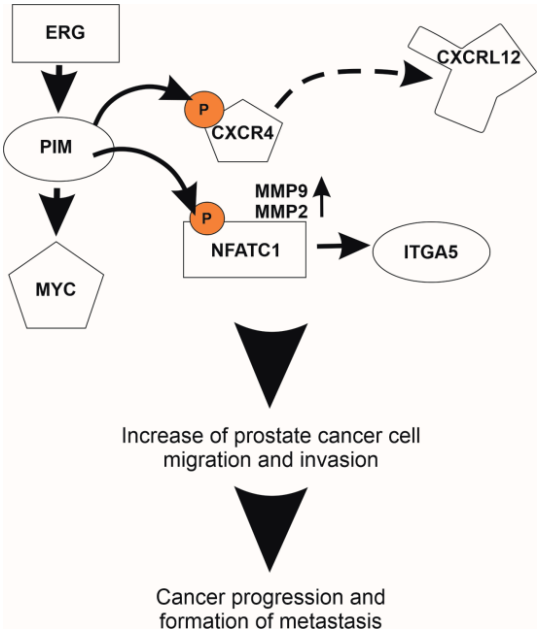

Figure 18. PIM kinases in prostate cancer progression.

ERG directly regulates *PIM* gene expression, while PIM kinases phosphorylate CXCR4 chemokine receptor and thereby induce CXCR4 expression on membrane. CXCR4-expressing cancer cells migrate towards CXCL12 expressing organs such as bones. Moreover, by phosphorylation PIM kinases enhance NFATC1 transcriptional activity and cell migration and invasion, which may occur through induction of MMP2 and MMP9 gelatinase activities and transcription of ITGA5. Expression of *PIM1* and *PIM3* are associated with *MYC* expression levels in prostate cancer and PIM1 stimulates MYC activity.

ACKNOWLEDGEMENTS

The research for this thesis was performed at the Faculty of Medicine and Health Technology of Tampere University and partly in the University of Turku. I would like to acknowledge Doctoral Programme in Medicine and Life Sciences, Finnish Cultural Foundation – Pirkanmaa fund, Cancer Society of Finland, Cancer Foundation, Pirkanmaa Cancer Association, The University of Tampere Foundation, Björkvist Foundation, and Ida Montin Foundation for funding my doctoral thesis research. Moreover, I want to acknowledge Tampereen kaupungin tiederahasto, from where I got support for covering expenses of printing my thesis. The greatest gratitude of course goes to my supervisor and our group leader, Prof. Tapio Visakorpi MD, PhD, for the opportunity to work in the Molecular Biology of Prostate Cancer group. I also indicate my appreciation to Prof. Visakorpi MD, PhD, for the flexible attitude towards my research and experiments and his great expertise in prostate cancer. I also want to thank our other group leader Prof. Teuvo Tammela, MD, PhD, for his wide clinical knowledge and invaluable collaboration and expertise in prostate cancer.

Especially I want to thank my other supervisor Adj. Prof. Päivi Koskinen, PhD, in whose research group I also started my carrier in science and my research related to PIM kinases. In addition, I want to thank my third supervisor Adj. Prof. Leena Latonen, PhD, who has been great support, especially during the third project. I am grateful for everything I have learned over the years and the excellent mentoring I have received. I would also like to thank the members of my thesis follow-up group, Adj. Prof. Paula Kujala MD, PhD, and Eeva Rainio, PhD for providing an important outside perspective to the projects. Eeva Rainio, PhD, was also the mastermind behind the NFAT-project; hence, I am sincerely thankful for her. Additionally, I would like to thank the pre-examiners Adj. Prof. Päivi Östling, PhD, and Adj. Prof. Tuomas Mirtti, MD, PhD, for the advice and constructive criticism concerning my thesis.

I also would like to thank all the co-authors for their contributions to the publications included in this thesis. Which would not have been possible without all

our collaborations; therefore, I want to thank our co-authors including Niina Santio, PhD, for her contribution in mouse experiments and analysis of the samples in the first project, and her contribution also in cell-based experiments in NFAT-project. Moreover, Prof. Yli-Kauhaluoma J, PhD, Anizon F, PhD, and Moreau P., PhD, for their expertise on PIM inhibitors. Additionally, sincere thanks to Prof. Pirkko Härkönen, MD, PhD, and Johanna Tuomela, PhD and Ilkka Paatero, PhD, for their expertise and contributions on animal experiments. I want also to thank Sanni Rinne, MSc for her expertise in cloning procedure. Special thanks to Mauro Scaravilli, PhD at the University of Eastern Finland helping me with microarray experiments. I am also grateful for the group of Prof. Dario Greco and his group members Giovanni Scala, PhD, and Angela Serra, PhD, who were helping me with the bioinformatics of microarray data. I also acknowledge Garry Corthals, PhD, and Petri Kouvonen, PhD, for their expertise in proteomics, and Adj. Prof. Pekka Ruusuvuori, PhD, for image analysis of invasion assays.

One key person, and also a co-author, who has been the greatest help for this project from the beginning, is Annika Kohvakka, MSc. We have learned and figured out a lot together over these years and surely without your unconditional assistance this thesis would never been possible. I would also like to thank all our group members that have worked in our group over these years including, our current team members Hanna Rauhala, PhD, Annika Kohvakka, MSc, Mina Sattari, DVM, Konsta Kukkonen, MSc, Kirsi Kaukoniemi, MSc, and Aurora Halkoluoto, MSc. Moreover, several former group members including Mauro Scaravilli, PhD, Gunilla Högnäs, PhD, Heini Kallio, PhD, Liisa Sjöblom, MSc, Benedikta Haflidadottir, PhD, and Katri Leinonen, MSc. Our lab technicians Päivi Martikainen, Paula Kosonen, Hanna Selin, and Riina Kaukoniemi, who have kept the lab running and helping with multiple practical issues. Special thanks for histology facility technician Sari Toivola for her help in IHC staining as well as friendship including important conversations which have been priceless. I would also like to specially thank Hanna Rauhala, PhD, for her advice and criticism towards my thesis, and our summer student Aurora Halkoluoto, MSc, because she made the last critical Western blots for my thesis project. Additionally, I would like to thank all co-workers in Arvo that have aided on my experiments or provided any support.

Eija Pehu, I want to thank for her support, advice, and mentor throughout my PhD studies, and also helping me pre-plan my steps for the life after PhD.

Yet separately, I would like to thank my friends for being part of my free-time activities. Special thanks for the time we have spent together in multiple occasions; Annika, Heini, Mina, Guni, Benny, Kristina, Anniina, Liisa, Ismaïl, Dafne, Niina, Lissu, Tiina, Nelly, Linda and Auri. We have had so many super fun trips and parties together throughout these many years. I also want to thank all my other friends; my biking group and training fellows as your friendship has been highly appreciated.

Finally, I would like to thank my family for their continuous support through this thesis. My parents and my dear sister Anni-Mari, and her daughters, my dearest nieces Reetta and Roosa. I would like to thank them for their company and all the precious moments and time outside the work.

Sini Eerola

10th of February 2022, Tampere

REFERENCES

Aaron, L., Franco, O., & Hayward, S. W. (2016). Review of prostate anatomy and embryology and the etiology of BPH. The Urologic Clinics of North America, 43(3), 279-288.

Adamo, P., & Ladomery, M. R. (2016). The oncogene ERG: A key factor in prostate cancer. Oncogene, 35(4), 403-414.

Adams, J. A. (2001). Kinetic and catalytic mechanisms of protein kinases. Chemical Reviews, 101(8), 2271-2290.

Aho, T. L. T., Sandholm, J., Peltola, K. J., Mankonen, H. P., Lilly, M., & Koskinen, P. J. (2004). Pim-1 kinase promotes inactivation of the pro-apoptotic bad protein by phosphorylating it on the Ser112 gatekeeper site. FEBS Letters, 571(1-3), 43-49.

Akashi, T., Koizumi, K., Tsuneyama, K., Saiki, I., Takano, Y., & Fuse, H. (2008). Chemokine receptor CXCR4 expression and prognosis in patients with metastatic prostate cancer. Cancer Science, 99(3), 539-542.

Akué-Gédu, R., Nauton, L., Théry, V., Bain, J., Cohen, P., Anizon, F., & Moreau, P. (2010). Synthesis, pim kinase inhibitory potencies and in vitro antiproliferative activities of diversely substituted pyrrolo[2,3-a]carbazoles. Bioorganic & Medicinal Chemistry, 18(18), 6865-6873.

Akué-Gédu, R., Rossignol, E., Azzaro, S., Knapp, S., Filippakopoulos, P., Bullock, A. N., Bain, J., Cohen, P., Prudhomme, M., Anizon, F., & Moreau, P. (2009). Synthesis, kinase inhibitory potencies, and in vitro antiproliferative evaluation of new pim kinase inhibitors. Journal of Medicinal Chemistry, 52(20), 6369-6381.

Allen, J. D., & Berns, A. (1996). Complementation tagging of cooperating oncogenes in knockout mice. Seminars in Cancer Biology, 7(5), 299-306.

Allen, J. D., Verhoeven, E., Domen, J., van der Valk, M., & Berns, A. (1997). Pim-2 transgene induces lymphoid tumors, exhibiting potent synergy with c-myc. Oncogene, 15(10), 1133-1141.

Amaravadi, R., & Thompson, C. B. (2005). The survival kinases akt and pim as potential pharmacological targets. The Journal of Clinical Investigation, 115(10), 2618-2624.

Annala, M., Kivinummi, K., Tuominen, J., Karakurt, S., Granberg, K., Latonen, L., Ylipää, A., Sjöblom, L., Ruusuvuori, P., Saramäki, O., Kaukoniemi, K. M., Yli-Harja, O., Vessella, R. L., Tammela, T. L. J., Zhang, W., Visakorpi, T., & Nykter, M. (2015). Recurrent SKIL-activating rearrangements in ETS-negative prostate cancer. Oncotarget, 6(8), 6235-6250.

Arora, M., Brown, A., Casey, D. C., Chen, A. Z., Coggeshall, M., Dilegge, T., Smith, A., Steiner, C., Abraham, B., Abubakar, I., Abu-Raddad, L. J., Agardh, E. E., Ajala, O. N., Al-Aly, Z., Alam, K., Assadi, R., Atique, S., Awasthi, A., Bazargan-Hejazi, S., Bell, M. L., Beyene, A. S., Bisanzio, D., Blore, J., Borschmann, R., Campuzano, J. C., Chibueze, C. E., Dargan, P. I., Derrett, S., Dharmaratne, S. D., Diaz-Torné, C., Duan, L., Duncan, B. B., Ellenbogen, R. G., Fereshtehnejad, S., Fernandes, J. G., Fischer, F., Fitchett, J. R. A., Frostad, J., Futran, N. D., Gebre, T., Gibney, K. B., Goodridge, A., Hailu, A. D., Handal, A. J., Harb, H. L., Harikrishnan, S., Hay, R. J., Horino, M., Huang, H., Jiang, Y., Karema, C. K., Kasaeian, A., Keiyoro, P. N., Koul, P. A., Lalloo, R., Leasher, J. L., Leigh, J., Lo, W. D., Lunevicius, R., Lyons, R. A., Memish, Z. A., Mitchell, P. B., Mohammed, S., Montico, M., Morawska, L., Mumford, J. E., Nagel, G., Nguyen, Q. L., Norheim, O. F., Oh, I., Olusanya, B. O., Piel, F. B., Rabiee, R. H. S., Radfar, A., Rahman, S. U., Reitsma, M. B., Remuzzi, G., Roy, A., Santos, I. S., Satpathy, M., Savic, M., Schöttker, B., Seedat, S., Sepanlou, S. G., Servan-Mori, E. E., Sharma, U., Shiue, I., Singh, O. P., Singh, P. K., Skogen, J. C., Sorensen, R. J. D., Sunguya, B. F., Szoeke, C. E. I., Truelsen, T., Ukwaja, K. N., Verma, R. K., Vlassov, V. V., Williams, H. C., Woodbrook, R., &

Yip, P. (2016). Global, regional, and national incidence, prevalence, and years lived with disability for 310 diseases and injuries, 1990–2015: A systematic analysis for the global burden of disease study 2015. The Lancet (British Edition), 388(10053), 1545-1602.

Aubrey, B. J., Strasser, A., & Kelly, G. L. (2016). Tumor-suppressor functions of the TP53 pathway. Cold Spring Harbor Perspectives in Medicine, 6(5), a026062.

Aumüller, I. B., & Yli-Kauhaluoma, J. (2009). Benzo[cd]azulene skeleton: Azulene, heptafulvene, and tropone derivatives. Organic Letters, 11(23), 5363-5365.

Bachmann, M., & Möröy, T. (2005). The serine/threonine kinase pim-1. The International Journal of Biochemistry & Cell Biology, 37(4), 726-730.

Barbieri, C. E., Baca, S. C., Lawrence, M. S., Demichelis, F., Blattner, M., Theurillat, J., White, T. A., Stojanov, P., Van Allen, E., Stransky, N., Nickerson, E., Chae, S., Boysen, G., Auclair, D., Onofrio, R. C., Park, K., Kitabayashi, N., MacDonald, T. Y., Sheikh, K., Vuong, T., Guiducci, C., Cibulskis, K., Sivachenko, A., Carter, S. L., Saksena, G., Voet, D., Hussain, W. M., Ramos, A. H., Winckler, W., Redman, M. C., Ardlie, K., Tewari, A. K., Mosquera, J. M., Rupp, N., Wild, P. J., Moch, H., Morrissey, C., Nelson, P. S., Kantoff, P. W., Gabriel, S. B., Golub, T. R., Meyerson, M., Lander, E. S., Getz, G., Rubin, M. A., & Garraway, L. A. (2012). Exome sequencing identifies recurrent SPOP, FOXA1 and MED12 mutations in prostate cancer. Nature Genetics, 44(6), 685-689.

Beals, C. R., Clipstone, N. A., Ho, S. N., & Crabtree, G. R. (1997). Nuclear localization of NF-ATc by a calcineurin-dependent, cyclosporin-sensitive intramolecular interaction. Genes & Development, 11(7), 824-834.

Bekelman, J. E., Rumble, R. B., Chen, R. C., Pisansky, T. M., Finelli, A., Feifer, A., Nguyen, P. L., Loblaw, D. A., Tagawa, S. T., Gillessen, S., Morgan. T. M., Liu, G., Vapiwala, N., Haluschak, J. J., Stephenson, A., Touijer, K., Kungel, T., and Freedland, S. J. (2018). Clinically Localized Prostate Cancer: ASCO Clinical Practice Guideline Endorsement of an American Urological Association/American Society for Radiation Oncology/Society of Urologic Oncology Guideline. Journal of Clinical Oncology, 36:32, 3251-3258.

Belinky, F., Nativ, N., Stelzer, G., Zimmerman, S., Iny Stein, T., Safran, M., & Lancet, D. (2015). PathCards: Multi-source consolidation of human biological pathways. Database: The Journal of Biological Databases and Curation, 2015, doi: 10.1093/database/bav006.

Bhattacharya, N., Wang, Z., Davitt, C., McKenzie, I. F. C., Xing, P., & Magnuson, N. S. (2002). Pim-1 associates with protein complexes necessary for mitosis. Chromosoma, 111(2), 80-95.

Brasó-Maristany, F., Filosto, S., Catchpole, S., Marlow, R., Quist, J., Francesch-Domenech, E., Plumb, D. A., Zakka, L., Gazinska, P., Liccardi, G., Meier, P., Gris-Oliver, A., Cheang, M. C. U., Perdrix-Rosell, A., Shafat, M., Noël, E., Patel, N., McEachern, K., Scaltriti, M., Castel, P., Noor, F., Buus, R., Mathew, S., Watkins, J., Serra, V., Marra, P., Grigoriadis, A., & Tutt, A. N. (2016). PIM1 kinase regulates cell death, tumor growth and chemotherapy response in triple-negative breast cancer. Nature Medicine, 22(11), 1303-1313.

Brault, L., Menter, T., Obermann, E. C., Knapp, S., Thommen, S., Schwaller, J., & Tzankov, A. (2012). PIM kinases are progression markers and emerging therapeutic targets in diffuse large B-cell lymphoma. British Journal of Cancer, 107(3), 491-500.

Brawer, M. K. (2005). Prostatic intraepithelial neoplasia: An overview. Reviews in Urology, 7 Suppl 3(Suppl 3), S11-S18.

Bregman, H., & Meggers, E. (2006). Ruthenium half-sandwich complexes as protein kinase inhibitors: An N-succinimidyl ester for rapid derivatizations of the cyclopentadienyl moiety. Organic Letters, 8(24), 5465-5468.

Breuer, M. L., Cuypers, H. T., & Berns, A. (1989). Evidence for the involvement of pim-2, a new common proviral insertion site, in progression of lymphomas. The EMBO Journal, 8(3), 743-748.

Bullock, A. N., Debreczeni, J., Amos, A. L., Knapp, S., & Turk, B. E. (2005). Structure and substrate specificity of the pim-1 kinase. The Journal of Biological Chemistry, 280(50), 41675-41682.

Burger, M. T., Nishiguchi, G., Han, W., Lan, J., Simmons, R., Atallah, G., Ding, Y., Tamez, V., Zhang, Y., Mathur, M., Muller, K., Bellamacina, C., Lindvall, M. K., Zang, R., Huh, K., Feucht, P.,

Zavorotinskaya, T., Dai, Y., Basham, S., Chan, J., Ginn, E., Aycinena, A., Holash, J., Castillo, J., Langowski, J. L., Wang, Y., Chen, M. Y., Lambert, A., Fritsch, C., Kauffmann, A., Pfister, E., Vanasse, K. G., & Garcia, P. D. (2015). Identification of N-(4-((1R,3S,5S)-3-amino-5-methylcyclohexyl)pyridin-3-yl)-6-(2,6-difluorophenyl)-5-fluoropicolinamide (PIM447), a potent and selective proviral insertion site of moloney murine leukemia (PIM) 1, 2, and 3 kinase inhibitor in clinical trials for hematological malignancies. Journal of Medicinal Chemistry, 58(21), 8373-8386.

Busillo, J. M., & Benovic, J. L. (2007). Regulation of CXCR4 signaling. Biochimica Et Biophysica Acta, 1768(4), 952-963.

Cai, X., Liu, C., Zhang, T., Zhu, Y., Dong, X., & Xue, P. (2018). Down-regulation of FN1 inhibits colorectal carcinogenesis by suppressing proliferation, migration, and invasion. Journal of Cellular Biochemistry, 119(6), 4717-4728.

Cancer Genome Atlas Research Network. (2015). The molecular taxonomy of primary prostate cancer. Cell, 163(4), 1011-1025.

Capriotti, K., & Capriotti, J. A. (2012). Dimethyl sulfoxide: History, chemistry, and clinical utility in dermatology. The Journal of Clinical and Aesthetic Dermatology, 5(9), 24-26.

Casillas, A. L., Toth, R. K., Sainz, A. G., Singh, N., Desai, A. A., Kraft, A. S., & Warfel, N. A. (2018). Hypoxia-inducible PIM kinase expression promotes resistance to antiangiogenic agents. Clinical Cancer Research: An Official Journal of the American Association for Cancer Research, 24(1), 169-180.

Castellano, G., Malaponte, G., Mazzarino, M. C., Figini, M., Marchese, F., Gangemi, P., Travali, S., Stivala, F., Canevari, S., & Libra, M. (2008). Activation of the osteopontin/matrix metalloproteinase-9 pathway correlates with prostate cancer progression. Clinical Cancer Research, 14(22), 7470-7480.

Catalona, W. J., Smith, D. S., Ratliff, T. L., Dodds, K. M., Coplen, D. E., Yuan, J. J., Petros, J. A., & Andriole, G. L. (1991). Measurement of prostate-specific antigen in serum as a screening test for prostate cancer. The New England Journal of Medicine, 324(17), 1156-1161.

Catalona, W. J., Richie, J. P., Ahmann, F. R., Hudson, M. A., Scardino, P. T., Flanigan, R. C., DeKernion, J. B., Ratliff, T. L., Kavoussi, L. R., Dalkin, B. L., Waters, W. B., MacFarlane, M. T., & Southwick, P. C. (1994). Comparison of digital rectal examination and serum prostate specific antigen in the early detection of prostate cancer: Results of a multicenter clinical trial of 6,630 men. The Journal of Urology, 151(5), 1283-1290.

Chen, H., Liu, H., & Qing, G. (2018). Targeting oncogenic Myc as a strategy for cancer treatment. Signal Transduction and Targeted Therapy, 3, 5.

Chen, J., Kobayashi, M., Darmanin, S., Qiao, Y., Gully, C., Zhao, R., Yeung, S. C., & Lee, M. H. (2009). Pim-1 plays a pivotal role in hypoxia-induced chemoresistance. Oncogene, 28(28), 2581-2592.

Cheng, L., Montironi, R., Bostwick, D. G., Lopez-Beltran, A., & Berney, D. M. (2012). Staging of prostate cancer. Histopathology, 60(1), 87-117.

Chen, L., Liu, S. & Tao, Y. (2020). Regulating tumor suppressor genes: post-translational modifications. Signal Transduction and Targeted Therapy, 5, 90.

Chen, L. S., Redkar, S., Taverna, P., Cortes, J. E., & Gandhi, V. (2011). Mechanisms of cytotoxicity to pim kinase inhibitor, SGI-1776, in acute myeloid leukemia. Blood, 118(3), 693-702.

Chen, W. W., Chan, D. C., Donald, C., Lilly, M. B., & Kraft, A. S. (2005). Pim family kinases enhance tumor growth of prostate cancer cells. Molecular Cancer Research: MCR, 3(8), 443-451.

Chen, X., Wang, Z., Li, B., Zhang, Y., & Li, Y. (2016). Pim-3 contributes to radioresistance through regulation of the cell cycle and DNA damage repair in pancreatic cancer cells. Biochemical and Biophysical Research Communications, 473(1), 296-302.

Chi, K. N., Agarwal, N., Bjartell, A., Chung, B. H., Pereira de Santana Gomes, A. J., Given, R., Juárez Soto, Á., Merseburger, A. S., Özgüroğlu, M., Uemura, H., Ye, D., Deprince, K., Naini, V., Li, J., Cheng, S., Yu, M. K., Zhang, K., Larsen, J. S., McCarthy, S., Chowdhury, S., TITAN Investigators (2019). Apalutamide for Metastatic, Castration-Sensitive Prostate Cancer. The New England journal of medicine, 381(1), 13–24.

Cibull, T. L., Jones, T. D., Li, L., Eble, J. N., Ann Baldridge, L., Malott, S. R., Luo, Y., & Cheng, L. (2006). Overexpression of pim-1 during progression of prostatic adenocarcinoma. Journal of Clinical Pathology, 59(3), 285-288.

Classon, M., & Harlow, E. (2002). The retinoblastoma tumour suppressor in development and cancer. Nature Reviews. Cancer, 2(12), 910-917.

Clipstone, N. A., Fiorentino, D. F., & Crabtree, G. R. (1994). Molecular analysis of the interaction of calcineurin with drug-immunophilin complexes. The Journal of Biological Chemistry, 269(42), 26431-26437.

Cohen, P. (2000). The regulation of protein function by multisite phosphorylation--a 25 year update. Trends in Biochemical Sciences, 25(12), 596-601.

Cohen, P. (2002). The origins of protein phosphorylation. Nature Cell Biology, 4(5), 127.

Cortes, J., Tamura, K., DeAngelo, D. J., de Bono, J., Lorente, D., Minden, M., Uy, G. L., Kantarjian, H., Chen, L. S., Gandhi, V., Godin, R., Keating, K., McEachern, K., Vishwanathan, K., Pease, J. E., & Dean, E. (2018). Phase I studies of AZD1208, a proviral integration moloney virus kinase inhibitor in solid and haematological cancers. British Journal of Cancer, 118(11), 1425-1433.

Crabtree, G. R., & Olson, E. N. (2002). NFAT signaling: Choreographing the social lives of cells. Cell, 109, 67.

Cross, D. A., Alessi, D. R., Cohen, P., Andjelkovich, M., & Hemmings, B. A. (1995). Inhibition of glycogen synthase kinase-3 by insulin mediated by protein kinase B. Nature, 378(6559), 785-789.

Crotti, T. N., Flannery, M., Walsh, N. C., Fleming, J. D., Goldring, S. R., & McHugh, K. P. (2006). NFATc1 regulation of the human beta3 integrin promoter in osteoclast differentiation. Gene, 372, 92-102.

Cuypers, H. T., Selten, G., Quint, W., Zijlstra, M., Maandag, E. R., Boelens, W., van Wezenbeek, P., Melief, C., & Berns, A. (1984). Murine leukemia virus-induced T-cell lymphomagenesis: Integration of proviruses in a distinct chromosomal region. Cell, 37(1), 141-150.

D'Amico, A. V, Whittington, R., Malkowicz, S. B., Schultz, D., Blank, K., Broderick, G. A., Tomaszewski, J. E., Renshaw, A. A., Kaplan, I., Beard, C. J., & Wein, A. (1998). Biochemical outcome after radical prostatectomy, external beam radiation therapy, or interstitial radiation therapy for clinically localized prostate cancer. JAMA, 280(11), 969-974.

Dai, H., Li, R., Wheeler, T., de Vivar, A. D., Frolov, A., Tahir, S., Agoulnik, I., Thompson, T., Rowley, D., & Ayala, G. (2005). Pim-2 upregulation: Biological implications associated with disease progression and perinueral invasion in prostate cancer. The Prostate, 65(3), 276-286.

Dang, C. V. (2012). MYC on the path to cancer. Cell, 149(1), 22-35.

Darash-Yahana, M., Pikarsky, E., Abramovitch, R., Zeira, E., Pal, B., Karplus, R., Beider, K., Avniel, S., Kasem, S., Galun, E., & Peled, A. (2004). Role of high expression levels of CXCR4 in tumor growth, vascularization, and metastasis. FASEB Journal: Official Publication of the Federation of American Societies for Experimental Biology, 18(11), 1240-1242.

Das, A., Monteiro, M., Barai, A., Kumar, S., Sen, S. (2017). MMP proteolytic activity regulates cancer invasiveness by modulating integrins. Scientific Reports, 7(1), 14219.

Datta, S. R., Dudek, H., Tao, X., Masters, S., Fu, H., Gotoh, Y., & Greenberg, M. E. (1997). Akt phosphorylation of BAD couples survival signals to the cell-intrinsic death machinery. Cell, 91(2), 231-241.

Davis, I. D., Martin, A. J., Stockler, M. R., Begbie, S., Chi, K. N., Chowdhury, S., Coskinas, X., Frydenberg, M., Hague, W. E., Horvath, L. G., Joshua, A. M., Lawrence, N. J., Marx, G., McCaffrey, J., McDermott, R., McJannett, M., North, S. A., Parnis, F., Parulekar, W., Pook, D. W., Reaume, M. N., Sandhu, S. K., Tan, A., Tan, T. H., Thomson, A., Tu, E., Vera-Badillo, F., Williams, S. G., Yip, S., Zhang, A. Y., Zielinski, R. R., Sweeney, C. J.; ENZAMET Trial Investigators and the Australian and New Zealand Urogenital and Prostate Cancer Trials Group. (2019). Enzalutamide with Standard First-Line Therapy in Metastatic Prostate Cancer. New England Journal of Medicine, 381(2), 121-131.

Debreczeni, J. E., Bullock, A. N., Atilla, G. E., Williams, D. S., Bregman, H., Knapp, S., & Meggers, E. (2006). Ruthenium half-sandwich complexes bound to protein kinase pim-1. Angewandte Chemie (International Ed. in English), 45(10), 1580-1585.

Decker, S., Finter, J., Forde, A. J., Kissel, S., Schwaller, J., Mack, T. S., Kuhn, A., Gray, N., Follo, M., Jumaa, H., Burger, M., Zirlik, K., Pfeifer, D., Miduturu, C. V., Eibel, H., Veelken, H., & Dierks, C. (2014). PIM kinases are essential for chronic lymphocytic leukemia cell survival (PIM2/3) and CXCR4-mediated microenvironmental interactions (PIM1). Molecular Cancer Therapeutics, 13(5), 1231-1245.

Dehm, S. M., Schmidt, L. J., Heemers, H. V., Vessella, R. L., & Tindall, D. J. (2008). Splicing of a novel androgen receptor exon generates a constitutively active androgen receptor that mediates prostate cancer therapy resistance. Cancer Research, 68(13), 5469-5477.

de la Pompa, J. L., Timmerman, L. A., Takimoto, H., Yoshida, H., Elia, A. J., Samper, E., Potter, J., Wakeham, A., Marengere, L., Langille, B. L., Crabtree, G. R., & Mak, T. W. (1998). Role of the NF-ATc transcription factor in morphogenesis of cardiac valves and septum. Nature, 392(6672), 182-186.

Deng, Y., Wan, Q., & Yan, W. (2019). Integrin α5/ITGA5 promotes the proliferation, migration, invasion and progression of oral squamous carcinoma by Epithelial–Mesenchymal transition. Cancer Management and Research, 11, 9609-9620.

Desgrosellier, J. S., & Cheresh, D. A. (2010). Integrins in cancer: Biological implications and therapeutic opportunities. Nature Reviews. Cancer, 10(1), 9-22.

Dhanasekaran, R., Park, J., Yevtodiyenko, A., Bellovin, D. I., Adam, S. J., Kd, A. R., Gabay, M., Fernando, H., Arzeno, J., Arjunan, V., Gryanzov, S., & Felsher, D. W. (2020). MYC ASO impedes tumorigenesis and elicits oncogene addiction in autochthonous transgenic mouse models of HCC and RCC. Molecular Therapy. Nucleic Acids, 21, 850-859.

Dhanasekaran, S. M., Barrette, T. R., Ghosh, D., Shah, R., Varambally, S., Kurachi, K., Pienta, K. J., Rubin, M. A., & Chinnaiyan, A. M. (2001). Delineation of prognostic biomarkers in prostate cancer. Nature, 412(6849), 822-826.

Domen, J., van der Lugt, N. M., Laird, P. W., Saris, C. J., & Berns, A. (1993). Analysis of pim-1 function in mutant mice. Leukemia, 7 Suppl 2, 108.

Duffy, M. J., O'Grady, S., Tang, M., & Crown, J. (2021). MYC as a target for cancer treatment. Cancer Treatment Reviews, 94, 102154.

Durnian, J. M., Stewart, R. M. K., Tatham, R., Batterbury, M., & Kaye, S. B. (2007). Cyclosporin-A associated malignancy. Clinical Ophthalmology (Auckland, N.Z.), 1(4), 421-430.

EAU Guidelines. Edn. presented at the EAU Annual Congress Milan 2021. ISBN 978-94-92671-13-4.

Eggener, S. E., Rumble, R. B., Armstrong, A. J., Morgan, T. M., Crispino, T., Cornford, P., van der Kwast, D., Grignon, D. J., Rai, A. J., Agarwal, N., Klein, E. A., Den, R. B., and Beltran, H., (2018). American Society of Clinical Oncology: Molecular Biomarkers in Localized Prostate Cancer. Published online December 12, 2019, doi: 10.1200/JCO.19.02768.

Eiring, A. M., Harb, J. G., Neviani, P., Garton, C., Oaks, J. J., Spizzo, R., Liu, S., Schwind, S., Santhanam, R., Hickey, C. J., Becker, H., Chandler, J. C., Andino, R., Cortes, J., Hokland, P., Huettner, C. S., Bhatia, R., Roy, D. C., Liebhaber, S. A., Caligiuri, M. A., Marcucci, G., Garzon, R., Croce, C. M., Calin, G. A., & Perrotti, D. (2010). miR-328 functions as an RNA decoy to modulate hnRNP E2 regulation of mRNA translation in leukemic blasts. Cell, 140(5), 652-665.

Ellwood-Yen, K., Graeber, T. G., Wongvipat, J., Iruela-Arispe, M., Zhang, J., Matusik, R., Thomas, G. V., & Sawyers, C. L. (2003). Myc-driven murine prostate cancer shares molecular features with human prostate tumors. Cancer Cell, 4(3), 223-238.

Epstein, J. I., Allsbrook, W. C., Amin, M. B., & Egevad, L. L. (2005). The 2005 international society of urological pathology (ISUP) consensus conference on gleason grading of prostatic carcinoma. The American Journal of Surgical Pathology, 29(9), 1228-1242.

Epstein, J. I., Egevad, L., Amin, M. B., Delahunt, B., Srigley, J. R., & Humphrey, P. A. (2016). The 2014 international society of urological pathology (ISUP) consensus conference on gleason

grading of prostatic carcinoma: Definition of grading patterns and proposal for a new grading system. The American Journal of Surgical Pathology, 40(2), 244-252.
Epstein, J. I. (2010). An update of the gleason grading system. The Journal of Urology, 183(2), 433-440.
Evans, A. J. (2018). Treatment effects in prostate cancer. Modern Pathology, 31(S1), 110.
Fares, J., Fares, M. Y., Khachfe, H. H., Salhab, H. A., & Fares, Y. (2020). Molecular principles of metastasis: A hallmark of cancer revisited. Signal Transduction and Targeted Therapy, 5(1), 1-17.
Feldman, J. D., Vician, L., Crispino, M., Tocco, G., Marcheselli, V. L., Bazan, N. G., Baudry, M., & Herschman, H. R. (1998). KID-1, a protein kinase induced by depolarization in brain. The Journal of Biological Chemistry, 273(26), 16535-16543.
Fischer-Valuck, B. W., Gay, H. A., Patel, S., Baumann, B. C., & Michalski, J. M. (2019). A brief review of low-dose rate (LDR) and high-dose rate (HDR) brachytherapy boost for high-risk prostate. Frontiers in Oncology, 9.
Fizazi, K., Shore, N., Tammela, T. L., Ulys, A., Vjaters, E., Polyakov, S., Jievaltas, M., Luz, M., Alekseev, B., Kuss, I., Le Berre, M. A., Petrenciuc, O., Snapir, A., Sarapohja, T., Smith, M. R., & ARAMIS Investigators (2020). Nonmetastatic, Castration-Resistant Prostate Cancer and Survival with Darolutamide. The New England journal of medicine, 383(11), 1040–1049.
Foster, C. S. (2000). Pathology of benign prostatic hyperplasia. The Prostate, 45(S9), 4-14.
Foulks, J. M., Carpenter, K. J., Luo, B., Xu, Y., Senina, A., Nix, R., Chan, A., Clifford, A., Wilkes, M., Vollmer, D., Brenning, B., Merx, S., Lai, S., McCullar, M. V., Ho, K., Albertson, D. J., Call, L. T., Bearss, J. J., Tripp, S., Liu, T., Stephens, B. J., Mollard, A., Warner, S. L., Bearss, D. J., & Kanner, S. B. (2014). A small-molecule inhibitor of PIM kinases as a potential treatment for urothelial carcinomas. Neoplasia (New York, N.Y.), 16(5), 403-412.
Fujita, K., & Nonomura, N. (2019). Role of androgen receptor in prostate cancer: A review. The World Journal of Men's Health, 37(3), 288-295.
Furusato, B., Mohamed, A., Uhlén, M., & Rhim, J. S. (2010). CXCR4 and cancer. Pathology International, 60(7), 497-505.
Förster T. (1948). Zwischenmolekulare Energiewanderung und Fluoreszenz. Annalen der Physik, 6:55-75.
GBD 2015, Disease and Injury Incidence and Prevalence Collaborators. (2016). Global, regional, and national incidence, prevalence, and years lived with disability for 310 diseases and injuries, 1990-2015: A systematic analysis for the global burden of disease study 2015. Lancet (London, England), 392(10159), 1789-1858.
Ghayor, C., Gjoksi, B., Dong, J., Siegenthaler, B., Caflisch, A., & Weber, F. E. (2017). N,N dimethylacetamide a drug excipient that acts as bromodomain ligand for osteoporosis treatment. Scientific Reports, 7(1), 42108.
Glazova, M., Aho, T. L. T., Palmetshofer, A., Murashov, A., Scheinin, M., & Koskinen, P. J. (2005). Pim-1 kinase enhances NFATc activity and neuroendocrine functions in PC12 cells. Brain Research. Molecular Brain Research, 138(2), 116-123.
Gleason, D. F. (1966). Classification of prostatic carcinomas. Cancer Chemotherapy Reports, 50(3), 125-128.
Gong, Y., Chippada-Venkata, U. D., & Oh, W. K. (2014). Roles of matrix metalloproteinases and their natural inhibitors in prostate cancer progression. Cancers, 6(3), 1298-1327.
Gosein, M. A., Narinesingh, D., Motilal, S., Ramkissoon, A. P., Goetz, C. M., Sadho, K., Mosodeen, M. D., and Banfield, R. (2020). Biparametric MRI prior to Radical Radiation Therapy for Prostate Cancer in a Caribbean Population: Implications for Risk Group Stratification and Treatment. Radiology: Imaging Cancer, 2:4.
Grasso, C. S., Wu, Y., Robinson, D. R., Cao, X., Dhanasekaran, S. M., Khan, A. P., Quist, M. J., Jing, X., Lonigro, R. J., Brenner, J. C., Asangani, I. A., Ateeq, B., Chun, S. Y., Siddiqui, J., Sam, L., Anstett, M., Mehra, R., Prensner, J. R., Palanisamy, N., Ryslik, G. A., Vandin, F., Raphael, B. J., Kunju, L. P., Rhodes, D. R., Pienta, K. J., Chinnaiyan, A. M., & Tomlins, S. A. (2012). The mutational landscape of lethal castration-resistant prostate cancer. Nature, 487(7406), 239-243.

Grundler, R., Brault, L., Gasser, C., Bullock, A. N., Dechow, T., Woetzel, S., Pogacic, V., Villa, A., Ehret, S., Berridge, G., Spoo, A., Dierks, C., Biondi, A., Knapp, S., Duyster, J., & Schwaller, J. (2009). Dissection of PIM serine/threonine kinases in FLT3-ITD–induced leukemogenesis reveals PIM1 as regulator of CXCL12–CXCR4-mediated homing and migration. Journal of Experimental Medicine, 206(9), 1957-1970.

Guan, X. (2015). Cancer metastases: Challenges and opportunities. Acta Pharmaceutica Sinica B, 5(5), 402-418.

Gu, H., Liu, M., Ding, C., Wang, X., Wang, R., Wu, X., & Fan, R. (2016). Hypoxia-responsive miR-124 and miR-144 reduce hypoxia-induced autophagy and enhance radiosensitivity of prostate cancer cells via suppressing PIM1. Cancer Medicine, 5(6), 1174-1182.

Gurel, B., Iwata, T., Koh, C. M., Jenkins, R. B., Lan, F., Van Dang, C., Hicks, J. L., Morgan, J., Cornish, T. C., Sutcliffe, S., Isaacs, W. B., Luo, J., & De Marzo, A.,M. (2008). Nuclear MYC protein overexpression is an early alteration in human prostate carcinogenesis. Modern Pathology: An Official Journal of the United States and Canadian Academy of Pathology, Inc, 21(9), 1156-1167.

Ha, S., Iqbal, N. J., Mita, P., Ruoff, R., Gerald, W. L., Lepor, H., Taneja, S. S., Lee, P., Melamed, J., Garabedian, M. J., & Logan, S. K. (2013). Phosphorylation of the androgen receptor by PIM1 in hormone refractory prostate cancer. Oncogene, 32(34), 3992-4000.

Hamidi, H., & Ivaska, J. (2018). Every step of the way: Integrins in cancer progression and metastasis. Nature Reviews. Cancer, 18(9), 533-548.

Hanahan, D. (2022). Hallmarks of Cancer: New Dimensions. Cancer discovery, 12(1), 31-46.

Hanahan, D., & Weinberg, R. A. (2000). The hallmarks of cancer. Cell, 100(1), 57-70.

Hanahan, D., & Weinberg, R. A. (2011). Hallmarks of cancer: The next generation. Cell, 144(5), 646-674.

Hanks, S. K., & Hunter, T. (1995). Protein kinases 6. the eukaryotic protein kinase superfamily: Kinase (catalytic) domain structure and classification. FASEB Journal: Official Publication of the Federation of American Societies for Experimental Biology, 9(8), 576-596.

Heavey, S., O'Byrne, K. J., & Gately, K. (2014). Strategies for co-targeting the PI3K/AKT/mTOR pathway in NSCLC. Cancer Treatment Reviews, 40(3), 445-456.

Heinlein, C. A., & Chang, C. (2004). Androgen receptor in prostate cancer. Endocrine Reviews, 25(2), 276-308.

Henry, R. E., Barry, E. R., Castriotta, L., Ladd, B., Markovets, A., Beran, G., Ren, Y., Zhou, F., Adam, A., Zinda, M., Reimer, C., Qing, W., Su, W., Clark, E., D'Cruz, C. M., & Schuller, A. G. (2016). Acquired savolitinib resistance in non-small cell lung cancer arises via multiple mechanisms that converge on MET-independent mTOR and MYC activation. Oncotarget, 7(36), 57651-57670.

Hernández, G. L., Volpert, O. V., Iñiguez, M. A., Lorenzo, E., Martínez-Martínez, S., Grau, R., Fresno, M., & Redondo, J. M. (2001). Selective inhibition of vascular endothelial growth factor-mediated angiogenesis by cyclosporin A: Roles of the nuclear factor of activated T cells and cyclooxygenase 2. The Journal of Experimental Medicine, 193(5), 607-620.

Hoang, D. T., Iczkowski, K. A., Kilari, D., See, W., & Nevalainen, M. T. (2017). Androgen receptor-dependent and -independent mechanisms driving prostate cancer progression: Opportunities for therapeutic targeting from multiple angles. Oncotarget, 8(2), 3724-3745.

Hoey, T., Sun, Y. L., Williamson, K., & Xu, X. (1995). Isolation of two new members of the NF-AT gene family and functional characterization of the NF-AT proteins. Immunity, 2(5), 461-472.

Hogan, P. G., Chen, L., Nardone, J., & Rao, A. (2003). Transcriptional regulation by calcium, calcineurin, and NFAT. Genes & Development, 17(18), 2205-2232.

Horiuchi, D., Camarda, R., Zhou, A. Y., Yau, C., Momcilovic, O., Balakrishnan, S., Corella, A. N., Eyob, H., Kessenbrock, K., Lawson, D. A., Marsh, L. A., Anderton, B. N., Rohrberg, J., Kunder, R., Bazarov, A. V., Yaswen, P., McManus, M. T., Rugo, H. S., Werb, Z., & Goga, A. (2016). PIM1 kinase inhibition as a targeted therapy against triple-negative breast tumors with elevated MYC expression. Nature Medicine, 22(11), 1321-1329.

Hsu, J., Leong, P., Ho, Y., Hsu, L., Lu, P., Chen, C., & Guh, J. (2012). Pim-1 knockdown potentiates paclitaxel-induced apoptosis in human hormone-refractory prostate cancers through inhibition of NHEJ DNA repair. Cancer Letters, 319(2), 214-222.

Hägglöf, C., Hammarsten, P., Strömvall, K., Egevad, L., Josefsson, A., Stattin, P., Granfors, T., & Bergh, A. (2014). TMPRSS2-ERG expression predicts prostate cancer survival and associates with stromal biomarkers. PloS One, 9(2), e86824.

Imanishi, S. Y., Kochin, V., Ferraris, S. E., de Thonel, A., Pallari, H., Corthals, G. L., & Eriksson, J. E. (2007). Reference-facilitated phosphoproteomics: Fast and reliable phosphopeptide validation by microLC-ESI-Q-TOF MS/MS. Molecular & Cellular Proteomics: MCP, 6(8), 1380-1391.

Jacobs, M. D., Black, J., Futer, O., Swenson, L., Hare, B., Fleming, M., & Saxena, K. (2005). Pim-1 ligand-bound structures reveal the mechanism of serine/threonine kinase inhibition by LY294002. The Journal of Biological Chemistry, 280(14), 13728-13734.

Jain, J., Burgeon, E., Badalian, T. M., Hogan, P. G., & Rao, A. (1995). A similar DNA-binding motif in NFAT family proteins and the rel homology region. The Journal of Biological Chemistry, 270(8), 4138-4145.

Jauliac, S., López-Rodriguez, C., Shaw, L. M., Brown, L. F., Rao, A., & Toker, A. (2002). The role of NFAT transcription factors in integrin-mediated carcinoma invasion. Nature Cell Biology, 4(7), 540-544.

Jiménez-García, M. P., Lucena-Cacace, A., Robles-Frías, M. J., Narlik-Grassow, M., Blanco-Aparicio, C., & Carnero, A. (2016). The role of PIM1/PIM2 kinases in tumors of the male reproductive system. Scientific Reports, 6, 38079.

Johnson, E. N., Lee, Y. M., Sander, T. L., Rabkin, E., Schoen, F. J., Kaushal, S., & Bischoff, J. (2003). NFATc1 mediates vascular endothelial growth factor-induced proliferation of human pulmonary valve endothelial cells*. Journal of Biological Chemistry, 278(3), 1686-1692.

Jolly, C., & Van Loo, P. (2018). Timing somatic events in the evolution of cancer. Genome Biology, 19.

Jung, S. J., Kim, C. I., Park, C. H., Chang, H. S., Kim, B. H., Choi, M. S., & Jung, H. R. (2011). Correlation between chemokine receptor CXCR4 expression and prognostic factors in patients with prostate cancer. Korean Journal of Urology, 52(9), 607-611.

Kalichamy, K. S., Ikkala, K., Pörsti, J., Santio, N. M., Tuomaala, J., Jha, S., Holmberg, C. I., & Koskinen, P. J. (2019). PIM-related kinases selectively regulate olfactory sensations in caenorhabditis elegans. eNeuro, 6(4), ENEURO.0003-19.2019.

Kawahara, T., Kashiwagi, E., Ide, H., Li, Y., Zheng, Y., Ishiguro, H., & Miyamoto, H. (2015). The role of NFATc1 in prostate cancer progression: Cyclosporine A and tacrolimus inhibit cell proliferation, migration, and invasion. The Prostate, 75(6), 573-584.

Keeton, E. K., McEachern, K., Dillman, K. S., Palakurthi, S., Cao, Y., Grondine, M. R., Kaur, S., Wang, S., Chen, Y., Wu, A., Shen, M., Gibbons, F. D., Lamb, M. L., Zheng, X., Stone, R. M., Deangelo, D. J., Platanias, L. C., Dakin, L. A., Chen, H., Lyne, P. D., & Huszar, D. (2014). AZD1208, a potent and selective pan-pim kinase inhibitor, demonstrates efficacy in preclinical models of acute myeloid leukemia. Blood, 123(6), 905-913.

Kennedy, S. P., O'Neill, M., Cunningham, D., Morris, P. G., Toomey, S., Blanco-Aparicio, C., Martinez, S., Pastor, J., Eustace, A. J., & Hennessy, B. T. (2020). Preclinical evaluation of a novel triple-acting PIM/PI3K/mTOR inhibitor, IBL-302, in breast cancer. Oncogene, 39(14), 3028-3040.

Kim, W., Youn, H., Kwon, T., Kang, J., Kim, E., Son, B., Yang, H. J., Jung, Y., & Youn, B. (2013). PIM1 kinase inhibitors induce radiosensitization in non-small cell lung cancer cells. Pharmacological Research, 70(1), 90-101.

Kim, W., Youn, H., Seong, K. M., Yang, H. J., Yun, Y. J., Kwon, T., Kim, Y. H., Lee, J. Y., Jin, Y., & Youn, B. (2011). PIM1-activated PRAS40 regulates radioresistance in non-small cell lung cancer cells through interplay with FOXO3a, 14-3-3 and protein phosphatases. Radiation Research, 176(5), 539-552.

Kiriazis, A., Vahakoski, R. L., Santio, N. M., Arnaudova, R., Eerola, S. K., Rainio, E., Aumüller, I. B., Yli-Kauhaluoma, J., & Koskinen, P. J. (2013). Tricyclic benzo[cd]azulenes selectively inhibit activities of pim kinases and restrict growth of epstein-barr virus-transformed cells. PLoS ONE, 8(2), e55409.

Kirschner, A. N., Wang, J., van der Meer, R., Anderson, P. D., Franco-Coronel, O. E., Kushner, M. H., Everett, J. H., Hameed, O., Keeton, E. K., Ahdesmaki, M., Grosskurth, S. E., Huszar, D., & Abdulkadir, S. A. (2015). PIM kinase inhibitor AZD1208 for treatment of MYC-driven prostate cancer. Journal of the National Cancer Institute, 107(2), dju407.

Kisseleva, T., Bhattacharya, S., Braunstein, J., & Schindler, C. W. (2002). Signaling through the JAK/STAT pathway, recent advances and future challenges. Gene, 285(1), 1-24.

Klezovitch, O., Risk, M., Coleman, I., Lucas, J. M., Null, M., True, L. D., Nelson, P. S., & Vasioukhin, V. (2008). A causal role for ERG in neoplastic transformation of prostate epithelium. Proceedings of the National Academy of Sciences of the United States of America, 105(6), 2105-2110.

Knudson, A. G. (1971). Mutation and cancer: Statistical study of retinoblastoma. Proceedings of the National Academy of Sciences of the United States of America, 68(4), 820-823.

Knudson, A. G. (2001). Two genetic hits (more or less) to cancer. Nature Reviews Cancer, 1(2), 157-162.

Kollerup Madsen, B., Hilscher, M., Zetner, D., & Rosenberg, J. (2019). Adverse reactions of dimethyl sulfoxide in humans: A systematic review. F1000Research, 7, 1746.

Kontomanolis, E. N., Koutras, A., Syllaios, A., Schizas, D., Mastoraki, A., Garmpis, N., Diakosavvas, M., Angelou, K., Tsatsaris, G., Pagkalos, A., Ntounis, T., & Fasoulakis, Z. (2020). Role of Oncogenes and Tumor-suppressor Genes in Carcinogenesis: A Review. Anticancer research, 40(11), 6009-6015.

Kouvonen, P., Rainio, E., Suni, V., Koskinen, P., & Corthals, G. L. (2011). Enrichment and sequencing of phosphopeptides on indium tin oxide coated glass slides. Molecular bioSystems, 7(6), 1828-1837.

Kuhn, C., Frank, D., Will, R., Jaschinski, C., Frauen, R., Katus, H. A., & Frey, N. (2009). DYRK1A is a novel negative regulator of cardiomyocyte hypertrophy. The Journal of Biological Chemistry, 284(25), 17320-17327.

Kukreja, P., Abdel-Mageed, A. B., Mondal, D., Liu, K., & Agrawal, K. C. (2005). Up-regulation of CXCR4 expression in PC-3 cells by stromal-derived factor-1alpha (CXCL12) increases endothelial adhesion and transendothelial migration: Role of MEK/ERK signaling pathway-dependent NF-kappaB activation. Cancer Research, 65(21), 9891-9898.

Kumar, A., Mandiyan, V., Suzuki, Y., Zhang, C., Rice, J., Tsai, J., Artis, D. R., Ibrahim, P., & Bremer, R. (2005). Crystal structures of proto-oncogene kinase Pim1: A target of aberrant somatic hypermutations in diffuse large cell lymphoma. Journal of Molecular Biology, 348(1), 183-193.

Kuriyama, M., Wang, M. C., Lee, C. I., Papsidero, L. D., Killian, C. S., Inaji, H., Slack, N. H., Nishiura, T., Murphy, G. P., & Chu, T. M. (1981). Use of human prostate-specific antigen in monitoring prostate cancer. Cancer Research, 41(10), 3874-3876.

Lamouille, S., Xu, J., & Derynck, R. (2014). Molecular mechanisms of epithelial–mesenchymal transition. Nature Reviews. Molecular Cell Biology, 15(3), 178-196.

Lawrentschuk, N., & Perera, M. (2000). Benign prostate disorders. Endotext. South Dartmouth (MA): MDText.com, Inc.

Le, X., Antony, R., Razavi, P., Treacy, D. J., Luo, F., Ghandi, M., Castel, P., Scaltriti, M., Baselga, J., & Garraway, L. A. (2016). Systematic functional characterization of resistance to PI3K inhibition in breast cancer. Cancer Discovery, 6(10), 1134-1147.

Leinonen, K. A., Saramäki, O. R., Furusato, B., Kimura, T., Takahashi, H., Egawa, S., Suzuki, H., Keiger, K., Ho Hahm, S., Isaacs, W. B., Tolonen, T. T., Stenman, U., Tammela, T. L. J., Nykter, M., Bova, G. S., & Visakorpi, T. (2013). Loss of PTEN is associated with aggressive behavior in ERG-positive prostate cancer. Cancer Epidemiol Biomarkers Prev, 22(12), 2333.

Liang, C., & Li, Y. (2014). Use of regulators and inhibitors of pim-1, a serine/threonine kinase, for tumour therapy (review). Molecular Medicine Reports, 9(6), 2051-2060.

Linn, P., Kohno, S., Sheng, J., Kulathunga, N., Yu, H., Zhang, Z., Voon, D., et al. (2021). Targeting RB1 Loss in Cancers. Cancers, 13(15), 3737.

Lilja, H., Vickers, A. J., & Ulmert, D. (2008). Prostate-specific antigen and prostate cancer: Prediction, detection and monitoring. Nature Reviews. Cancer, 8(4), 268-278.

Lilly, M., Sandholm, J., Cooper, J. J., Koskinen, P. J., & Kraft, A. (1999). The PIM-1 serine kinase prolongs survival and inhibits apoptosis-related mitochondrial dysfunction in part through a bcl-2-dependent pathway. Oncogene, 18(27), 4022-4031.

Lin, B., Ferguson, C., White, J. T., Wang, S., Vessella, R., True, L. D., Hood, L., & Nelson, P. S. (1999). Prostate-localized and androgen-regulated expression of the membrane-bound serine protease TMPRSS2. Cancer Research, 59(17), 4180-4184.

Linn, D. E., Yang, X., Xie, Y., Alfano, A., Deshmukh, D., Wang, X., Shimelis, H., Chen, H., Li, W., Xu, K., Chen, M., & Qiu, Y. (2012). Differential regulation of androgen receptor by PIM-1 kinases via phosphorylation-dependent recruitment of distinct ubiquitin E3 ligases. The Journal of Biological Chemistry, 287(27), 22959-22968.

Littlepage, L. E., Sternlicht, M. D., Rougier, N., Phillips, J., Gallo, E., Yu, Y., Williams, K., Brenot, A., Gordon, J. I., & Werb, Z. (2010). Matrix metalloproteinases contribute distinct roles in neuroendocrine prostate carcinogenesis, metastasis, and angiogenesis progression. Cancer Research, 70(6), 2224-2234.

Liu, H., Wang, K., Chen, S., Sun, Q., Zhang, Y., Chen, L., & Sun, X. (2017). NFATc1 phosphorylation by DYRK1A increases its protein stability. PloS One, 12(2), e0172985.

Liu, W., Liu, X., Tian, L., Gao, Y., Liu, W., Chen, H., Jiang, X., Xu, Z., Ding, H., & Zhao, Q. (2021). Design, synthesis and biological evaluation of harmine derivatives as potent GSK-3β/DYRK1A dual inhibitors for the treatment of alzheimer's disease. European Journal of Medicinal Chemistry, 222, 113554.

Liu, Y., Liang, T., Qiu, X., Ye, X., Li, Z., Tian, B., & Yan, D. (2019). Down-Regulation of Nfatc1 Suppresses Proliferation, Migration, Invasion, and Warburg Effect in Prostate Cancer Cells. Medical science monitor: international medical journal of experimental and clinical research, 25, 1572–1581.

Lomas, D. J., & Ahmed, H. U. (2020). All change in the prostate cancer diagnostic pathway. Nature Reviews. Clinical Oncology, 17(6), 372-381.

López-Rodríguez, C., Aramburu, J., Rakeman, A. S., Copeland, N. G., Gilbert, D. J., Thomas, S., Disteche, C., Jenkins, N. A., & Rao, A. (1999). NF-AT5: The NF-AT family of transcription factors expands in a new direction. Cold Spring Harbor Symposia on Quantitative Biology, 64, 517-526.

Losman, J. A., Chen, X. P., Vuong, B. Q., Fay, S., & Rothman, P. B. (2003). Protein phosphatase 2A regulates the stability of pim protein kinases. The Journal of Biological Chemistry, 278(7), 4800-4805.

Luszczak, S., Kumar, C., Sathyadevan, V. K., Simpson, B. S., Gately, K. A., Whitaker, H. C., & Heavey, S. (2020a). PIM kinase inhibition: Co-targeted therapeutic approaches in prostate cancer. Signal Transduction and Targeted Therapy, 5(1), 7.

Luszczak, S., Simpson, B. S., Stopka-Farooqui, U., Sathyadevan, V. K., Echeverria, L. M. C., Kumar, C., Costa, H., Haider, A., Freeman, A., Jameson, C., Ratynska, M., Ben-Salha, I., Sridhar, A., Shaw, G., Kelly, J. D., Pye, H., Gately, K. A., Whitaker, H. C., & Heavey, S. (2020b). Co-targeting PIM and PI3K/mTOR using multikinase inhibitor AUM302 and a combination of AZD-1208 and BEZ235 in prostate cancer. Scientific Reports, 10(1), 14380.

Ma, J., Arnold, H. K., Lilly, M. B., Sears, R. C., & Kraft, A. S. (2007). Negative regulation of pim-1 protein kinase levels by the B56b subunit of PP2A. Oncogene, 26(35), 5145-5153.

Macdonald, A., Campbell, D. G., Toth, R., McLauchlan, H., Hastie, C. J., & Arthur, J. S. C. (2006). Pim kinases phosphorylate multiple sites on bad and promote 14-3-3 binding and dissociation from bcl-XL. BMC Cell Biology, 7, 1.

Macian, F. (2005). NFAT proteins: Key regulators of T-cell development and function. Nature Reviews. Immunology, 5(6), 472-484.

Madden, S. K., de Araujo, A. D., Gerhardt, M., Fairlie, D. P., & Mason, J. M. (2021). Taking the myc out of cancer: Toward therapeutic strategies to directly inhibit c-myc. Molecular Cancer, 20(1), 3.

Magi-Galluzzi, C. (2018). Prostate cancer: Diagnostic criteria and role of immunohistochemistry. Modern Pathology, 31(S1), 12.

Magistroni, V., Mologni, L., Sanselicio, S., Reid, J. F., Redaelli, S., Piazza, R., Viltadi, M., Bovo, G., Strada, G., Grasso, M., Gariboldi, M., & Gambacorti-Passerini, C. (2011). ERG deregulation induces PIM1 over-expression and aneuploidy in prostate epithelial cells. Plos One, 6(11), e28162.

Malinen, M., Jääskeläinen, T., Pelkonen, M., Heikkinen, S., Väisänen, S., Kosma, V., Nieminen, K., Mannermaa, A., & Palvimo, J. J. (2013). Proto-oncogene PIM-1 is a novel estrogen receptor target associating with high grade breast tumors. Molecular and Cellular Endocrinology, 365(2), 270-276.

Malone, T., Schäfer, L., Simon, N., Heavey, S., Cuffe, S., Finn, S., Moore, G., & Gately, K. (2020). Current perspectives on targeting PIM kinases to overcome mechanisms of drug resistance and immune evasion in cancer. Pharmacology & Therapeutics, 207, 107454.

Mancini, M., & Toker, A. (2009). NFAT proteins: Emerging roles in cancer progression. Nature Reviews.Cancer, 9(11), 810-820.

Manda, K. R., Tripathi, P., Hsi, A. C., Ning, J., Ruzinova, M. B., Liapis, H., Bailey, M., Zhang, H., Maher, C. A., Humphrey, P. A., Andriole, G. L., Ding, L., You, Z., & Chen, F. (2016). NFATc1 promotes prostate tumorigenesis and overcomes PTEN loss-induced senescence. Oncogene, 35(25), 3282-3292.

Maroni, P., Bendinelli, P., Matteucci, E., & Desiderio, M. A. (2007). HGF induces CXCR4 and CXCL12-mediated tumor invasion through Ets1 and NF-kappaB. Carcinogenesis, 28(2), 267-279.

Masuda, E. S., Naito, Y., Tokumitsu, H., Campbell, D., Saito, F., Hannum, C., Arai, K., & Arai, N. (1995). NFATx, a novel member of the nuclear factor of activated T cells family that is expressed predominantly in the thymus. Molecular and Cellular Biology, 15(5), 2697-2706.

Matikainen, S., Sareneva, T., Ronni, T., Lehtonen, A., Koskinen, P. J., & Julkunen, I. (1999a). Interferon-α activates multiple STAT proteins and upregulates proliferation-associated IL-2Rα, c-myc, and pim-1 genes in human T cells. Blood, 93(6), 1980-1991.

McAllister, M. J., McCall, P., Dickson, A., Underwood, M. A., Andersen, D., Holmes, E., Markert, E., Leung, H. Y., & Edwards, J. (2020). Androgen receptor phosphorylation at serine 81 and serine 213 in castrate-resistant prostate cancer. Prostate cancer and prostatic diseases, 23(4), 596–606.

McCaffrey, P. G., Luo, C., Kerppola, T. K., Jain, J., Badalian, T. M., Ho, A. M., Burgeon, E., Lane, W. S., Lambert, J. N., & Curran, T. (1993). Isolation of the cyclosporin-sensitive T cell transcription factor NFATp. Science (New York, N.Y.), 262(5134), 750-754.

McNeal, J. E., Redwine, E. A., Freiha, F. S., & Stamey, T. A. (1988). Zonal distribution of prostatic adenocarcinoma. correlation with histologic pattern and direction of spread. The American Journal of Surgical Pathology, 12(12), 897-906.

McNeal, J. E. (1981). The zonal anatomy of the prostate. The Prostate, 2(1), 35-49.

Medyouf, H., Alcalde, H., Berthier, C., Guillemin, M. C., dos Santos, N. R., Janin, A., Decaudin, D., de Thé, H., & Ghysdael, J. (2007). Targeting calcineurin activation as a therapeutic strategy for T-cell acute lymphoblastic leukemia. Nature Medicine, 13(6), 736-741.

Mikkers, H., Nawijn, M., Allen, J., Brouwers, C., Verhoeven, E., Jonkers, J., & Berns, A. (2004). Mice deficient for all PIM kinases display reduced body size and impaired responses to hematopoietic growth factors. Molecular and Cellular Biology, 24(13), 6104-6115.

Miyakawa, H., Woo, S. K., Dahl, S. C., Handler, J. S., & Kwon, H. M. (1999). Tonicity-responsive enhancer binding protein, a rel-like protein that stimulates transcription in response to hypertonicity. Proceedings of the National Academy of Sciences of the United States of America, 96(5), 2538-2542.

Mizuno, K., Shirogane, T., Shinohara, A., Iwamatsu, A., Hibi, M., & Hirano, T. (2001). Regulation of pim-1 by Hsp90. Biochemical and Biophysical Research Communications, 281(3), 663-669.

Moch, H., Cubilla, A. L., Humphrey, P. A., Reuter, V. E., & Ulbright, T. M. (2016). The 2016 WHO classification of tumours of the urinary system and male genital organs-part A: Renal, penile, and testicular tumours. European Urology, 70(1), 93-105.

Mochizuki, H., Matsubara, A., Teishima, J., Mutaguchi, K., Yasumoto, H., Dahiya, R., Usui, T., & Kamiya, K. (2004). Interaction of ligand-receptor system between stromal-cell-derived factor-1 and CXC chemokine receptor 4 in human prostate cancer: A possible predictor of metastasis. Biochemical and Biophysical Research Communications, 320(3), 656-663.

Mohamed, A. A., Xavier, C. P., Sukumar, G., Tan, S., Ravindranath, L., Seraj, N., Kumar, V., Sreenath, T., McLeod, D. G., Petrovics, G., Rosner, I. L., Srivastava, M., Strovel, J., Malhotra, S. V., LaRonde, N. A., Dobi, A., Dalgard, C. L., & Srivastava, S. (2018). Identification of a small molecule that selectively inhibits ERG-positive cancer cell growth. Cancer Research, 78(13), 3659-3671.

Mohlin, S., Hansson, K., Radke, K., Martinez, S., Blanco-Aparicio, C., Garcia-Ruiz, C., Welinder, C., Esfandyari, J., O'Neill, M., Pastor, J., von Stedingk, K., & Bexell, D. (2020). Anti-tumor effects of PIM/PI3K/mTOR triple kinase inhibitor IBL-302 in neuroblastoma. EMBO Molecular Medicine, 12(1), e11749.

Moilanen, A. M., Riikonen, R., Oksala, R., Ravanti, L., Aho, E., Wohlfahrt, G., Nykänen, P. S., Törmäkangas, O. P., Palvimo, J. J., & Kallio, P. J. (2015). Discovery of ODM-201, a new-generation androgen receptor inhibitor targeting resistance mechanisms to androgen signaling-directed prostate cancer therapies. Scientific reports, 5, 12007.

Mollica Poeta, V., Massara, M., Capucetti, A., & Bonecchi, R. (2019). Chemokines and Chemokine Receptors: New Targets for Cancer Immunotherapy. Frontiers in immunology, 10, 379.

Mologni, L., Magistroni, V., Casuscelli, F., Montemartini, M., & Gambacorti-Passerini, C. (2017). The novel PIM1 inhibitor NMS-P645 reverses PIM1-dependent effects on TMPRSS2/ERG positive prostate cancer cells and shows anti-proliferative activity in combination with PI3K inhibition. Journal of Cancer, 8(1), 140-145.

Mondello, P., Cuzzocrea, S., & Mian, M. (2014). Pim kinases in hematological malignancies: Where are we now and where are we going? Journal of Hematology & Oncology, 7, 95.

Moore, G., Lightner, C., Elbai, S., Brady, L., Nicholson, S., Ryan, R., O'Sullivan, K. E., O'Byrne, K. J., Blanco-Aparicio, C., Cuffe, S., O'Neill, M., Heavey, S., Finn, S. P., & Gately, K. (2021). Co-targeting PIM kinase and PI3K/mTOR in NSCLC. Cancers, 13(9), 2139.

Mori, M., Tintori, C., Christopher, R. S. A., Radi, M., Schenone, S., Musumeci, F., Brullo, C., Sanità, P., Delle Monache, S., Angelucci, A., Kissova, M., Crespan, E., Maga, G., & Botta, M. (2013). A combination strategy to inhibit pim-1: Synergism between noncompetitive and ATP-competitive inhibitors. ChemMedChem, 8(3), 484-496.

Mukherjee, D., & Zhao, J. (2013). The role of chemokine receptor CXCR4 in breast cancer metastasis. American Journal of Cancer Research, 3(1), 46-57.

Müller, M. R., & Rao, A. (2010). NFAT, immunity and cancer: A transcription factor comes of age. Nature Reviews. Immunology, 10(9), 645-656.

Nawijn, M. C., Alendar, A., & Berns, A. (2011). For better or for worse: The role of pim oncogenes in tumorigenesis. Nature Reviews. Cancer, 11(1), 23-34.

Northrop, J. P., Ho, S. N., Chen, L., Thomas, D. J., Timmerman, L. A., Nolan, G. P., Admon, A., & Crabtree, G. R. (1994). NF-AT components define a family of transcription factors targeted in T-cell activation. Nature, 369(6480), 497-502.

Okamura, H., Aramburu, J., García-Rodríguez, C., Viola, J. P., Raghavan, A., Tahiliani, M., Zhang, X., Qin, J., Hogan, P. G., & Rao, A. (2000). Concerted dephosphorylation of the transcription factor NFAT1 induces a conformational switch that regulates transcriptional activity. Molecular Cell, 6(3), 539-550.

Palaty, C. K., Clark-Lewis, I., Leung, D., & Pelech, S. L. (1997). Phosphorylation site substrate specificity determinants for the pim-1 protooncogene-encoded protein kinase. Biochemistry and Cell Biology = Biochimie Et Biologie Cellulaire, 75(2), 153-162.

Paschalis, A., Sharp, A., Welti, J. C., Neeb, A., Raj, G. V., Luo, J., Plymate, S. R., & de Bono, J. S. (2018). Alternative splicing in prostate cancer. Nature Reviews. Clinical Oncology, 15(11), 663-675.

Peltola, K. J., Paukku, K., Aho, T. L. T., Ruuska, M., Silvennoinen, O., & Koskinen, P. J. (2004). Pim-1 kinase inhibits STAT5-dependent transcription via its interactions with SOCS1 and SOCS3. Blood, 103(10), 3744-3750.

Peng, C., Knebel, A., Morrice, N. A., Li, X., Barringer, K., Li, J., Jakes, S., Werneburg, B., & Wang, L. (2007). Pim kinase substrate identification and specificity. Journal of Biochemistry, 141(3), 353-362.

Peng, S. L., Gerth, A. J., Ranger, A. M., & Glimcher, L. H. (2001). NFATc1 and NFATc2 together control both T and B cell activation and differentiation. Immunity, 14(1), 13-20.

Pernar CH, Ebot EM, Wilson KM, Mucci LA. The Epidemiology of Prostate Cancer. (2018). Cold Spring Harb Perspect Med. 8(12):a030361.

Petersen Shay, K., Wang, Z., Xing, P., McKenzie, I. F. C., & Magnuson, N. S. (2005). Pim-1 kinase stability is regulated by heat shock proteins and the ubiquitin-proteasome pathway. Molecular Cancer Research, 3(3), 170-181.

Pflueger, D., Rickman, D. S., Sboner, A., Perner, S., LaFargue, C. J., Svensson, M. A., Moss, B. J., Kitabayashi, N., Pan, Y., de la Taille, A., Kuefer, R., Tewari, A. K., Demichelis, F., Chee, M. S., Gerstein, M. B., & Rubin, M. A. (2009). N-myc downstream regulated gene 1 (NDRG1) is fused to ERG in prostate cancer. Neoplasia (New York, N.Y.), 11(8), 804-811.

Pircher, T. J., Zhao, S., Geiger, J. N., Joneja, B., & Wojchowski, D. M. (2000). Pim-1 kinase protects hematopoietic FDC cells from genotoxin-induced death. Oncogene, 19(32), 3684-3692.

Qian, K. C., Wang, L., Hickey, E. R., Studts, J., Barringer, K., Peng, C., Kronkaitis, A., Li, J., White, A., Mische, S., & Farmer, B. (2005). Structural basis of constitutive activity and a unique nucleotide binding mode of human pim-1 kinase. The Journal of Biological Chemistry, 280(7), 6130-6137.

Qin, J., Nag, S., Wang, W., Zhou, J., Zhang, W., Wang, H., & Zhang, R. (2014). NFAT as cancer target: Mission possible? Biochimica Et Biophysica Acta, 1846(2), 297-311.

Qin, L., Chen, X., Wu, Y., Feng, Z., He, T., Wang, L., Liao, L., & Xu, J. (2011). Steroid receptor coactivator-1 upregulates integrin αs expression to promote breast cancer cell adhesion and migration. Cancer Research, 71(5), 1742-1751.

Qu, Y., Zhang, C., Du, E., Wang, A., Yang, Y., Guo, J., Wang, A., Zhang, Z., & Xu, Y. (2016). Pim-3 is a critical risk factor in development and prognosis of prostate cancer. Medical Science Monitor: International Medical Journal of Experimental and Clinical Research, 22, 4254-4260.

Quigley, D. A., Dang, H. X., Zhao, S. G., Lloyd, P., Aggarwal, R., Alumkal, J. J., Foye, A., Kothari, V., Perry, M. D., Bailey, A. M., Playdle, D., Barnard, T. J., Zhang, L., Zhang, J., Youngren, J. F., Cieslik, M. P., Parolia, A., Beer, T. M., Thomas, G., Chi, K. N., Gleave, M., Lack, N. A., Zoubeidi, A., Reiter, R. E., Rettig, M. B., Witte, O., Ryan, C. J., Fong, L., Kim, W., Friedlander, T., Chou, J., Li, H., Das, R., Li, H., Moussavi-Baygi, R., Goodarzi, H., Gilbert, L. A., Lara, P. N., Evans, C. P., Goldstein, T. C., Stuart, J. M., Tomlins, S. A., Spratt, D. E., Cheetham, R. K., Cheng, D. T., Farh, K., Gehring, J. S., Hakenberg, J., Liao, A., Febbo, P. G., Shon, J., Sickler, B., Batzoglou, S., Knudsen, K. E., He, H. H., Huang, J., Wyatt, A. W., Dehm, S. M., Ashworth, A., Chinnaiyan, A. M., Maher, C. A., Small, E. J., & Feng, F. Y. (2018). Genomic hallmarks and structural variation in metastatic prostate cancer. Cell, 174(3), 758-769.e9.

Raab, M. S., Thomas, S. K., Ocio, E. M., Guenther, A., Goh, Y. T., Talpaz, M., Hohmann, N., Zhao, S., Xiang, F., Simon, C., Vanasse, K. G., & Kumar, S. K. (2019). The first-in-human study of the pan-PIM kinase inhibitor PIM447 in patients with relapsed and/or refractory multiple myeloma. Leukemia, 33, 2924-2933.

Rainio, E., Sandholm, J., & Koskinen, P. (2002). Cutting edge: Transcriptional activity of NFATc1 is enhanced by the pim-1 kinase. The Journal of Immunology, 168(4), 1524.

Rao, A., Luo, C., & Hogan, P. G. (1997). Transcription factors of the NFAT family: Regulation and function. Annual Review of Immunology, 15, 707-747.

Rawla, P. (2019). Epidemiology of prostate cancer. World Journal of Oncology, 10(2), 63-89.
Ren, K., Gou, X., Xiao, M., He, W., & Kang, J. (2019). Pim-2 cooperates with downstream factor XIAP to inhibit apoptosis and intensify malignant grade in prostate cancer. Pathology Oncology Research : POR, 25(1), 341-348.
Ren, K., Gou, X., Xiao, M., Wang, M., Liu, C., Tang, Z., & He, W. (2013). The over-expression of pim-2 promote the tumorigenesis of prostatic carcinoma through phosphorylating eIF4B. The Prostate, 73(13), 1462-1469.
Ritchie, M. E., Phipson, B., Wu, D., Hu, Y., Law, C. W., Shi, W., & Smyth, G. K. (2015). Limma powers differential expression analyses for RNA-sequencing and microarray studies. Nucleic Acids Research, 43(7), e47.
Robinson, D., Van Allen, E. M., Wu, Y., Schultz, N., Lonigro, R. J., Mosquera, J., Montgomery, B., Taplin, M., Pritchard, C. C., Attard, G., Beltran, H., Abida, W., Bradley, R. K., Vinson, J., Cao, X., Vats, P., Kunju, L. P., Hussain, M., Feng, F. Y., Tomlins, S. A., Cooney, K. A., Smith, D. C., Brennan, C., Siddiqui, J., Mehra, R., Chen, Y., Rathkopf, D. E., Morris, M. J., Solomon, S. B., Durack, J. C., Reuter, V. E., Gopalan, A., Gao, J., Loda, M., Lis, R. T., Bowden, M., Balk, S. P., Gaviola, G., Sougnez, C., Gupta, M., Yu, E. Y., Mostaghel, E. A., Cheng, H. H., Mulcahy, H., True, L. D., Plymate, S. R., Dvinge, H., Ferraldeschi, R., Flohr, P., Miranda, S., Zafeiriou, Z., Tunariu, N., Mateo, J., Perez-Lopez, R., Demichelis, F., Robinson, B. D., Schiffman, M., Nanus, D. M., Tagawa, S. T., Sigaras, A., Eng, K. W., Elemento, O., Sboner, A., Heath, E. I., Scher, H. I., Pienta, K. J., Kantoff, P., de Bono, J. S., Rubin, M. A., Nelson, P. S., Garraway, L. A., Sawyers, C. L., & Chinnaiyan, A. M. (2015). Integrative clinical genomics of advanced prostate cancer. Cell, 161(5), 1215-1228.
Rodrigues, G., Warde, P., Pickles, T., Crook, J., Brundage, M., Souhami, L., & Lukka, H. (2012). Pre-treatment risk stratification of prostate cancer patients: A critical review. Canadian Urological Association Journal, 6(2), 121-127.
Ruff, S. E., Vasilyev, N., Nudler, E., Logan, S. K., & Garabedian, M. J. (2021). PIM1 phosphorylation of the androgen receptor and 14-3-3 ζ regulates gene transcription in prostate cancer. Communications Biology, 4, 1221.
Ruohola, J. K., Valve, E. M., Karkkainen, M. J., Joukov, V., Alitalo, K., & Härkönen, P. L. (1999). Vascular endothelial growth factors are differentially regulated by steroid hormones and antiestrogens in breast cancer cells. Molecular and Cellular Endocrinology, 149(1-2), 29-40.
Ryeom, S., Baek, K., Rioth, M. J., Lynch, R. C., Zaslavsky, A., Birsner, A., Yoon, S. S., & McKeon, F. (2008). Targeted deletion of the calcineurin inhibitor DSCR1 suppresses tumor growth. Cancer Cell, 13(5), 420-431.
Sandhu, S., Moore, C. M., Chiong, E., Beltran, H., Bristow, R. G., & Williams, S. G. (2021). Prostate cancer. The Lancet, 398(10305), 1075-1090.
Saris, C. J., Domen, J., & Berns, A. (1991). The pim-1 oncogene encodes two related protein-serine/threonine kinases by alternative initiation at AUG and CUG. The EMBO Journal, 10(3), 655-664.
Santio, N. M., & Koskinen, P. J. (2017). PIM kinases: From survival factors to regulators of cell motility. The International Journal of Biochemistry & Cell Biology, 93, 74-85.
Santio, N. M., Salmela, M., Arola, H., Eerola, S. K., Heino, J., Rainio, E., & Koskinen, P. J. (2016). The PIM1 kinase promotes prostate cancer cell migration and adhesion via multiple signalling pathways. Experimental Cell Research, 342(2), 113-124.
Santio, N. M., Vahakoski, R. L., Rainio, E., Sandholm, J. A., Virtanen, S. S., Prudhomme, M., Anizon, F., Moreau, P., & Koskinen, P. J. (2010). Pim-selective inhibitor DHPCC-9 reveals pim kinases as potent stimulators of cancer cell migration and invasion. Molecular Cancer, 9, 279.
Sedarsky, J., Degon, M., Srivastava, S., & Dobi, A. (2018). Ethnicity and ERG frequency in prostate cancer. Nature Reviews. Urology, 15(2), 125-131.
Seifert, A., Rau, S., Küllertz, G., Fischer, B., & Santos, A. N. (2009). TCDD induces cell migration via NFATc1/ATX-signaling in MCF-7 cells. Toxicology Letters, 184(1), 26-32.

Shaw, J. P., Utz, P. J., Durand, D. B., Toole, J. J., Emmel, E. A., & Crabtree, G. R. (1988). Identification of a putative regulator of early T cell activation genes. Science (New York, N.Y.), 241(4862), 202-205.

Sheridan, C. M., Heist, E. K., Beals, C. R., Crabtree, G. R., & Gardner, P. (2002). Protein kinase A negatively modulates the nuclear accumulation of NF-ATc1 by priming for subsequent phosphorylation by glycogen synthase kinase-3. The Journal of Biological Chemistry, 277(50), 48664-48676.

Sherr, C. J. (2004). Principles of tumor suppression. Cell, 116(2), 235-246.

Sieber, M., Karanik, M., Brandt, C., Blex, C., Podtschaske, M., Erdmann, F., Rost, R., Serfling, E., Liebscher, J., Pätzel, M., Radbruch, A., Fischer, G., & Baumgrass, R. (2007). Inhibition of calcineurin-NFAT signaling by the pyrazolopyrimidine compound NCI3. European Journal of Immunology, 37(9), 2617-2626.

Siegel, R., DeSantis, C., Virgo, K., Stein, K., Mariotto, A., Smith, T., Cooper, D., Gansler, T., Lerro, C., Fedewa, S., Lin, C., Leach, C., Cannady, R. S., Cho, H., Scoppa, S., Hachey, M., Kirch, R., Jemal, A., & Ward, E. (2012). Cancer treatment and survivorship statistics, 2012. CA: A Cancer Journal for Clinicians, 62(4), 220-241.

Singareddy, R., Semaan, L., Conley-LaComb, M. K., St. John, J., Powell, K., Iyer, M., Smith, D., Heilbrun, L. K., Shi, D., Sakr, W., Cher, M. L., & Chinni, S. R. (2013). Transcriptional regulation of CXCR4 in prostate cancer: Significance of TMPRSS2-ERG fusions. Molecular Cancer Research, 11(11), 1349-1361.

Singh, S., Singh, U. P., Grizzle, W. E., & Lillard, J. W. (2004). CXCL12-CXCR4 interactions modulate prostate cancer cell migration, metalloproteinase expression and invasion. Laboratory Investigation; a Journal of Technical Methods and Pathology, 84(12), 1666-1676.

Song, J. H., Singh, N., Luevano, L. A., Padi, S. K. R., Okumura, K., Olive, V., Black, S. M., Warfel, N. A., Goodrich, D. W., & Kraft, A. S. (2018). Mechanisms behind resistance to PI3K inhibitor treatment induced by the PIM kinase. Molecular Cancer Therapeutics, 17(12), 2710-2721.

Stephenson, R. A., Dinney, C. P., Gohji, K., Ordóñez, N. G., Killion, J. J., & Fidler, I. J. (1992). Metastatic model for human prostate cancer using orthotopic implantation in nude mice. Journal of the National Cancer Institute, 84(12), 951-957.

Ström P., Nordström T., Aly M., Egevad L., Grönberg H., Eklund M. (2018). The Stockholm-3 Model for Prostate Cancer Detection: Algorithm Update, Biomarker Contribution, and Reflex Test Potential. European Urology, 74(2), 204-210.

Sung, H., Ferlay, J., Siegel, R. L., Laversanne, M., Soerjomataram, I., Jemal, A., & Bray, F. (2021). Global cancer statistics 2020: GLOBOCAN estimates of incidence and mortality worldwide for 36 cancers in 185 countries. CA: A Cancer Journal for Clinicians, 71(3), 209-249.

Sun, Y., Fang, M., Wang, J., Cooper, C. R., Pienta, K. J., & Taichman, R. S. (2007). Expression and activation of alpha v beta 3 integrins by SDF-1/CXC12 increases the aggressiveness of prostate cancer cells. The Prostate, 67(1), 61-73.

Sun, Y., Wang, J., Shelburne, C. E., Lopatin, D. E., Chinnaiyan, A. M., Rubin, M. A., Pienta, K. J., & Taichman, R. S. (2003). Expression of CXCR4 and CXCL12 (SDF-1) in human prostate cancers (PCa) in vivo. Journal of Cellular Biochemistry, 89(3), 462-473.

Taichman, R. S., Cooper, C., Keller, E. T., Pienta, K. J., Taichman, N. S., & McCauley, L. K. (2002). Use of the stromal cell-derived factor-1/CXCR4 pathway in prostate cancer metastasis to bone. Cancer Research, 62(6), 1832-1837.

Taylor, B. S., Schultz, N., Hieronymus, H., Gopalan, A., Xiao, Y., Carver, B. S., Arora, V. K., Kaushik, P., Cerami, E., Reva, B., Antipin, Y., Mitsiades, N., Landers, T., Dolgalev, I., Major, J. E., Wilson, M., Socci, N. D., Lash, A. E., Heguy, A., Eastham, J. A., Scher, H. I., Reuter, V. E., Scardino, P. T., Sander, C., Sawyers, C. L., & Gerald, W. L. (2010). Integrative genomic profiling of human prostate cancer (2010/06/24 ed.)

te Riele, H., Maandag, E. R., Clarke, A., Hooper, M., & Berns, A. (1990). Consecutive inactivation of both alleles of the pim-1 proto-oncogene by homologous recombination in embryonic stem cells. Nature, 348(6302), 649-651.

Teicher, B. A., & Fricker, S. P. (2010). CXCL12 (SDF-1)/CXCR4 pathway in cancer. Clinical Cancer Research: An Official Journal of the American Association for Cancer Research, 16(11), 2927-2931.

Teo, M. Y., Rathkopf, D. E., & Kantoff, P. (2019). Treatment of advanced prostate cancer. Annual Review of Medicine, 70(1), 479-499.

Thomas, M., Lange-Grünweller, K., Weirauch, U., Gutsch, D., Aigner, A., Grünweller, A., & Hartmann, R. K. (2012). The proto-oncogene pim-1 is a target of miR-33a. Oncogene, 31(7), 918-928.

Tolcher, A. W., Papadopoulos, K. P., Patnaik, A., Rasco, D. W., Martinez, D., Wood, D. L., Fielman, B., Sharma, M., Janisch, L. A., Brown, B. D., Bhargava, P., & Ratain, M. J. (2015). Safety and activity of DCR-MYC, a first-in-class dicer-substrate small interfering RNA (DsiRNA) targeting MYC, in a phase I study in patients with advanced solid tumors. Journal of Clinical Oncology, 33(15_suppl), 11006-11006.

Tomlins, S. A., Laxman, B., Varambally, S., Cao, X., Yu, J., Helgeson, B. E., Cao, Q., Prensner, J. R., Rubin, M. A., Shah, R. B., Mehra, R., & Chinnaiyan, A. M. (2008). Role of the TMPRSS2-ERG gene fusion in prostate cancer. Neoplasia (New York, N.Y.), 10(2), 177-188.

Tomlins, S. A., Rhodes, D. R., Perner, S., Dhanasekaran, S. M., Mehra, R., Sun, X., Varambally, S., Cao, X., Tchinda, J., Kuefer, R., Lee, C., Montie, J. E., Shah, R. B., Pienta, K. J., Rubin, M. A., & Chinnaiyan, A. M. (2005). Recurrent fusion of TMPRSS2 and ETS transcription factor genes in prostate cancer. Science, 310(5748), 644.

Tuomela, J. M., Valta, M. P., Väänänen, K., & Härkönen, P. L. (2008). Alendronate decreases orthotopic PC-3 prostate tumor growth and metastasis to prostate-draining lymph nodes in nude mice. BMC Cancer, 8, 81.

Tuomela, J., Valta, M., Seppänen, J., Tarkkonen, K., Väänänen, H. K., & Härkönen, P. (2009). Overexpression of vascular endothelial growth factor C increases growth and alters the metastatic pattern of orthotopic PC-3 prostate tumors. BMC Cancer, 9, 362.

Urological Illustrations by Fairman Studios for American Urological Association patient education materials. (2021). This Article was last updated on: July 18, 2020. The prostate gland - medika life: Understanding human anatomy: https://medika.life/the-prostate-gland/: September 29, 2021.

Vaarala, M. H., Porvari, K., Kyllönen, A., Lukkarinen, O., & Vihko, P. (2001). The TMPRSS2 gene encoding transmembrane serine protease is overexpressed in a majority of prostate cancer patients: Detection of mutated TMPRSS2 form in a case of aggressive disease. International Journal of Cancer, 94(5), 705-710.

Valdman, A., Fang, X., Pang, S., Ekman, P., & Egevad, L. (2004). Pim-1 expression in prostatic intraepithelial neoplasia and human prostate cancer. The Prostate, 60(4), 367-371.

van der Poel, H. G., Zevenhoven, J., & Bergman, A. M. (2010). Pim1 regulates androgen-dependent survival signaling in prostate cancer cells. Urologia Internationalis, 84(2), 212-220.

van Lohuizen, M., Verbeek, S., Krimpenfort, P., Domen, J., Saris, C., Radaszkiewicz, T., & Berns, A. (1989). Predisposition to lymphomagenesis in pim-1 transgenic mice: Cooperation with c-myc and N-myc in murine leukemia virus-induced tumors. Cell, 56(4), 673-682.

Virtanen, S. S., Väänänen, H. K., Härkönen, P. L., & Lakkakorpi, P. T. (2002). Alendronate inhibits invasion of PC-3 prostate cancer cells by affecting the mevalonate pathway. Cancer Research, 62(9), 2708-2714.

Vivanco, I., & Sawyers, C. L. (2002). The phosphatidylinositol 3-Kinase–AKT pathway in human cancer. Nature Reviews Cancer, 2(7), 489-501.

Waltering, K. K., Urbanucci, A., & Visakorpi, T. (2012). Androgen receptor (AR) aberrations in castration-resistant prostate cancer. Molecular and Cellular Endocrinology, 360(1-2), 38-43.

Wang, G., Zhao, D., Spring, D. J., & DePinho, R. A. (2018). Genetics and biology of prostate cancer. Genes Development, 32(17-18), 1105-1140.

Wang, M. C., Valenzuela, L. A., Murphy, G. P., & Chu, T. M. (1979). Purification of a human prostate specific antigen. Investigative Urology, 17(2), 159-163.

Warfel, N. A., & Kraft, A. S. (2015). PIM kinase (and akt) biology and signaling in tumors. Pharmacology & Therapeutics, 151, 41-49.

Weaver, R. P., Noble, M. J., & Weigel, J. W. (1991). Correlation of ultrasound guided and digitally directed transrectal biopsies of palpable prostatic abnormalities. The Journal of Urology, 145(3), 516-518.

Winkler, J., Abisoye-Ogunniyan, A., Metcalf, K. J., & Werb, Z. (2020). Concepts of extracellular matrix remodelling in tumour progression and metastasis. Nature communications, 11(1), 5120.

Wong, A. W., Paulson, Q. X., Hong, J., Stubbins, R. E., Poh, K., Schrader, E., & Nunez, N. P. (2011). Alcohol promotes breast cancer cell invasion by regulating the Nm23-ITGA5 pathway. Journal of Experimental & Clinical Cancer Research: CR, 30(1), 75.

Wood, M., Fudge, K., Mohler, J. L., Frost, A. R., Garcia, F., Wang, M., & Stearns, M. E. (1997). In situ hybridization studies of metalloproteinases 2 and 9 and TIMP-1 and TIMP-2 expression in human prostate cancer. Clinical & Experimental Metastasis, 15(3), 246-258.

Xiong, J., Yan, L., Zou, C., Wang, K., Chen, M., Xu, B., Zhou, Z., & Zhang, D. (2021). Integrins regulate stemness in solid tumor: an emerging therapeutic target. Journal of hematology & oncology, 14(1), 177.

Xu, Y., Zhang, T., Tang, H., Zhang, S., Liu, M., Ren, D., & Niu, Y. (2005). Overexpression of PIM-1 is a potential biomarker in prostate carcinoma. Journal of Surgical Oncology, 92(4), 326-330.

Yadav, A. K., Kumar, V., Bailey, D. B., & Jang, B. (2019). AZD1208, a pan-pim kinase inhibitor, has anti-growth effect on 93T449 human liposarcoma cells via control of the expression and phosphorylation of pim-3, mTOR, 4EBP-1, S6, STAT-3 and AMPK. International Journal of Molecular Sciences, 20(2)

Yan, B., Zemskova, M., Holder, S., Chin, V., Kraft, A., Koskinen, P. J., & Lilly, M. (2003). The PIM-2 kinase phosphorylates BAD on serine 112 and reverses BAD-induced cell death. The Journal of Biological Chemistry, 278(46), 45358-45367.

Yang, J., Nie, J., Ma, X., Wei, Y., Peng, Y., & Wei, X. (2019). Targeting PI3K in cancer: Mechanisms and advances in clinical trials. Molecular Cancer, 18(1), 26.

Ye, C., Zhang, C., Huang, H., Yang, B., Xiao, G., Kong, D., Tian, Q., Song, Q., Song, Y., Tan, H., Wang, Y., Zhou, T., Zi, X., & Sun, Y. (2018). The natural compound myricetin effectively represses the malignant progression of prostate cancer by inhibiting PIM1 and disrupting the PIM1/CXCR4 interaction. Cellular Physiology and Biochemistry, 48(3), 1230-1244.

Ylipää, A., Kivinummi, K., Kohvakka, A., Annala, M., Latonen, L., Scaravilli, M., Kartasalo, K., Leppänen, S., Karakurt, S., Seppälä, J., Yli-Harja, O., Tammela, T. L. J., Zhang, W., Visakorpi, T., & Nykter, M. (2015). Transcriptome sequencing reveals PCAT5 as a novel ERG-regulated long noncoding RNA in prostate cancer. Cancer Research, 75(19), 4026-4031.

Yu, J., Yu, J., Mani, R., Cao, Q., Brenner, C. J., Cao, X., Wang, X., Wu, L., Li, J., Hu, M., Gong, Y., Cheng, H., Laxman, B., Vellaichamy, A., Shankar, S., Li, Y., Dhanasekaran, S. M., Morey, R., Barrette, T., Lonigro, R. J., Tomlins, S. A., Varambally, S., Qin, Z. S., & Chinnaiyan, A. M. (2010). An integrated network of androgen receptor, polycomb, and TMPRSS2-ERG gene fusions in prostate cancer progression. Cancer Cell, 17(5), 443-454.

Zakut-Houri, R., Hazum, S., Givol, D., & Telerman, A. (1987). The cDNA sequence and gene analysis of the human pim oncogene. Gene, 54(1), 105-111.

Zemskova, M., Sahakian, E., Bashkirova, S., & Lilly, M. (2008). The PIM1 kinase is a critical component of a survival pathway activated by docetaxel and promotes survival of docetaxel-treated prostate cancer cells. The Journal of Biological Chemistry, 283(30), 20635-20644.

Zhang, F., Beharry, Z. M., Harris, T. E., Lilly, M. B., Smith, C. D., Mahajan, S., & Kraft, A. S. (2009). PIM1 protein kinase regulates PRAS40 phosphorylation and mTOR activity in FDCP1 cells. Cancer Biology & Therapy, 8(9), 846-853.

Zhang, J., Feng, H., Zhao, J., Feldman, E. R., Chen, S., Yuan, W., Huang, C., Akbari, O., Tibbetts, S. A., & Feng, P. (2016). IκB kinase ε is an NFATc1 kinase that inhibits T cell immune response. Cell Reports, 16(2), 405-418.

Zhang, X., Song, M., Kundu, J. K., Lee, M., & Liu, Z. (2018). PIM kinase as an executional target in cancer. Journal of Cancer Prevention, 23(3), 109-116.

Zhang, Y., Wang, Z., Li, X., & Magnuson, N. S. (2008). Pim kinase-dependent inhibition of c-myc degradation. Oncogene, 27(35), 4809-4819.

Zhao, Y., Hamza, M. S., Leong, H. S., Lim, C. -., Pan, Y. -., Cheung, E., Soo, K. -., & Iyer, N. G. (2008). Kruppel-like factor 5 modulates p53-independent apoptosis through Pim1 survival kinase in cancer cells. Oncogene, 27(1), 1-8.

Zhong, W., Han, Z., He, H., Bi, X., Dai, Q., Zhu, G., Ye, Y., Liang, Y., Qin, W., Zhang, Z., Zeng, G., & Chen, Z. (2008). CD147, MMP-1, MMP-2 and MMP-9 protein expression as significant prognostic factors in human prostate cancer. Oncology, 75(3-4), 230-236.

Zhou, Y., Cao, H., Li, W., & Zhao, L. (2018). The CXCL12 (SDF-1)/CXCR4 chemokine axis: Oncogenic properties, molecular targeting, and synthetic and natural product CXCR4 inhibitors for cancer therapy. Chinese Journal of Natural Medicines, 16(11), 801-810.

Zhu, N., Ramirez, L. M., Lee, R. L., Magnuson, N. S., Bishop, G. A., & Gold, M. R. (2002). CD40 signaling in B cells regulates the expression of the pim-1 kinase via the NF-kappa B pathway. Journal of Immunology (Baltimore, Md.: 1950), 168(2), 744-754.

Zippo, A., De Robertis, A., Serafini, R., & Oliviero, S. (2007). PIM1-dependent phosphorylation of histone H3 at serine 10 is required for MYC-dependent transcriptional activation and oncogenic transformation. Nature Cell Biology, 9(8), 932-944.

Zlotnik, A., Burkhardt, A. & Homey, B. (2011). Homeostatic chemokine receptors and organ-specific metastasis. Nature Reviews Immunology, 11, 597–606.

PUBLICATIONS

Publication I Santio NM, Eerola SK, Paatero I, Yli-Kauhaluoma J, Anizon F, Moreau P, Tuomela J, Härkönen P, Koskinen PJ. Pim kinases promote migration and metastatic growth of prostate cancer xenografts by employing the CXCL12/CXCR4 pathway. PLOS One, 2015; 10(6): e0130340.

Publication II Eerola SK, Santio NM, Rinne S, Kouvonen P, Corthals G, Scaravilli M, Scala G, Serra A, Greco D, Ruusuvuori P, Rainio EM, Latonen L, Visakorpi T, Koskinen PJ. Phosphorylation of NFATC1 at multiple sites is essential for its ability to promote prostate cancer cell migration and invasion. Cell Communication and Signaling, 2019; 17(1):148.

Publication III Eerola SK, Kohvakka A, Tammela TLJ, Koskinen PJ, Latonen L, Visakorpi T. Expression and ERG-regulation of PIM kinases in prostate cancer. Cancer Medicine, 2021; 10(10):3427-3436.

PUBLICATION I

Pim kinases promote migration and metastatic growth of prostate cancer xenografts by employing the CXCL12/CXCR4 pathway

Santio NM, Eerola SK, Paatero I, Yli-Kauhaluoma J, Anizon F, Moreau P, Tuomela J, Härkönen P, Koskinen PJ

PLOS One, 2015; 10(6): e0130340
DOI: 10.1371/journal.pone.0130340

PLOS | ONE

RESEARCH ARTICLE

Pim Kinases Promote Migration and Metastatic Growth of Prostate Cancer Xenografts

Niina M. Santio[1,2], Sini K. Eerola[1], Ilkka Paatero[3], Jari Yli-Kauhaluoma[4], Fabrice Anizon[5,6], Pascale Moreau[5,6], Johanna Tuomela[7,8], Pirkko Härkönen[7], Päivi J. Koskinen[1]*

1 Section of Genetics and Physiology, Department of Biology, University of Turku, 20500 Turku, Finland, **2** Drug Research Doctoral Programme, University of Turku, 20520 Turku, Finland, **3** Institute of Biomedicine, Department of Medical Biochemistry and Genetics, University of Turku, 20520 Turku, Finland, **4** Division of Pharmaceutical Chemistry and Technology, Faculty of Pharmacy, University of Helsinki, 00014 Helsinki, Finland, **5** Institut de Chimie de Clermont-Ferrand, Université Clermont Auvergne, Université Blaise Pascal, 63000 Clermont-Ferrand, France, **6** Centre National de la Recherche Scientifique, 63178 Aubiere, France, **7** Institute of Biomedicine, Department of Cell Biology and Anatomy, University of Turku, 20520 Turku, Finland, **8** Pharmatest Services Ltd, 20520 Turku, Finland

* paivi.koskinen@utu.fi

OPEN ACCESS

Citation: Santio NM, Eerola SK, Paatero I, Yli-Kauhaluoma J, Anizon F, Moreau P, et al. (2015) Pim Kinases Promote Migration and Metastatic Growth of Prostate Cancer Xenografts. PLoS ONE 10(6): e0130340. doi:10.1371/journal.pone.0130340

Academic Editor: Jeffrey K. Harrison, University of Florida, UNITED STATES

Received: November 20, 2014

Accepted: May 19, 2015

Published: June 15, 2015

Data Availability Statement: All relevant data are within the paper and its Supporting Information files.

Funding: This work was supported by the Academy of Finland (grant 121533 to PJK, grant 269541 to PH), TULI Program of the University of Turku (PJK), Sigrid Jusélius Foundation (PH), FinPharma Doctoral Program (NMS), Emil Aaltonen Foundation (NMS), Cancer Organizations for the Western Finland (NMS), Orion-Farmos Research Foundation (NMS), Finnish Cultural Foundation (NMS), Turku University Foundation (SKE), and Walter och Lisi Wahls Stiftelse för Naturvetenskaplig Forskning (JYK). The funders had no role in study design, data collection

Abstract

Background and methods

Pim family proteins are oncogenic kinases implicated in several types of cancer and involved in regulation of cell proliferation, survival as well as motility. Here we have investigated the ability of Pim kinases to promote metastatic growth of prostate cancer cells in two xenograft models for human prostate cancer. We have also evaluated the efficacy of Pim-selective inhibitors to antagonize these effects.

Results

We show here that tumorigenic growth of both subcutaneously and orthotopically inoculated prostate cancer xenografts is enhanced by stable overexpression of either Pim-1 or Pim-3. Moreover, Pim-overexpressing orthotopic prostate tumors are highly invasive and able to migrate not only to the nearby prostate-draining lymph nodes, but also into the lungs to form metastases. When the xenografted mice are daily treated with the Pim-selective inhibitor DHPCC-9, both the volumes as well as the metastatic capacity of the tumors are drastically decreased. Interestingly, the Pim-promoted metastatic growth of the orthotopic xenografts is associated with enhanced angiogenesis and lymphangiogenesis. Furthermore, forced Pim expression also increases phosphorylation of the CXCR4 chemokine receptor, which may enable the tumor cells to migrate towards tissues such as the lungs that express the CXCL12 chemokine ligand.

and analysis, decision to publish, or preparation of the manuscript. Johanna Tuomela was employed by Pharmatest Services Ltd for a period during the study. Pharmatest did not have any additional role in the study design, data collection and analysis, decision to publish, or preparation of the manuscript. The specific role of JT is articulated in the 'author contributions' section.

Competing Interests: Johanna Tuomela was employed by Pharmatest Services Ltd for a period during the study. There are no patents, products in development, or marketed products to declare. This does not alter JT's adherence to all the PLOS ONE policies on sharing data and materials. Pirkko Härkönen is a PLOS ONE Editorial Board member, but this does not alter the authors' adherence to PLOS ONE policies on sharing data and materials.

Conclusions

Our results indicate that Pim overexpression enhances the invasive properties of prostate cancer cells *in vivo*. These effects can be reduced by the Pim-selective inhibitor DHPCC-9, which can reach tumor tissues without serious side effects. Thus, Pim-targeting therapies with DHPCC-9-like compounds may help to prevent progression of local prostate carcinomas to fatally metastatic malignancies.

Introduction

The *pim* family genes were first identified as proviral integration sites for Moloney murine leukemia virus [1], but have later been shown to be involved in development of human lymphoid malignancies as well as solid tumors [2]. The proteins encoded by the three *pim* family genes are serine/threonine-specific kinases that have been shown to promote tumorigenesis by increasing both proliferation and survival of cells [2,3]. More recently, we and others have also implicated them in the regulation of migration and invasion of adherent cancer cells [4–6], while results from clinical studies show association of abnormally high levels of Pim kinases with more malignant cancers of epithelial origin [7–9].

Because of their emerging roles in cancer development, Pim kinases have become highly attractive as therapeutic targets [10–12]. There are also physiological and structural reasons to justify Pim kinases as drug targets. First, inactivation of Pim kinases is not expected to cause serious side effects, since mice deficient for all three Pim family members are viable [13]. Secondly, unique structural features within the hinge region connecting the N- and C-terminal lobes around the ATP-binding pocket render the Pim kinases constitutively active and enable design of highly selective inhibitors [14]. We have recently identified potent and selective Pim kinase inhibitors within two structurally unrelated groups of compounds, tetracyclic pyrrolocarbazoles [15] and tricyclic benzo[*cd*]azulenes [16]. We have also functionally validated them in both *in vitro* and cell-based assays [6, 17].

Tumor xenografts provide excellent physiological settings for preclinical proof-of-concept studies, both to identify therapeutic targets and to evaluate *in vivo* efficacy of compounds targeting them. Subcutaneous inoculation of PC-3 prostate cancer cells overexpressing either Pim-1 or Pim-2 into immunodeficient mice has previously been shown to result in larger tumors [18], but comparable data on Pim-3 has been lacking as also direct evidence for the ability of Pim kinases to contribute to formation of metastases. Yet information from cell-based motility assays as well as clinical data connect upregulation of Pim kinases to cancer cell migration, invasion and more malignant behaviour [4–9]. In addition, Pim-1 has been shown to regulate the CXCR4/CXCL12 chemokine pathway, which plays an important role in migration and invasion of both leukemic [4, 19] and prostate cancer cells [20–23].

In this study, we have assessed the effects of Pim kinases and their inhibitors using both subcutaneous and orthotopic mouse xenograft models for human prostate cancer. We demonstrate that overexpressed Pim-1 or Pim-3 kinases promote not only growth of PC-3 cell-derived xenografts, but also metastatic properties of orthotopically induced tumors, and that Pim-inhibitory compounds can prevent these effects. We also show that the Pim-promoted metastatic growth is associated with increased angiogenesis, lymphangiogenesis and CXCR4 phosphorylation.

Results

Pim-3 kinase enhances growth and metastatic properties of prostate cancer xenografts

To investigate the ability of Pim-3 to promote tumor growth and metastasis under *in vivo* conditions, we established a stable PC-3/Pim-3 prostate cancer cell line expressing human Pim-3 together with Tomato as a fluorescent follow-up marker. In order to evaluate the tumorigenic potential of the PC-3/Pim-3 cell line as compared to the mock-transfected PC-3 control cell line, cells were subcutaneously inoculated into athymic nude male mice. During the follow-up period of up to 24 days, tumor volumes were measured both with a caliper and by fluorescent imaging of Tomato expression. After sacrifice, tumors and tissue samples were excised for fluoro- and morphometric analyses. These revealed that the Pim-3-overexpressing xenografts had grown significantly faster than the mock-transfected cells, even though tumors had remained local without any signs of metastases (Fig 1A and 1B). The manually measured tumor volumes correlated with the areas determined by fluorescent imaging (S1 Fig). To further analyse the growth properties of these tumors, mitotic cells were stained from paraffin-embedded tissues samples. Interestingly, the proportion of mitotic cells was clearly higher in the Pim-3-overexpressing tumor tissues than in the controls (Fig 1C and S1 Fig). The differences in the tumor volumes could also be detected from the whole tumor scans used for analysis of the mitotic cells (S1 Fig). Simultaneously to the subcutaneous experiments, cells were cultured for three weeks without antibiotic selection to confirm the stability of Pim-3 overexpression (S1 Fig).

Since the subcutaneous xenografts had not invaded into the body, we continued our studies with an orthotopic prostate cancer model, where the tumor microenvironment was expected to be more favorable towards metastatic growth [24–26]. In the first pilot set of experiments, control or Pim-3-overexpressing cells were orthotopically inoculated into the prostates of nude male mice. Tumor growth was followed during a three-week period, after which the animals were sacrificed and tumors along with selected organs were collected. In this study, no major differences in tumor volumes were detected. However, analysis of paraffin-embedded tissue samples not only revealed the higher mitotic potential of the Pim-3-overexpressing cells, but also their ability to invade into the lungs (Fig 1D and 1E). By contrast, the milder metastatic behaviour of the mock-transfected control cells confirmed our previous observations on the ability of parental PC-3 cells to invade into prostate-draining lymph nodes, but rarely to more distant organs [25–26].

Pim inhibition is tolerated by zebrafish embryos and adult mice

The promising results with invasive Pim-3-overexpressing orthotopic tumors prompted us to perform another set of experiments, where we also tested the effects of Pim inhibition by the tetracyclic pyrrolocarbazole DHPCC-9 [6] and the tricyclic benzo[*cd*]azulene BA-1a [17]. For comparison, we also established another stable PC-3 cell line overexpressing human Pim-1.

Prior to animal experimentation, the efficacy and toxicity of the Pim-selective inhibitors were tested in cell-based assays and *in vivo*. Both inhibitors efficiently antagonized the pro-migratory effects of Pim-1 and Pim-3, and decreased migration of all stable cell lines to a similar extent (S2 Fig). Within the 24 h follow-up period of the wound healing assay, cell viability was only slightly affected, while both inhibitors dramatically reduced it in all cell lines by a later 72 h time-point. When the *in vivo* safety of the inhibitors was analysed with zebrafish embryos within their aquatic environment, both DHPCC-9 and BA-1a were well tolerated, while our cytotoxic control compound BA-2c [17] led to massive developmental problems and death (S3

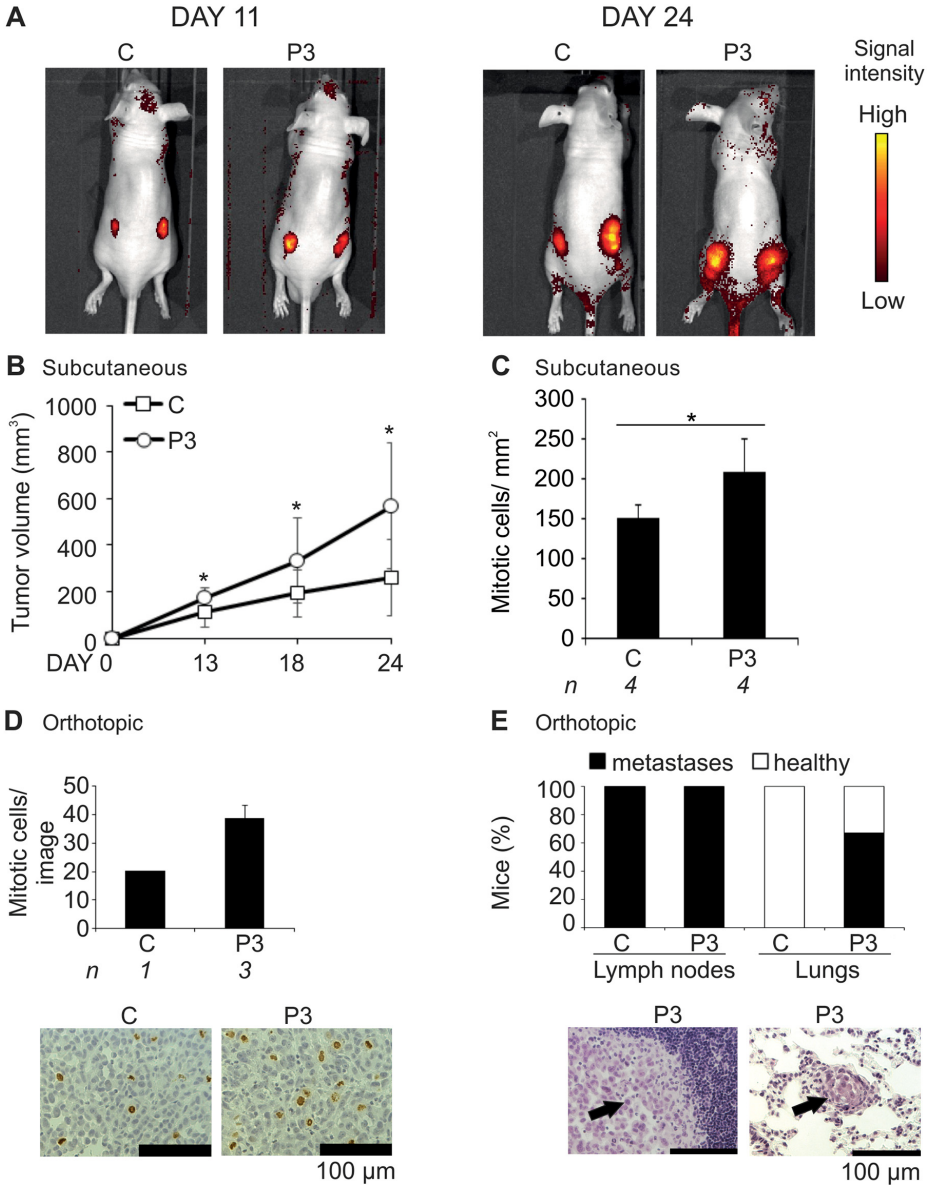

Fig 1. Pim-3 overexpression promotes metastatic growth of prostate tumor xenografts. PC-3-derived cell lines that had been stably transfected with an empty vector (C) or a vector expressing Pim-3 (P3) were subcutaneously or orthotopically injected into athymic nude mice. Tumors and isolated tissues were stained with Hematoxylin and Eosin for visualization of their structure. Additional stainings were carried out with anti-phospho-histone H3 antibody to visualize the number of mitotic cells. In the subcutaneous experiments, tumor formation was followed by fluorescence imaging of Tomato expression (A) and approximate tumor sizes were measured by palpation at different time-points (B). After 24 days, mice were sacrificed and their tumors and tissues were collected. Shown are average values from all fully imaged tumor sections from indicated numbers (*n*) of mice after staining of mitotic cells (C). In the orthotopic experiments, the stable PC-3 cells were allowed to grow in the prostates for three weeks. Thereafter mitotic cells (brown) were analysed from sample images (D), while metastases (indicated by arrows) were counted from prostate-draining lymph nodes and lungs (E).

doi:10.1371/journal.pone.0130340.g001

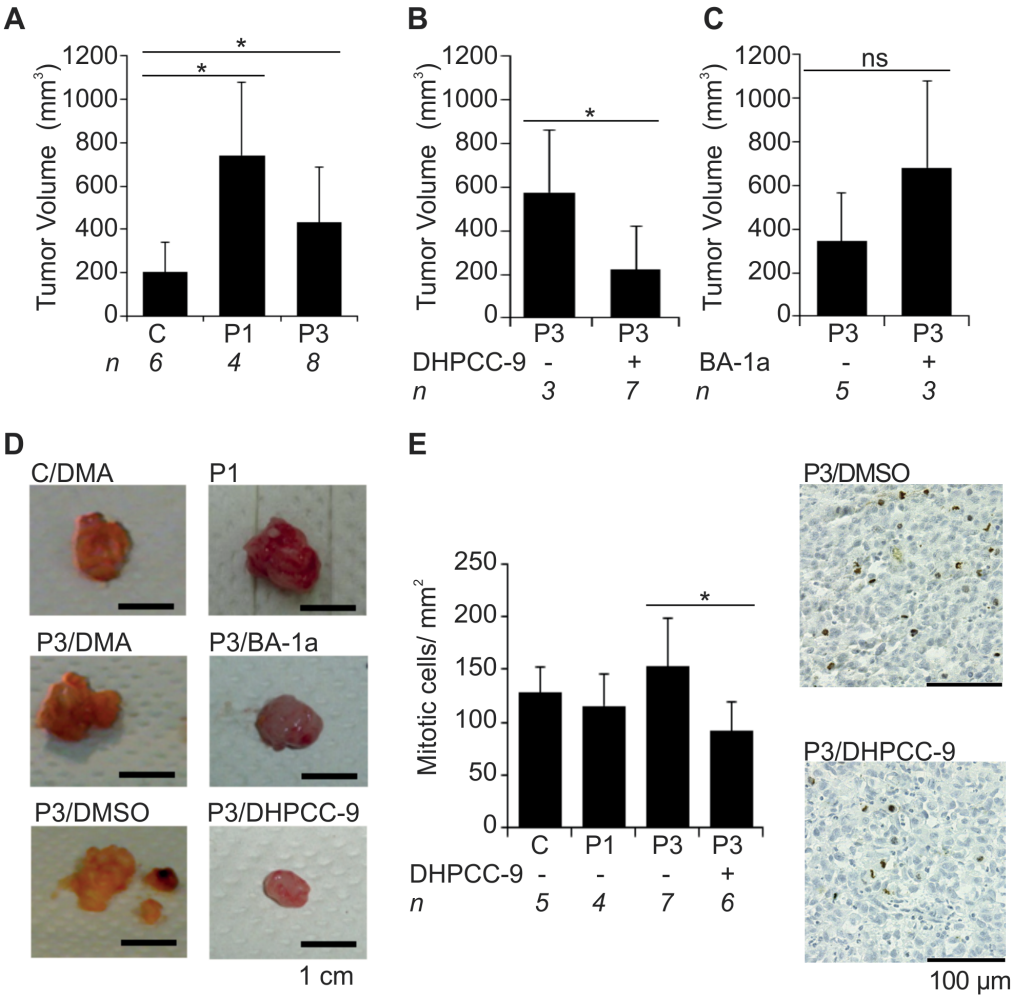

Fig 2. Pim overexpression increases and Pim inhibition by DHPCC-9 decreases growth of orthotopic prostate xenografts. PC-3-derived stably transfected cells (Mock = C, Pim-1 = P1, Pim-3 = P3) were orthotopically inoculated into the prostates of athymic nude mice. Mice were treated daily with either DMSO or DMA (control treatments) or with Pim inhibitors (50 mg/kg of DHPCC9 in DMSO or 20 mg/kg of BA-1a in DMA). After three weeks of treatments, mice were sacrificed and their tumor volumes were measured. First the volumes were compared between indicated numbers (*n*) of mice without inhibitor treatments (A). Then the volumes of tumors derived from inhibitor-treated animals were compared to tumors from animals with appropriate control treatments DMSO (B) or DMA (C). Before tumor fixation, representative images were taken (D). Later on paraffin-embedded tumor sections were stained with anti-phospho-histone H3 antibody to visualize mitotic cells (brown). Shown are average values combined from all fully imaged tumor tissue sections from DHPCC-9-treated and DMSO- or DMA-treated control groups as well as representative images from Pim-3-overexpressing tumors (E).

doi:10.1371/journal.pone.0130340.g002

Fig and S1 Table). However, slightly curved tails and enlarged pericardiac sacs were observed in embryos treated with 10 µM DHPCC-9 (S3 Fig), suggesting that proper Pim activity is needed for normal embryonal development. Yet these data did not allow for reliable conclusions on the safety of the inhibitors in adult organisms.

Additional safety tests were then carried out with adult mice. However, with the high concentrations needed for these tests, only DHPCC-9 could be suspended in DMSO, while BA-1a was soluble only in N,N-dimethylacetamide (DMA).

During an initial ten-day follow-up period, DHPCC-9 treatments (50 mg/kg) caused no major changes in mouse behavior, injection area or body weight (S4 Fig). By contrast, DMA-based treatments (25 mg/kg) caused restless behavior and slightly decreased body weight. In addition, DMA seemed to induce scar tissue formation in the injection area. Thereafter, safety testing was continued with smaller amounts of DMA (10–20 mg/kg), which did not cause any visible changes in the injection area, mouse behavior or weight gain during the 17-day follow-up (S4 Fig). Based on these results, 50 mg/kg of DHPCC-9 in 20 μl of DMSO and 20 mg/kg of BA-1a in 10 μl of DMA were decided to be used daily to test their effects on orthotopic Pim-3-overexpressing prostate xenografts.

Pim inhibition reduces Pim-dependent metastatic growth of orthotopic prostate xenografts

In the second set of orthotopic experiments, mock-transfected PC-3 cells or cells stably overexpressing Pim-1 or Pim-3 were orthotopically inoculated into the prostates of nude male mice. Mice with Pim-3-overexpressing xenografts were randomized into 4 groups and administered with daily dosages of the inhibitors or equal volumes of DMSO or DMA as controls. Mouse behavior and weight gain was followed during the experiment, but no major inhibitor-related changes were detected (S5 Fig). After sacrifice, tumors were excised and mice without tumors were excluded from further analyses (S2 Table). To confirm the stability of the cell lines, *ex vivo* scanning was performed to detect Tomato signals in tumors (S6 Fig), while immunohistochemistry was used to visualize the xenografted tumor cells expressing Pim proteins from V5-tagged constructs (S7 Fig).

When tumor volumes were calculated, Pim-overexpressing tumors were again significantly larger than those formed by mock-transfected cells (Fig 2A and 2D). However, the Pim-1 xenografts could not be directly compared to others, since mice carrying them had not obtained any chemical treatments. DHPCC-9 treatment significantly decreased the volume of Pim-3-overexpressing tumors, suggesting that this compound had been able to reach the tumor tissue and inhibit Pim-3 activity there (Fig 2B and 2D). By contrast, BA-1a did not show any efficacy in terms of reducing tumor volume (Fig 2C and 2D). Apparently this compound had not reached its target tissue, as also suggested by the presence of a yellow precipitate around the injection site.

The mitotic rates were also measured from tissue sections derived from the orthotopic tumors. While in the subcutaneous experiments and in the first set of orthotopic experiments, there had been clearly more mitotic cells in tumors formed by Pim-3-overexpressing cells as compared to mock-transfected cells (Fig 1C and 1D), in the second orthotopic set the differences were smaller (Fig 2E). However, treatment with DHPCC-9 had decreased the number of mitotic cells in Pim-3 xenografts (Fig 2E).

Since the Tomato-derived fluorescence was not strong enough to clearly reveal the micrometastases (S6 Fig), histological analyses were carried out with tissue sections from kidneys, spleen, liver, lungs as well as the prostate-draining lymph nodes. After staining with haematoxylin and eosin, metastases were sought for from different tissue samples, but especially from lymph nodes and lungs. Intriguingly, while more than half of mock-transfected and most Pim-1 or Pim-3 xenografts had been able to metastasize into the prostate-draining lymph nodes, only Pim-overexpressing cells had invaded as far as into the lungs (Fig 3A–3C, S3 Table). Even more interestingly, DHPCC-9 treatment had efficiently inhibited formation of metastases in

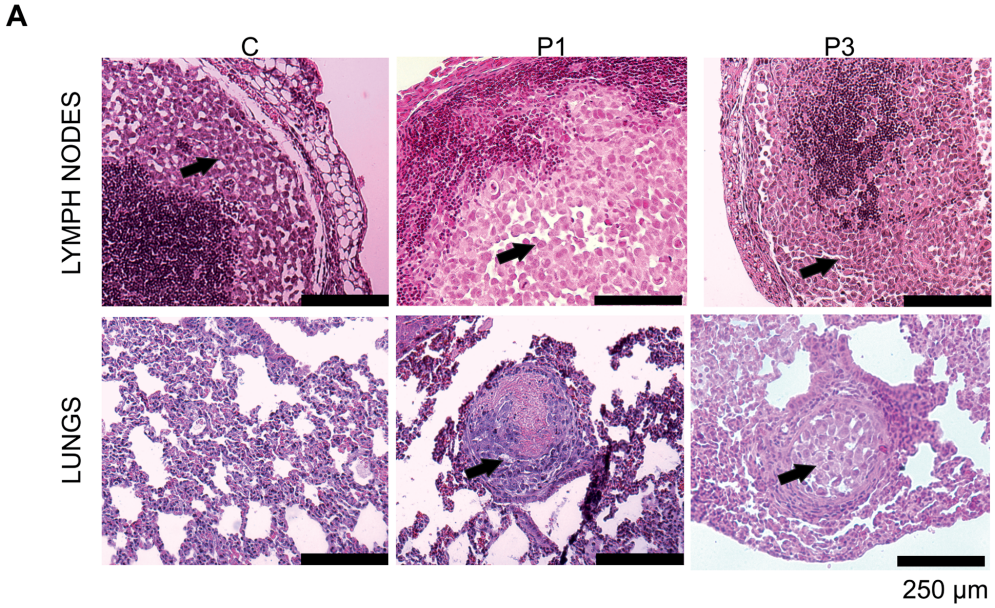

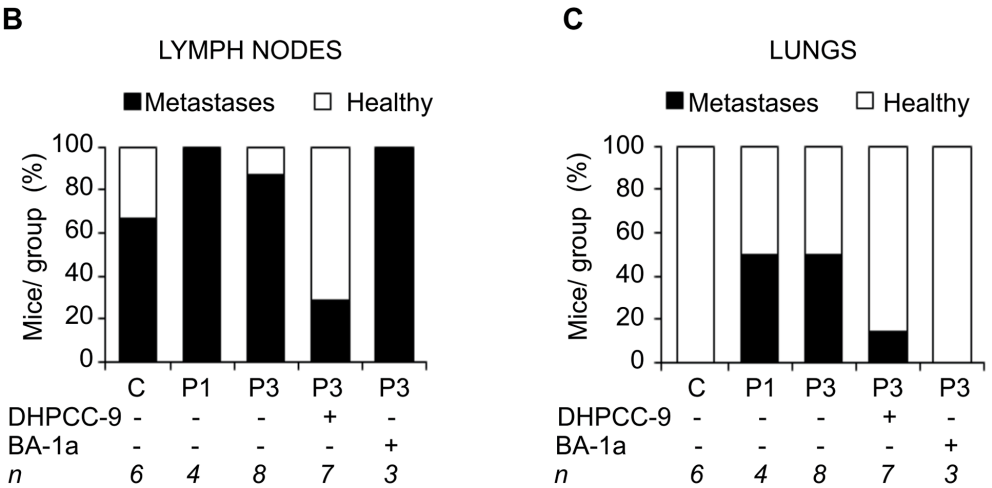

Fig 3. Pim inhibition by DHPCC-9 reduces the number of metastases in orthotopic prostate tumors overexpressing Pim-3. Different organs were collected from mice with orthotopic prostate tumor xenografts formed by PC-3 cells stably overexpressing an empty vector (C), Pim-1 (P1) or Pim-3 (P3). Paraffin-embedded tissue sections were stained with hematoxylin and eosin and analysed for the presence of metastases. Shown are representative images (A) from lymph node and lung sections (tumor cells indicated by arrows). The metastatic properties of xenografts from mice treated with DHPCC-9, BA-1a or their solvents were also analysed. Shown are percentages of mice positive for either lymph node metastases (B) or lung metastases (C) in each group.

doi:10.1371/journal.pone.0130340.g003

both organs. Both metastatic and necrotic areas were measured, but there was no clear connection to Pim activity (S6 Fig), suggesting that once a metastatic tumor is formed, the tumor cells may acquire other properties in addition to Pim activity to support their growth.

To visualize the vasculature of the orthotopic tumors, blood vessels and lymphatic vessels were stained. After quantitative analyses, a significant increase was detected in the areas of blood vessels per tumor in the xenografts formed by the Pim-overexpressing cells as compared to the control cells (Fig 4A). Slightly smaller differences were detected also in the areas of

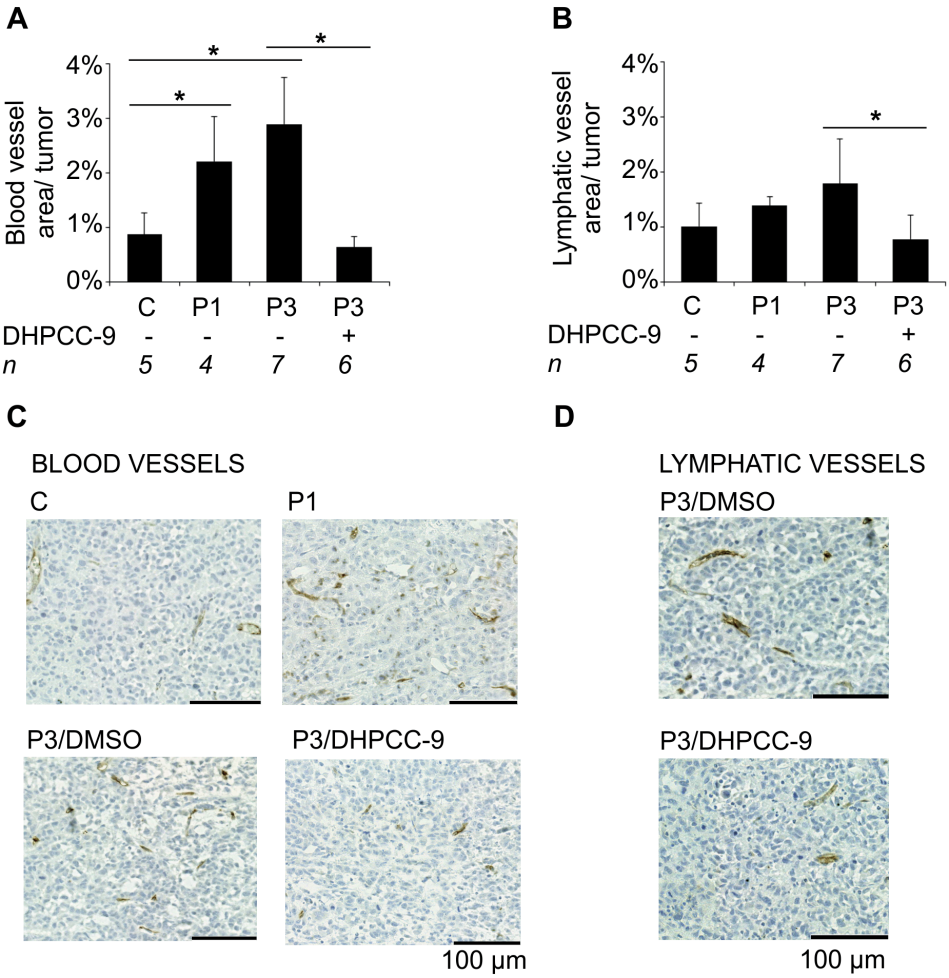

Fig 4. Pim kinases promote angiogenesis and lymphangiogenesis of prostate tumor xenografts. Angiogenic properties of the orthotopic prostate xenografts (Mock = C, Pim-1 = P1, Pim-3 = P3) were analysed by immunohistochemical staining of the paraffin-embedded tissue sections with anti-CD34 (blood vessels) and anti-m-LYVE-1 (lymphatic vessels) antibodies. Shown are average areas of all analysed blood (A) and lymphatic vessels (B) along with representative images (vessels in brown) (C-D) from fully imaged tumor tissue sections.

doi:10.1371/journal.pone.0130340.g004

lymphatic vessels (Fig 4B). However, after treatment with the Pim inhibitor DHPCC-9, the areas of both blood as well as lymphatic vessels were significantly decreased (Fig 4A–4D).

Pim-1 and Pim-3 enhance phosphorylation and cell surface expression of CXCR4

The CXCR4 chemokine receptor protein has previously been implicated in PC-3 cell migration and interaction with endothelial cells [20–23]. Moreover, in hematopoietic cells Pim-1 has been shown to phosphorylate CXCR4 at Ser339, and thereby promote cell surface expression of CXCR4 and its interaction with the CXCL12 chemokine ligand [4]. In addition, we have previously shown Pim inhibition or silencing to efficiently reduce invasion of PC-3 cells towards MG-63 osteosarcoma cell conditioned medium, where the major chemoattractant is CXCL12 [6, 23]. To find out whether Pim/CXCR4 interaction plays a role also in our prostate cancer xenograft model, we first assessed whether there were differences in the phosphorylation status of CXCR4 between our stable cell lines. By Western blotting, we observed a marked increase in the Ser339-phosphorylated CXCR4 levels in both Pim-overexpressing stable cell lines as compared to the control cell line (Fig 5A). In addition, a decrease in phosphorylated CXCR4 levels was seen after treatment of parental PC-3 cells with the Pim inhibitor DHPCC-9 (Fig 5B).

Since stable overexpression of either Pim-1 or Pim-3 clearly enhanced CXCR4 phosphorylation, we wanted to compare the *in vitro* activities of all three Pim family members towards CXCR4. Therefore, we incubated GST-tagged Pim proteins together with GST-tagged C-terminal 46 aa fragments of CXCR4 (WT) or its mutated S339A form (SA), where the serine residue had been replaced by an alanine residue. When the *in vitro* phosphorylated fragments were detected with the anti-phospho(Ser339)-CXCR4 antibody, it became evident that both Pim-1 and Pim-3, but not Pim-2 can phosphorylate CXCR4 on Ser339 (Fig 5C). Similar differences were also detected in PC-3 cells after transient Pim overexpression, whereas the Pim inhibitor DHPCC-9 efficiently inhibited CXCR4 phosphorylation there (S8 Fig).

Thereafter we carried out immunofluorescence stainings to visualize the localization of CXCR4 protein in the stable PC-3 cell lines that had been treated for 24 h with DMSO or DHPCC-9. While CXCR4 was ubiquitously expressed, its phosphorylated form recognized by the anti-phospho(Ser339)-CXCR4 antibody displayed more membrane-associated expression in DMSO-treated samples, but rather dispersed and weaker cytoplasmic expression in DHPCC-9-treated samples (Fig 5D and 5E). While both Pim-1 and Pim-3 enhanced the phospho-CXCR4 signals as compared to overall CXCR4 levels, Pim inhibition efficiently reduced them, resulting also in slightly stronger nuclear expression of CXCR4 (Fig 5D and 5E).

To analyse the role of CXCR4 phosphorylation in our *in vivo* experiments, we used immunohistochemistry to measure the relative amounts of orthotopic prostate tumor cells positive for phosphorylated CXCR4. Comparison of phospho-CXCR4 signals to the average CXCR4 signals in each tumor revealed that both Pim-1 and Pim-3 had significantly increased the relative amounts of phospho-CXCR4, while Pim inhibition by DHPCC-9 had decreased it even below the level observed in the mock-transfected samples (Fig 5F). Altogether, both the *in vitro* and *in vivo* data suggest that tumors overexpressing Pim-1 or Pim-3 may take advantage of the CXCL12/CXCR4 chemokine pathway to spread into other organs such as the lungs.

Discussion

Here we show that PC-3 prostate cancer cells overexpressing either Pim-1 or Pim-3 kinases form larger xenograft tumors than the parental PC-3 cells. These results are well in line with previous observations on the ability of Pim-1 and Pim-2 to enhance growth of PC-3 cell-derived subcutaneous prostate cancer xenografts [18], while here we demonstrate that Pim-3 is

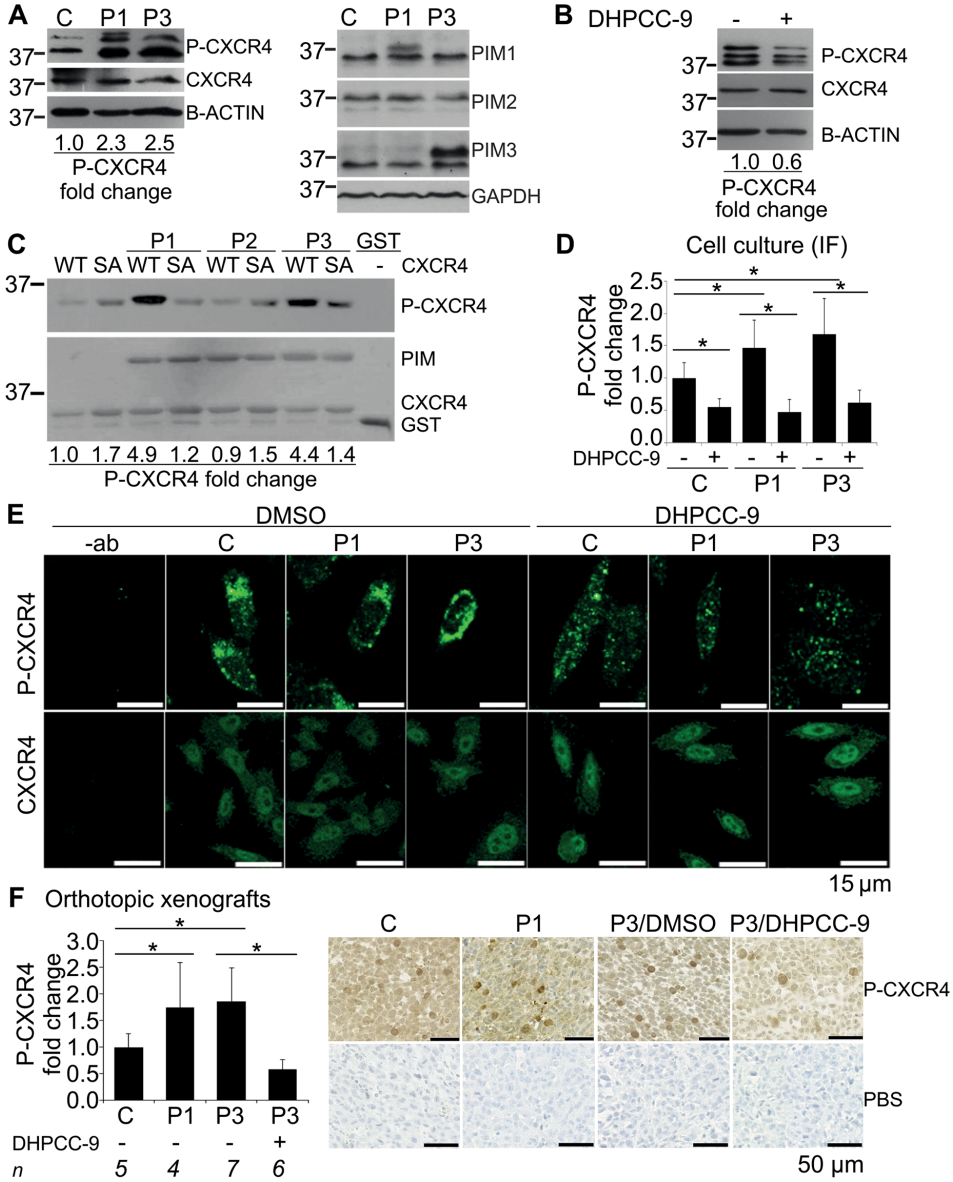

Fig 5. Pim-1 and Pim-3 enhance CXCR4 phosphorylation and cell surface expression in prostate cancer cells. Phosphorylation of CXCR4 at S339 as well as Pim levels were analysed by western blotting in the stable Pim-1 (P1), Pim-3 (P3) or control vector (C) overexpressing PC-3 cells or the parental PC-3 cell line treated with 0.1% DMSO or 10 µM DHPCC-9. Shown are results from one representative experiment with loading controls and molecular weight (kDa) markers (A-B). The ability of Pim family members to phosphorylate CXCR4 *in vitro* was analysed by incubating GST-tagged Pim-1 (P1), Pim-2 (P2) or Pim-3 (P3) proteins with GST-tagged fragments of wild-type (WT) or Ser339>Ala (SA) mutant human CXCR4. Phosphorylated CXCR4 was detected by phospho(Ser339)-CXCR4 antibody and protein loading by Ponceau S staining. Shown are results from one representative experiment (C). Localization and signal intensity of phosphorylated versus overall CXCR4 expression was analysed by immunofluorescent (IF) staining of stably transfected cells treated with either 0.1% DMSO or 10 µM DHPCC-9. The experiment was controlled by parallel samples stained only with the secondary antibody (-ab). Stainings were

repeated twice and stacks of images were taken by confocal microscopy from at least 30 cells per sample per experiment. Shown are the signal intensities of phospho-CXCR4 stainings compared to overall CXCR4 levels along with representative images from phospho-CXCR4 and CXCR4 stainings (D-E). Phosphorylation and localization of CXCR4 was also analysed by immunohistochemical staining of the paraffin-embedded tissue sections from orthopic prostate tumors. Shown is the relative increase in the amount of phospho-CXCR4-positive cells versus overall CXCR4 expression measured by whole tumor scanning. PBS instead of the primary antibody was used as a negative control. Representative images were taken to visualize the differences in phospho-CXCR4 (dark brown) stainings (F).

doi:10.1371/journal.pone.0130340.g005

also equally effective. More intriguingly, when orthotopically inoculated into mouse prostates, cells overexpressing Pim-1 or Pim-3 have an increased capacity to metastasize from the prostate-based tumors to other organs such as the lungs. In addition, one of the tested Pim-inhibitory compounds, DHPCC-9, is able to decrease Pim-dependent tumor growth as well as formation of metastases without severe side effects, suggesting that it is able to penetrate into tumor cells to inactivate Pim kinases there.

While we have previously shown that Pim kinases are able to promote motility of prostate cancer cells [6], the present study is the first to demonstrate similar effects also under *in vivo* conditions. This is of interest, since orthotopically inoculated PC-3 cells have previously been shown to migrate from the prostate to the local prostate-draining sacral and iliac lymph nodes, but rarely anywhere else [24–26]. These findings were confirmed in our studies, where metastatic growth was observed in the prostate-draining lymph nodes of most tumor-bearing mice. However, only the Pim-overexpressing xenografts were able to metastasize into the lungs, while no metastases were detected in other collected tissues.

To address the tumorigenic mechanisms driven by Pim kinases and opposed by Pim inhibition, tissue samples from the primary xenograft tumors were analysed by immunohistochemistry for markers of mitotic activity, angiogenicity and invasiveness. Slight Pim-dependent increases were observed in the proportion of mitotic cells and in the areas of lymphatic vessels, while more significant upregulation was detected in the formation of tumor vasculature and in the phosphorylation and cell surface expression of CXCR4. By contrast, all these parameters were strongly decreased by the Pim-selective inhibitor DHPCC-9. Thus, these observations may explain not only the enhanced growth of tumors overexpressing Pim kinases, but also their metastatic properties.

The CXCL12/CXCR4 chemokine pathway is essential for lymphocyte trafficking and especially for homing of hematopoietic stem cells into the bone marrow [19, 27]. In addition, the CXCL12 chemokine is constitutively expressed in several other organs including lymph nodes and lungs and can thereby attract not only hematopoietic cells, but also migrating cancer cells that often show high expression levels of the CXCR4 receptor on their cell surface. Furthermore, CXCR4 can support tumor survival e.g. by promoting tumor vascularization.

Pim-1 overexpression has been associated with upregulated cell surface expression of CXCR4 in hematopoietic malignancies such as acute myeloid leukemia [4], diffuse large B-cell lymphoma [28] and chronic lymphocytic leukemia [29]. The intracellular tail of CXCR4 can be phosphorylated *in vitro* at Ser339 by Pim-1 kinase [4] and by Pim-3, as shown here, but not by Pim-2. Interestingly, Ser339 is among several serine residues targeted by G-protein receptor kinases (GRKs), resulting in receptor endocytosis [30]. By contrast, Pim-dependent phosphorylation of CXCR4 has been reported to lead to increased externalization of the receptor, allowing cells to migrate towards a CXCL12 gradient [4]. In PC-3 cells, CXCR4 surface levels are relatively low, unless the cells are treated with the CXCL12 ligand, which also clearly increases the invasive properties of these cells [20–23]. Thus, while additional studies on the effects of Pim kinases on CXCR4 in PC-3 cells cultured in the absence or presence of CXCL12 would be of interest, one can already speculate that the Pim-CXCR4 interaction has helped our Pim-overexpressing orthotopic tumor cells to form metastases into the prostate-draining

lymph nodes and the lungs, while the tumor microenvironment around the subcutaneous tumors may not have been permissive enough to promote the invasion.

Since the CXCL12/CXCR4 pathway is an attractive therapeutic target, several small molecule compounds have been developed that either block the interaction of the chemokine with its receptor or inhibit signaling downstream from the receptor [19, 27]. Promising results have already been obtained from clinical trials that have aimed to increase chemosensitivity of hematopoietic malignancies, but CXCL12/CXCR4 inhibitors may also help to reduce the metastatic potential of solid cancers. One problem with these inhibitors is that they induce a counter-regulatory upregulation of CXCR4 on the cell surface, resulting in only short-lived responses. Therefore it might be more efficient to block externalization of the CXCR4 receptor by Pim-selective inhibitors that may also have less harmful side effects.

Here we have shown preliminary *in vivo* safety and efficacy data for one Pim-selective inhibitor, the pyrrolocarbazole DHPCC-9, whereas the benzo[*cd*]azulene BA-1a turned out to be too insoluble. DHPCC-9 did not show any cytotoxic effects in mice, even though some malformations were detected in the early-stage zebrafish embryos. These results suggest that at least a short-term inhibition of Pim activity can be well tolerated in adult organisms and that it may even be possible to use higher doses of this inhibitor to magnify the observed effects. It may also be advantageous to combine Pim inhibition with other treatments affecting cell survival or motility.

Data from cell-based wound healing experiments indicate that DHPCC-9 is able to block motility of PC-3 prostate cancer cells [6]. As shown also in this study, this is not simply due to decreased proliferation, since cell viability was not substantially reduced during the 24 h wound recovery follow-up period. However, longer exposure of PC-3 cells to DHPCC-9 reduced viable cell numbers in culture, which was well in line with the decreased tumor growth during the three-week test period. Yet for the prostate cancer patients, it is not the primary tumors but the metastases that are usually fatal. Therefore it will be important to be able to reduce the metastatic properties of the tumors e.g. by DHPCC-9-like compounds.

Even though the results with DHPCC-9 look promising, there are several obstacles to overcome if it was to be developed towards an actual drug compound. DHPCC-9 is soluble in DMSO, but this solvent is too toxic to be used within human patients. Therefore oral derivatives should be searched for. The putative cardiotoxicity of the compound should also be tested, since Pim kinases regulate cytokine responses and have essential functions in endothelial cells [31]. Here it should be noted that the first clinical Phase 1 trial with a Pim inhibitor, SGI-1776, had to be ended due to hERG channel toxicity [32]. However, its derivatives have displayed more favorable profiles, suggesting that the cardiotoxicity problems were due to the properties of the original compound, and not the Pim kinases targeted by it [32].

Conclusions

Taken together, we have shown that Pim kinases play an important role in cancer progression by increasing the potential of tumor cells to grow as well as to invade not only to the surrounding tissues but also much further into the body. In addition to enhancing angiogenesis and lymphangiogenesis, Pim kinases are likely to promote metastatic prostate cancer growth by employing the CXCL12/CXCR4 chemokine pathway. Furthermore, we have provided preliminary evidence for the safety and efficacy of the Pim-selective inhibitor DHPCC-9 as a promising compound to decrease Pim-induced cell proliferation and motility also *in vivo*. Such compounds are clearly needed to combat the fatal metastases associated with prostate cancer and other solid tumors.

Materials and Methods

Cell culture and transfections

The human androgen-independent prostate epithelial adenocarcinoma cell line PC-3 (American Type Culture Collection) was maintained in Roswell Park Memorial Institute (RPMI) -1640 medium, supplemented with 10% fetal bovine serum, L-glutamine and antibiotics. To prepare PC-3-derived cell lines stably overexpressing human Pim family members, PC-3 cells were transfected with pcDNA3.1/V5-His-C-based expression vectors for Pim-1 or Pim-3 (kindly provided by Markku Varjosalo, University of Helsinki, Finland) or mock-transfected with the empty vector (Thermo Fisher Scientific, Waltham, MA, USA). In addition, all cells were cotransfected with the pCMV-Td-Tomato plasmid (Clontech Laboratories Inc., Mountain View, CA, USA) to be used as a fluorescent follow-up marker. All transfections were performed with Fugene 6 (Promega, Madison, WI) in 3:1 ratio to DNA. After an overnight incubation, positively transfected cells were enriched by antibiotic selection with G418 (Fisher Scientific, Geel, Belgium), first using 300 μg/ml for 48 h and thereafter 500 μg/ml for 14 days. Medium was changed every day during the selection. After selection, maintenance of the transfected plasmids in the stable cell lines generated from pools of cells was ensured by supplementing culture medium with 200 μg/ml of G418.

Kinase inhibitors

Two structurally distinct types of Pim-selective inhibitors were used that have been described and validated before: the pyrrolozarbazole DHPCC-9 (1,10-dihydropyrrolo[2,3-*a*]carbazole-3-carbaldehyde) [6, 15] and the benzo[*cd*]azulenes BA-1a and BA-2c [16, 17].

Migration assays

Cells were plated on 24-well plates (100 000 cells/well). After 24 or 48 hours, confluent cell layers were scratched with 10 μl pipette tips. Thereafter, the cells were treated with 10 μM DHPCC-9 or BA-1a or control-treated with DMSO (0.1%). Images were taken by 20× magnification at indicated time-points. The width of the wound was analysed by ImageJ software (1.37v, Wayne Rasband, National Institute of Health, Bethesda, MD, USA) by manually drawing the wound lines and analysing the wound area in square pixels.

Viability assays

Cells were plated on 96-well plates (35 000 cells/ well). After attachment, the cells were treated with 10 μM DHPCC-9 or BA-1a or control-treated with DMSO (0.1%). Cell viability was analysed by MTT assay as previously described [6].

Toxicity assays with zebrafish embryos

Housing and experiments of wild-type zebrafish (*Danio rerio*) were performed according to the European Convention for the Protection of Vertebrate Animals used for Experimental and other Scientific Purposes, and the Statutes 1076/85 and 62/2006 of The Animal Protection Law in Finland and EU Directive 86/609. Briefly, the animals were maintained at 26°C according to standard procedures [33] in the aquatic facilities of the Laboratory of Animal Physiology, University of Turku, Finland under the licence ID ESAVI/4068/04.10.07/2013 from the Provincial State Office of Western Finland. Breeding traps were placed in the fish tanks and after natural spawning, the fertilized embryos were collected and cultured in E3 medium (5 mM NaCl, 0.17 mM KCl, 0.33 mM $CaCl_2$, 0.33 mM $MgSO_4$, 0.01% methylene blue) at 28°C. Treatments with Pim inhibitors or 0.1% DMSO (control) were started at 6 h post-fertilization (hpf). Toxicity

was assessed by scoring embryos as live or dead at 26 hpf under stereomicroscope (Zeiss StereoLumar V.12, Carl Zeiss Microscopy GmBH, Jena Germany). For more detailed morphological analysis, embryos treated with DMSO or DHPCC-9 embryos were dechorionated and imaged with stereomicroscope at 50 hpf. Embryo length was measured as greatest length from head to tail. The developmental stage (head-trunk angle) was measured as described earlier [34]. Body curvature was measured as an angle between center line of notochord extending to the level of the posterior end of yolk sac extension (yolk-anus-tail angle), and as a line from this point to the most posterior end of the last somite. Pericardiac oedema was quantitated by measuring the area of pericardiac space. All image analyses were performed using ImageJ software (1.48s, Fiji, Wayne Rasband, National Institutes of Health, Bethesda, MD, USA).

Toxicity assays with mice

All mouse experiments were carried out at the Central Animal Laboratory of the University of Turku, Finland according to the European Convention for the Protection of Vertebrate Animals used for Experimental and other Scientific Purposes, and the Statutes 1076/85 and 1360/90 of The Animal Protection Law in Finland and EU Directive 86/609. Accordingly, the clinical signs of mice were daily recorded, and if the criteria of humane endpoints were met, animals were sacrificed. Humane endpoints were considered as rapid or gradual weight loss, abnormal changes in behavior and motion (social and eating behavior), subcutanic tumor size greater than 1.5 cm in diameter or skin problems (wounds or signs of inflammation). The experimental procedures were reviewed by the local Ethics Committee on Animal Experimentation of the University of Turku and approved by the Provincial State Office of Western Finland with the licence IDs ESAVI/2008-05531 and ESAVI/3937/04.10.03/2011. Two available batches of mice from Harlan Laboratories (Horst, the Netherlands) were initially used, males (FVB/NhanHsd) and females (BALB/cOlaHsd), and maintained under controlled conditions (20–21°C, 30–60% relative humidity and 12-hour lighting cycle).

DHPCC-9 was dissolved in DMSO and intraperitoneally injected in 20 μl total volume of DMSO into FVB/NHanHsd male mice in concentration of 100 mg/kg/day for two days and thereafter 50 mg/kg/day for 8 days. BA-1a was dissolved in DMA and intraperitoneally injected into BALB/cOlaHsd female mice, either 25 mg/kg/day in 25 μl of total volume of DMA for 6 days or 10–20 mg/kg/day in 10 μl of total volume of DMA for 17 days. Animal welfare and weight was monitored daily until the mice were anesthesized by CO_2 and sacrificed. Tissue samples from liver, spleen and kidneys were collected to search for possible abnormalities.

Efficacy assays with xenografted mice

The follow-up periods of both subcutaneous and orthotopic experiments were designed according to previous PC-3 xenograft studies [18, 25–26]. For subcutaneous inoculations, PC-3 cells stably transfected with Pim-1, Pim-3 or the empty vector were collected, while cells were growing in a logarithmic phase. The cells were suspended in sterile PBS (4.5×10^6 cells in 100 μl) and injected into both flanks of athymic nude male mice (Balb/cOlaHsd-Foxn1nu/nu, Harlan Laboratories, Horst, the Netherlands), which were maintained in controlled and pathogen-free environment. Animal welfare was monitored daily, and animals were weighed and tumors palpated every other day. Tumor volume was calculated according to the formula $V = (\pi/6)(d_1 \times d_2)^{3/2}$ (20), where d_1 and d_2 are perpendicular tumor diameters (width, length). The fluorescently labelled tumor cells were imaged by IVIS Lumina II (Xenogen corp./ Caliper Life Sciences, Inc., Hopkinton, MA, USA) at different time points during the experiment, after which tumor areas (square pixels) and average signal intensities were measured by ImageJ.

After three weeks, mice were sacrificed and tumors as well as selected tissues (kidneys, spleen, liver, lungs and prostate-draining lymph nodes) were collected.

For orthotopic inoculations, cells were suspended in sterile PBS (Biochrom AG, Berlin, Germany; 10^6 cells in 20 μl) containing green food color 33022 (5 μg/ml; Roberts Oy, Turku, Finland) and kept on ice until usage. Cells were inoculated into the ventral prostates of anesthetized mice as previously described [25]. Analgesic drug Temgesic (Reckitt Benckiser Healthcare Ltd, Hull, UK) was given to mice prior to operation, 24 h and 48 h after them and also during the three-week follow-up period when needed.

Two separate orthotopical sets of experiments were performed. In the second set, part of the mice inoculated with Pim-3-overexpressing cells were daily treated with intraperitoneal injections of either 50 mg/kg of DHPCC-9 in 20 μl of DMSO or 20 mg/kg of BA-1a in 10 μl of DMA or equal amounts of the dissolvents as controls. All treatments were initiated one day after the orthotopic inoculations. Animal welfare and weight was monitored daily until the mice were sacrificed, after which the tumors as well as tissue samples were first imaged by IVIS Lumina II (Xenogen corp./ Caliper Life Sciences, Inc., Hopkinton, MA, USA) and then collected and stored for further analysis as described below. Fluorescent signals in each animal or isolated organ were normalized according to background signals given by tissues not expected to contain metastases or by signals originating from food. Tumor volume was calculated according to the formula $V = (\pi/6)(d_1 \times d_2 \times d_3)$, where d_1_d_3 are perpendicular tumor diameters (width, length, height) [35].

Histology and immunohistochemistry

Tumors and tissue samples were fixed for 24 h in 4% paraformaldehyde, after which they were stored in 70% EtOH. After paraffin embedding, 5 μm sections were cut and sections were stored at +4°C until they were deparaffinized, stained and rehydrated. All tumor and tissue samples were first stained by Mayer's Hematoxylin and Eosin (H&E). Additional immunohistochemical stainings were performed to visualize mitotic cells, expression of V5-tagged constructs, blood vessels, lymphatic vessels and phosphorylation of CXCR4 (S4 Table). For each staining, paraffin-embedded tissue sections were deparaffinized, microwaved, washed in water and blocked in 3% hydrogen peroxide in methanol. Samples were washed first in water and then in PBS or TBS, after which they were blocked and stained with antibodies. In addition, sections were counterstained by dipping them for 5–10 s in Mayer's hematoxylin, after which samples were washed in water and dehydrated. As a negative staining control, primary antibody was replaced by PBS or TBS in each sample. Stable PC-3/pcDNA3.1-VEGF-C tumor tissue [26] was used as a negative control for V5 staining.

To analyse the stainings representative images were taken by Leica DMRXA microscope (Leica Microsystems CMS GmbH, Mannheim, Germany) and ISCapture V2.6. software (Xintu Photonics Co., Ltd, Tucsen, Fuzhou, China), while whole tumor scans were performed either by Olympus BX51 microscope with DotSlide software (Olympus Corporation, Tokyo, Japan) or the Pannoramic 250 slide scanner with Pannoramic Viewer (3DHistech Ltd., Budapest, Hungary). Images were further analysed by ImageJ. For analysis of signal intensities and stained areas, a color deconvolution by H&E DAB was performed, then images were turned into grayscale and colors were inverted, background was subtracted and threshold levels were adjusted. Thereafter particles were analysed. For other than vessel analyses, necrotic areas were avoided. In addition, fully necrotic tumors were left out from analyses (one fully necrotic tumor/ each group except for none among PC-3/Pim-1-derived tumors, S5 Table).

Western blotting

Cells were washed once with PBS and resuspended in 2x Laemmli Sample Buffer. Samples were vortexed for 5 s and heated at 95°C for 5 min. Protein samples were then separated by

SDS-PAGE, immobilized onto PVDF-membrane (Merck Millipore, Billerica, MA, USA) and incubated with primary antibodies (S6 Table). Signal was created using mouse (#7076, Cell Signaling Technology, 1:5000) or rabbit (#7074, Cell Signaling Technology, 1:5000) HRP-linked secondary antibodies and Amersham ECL Plus or Prime (GE Healthcare, Fairfield, CT, USA) or Pierce ECL (Thermo Fisher Scientific Inc.) chemiluminescence reagents. In addition, for analysing the phospho-CXCR4 levels, the signal intensities were calculated by ChemiDoc MP System with Image Lab software (Bio-Rad Laboratories, Inc., Hercules, CA, USA). Thereafter the phospho-CXCR4 signal values were compared to overall CXCR4 values.

In vitro phosphorylation assays

GST-tagged constructs expressing human CXCR4 C46-WT and C46-S339A fragments [4] were kindly provided by Alex Bullock (University of Oxford, Oxford, UK). These fragments as well as full-length human Pim-1, human Pim-2 and mouse Pim-3 proteins were produced in bacteria, purified and analysed by *in vitro* phosphorylation assays as previously described [17] except that no radioactively labelled ATP was used. Samples were separated on SDS-PAGE, after which Western blotting with anti-phospho(Ser339)-CXCR4 was used to detect CXCR4 phosphorylation. Protein loading was analysed from PVDF-membrane by staining with Ponceau S solution (Sigma, St.Louis, MO, USA). Signal intensities were analysed by the ChemiDoc MP System.

Immunofluorescence

For confocal microscopy, cells were plated on coverslips on 12-well plates (100 000 cells/well). After 24 hours, cells were treated with DMSO or the Pim inhibitor DHPCC-9 (10 μM). After another 24 h incubation, samples were fixed in 4% PFA, permeabilized in 0,25% Triton X-100/PBS and blocked in 1% BSA for 30 min at +37°C. Thereafter samples were stained with anti-phospho(Ser339)-CXCR4 or anti-CXCR4 antibodies (1:1000) overnight. For secondary antibody, Alexa-Fluor 488-labelled chicken anti-rabbit IgG (H+L) antibody (A21441, Life Technologies, 1:1000) was used for 30 min at +37°C and 30 min at RT. Cells were imaged by Leica DMRXA TCS SP5 Matrix confocal microscope with LAS AF Application (Leica Microsystems CMS GmbH, Mannheim, Germany). Signal intensities were analysed by ImageJ.

Statistical analyses

Statistical analyses were performed by one-way ANOVA variance analyses with LSD post hoc multiple comparison tests (IBM SPSS Statistics 22, Chicago, Illinois, USA). In addition, Microsoft Excel data analysis tool t-Test: Two-Sample Assuming Unequal Variances was used in the supplementary assays. Pearson's correlations were determined by Microsoft Excel data analysis tools and interpreted according to common quidelines [36]. The mean differences of ≤ 0.05 were considered significant. The graphs with means and standard deviations have been produced by Microsoft Excel.

Supporting Information

S1 Fig. Subcutaneous tumor imaging and cell culture control. PC-3-derived cell lines that had been stably transfected with the fluorescent Tomato vector and an empty vector (C) or a vector expressing Pim-3 (P3) were subcutaneously inoculated into the left and right backsides of nude mice (n = 4 +4). During the test period of 24 days, manual palpation and fluorescent imaging were perfomed three times. Correlations were analysed between the manually measured tumor volumes and either the areas or average signal intensities measured by fluorescent

scanning. Shown are average results per each mouse at every time point (A). For analysis of mitotic cells, phospho-histone H3 staining (brown) was performed. Shown are representative images from control (C) and Pim-3 (P3) overexpressing tumors as well as whole tumor scan images for visualization of the differences in tumor size (B-C). Simultaneously to the animal experiment, cells were cultured in the absence of antibiotic selection to confirm stability of Pim-3 overexpression during the three-week test period (D).
(TIF)

S2 Fig. Both DHPCC-9 and BA-1a Pim inhibitors decrease migration and viability of stable Pim-overexpressing PC-3 cells. Cell motility of stable control (C), Pim-1 (P1) or Pim-3 (P3) overexpressing PC-3 prostate cancer cells was analysed by wound healing assays. Cells were cultured on 24-well plates until confluency, after which wounds were scratched with 10 μl pipette tips. Cells were treated with 0.1% DMSO or DMSO-dissolved Pim inhibitors and samples were imaged and analysed at 0 and 24 h time-points. Shown are representative images along with average values from cells treated with either DHPCC-9 (A) or BA-1a (B). After 24 and 72 hours, viability of the cells was analysed by MTT assays. Shown are average OD_{570} values from triplicate samples from one representative experiment (C). For each assay, at least three separate experiments were carried out with highly similar results.
(TIF)

S3 Fig. DHPCC-9 tolerance in zebrafish embryos. Zebrafish embryos were treated at 6 h post-fertilization and analysed at 50 h post-fertilization. Shown is average survival in two experiments (A), and body curvatures (B-C) as well as pericardial sac sizes (D) in one experiment with representative images to visualize the angles and the pericardiac sac indicated by an arrow.
(TIF)

S4 Fig. Mouse weight gain during toxicity testing. White male or female mice were treated with various concentrations of either DMSO (A) or DMA (B-C) diluted Pim inhibitors and followed up for indicated time-periods to gain information about the possible cytotoxicity of the compounds.
(TIF)

S5 Fig. Mouse weight gain during the second orthotopic experiment. Stable control (C) or Pim-1 (P1) or Pim-3 (P3) overexpressing PC-3 cells were orthotopically inoculated into nude mice. Mice were treated with DMSO or DMA as a control or with Pim inhibitors DHPCC-9 or BA-1a. Shown is the average mouse weight gain in each group during the test period.
(TIF)

S6 Fig. Fluorescent imaging of the second orthotopic set tissue samples. At the second orthotopic set, tumors and tissue samples were fluorescently imaged to obtain information on the Tomato-derived signal of stably transfected PC-3 cells (Mock = C, Pim-1 = P1, Pim-3 = P3). Mice with control or Pim-3-overexpressing tumors were treated with 50 mg/kg of DHPCC9 in DMSO or 20 mg/kg of BA-1a in DMA or vehicles only. After approximately three weeks, mice were sacrificed and tissues were imaged. In each animal, signal intensity was normalized according to background signal given by a kidney. Lymph nodes are pointed out by arrows. Shown are images from tumors and collected tissue samples (A). After detection of metastases in the lymph node and lung sections, the average areas of the metastases and the average necrotic areas in them were analysed. Shown are areas as well as the number (n) of mice with metastases in control treated and DHPCC-9 treated animals (B).
(TIF)

S7 Fig. V5-immunostaining of xenografted cells within orthotopic tumors and their lymph node metastases. Paraffin-embedded tissue sections from the second orthotopic set of tumors (Mock = C, Pim-1 = P1 and Pim-3 = P3), their surrounding mouse tissues and one control tumor (Neg. Ctrl) were stained with anti-V5 antibody. Shown are representative images from V5-positive or—negative samples.
(TIF)

S8 Fig. Pim-1 and Pim-3 increase and DHPCC-9 decreases CXCR4 phosphorylation in PC-3 cells. PC-3 cells transiently overexpressing an empty vector (C), Pim-1 (P1), Pim-2 (P2) or Pim-3 (P3) were treated with DMSO or 10 μM DHPCC-9 for 24 hours. CXCR4 phosphorylation was detected by phospho(Ser339)-CXCR4 antibody, after which the signal intensity was compared to the intensity of the CXCR4 signal. Pim overexpression was confirmed by Pim-specific antibodies, while β-actin was used as a loading control.
(TIF)

S1 Table. Pim inhibitor tolerance in zebrafish embryos. List of zebrafish embryos treated with Pim inhibitors or DMSO at 6 h post-fertilization and analysed for their viability and possible abnormalities at 50 h post-fertilization.
(XLSX)

S2 Table. Animal numbers in the orthotopic experiments. List of mice with or without prostate xenograft tumors derived from the stable PC-3 cell lines in the presence of control (DMSO or DMA) or Pim inhibitor treatments.
(XLSX)

S3 Table. Metastases from orthotopic tumors. List of mice with prostate xenograft tumors and metastases in the prostate-draining lymph nodes and/or the lungs. In addition, the groups were compared based on the number of metastases in different organ types (lymph nodes or/and lungs). DMSO or DMA treatments have been combined as control treatments.
(XLSX)

S4 Table. Protocols for immunohistochemistry. Immunohistochemical staining of paraffin-embedded tissue samples was done according to following protocols for antigen retrieval (1), blocking (2), primary (3) and secondary antibody stainings (4), Avidin-Biotin reaction (5) and DAB reaction (6).
(XLSX)

S5 Table. Detailed information for excluding samples in immunohistochemical analysis of the second orthotopic set samples. Original sample number represents the number of mice with tumors in each group. DMSO or DMA treatments are combined as control treatments.
(XLSX)

S6 Table. Antibody dilutions for Western blotting. Table contains details for primary antibody dilutions incubated at +4°C overnight.
(XLSX)

Acknowledgments

We thank S. Jussila, J. Kujala, H. Rantanen, J. Sandholm and L. Shumskaya from the University of Turku, A. Kiriazis and M. Varjosalo from the University of Helsinki, and A. Luostarinen and J. Seppänen from the Pharmatest Services Ltd for reagents or technical assistance. We also thank the Laboratory of Animal Physiology and the Turku Central Animal laboratory unit for

assistance in animal experiments and imaging. Microscopy was carried out in the facilities of the Cell Imaging Core of Turku Centre for Biotechnology.

Author Contributions

Conceived and designed the experiments: PJK NMS PH. Performed the experiments: NMS SKE IP JT. Analyzed the data: NMS SKE IP JT PJK PH. Contributed reagents/materials/analysis tools: JYK FA PM. Wrote the paper: NMS PJK PH JT.

References

1. Cuypers HT, Selten G, Quint W, Zijlstra M, Maandag ER, Boelens W, et al. Murine leukemia virus-induced T-cell lymphomagenesis: integration of proviruses in a distinct chromosomal region. Cell 1984: 37: 141–150. PMID: 6327049
2. Brault L, Gasser C, Bracher F, Huber K, Knapp S, Schwaller J. PIM serine/threonine kinases in pathogenesis and therapy of hematological malignancies and solid cancers. Haematologica 2010; 95: 1004–1015. doi: 10.3324/haematol.2009.017079 PMID: 20145274
3. Bachmann M, Möröy T. The serine/threonine kinase Pim-1. Int J Biochem Cell Biol 2005; 37: 726–730. PMID: 15694833
4. Grundler R, Brault L, Gasser C, Bullock AN, Dechow T, Woetzel S, et al. Dissection of PIM serine/threonine kinases in FLT3-ITD-induced leukemogenesis reveals PIM1 as regulator of CXCL12-CXCR4-mediated homing and migration. J Exp Med 2009; 206: 1957–1970. doi: 10.1084/jem.20082074 PMID: 19687226
5. Zhang P, Wang H, Min X, Wang Y, Tang J, Cheng J, et al. Pim-3 is expressed in endothelial cells and promotes vascular tube formation. J Cell Physiol 2009; 220: 82–90. doi: 10.1002/jcp.21733 PMID: 19229879
6. Santio NM, Vahakoski RL, Rainio EM, Sandholm JA, Virtanen SS, Prudhomme M, et al. Pim-selective inhibitor DHPCC-9 reveals Pim kinases as potent stimulators of cancer cell migration and invasion. Mol Cancer 2010; 9: 279. doi: 10.1186/1476-4598-9-279 PMID: 20958956
7. Peltola K, Hollmen M, Maula SM, Rainio E, Ristamäki R, Luukkaa M, et al. Pim-1 kinase expression predicts radiation response in squamocellular carcinoma of head and neck and is under the control of epidermal growth factor receptor. Neoplasia 2009; 11: 629–636. PMID: 19568408
8. Tanaka S, Kitamura T, Higashino F, Hida K, Ohiro Y, Ono M, et al. Pim-1 activation of cell motility induces the malignant phenotype of tongue carcinoma. Mol Med Report 2009; 2: 313–318. doi: 10.3892/mmr_00000102 PMID: 21475831
9. Liu HT, Wang N, Wang X, Li SL. Overexpression of Pim-1 is associated with poor prognosis in patients with esophageal squamous cell carcinoma. J Surg Oncol 2010; 102: 683–688. doi: 10.1002/jso.21627 PMID: 20544717
10. Anizon F, Shtil AA, Danilenko VN, Moreau P. Fighting tumor cell survival: Advances in the design and evaluation of Pim Inhibitors. Curr Med Chem 2010; 17: 4114–4133. PMID: 20939820
11. Morwick T. Pim kinase inhibitors: a survey of the patent literature. Expert Opin Ther Pat 2010; 20: 193–212. doi: 10.1517/13543770903496442 PMID: 20100002
12. Arunesh GM, Shanthi E, Krishna MH, Sooriya Kumar J, Viswanadhan VN. Small molecule inhibitors of PIM1 kinase: July 2009 to February 2013 patent update. Expert Opin Ther Pat 2014; 24: 5–17. doi: 10.1517/13543776.2014.848196 PMID: 24131033
13. Mikkers H, Nawijn M, Allen J, Brouwers C, Verhoeven E, Berns A, et al. Mice deficient for all PIM kinases display reduced body size and impaired responses to hematopoietic growth factors. Mol Cell Biol 2004; 24: 6104–6115. PMID: 15199164
14. Qian KC, Wang L, Hickey ER, Studts J, Barringer K, Peng C, et al. Structural basis of constitutive activity and a unique nucleotide binding mode of human Pim-1 kinase. J Biol Chem 2005; 280: 6130–6137. PMID: 15525646
15. Akué-Gédu R, Rossignol E, Azzaro S, Knapp S, Filippakopoulos P, Bullock AN, et al. Synthesis, kinase Inhibitory potencies, and *in vitro* antiproliferative evaluation of new Pim kinase inhibitors. J Med Chem 2009; 52: 6369–6381. doi: 10.1021/jm901018f PMID: 19788246
16. Aumüller IB, Yli-Kauhaluoma J. Benzo[*cd*]azulene skeleton: Azulene, heptafulvene, and tropone derivatives. Org Lett 2009; 11: 5363–5365. doi: 10.1021/ol902283q PMID: 19904921
17. Kiriazis A, Vahakoski RL, Santio NM, Arnaudova R, Eerola SK, Rainio EM, et al. Tricyclic benzo[*cd*]azulenes selectively inhibit activities of Pim kinases and restrict growth of Epstein-Barr virus-transformed cells. PLoS One 2013; 8: e55409. doi: 10.1371/journal.pone.0055409 PMID: 23405147

18. Chen WW, Chan DC, Donald C, Lilly MB, Kraft AS. Pim family kinases enhance tumor growth of prostate cancer cells. Mol Cancer Res 2005; 3: 443–451. PMID: 16123140

19. Teicher BA, Fricker SP. CXCL12 (SDF-1)/CXCR4 pathway in cancer. Clin Cancer Res 2010; 16: 2927–2931. doi: 10.1158/1078-0432.CCR-09-2329 PMID: 20484021

20. Chinni SR, Sivalogan S, Dong Z, Trindade Filho JC, Deng X, Bonfil RD, et al. CXCL12/CXCR4 signaling activates Akt-1 and MMP-9 expression in prostate cancer cells: The role of bone microenvironment-associated CXCL12. Prostate 2006; 66: 32–48. PMID: 16114056

21. Kukreja P1, Abdel-Mageed AB, Mondal D, Liu K, Agrawal KC. Up-regulation of CXCR4 expression in PC-3 cells by stromal-derived factor-1alpha (CXCL12) increases endothelial adhesion and transendothelial migration: role of MEK/ERK signaling pathway-dependent NF-kappaB activation. Cancer Res 2005; 65: 9891–9898. PMID: 16267013

22. Singh S, Singh UP, Grizzle WE, Lillard JW Jr. CXCL12-CXCR4 interactions modulate prostate cancer cell migration, metalloproteinase expression and invasion. Lab Invest 2004; 84:1666–1676. PMID: 15467730

23. Taichman RS, Cooper C, Keller ET, Pienta KJ, Taichman NS, McCauley LK. Use of the stromal cell-derived factor-1/CXCR4 pathway in prostate cancer metastasis to bone. Cancer Res 2002; 62:1832–1837. PMID: 11912162

24. Stephenson RA, Dinney CP, Gohji K, Ordonez NG, Killion JJ, Fidler IJ. Metastatic model for human prostate cancer using orthotopic implantation in nude mice. J Natl Cancer Inst 1992; 84: 951–957. PMID: 1378502

25. Tuomela JM, Valta MP, Väänänen K, Härkönen PL. Alendronate decreases orthotopic PC-3 prostate tumor growth and metastasis to prostate-draining lymph nodes in nude mice. BMC Cancer 2008; 8: 81. doi: 10.1186/1471-2407-8-81 PMID: 18371232

26. Tuomela J, Valta M, Seppänen J, Tarkkonen K, Väänänen K, Härkönen P. Overexpression of vascular endothelial growth factor C increases growth and alters the metastatic pattern of orthotopic PC-3 prostate tumors. BMC Cancer 2009; 9: 362. doi: 10.1186/1471-2407-9-362 PMID: 19821979

27. Furusato B, Mohamed A, Uhlén M, Rhim JS. CXCR4 and cancer. Pathol Int 2010; 60: 497–505. doi: 10.1111/j.1440-1827.2010.02548.x PMID: 20594270

28. Brault L, Menter T, Obermann EC, Knapp S, Thommen S, Schwaller J, et al. PIM kinases are progression markers and emerging therapeutic targets in diffuse large B-cell lymphoma. Br J Cancer 2012; 107: 491–500. doi: 10.1038/bjc.2012.272 PMID: 22722314

29. Decker S, Finter J, Forde A, Kissel S, Schwaller J, Mack TS, et al. PIM kinases are essential for chronic lymphocytic leukemia cell survival (PIM2/3) and CXCR4 mediated microenvironmental interactions (PIM1). Mol Cancer Ther 2014; 13: 1231–1245. doi: 10.1158/1535-7163.MCT-13-0575-T PMID: 24659821

30. Busillo JM, Armando S, Sengupta R, Meucci O, Bouvier M, Benovic JL. Site-specific phosphorylation of CXCR4 is dynamically regulated by multiple kinases and results in differential modulation of CXCR4 signaling. J Biol Chem 2010; 285: 7805–7817. doi: 10.1074/jbc.M109.091173 PMID: 20048153

31. Sussman MA. Mitochondrial integrity: preservation through Akt/Pim-1 kinase signaling in the cardiomyocyte. Expert Rev Cardiovasc Ther 2009; 7: 929–938. doi: 10.1586/erc.09.48 PMID: 19673671

32. Foulks JM, Carpenter KJ, Luo B, Xu Y, Senina A, Nix R, et al. A small-molecule inhibitor of PIM kinases as a potential treatment for urothelial carcinomas. Neoplasia 2014; 16: 403–412. doi: 10.1016/j.neo.2014.05.004 PMID: 24953177

33. Kimmel CB, Ballard WW, Kimmel SR, Ullmann B, Schilling TF. Stages of embryonic development of the zebrafish. Dev Dyn 1995; 203: 253–310. PMID: 8589427

34. Nuüsslein-Volhard C, Dahm R. Zebrafish: a practical approach. 1st ed. Oxford, UK: Oxford University Press; 2002.

35. Ruohola JK, Valve EM, Kärkkäinen MJ, Joukov V, Alitalo K, Härkönen PL. Vascular endothelial growth factors are differentially regulated by steroid hormones and antiestrogens in breast cancer cells. Mol Cell Endocrinol 1999; 149: 29–40. PMID: 10375015

36. Evans JD. Straightforward statistics for the behavioral sciences. Pacific Grove,CA: Brooks Cole Publishing Company; 1996.

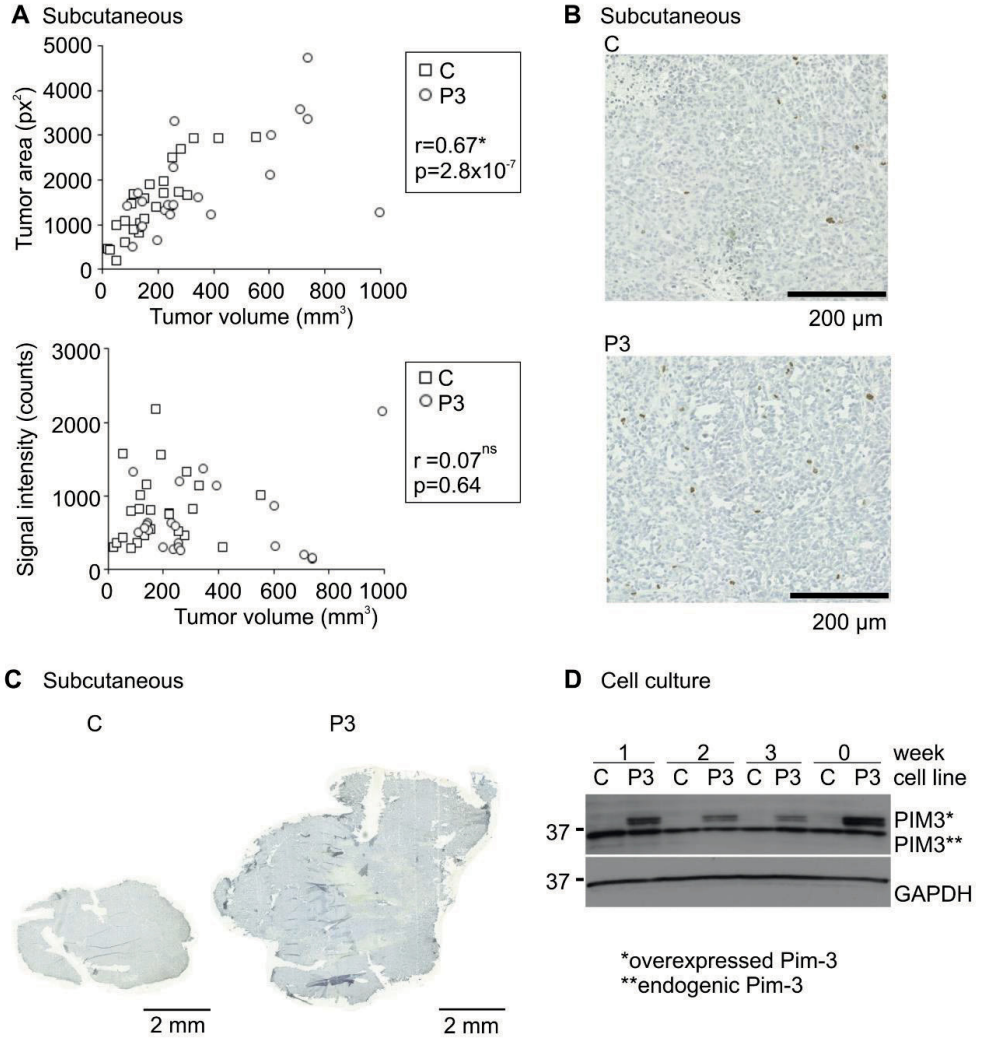

S1 Fig Subcutaneous tumor imaging and cell culture control.

PC-3-derived cell lines that had been stably transfected with the fluorescent Tomato vector and an empty vector (C) or a vector expressing Pim-3 (P3) were subcutaneously inoculated into the left and right backsides of nude mice (n = 4 +4). During the test period of 24 days, manual palpation and fluorescent imaging were performed three times. Correlations were analysed between the manually measured tumor volumes and either the areas or average signal intensities measured by fluorescent scanning. Shown are average results per each mouse at every time point (A). For analysis of mitotic cells, phospho-histone H3 staining (brown) was performed. Shown are representative images from control (C) and Pim-3 (P3) overexpressing tumors as well as whole tumor scan images for visualization of the differences in tumor size (B-C). Simultaneously to the animal experiment, cells were cultured in the absence of antibiotic selection to confirm stability of Pim-3 overexpression during the three-week test period (D).

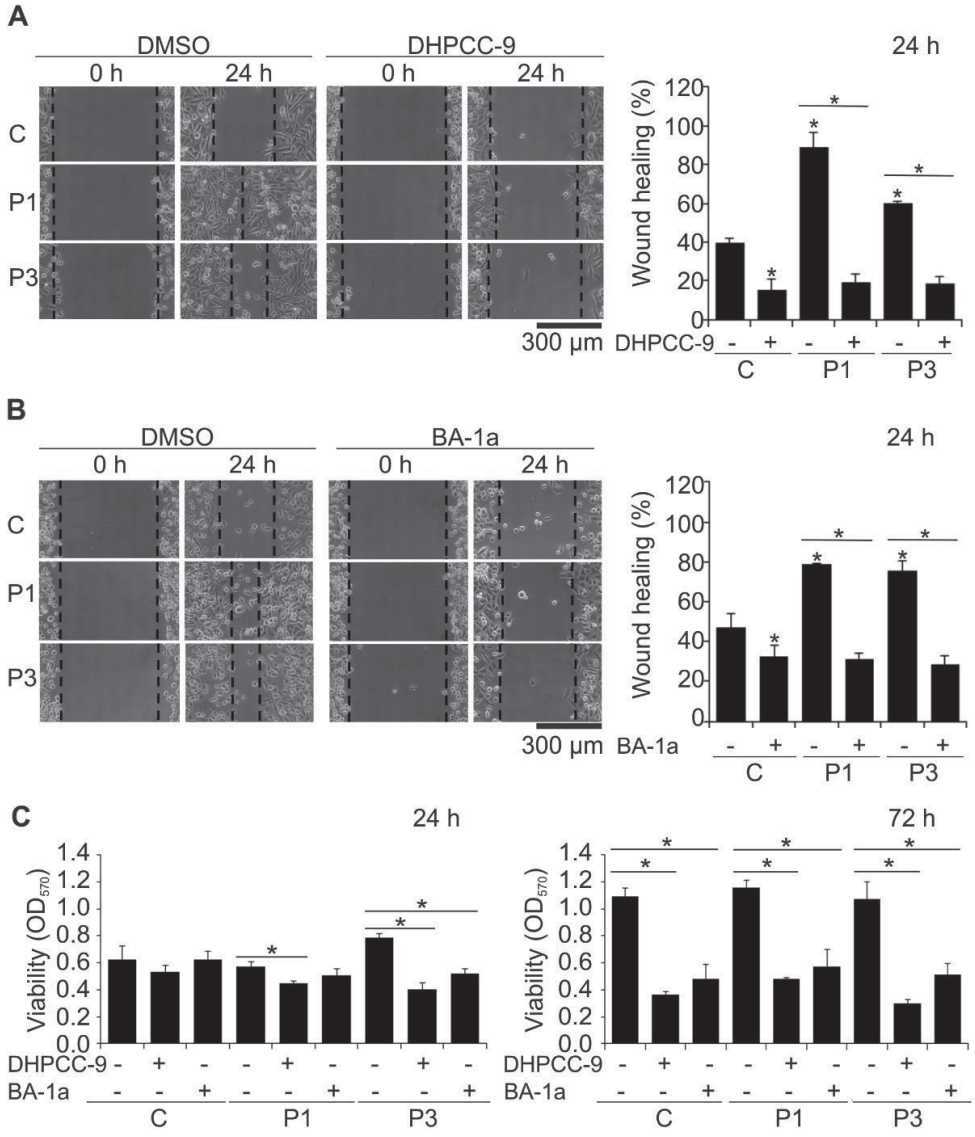

S2 Fig Both DHPCC-9 and BA-1a Pim inhibitors decrease migration and viability of stable Pim-overexpressing PC-3 cells.

Cell motility of stable control (C), Pim-1 (P1) or Pim-3 (P3) overexpressing PC-3 prostate cancer cells was analysed by wound healing assays. Cells were cultured on 24-well plates until confluency, after which wounds were scratched with 10 µl pipette tips. Cells were treated with 0.1% DMSO or DMSO-dissolved Pim inhibitors and samples were imaged and analysed at 0 and 24 h time-points. Shown are representative images along with average values from cells treated with either DHPCC-9 (A) or BA-1a (B). After 24 and 72 hours, viability of the cells was analysed by MTT assays. Shown are average OD_{570} values from triplicate samples from one representative experiment (C). For each assay, at least three separate experiments were carried out with highly similar results.

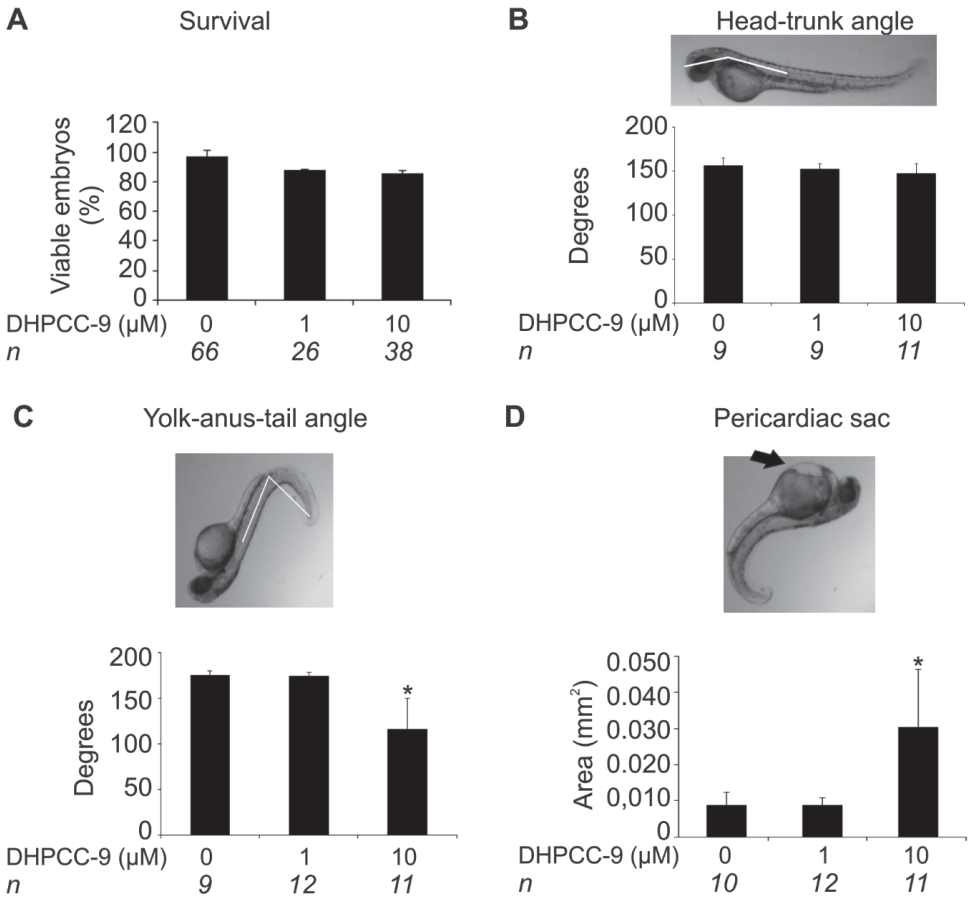

S3 Fig DHPCC-9 tolerance in zebrafish embryos.

Zebrafish embryos were treated at 6 h post-fertilization and analysed at 50 h post-fertilization. Shown is average survival in two experiments (A), and body curvatures (B-C) as well as pericardial sac sizes (D) in one experiment with representative images to visualize the angles and the pericardiac sac indicated by an arrow.

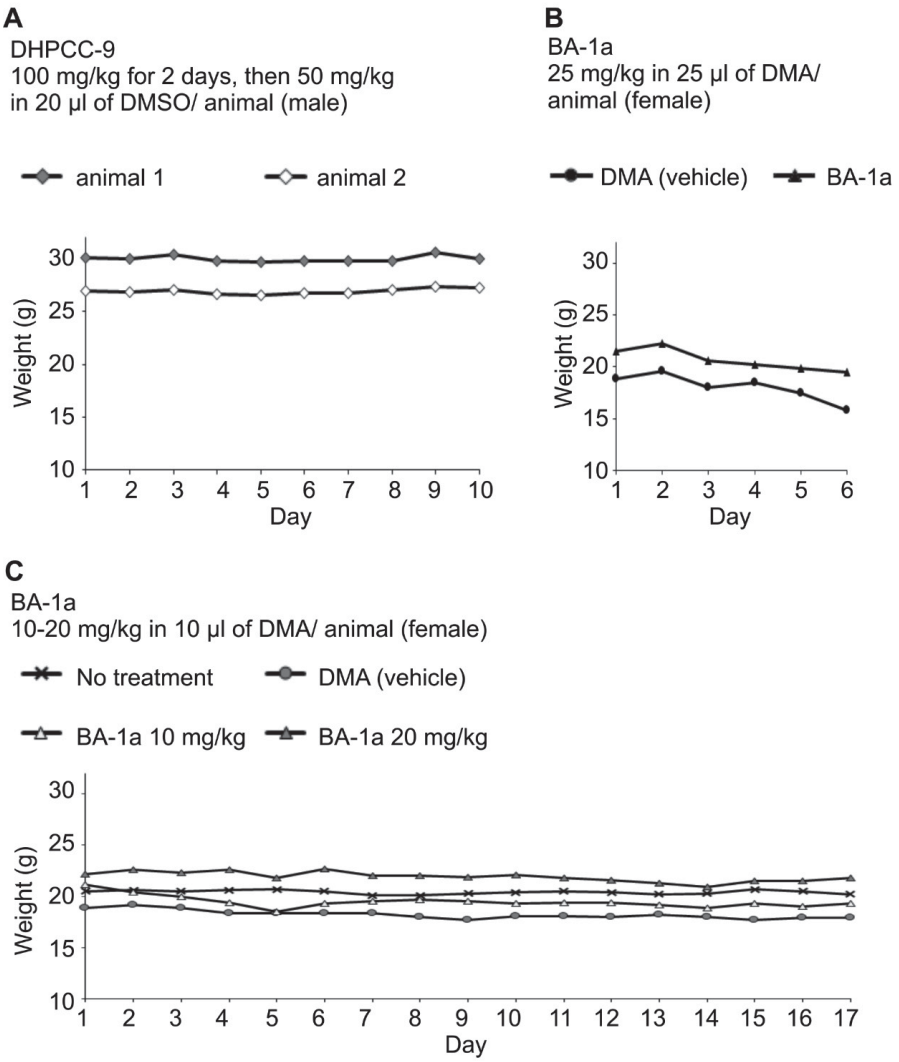

S4 Fig Mouse weight gain during toxicity testing.

White male or female mice were treated with various concentrations of either DMSO (A) or DMA (B-C) diluted Pim inhibitors and followed up for indicated time-periods to gain information about the possible cytotoxicity of the compounds.

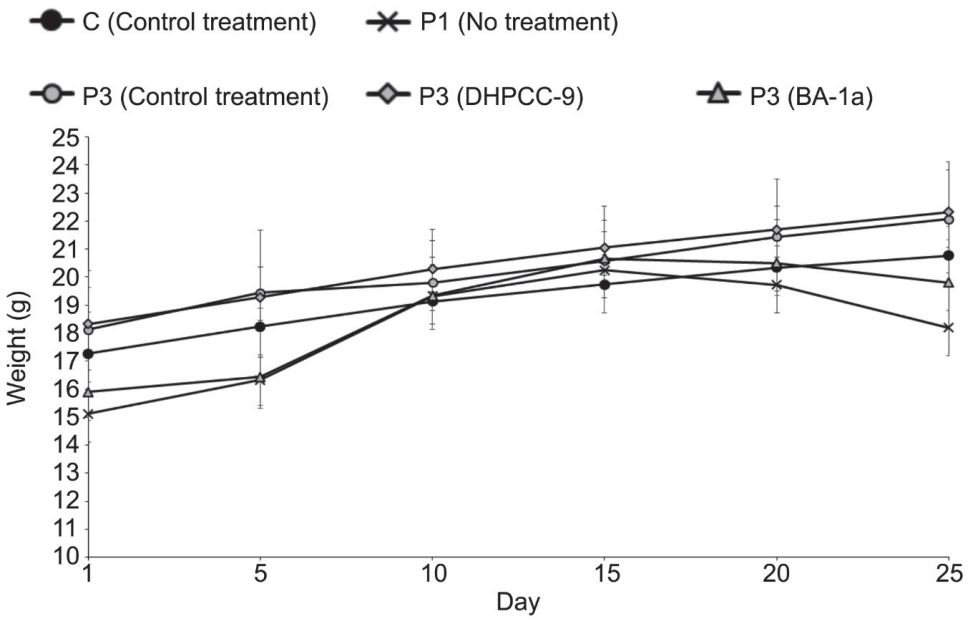

S5 Fig Mouse weight gain during the second orthotopic experiment.

Stable control (C) or Pim-1 (P1) or Pim-3 (P3) overexpressing PC-3 cells were orthotopically inoculated into nude mice. Mice were treated with DMSO or DMA as a control or with Pim inhibitors DHPCC-9 or BA-1a. Shown is the average mouse weight gain in each group during the test period.

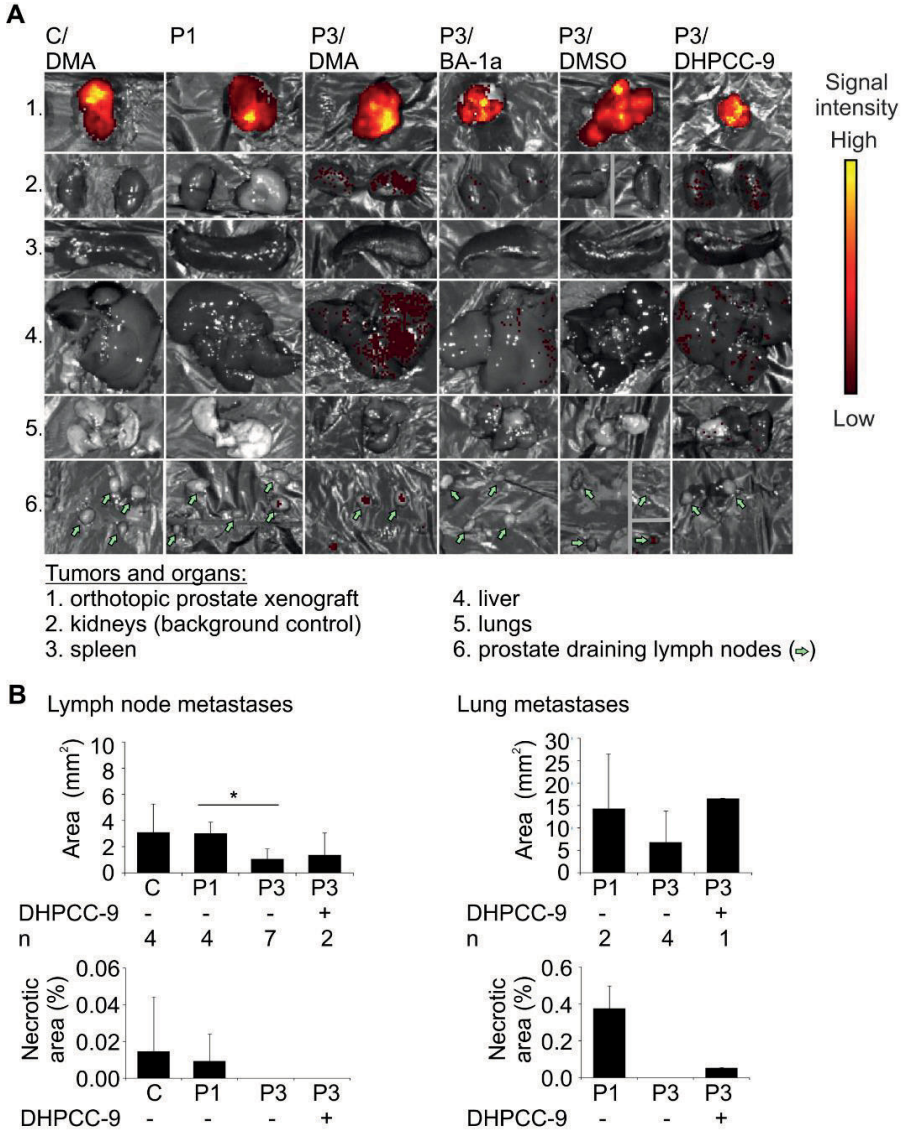

S6 Fig Fluorescent imaging of the second orthotopic set tissue samples.

At the second orthotopic set, tumors and tissue samples were fluorescently imaged to obtain information on the Tomato-derived signal of stably transfected PC-3 cells (Mock = C, Pim-1 = P1, Pim-3 = P3). Mice with control or Pim-3-overexpressing tumors were treated with 50 mg/kg of DHPCC9 in DMSO or 20 mg/kg of BA-1a in DMA or vehicles only. After approximately three weeks, mice were sacrificed, and tissues were imaged. In each animal, signal intensity was normalized according to background signal given by a kidney. Lymph nodes are pointed out by arrows. Shown are images from tumors and collected tissue samples (A). After detection of metastases in the lymph node and lung sections, the average areas of the metastases and the average necrotic areas in them were analysed. Shown are areas as well as the number (n) of mice with metastases in control treated and DHPCC-9 treated animals (B).

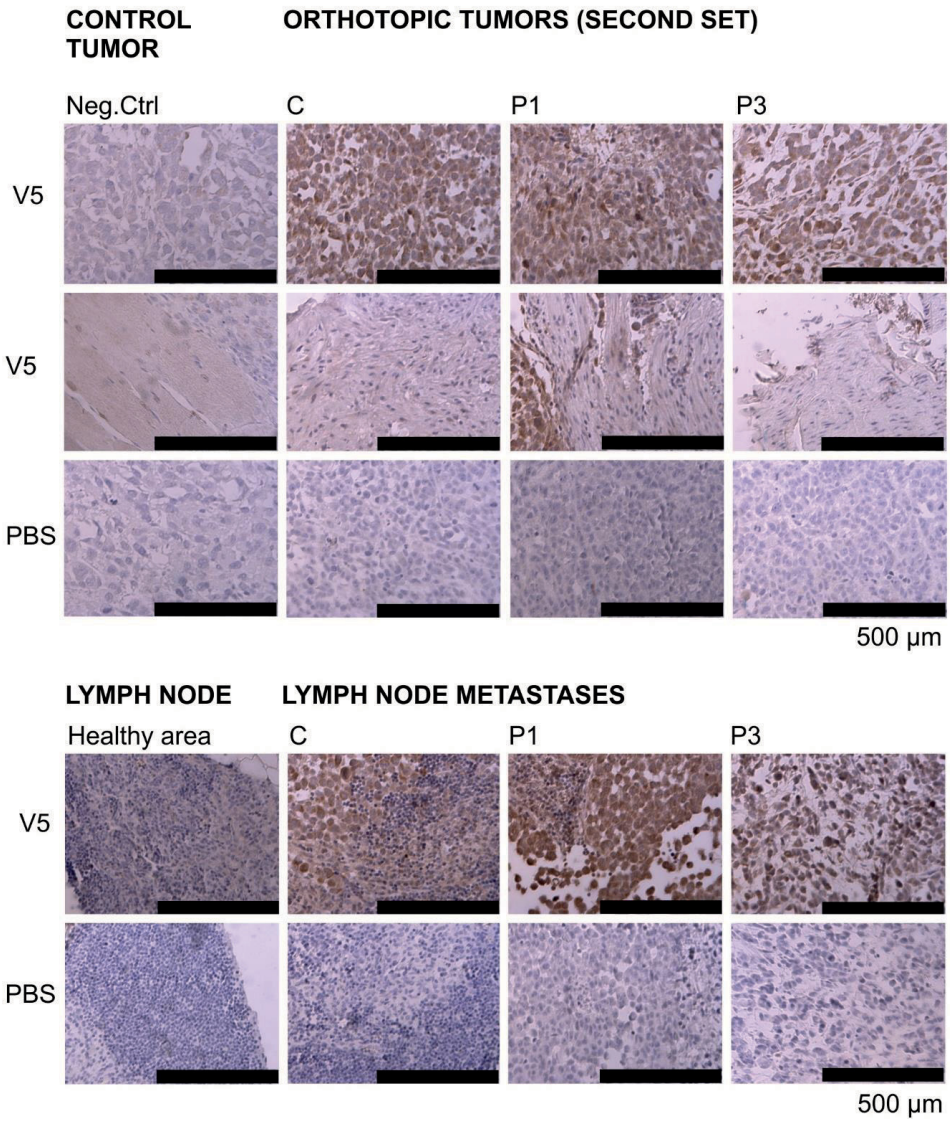

S7 Fig V5-immunostaining of xenografted cells within orthotopic tumors and their lymph node metastases.

Paraffin-embedded tissue sections from the second orthotopic set of tumors (Mock = C, Pim-1 = P1 and Pim-3 = P3), their surrounding mouse tissues and one control tumor (Neg. Ctrl) were stained with anti-V5 antibody. Shown are representative images from V5-positive or—negative samples.

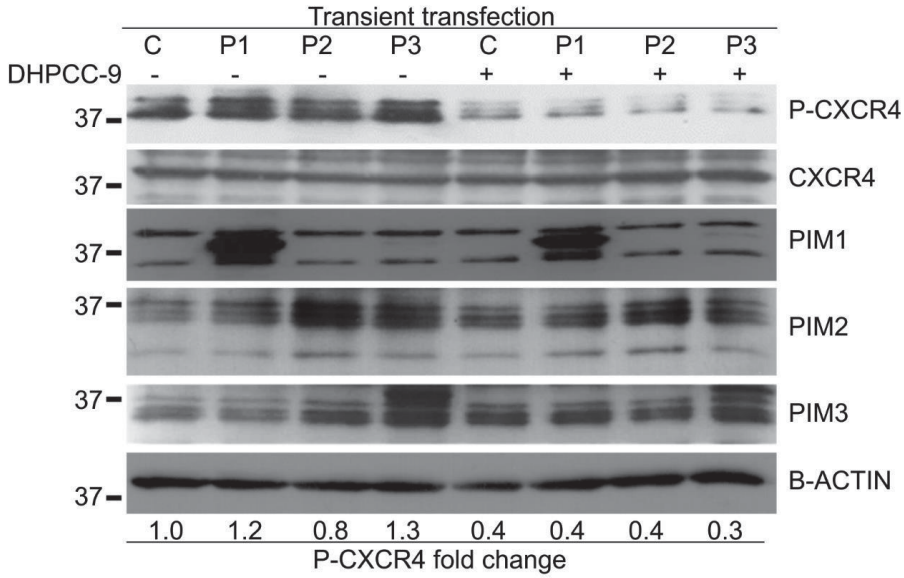

S8 Fig Pim-1 and Pim-3 increase, and DHPCC-9 decreases CXCR4 phosphorylation in PC-3 cells.

PC-3 cells transiently overexpressing an empty vector (C), Pim-1 (P1), Pim-2 (P2) or Pim-3 (P3) were treated with DMSO or 10 μM DHPCC-9 for 24 hours. CXCR4 phosphorylation was detected by phospho(Ser339)-CXCR4 antibody, after which the signal intensity was compared to the intensity of the CXCR4 signal. Pim overexpression was confirmed by Pim-specific antibodies, while β-actin was used as a loading control.

S1 Table. Pim inhibitor tolerance in zebrafish embryos.

List of zebrafish embryos treated with Pim inhibitors or DMSO at 6 h post-fertilization and analysed for their viability and possible abnormalities at 50 h post-fertilization.

Treatment	Concentration	Viable embryos	Normal body structure	Number of embryos
DMSO	0.1 %	100 %	100 %	8
BA-1a	1 µM	83 %	100 %	6
	5 µM	100 %	100 %	6
BA-2c	1 µM	86 %	100 %	7
	5 µM	57 %	0 %	7
DHPCC-9	10 µM	88 %	100 %	8

S2 Table. Animal numbers in the orthotopic experiments.

List of mice with or without prostate xenograft tumors derived from the stable PC-3 cell lines in the presence of control (DMSO or DMA) or Pim inhibitor treatments.

Experiment	Stable PC-3 cell line	Treatment	Animals		
			Tumor	No tumor	Total
Orthotopic 1 (preliminary)	Mock	-	1	-	1
	Pim-3	-	3	3	6
Orthotopic 2	Mock	DMSO	1	3	4
		DMA	5	-	5
	Pim-1	-	4	-	4
	Pim-3	DMSO	3	2	5
		DMA	5	3	8
		DHPCC-9	7	3	10
		BA-1a	3	3	6

S3 Table. Metastases from orthotopic tumors.

List of mice with prostate xenograft tumors and metastases in the prostate-draining lymph nodes and/or the lungs. In addition, the groups were compared based on the number of metastases in different organ types (lymph nodes or/and lungs). DMSO or DMA treatments have been combined as control treatments.

Experiment	Cell line	Treatment	Animals with metastases/group			
			Lymph nodes	Lungs	Lymph nodes or lungs	Lymph nodes and lungs
Orthotopic 1 (preliminary)	Mock	-	1/1	0/1	1/1	0/1
	Pim-3	-	3/3	2/3	3/3	2/3
Orthotopic 2	Mock	Control	4/6	0/6	4/6	0/6
	Pim-1	-	4/4	2/4	4/4	2/4
	Pim-3	Control	7/8	4/8	8/8	3/8
		DHPCC-9	2/7	1/7	3/7	0/7
		BA-1a	3/3	0/3	3/3	0/3

S4 Table. Protocols for immunohistochemistry.

Immunohistochemical staining of paraffin-embedded tissue samples was done according to following protocols for antigen retrieval (1), blocking (2), primary (3) and secondary antibody staining (4), Avidin-Biotin reaction (5) and DAB reaction (6)

Target	Step	Protocol
Mitotic cells	1	10 mM natrium citrate buffer, pH 6, 750 W, 10 min
	2	normal goat serum, S-1000 Vector, 2 %/ PBS, RT, 30 min
	3	rabbit polyclonal, Phospho-Histone H3, #9701 Cell Signaling Technology, 1:200/PBS, 4 °C, o/n
	4	goat anti-rabbit IgG, BA-1000 Vector, 1:200/ PBS, RT, 1 h
	5	PK-4000 Vector kit , RT, 1h
	6	SK-4100 Vector kit , RT, 5 min
V5-tag	1	0.1 M Tris-HCl + 2 mM EDTA, pH 9.0, 750 W, 10 min
	2	Normal horse serum, S-2000 Vector, 10%/ TBS, RT, 2 h
	3	goat polyclonal, V5, ab95038 Abcam, 1:500/ TBS, RT, 2 h
	4	horse anti-goat IgG, BA-9500 Vector, 1:200/ TBS, RT, 1 h
	5	PK-4000 Vector kit , RT, 30 min
	6	SK-4100 Vector kit , RT, 15 min
Blood vessels	1	10 mM natrium citrate buffer, pH 6, 750 W, 15 min
	2	normal rabbit serum, S-5000 Vector, 10 %/ PBS, RT, 2h
	3	rat monoclonal, CD34, ME 14.7, sc-18917 Santa Cruz, 1:50/ PBS, 4 °C, o/n
	4	rabbit anti-rat, DAKO 097(101)E0468, 1:200/ PBS, RT 1 h
	5	PK-4000 Vector kit , RT, 1 h
	6	SK-4100 Vector kit , RT, 15 min
Lymphatic vessels	1	0.1 M Tris-HCl + 2 mM EDTA, pH 9.0, 750 W, 10 min
	2	normal goat serum, S-1000 Vector, 25 %/ 5 % BSA/ PBS, RT, 30 min
	2	Avidin (A), RT, 10 min - Biotin (B), RT, 10 min blocking, 00-4304 Zymed
	3	rabbit polyclonal, m-LYVE-1 (Dr. Jackson, WIMM, Oxford, UK), 1:200/ blocking buffer, RT, 2.5 h
	4	goat anti-rabbit IgG, BA-1000 Vector, 1:200/ blocking buffer, RT, 1 h
	5	PK-4000 Vector kit , RT, 30 min
	6	SK-4100 Vector kit , RT, 10 min
Phosphor-ylated CXCR4 (S339)	1	10 mM natrium citrate buffer, pH 6, 750 W, 20 min
	2	normal goat serum, S-1000 Vector, 10 %/ PBS, RT, 2 h
	3	rabbit polyclonal, CXCR4 phospho S339, ab74012 Abcam, 1:500/ PBS, 4 °C, o/n
	4	goat anti-rabbit IgG, BA-1000 Vector, 1:200/ PBS, RT, 1 h
	5	PK-4000 Vector kit , RT, 30 min
	6	SK-4100 Vector kit , RT, 15 min
CXCR4	1	10 mM natrium citrate buffer, pH 6, 750W, 20 min
	2	normal goat serum, S-1000 Vector, 10 %/ PBS, RT, 2 h
	3	rabbit polyclonal, CXCR4, ab2074 Abcam, 1:200/ PBS, 4 °C, o/n
	4	goat anti-rabbit IgG, BA-1000 Vector, 1:200/ PBS, RT, 1 h
	5	PK-4000 Vector kit , RT, 30 min
	6	SK-4100 Vector kit , RT, 15 min

S5 Table. Detailed information for excluding samples in immunohistochemical analysis of the second orthotopic set samples.

Original sample number represents the number of mice with tumors in each group. DMSO or DMA treatments are combined as control treatments.

Cell line	Treatment	Original sample number *(n)*	Excluded samples (mice with a fully necrotic tumor)	Number of samples *(n)* in analysis
Mock	Control	6	1	5
Pim-1	-	4	0	4
Pim-3	Control	8	1	7
Pim-3	DHPCC-9	7	1	6
Pim-3	BA-1a	3	0	not analysed

S6 Table. Antibody dilutions for Western blotting.

Table contains details for primary antibody dilutions incubated at +4°C overnight.

Antibody	Product number	Species/ details	Dilution
anti-phospho (Ser339)-CXCR4	ab74012, Abcam	rabbit polyclonal	1:1000
anti-CXCR4	ab2074, Abcam	rabbit polyclonal	1:1000
anti-Pim-1	12H8; Santa Cruz	mouse monoclonal	1:500
anti-Pim-2	D1D2; Cell Signaling Technology	rabbit monoclonal	1:1000
anti-Pim-3	D17C9; Cell Signaling Technology	rabbit monoclonal	1:1000
anti-ß-actin	13E5, #4970S, Cell Signaling Technology	rabbit monoclonal	1:1000
anti-GAPDH	G8795, Sigma-Aldrich	mouse monoclonal	1:20 000

PUBLICATION II

Phosphorylation of NFATC1 at multiple sites is essential for its ability to promote prostate cancer cell migration and invasion

Eerola SK, Santio NM, Rinne S, Kouvonen P, Corthals G, Scaravilli M, Scala G, Serra A, Greco D, Ruusuvuori P, Rainio EM, Latonen L, Visakorpi T, Koskinen PJ

Cell Communication and Signaling, 2019; 17(1):148
DOI: 10.1186/s12964-019-0463-y

Eerola et al. Cell Communication and Signaling (2019) 17:148
https://doi.org/10.1186/s12964-019-0463-y

Cell Communication and Signaling

RESEARCH Open Access

Phosphorylation of NFATC1 at PIM1 target sites is essential for its ability to promote prostate cancer cell migration and invasion

Sini K. Eerola[1,2], Niina M. Santio[1], Sanni Rinne[1], Petri Kouvonen[3], Garry L. Corthals[3], Mauro Scaravilli[2,4], Giovanni Scala[2,5], Angela Serra[2], Dario Greco[2,5], Pekka Ruusuvuori[2,6], Leena Latonen[2,4], Eeva-Marja Rainio[1], Tapio Visakorpi[2,7] and Päivi J. Koskinen[1*]

Abstract

Background: Progression of prostate cancer from benign local tumors to metastatic carcinomas is a multistep process. Here we have investigated the signaling pathways that support migration and invasion of prostate cancer cells, focusing on the role of the NFATC1 transcription factor and its post-translational modifications. We have previously identified NFATC1 as a substrate for the PIM1 kinase and shown that PIM1-dependent phosphorylation increases NFATC1 activity without affecting its subcellular localization. Both PIM kinases and NFATC1 have been reported to promote cancer cell migration, invasion and angiogenesis, but it has remained unclear whether the effects of NFATC1 are phosphorylation-dependent and which downstream targets are involved.

Methods: We used mass spectrometry to identify PIM1 phosphorylation target sites in NFATC1, and analysed their functional roles in three prostate cancer cell lines by comparing phosphodeficient mutants to wild-type NFATC1. We used luciferase assays to determine effects of phosphorylation on NFAT-dependent transcriptional activity, and migration and invasion assays to evaluate effects on cell motility. We also performed a microarray analysis to identify novel PIM1/NFATC1 targets, and validated one of them with both cellular expression analyses and in silico in clinical prostate cancer data sets.

Results: Here we have identified ten PIM1 target sites in NFATC1 and found that prevention of their phosphorylation significantly decreases the transcriptional activity as well as the pro-migratory and pro-invasive effects of NFATC1 in prostate cancer cells. We observed that also PIM2 and PIM3 can phosphorylate NFATC1, and identified several novel putative PIM1/NFATC1 target genes. These include the ITGA5 integrin, which is differentially expressed in the presence of wild-type versus phosphorylation-deficient NFATC1, and which is coexpressed with PIM1 and NFATC1 in clinical prostate cancer specimens.

Conclusions: Based on our data, phosphorylation of PIM1 target sites stimulates NFATC1 activity and enhances its ability to promote prostate cancer cell migration and invasion. Therefore, inhibition of the interplay between PIM kinases and NFATC1 may have therapeutic implications for patients with metastatic forms of cancer.

Keywords: Prostate cancer, Metastatic carcinoma, NFATC1, PIM kinases, Cell motility

* Correspondence: paivi.koskinen@utu.fi
[1]Department of Biology, University of Turku, Vesilinnantie 5, FI-20500 Turku, Finland
Full list of author information is available at the end of the article

Background

Prostate cancer is globally one of the most prevalent cancers in men. Locally restricted prostate cancer is usually not fatal, but there is a clear need for effective therapies to prevent or stop progression of local tumors to a metastatic state spreading to bones and other vital organs. Formation of metastases is a multistep process, which includes detachment of cancer cells from the primary tumor, migration, adhesion and invasion of cancer cells into blood or lymph vessels, and infiltration of the cells to secondary sites. Thus, improved understanding of the proteins and signaling pathways that regulate the metastatic growth of cancer cells is essential when developing therapies to treat prostate cancer patients.

NFAT (Nuclear Factor of Activated T cells) transcription factors are ubiquitously expressed in human tissues, where they control cellular processes, such as immune responses [1]. However, one of the family members, NFATC1, has also been shown to act as an oncogene that promotes cancer cell proliferation and transformation [2]. Accordingly, elevated levels as well as increased transcriptional activity of NFATC1 have been detected in both solid cancers and hematological malignancies. NFATC1 has been shown to support cell migration or invasion in multiple types of cancer, such as ovarian, breast and prostate cancer as well as glioblastoma [3–7]. Furthermore, it has been reported to support metastatic behavior of prostate or breast cancer cells via increased osteoclastogenesis [8, 9].

Both the subcellular localization and transcriptional activity of NFAT proteins are post-translationally regulated. Most previously identified phosphorylation sites in NFATC1 have been located to the serine-rich regions (SRRs) and SPXX motifs within the NFAT homology region [10, 11]. Phosphorylation of these sites by kinases such as PKA and GSK3 results in nuclear exit and inactivation of NFATC1. By contrast, dephosphorylation of these sites by the calcium-dependent phosphatase calcineurin leads to nuclear translocation and transcriptional activation.

We have previously shown that the oncogenic PIM1 kinase directly interacts with NFATC1 and phosphorylates it in vitro [12]. However, in contrast to other kinases, PIM1 does not affect the subcellular localization of NFATC1, but stimulates its transcriptional activity in both immune and neuronal cells [12, 13]. PIM1 belongs to a family of three serine/threonine-specific kinases, which have partially overlapping expression patterns, but share several functions to support cell proliferation and survival [14–16]. Increased expression of PIM family members has been detected both in hematological malignancies and in solid tumors. In prostate cancer, overexpression of either PIM1 or PIM3 positively correlates with tumor size, aggressiveness and/or poor patient survival [17–21]. Furthermore, PIM kinases have been linked to regulation of prostate cancer cell motility in several cell-based and animal models, where they have supported cell migration, invasion, tumor angiogenesis and the formation of metastases [4, 16, 22]. As also NFATC1 promotes motility of prostate cancer cells and as PIM-selective inhibitors can block this [4], we now wanted to investigate whether or not PIM-dependent phosphorylation of NFATC1 is important for migration and invasion of prostate cancer cells. Therefore, we identified and mutated the PIM targets sites from NFATC1 and analysed the impact of these mutations in three prostate cancer cell lines, the hormone-insensitive PC-3 and DU-145 cells and the hormone-sensitive LNCaP cells. We also performed a microarray analysis to identify putative phosphorylation-dependent target genes for NFATC1.

Methods

Cell culture

The cell culture conditions for prostate epithelial adenocarcinoma cell line PC-3 and the stable cell lines overexpressing human PIM1 have been previously described [22]. DU145 and LNCaP prostate cancer cell lines were obtained from American Type Culture Collection (Manassas, VA) and cultured under recommended conditions. For transient transfections, Fugene 6 or HD reagents (Promega, Fitchburg, WI, USA) were used in 1:2 or 1:3 ratio to DNA according to manufacturer's instructions. All the cell lines were frequently tested for mycoplasma contamination. Viability of cells was analysed by the MTT assay [4] or the AlamarBlue® cell viability assay (Thermo Fisher Scientific, Waltham, MA, USA).

DNA constructs and cloning

The pcDNA3.1/V5-HisC, pGEX-6P-1 and pTag-RFP vectors expressing wild-type (WT) or kinase-deficient (KD) human PIM1, 2 or 3 or mouse PIM3 have been previously described [23]. The NFAT-luciferase reporter plasmids as well as wild-type (WT), N-terminally truncated (amino acids 1–418), dominant negative (DN, amino acids 410–680) and constitutively active SRR mutant (mSRR) human NFATC1 expression vectors based on pGEX-3X or pBJ5-Flag were kindly provided by the group of G.R. Crabtree (Stanford University, CA, USA) [10, 24]. Truncated NFATC1 was digested from pGEX-3X with PflMI and ligated to pEYFP-C2 (Clontech Laboratories, Mountain View, CA, USA). Full-length NFATC1 was multiplied by PCR from pBJ5-NFATC1-Flag by using a forward primer (5′ GCG GTA CCG CCA CCA TGG ACT ACA AGG CA 3′) and a reverse primer (5′ CCC GGA TCC CTG CGT CTT TAG 3′), digested with KpnI and BamHI, and ligated into pFlag-CMV-2 (Sigma-Aldrich), from where it was further

transfered to pEGFP-C3 (Clontech) by BglI and BamHI digestion, followed by ligation.

NFATC1 mutagenesis

The QuikChange™ site-directed mutagenesis kit (Stratagene, Agilent Technologies, Santa Clara, CA, USA) was used to prepare phosphodeficient mutants of NFATC1. Mutations to replace serines or threonines with alanine residues were introduced into ten PIM1 target sites with the help of five different primer pairs (Additional file 1: Table S1), resulting in production of double mutant (DM, two primer pairs, 1–2), triple mutant (TM, three primer pairs, 3–5) or multi mutant (MM, all primer pairs) NFATC1.

In vitro kinase assays

GST fusion proteins were produced in the *E. coli* BL21 strain as previously described [25] with minor modifications. Protein production was induced with 0,5 mM IPTG and protease activity was inhibited by Aprotinin (1:200; Sigma-Aldrich) during cell lysis. Proteins were either eluted as fusion proteins or cleaved by the PreScission protease according to manufacturer's protocol (GE Healthcare Life Sciences, Little Chalfont, UK). For in vitro kinase assays, cleaved PIM kinase (0.5 μg) and GST-tagged NFATC1 (amino acids 1–418) fusion protein (1 μg) were mixed prior to addition of the 2x kinase buffer (20 mM Pipes, pH 7.0, 5 mM $MnCl_2$, 0.25 mM β-glycerophophate, 0.4 mM spermine, 10 μM ATP) with 0.5 MBq of [^{32}P] adenosine triphosphate. To inhibit PIM kinase activity, samples were pre-treated for 15 min with 10 μM DHPCC-9, a pan-PIM inhibitor, which was kindly provided by P. Moreau (University of Clermont Auvergne, France) and dissolved in 0,1% DMSO. This ATP-competitive pyrrolocarbazole compound selectively inhibits catalytic activities of all PIM family members in vitro [26], in cell-based assays [4] and in mice xenografted with PIM-expressing prostate cancer cells [22]. After 15 to 30 min kinase reactions at 30 °C, samples were heated in 2x Laemmli sample buffer (LSB) for 5 min at 95 °C. Phosphorylated proteins were resolved in SDS-PAGE, stained by Page Blue solution (Thermo Fisher Scientific) and detected by autoradiography.

Identification of NFATC1 in vivo phosphorylation sites by mass spectrometry

PC-3 cells were transiently transfected with the pEYFP-NFATC1 expression vector. After 48 h, cells were stimulated with TPA and IM for 1 h prior to cell lysis in RIPA buffer supplemented with complete mini EDTA-free protease inhibitors (Roche, Basel, Switzerland). Protein concentrations were determined by the DC Lowry method (Bio-Rad Laboratories, Inc., Hercules, CA, USA). 1 mg aliquots of proteins were mixed with Chromotek-GFP-Trap® Magnetic beads (Allele Biotechnology, San Diego, CA, USA), after which GFP-tagged proteins were immunoprecipitated according to manufacturer's protocol, heated in 2x LSB, resolved in 10% Bis-Tris gel (Bio-Rad) and stained with colloidal coomassie blue solution (Thermo Fisher Scientific). NFATC1 protein isolation, trypsin digestion and titanium dioxide enrichment without salt extraction were performed as previously described [27, 28]. Thereafter, samples were analysed by LTQ Orbitrap Velos mass spectrometer (Thermo Fisher Scientific), using the HCD Top 10 method with 10 min gradient and mass value of 300 to 2000.

Luciferase assays

To measure NFAT-dependent transcriptional activity, PC-3 cells were transiently transfected with the pGL3-IL-2-luciferase reporter and either pBJ5-NFATC1-Flag or an empty control vector. To stimulate NFATC1 activity and nuclear translocation, cells were treated for 7 h with 15 ng/ml of 12–0-tetradecanoyl-phorbol-13-asetate (TPA; Sigma-Aldrich, St. Louis, MO, USA) in DMSO and 1 μM ionomycin (IM; Merck KGaA, Darmstadt, Germany) in EtOH. To inhibit PIM kinase activity, cells were treated for 24 h with 10 μM DHPCC-9 in 0,1% DMSO. As controls for all chemical compounds, their solvents were used. 24 or 48 h after transfections, cells were collected, lysed in 1% NP-40 buffer by repeated freezing and thawing, and analysed for luciferase activity using the Luminoscan Ascent luminometer (Thermo Fisher Scientific).

To compare activities of wild-type (WT) and multi mutant (MM) NFATC1 in PC-3, DU-145 and LNCaP cell lines, cells were transiently transfected with the pGL3-NFAT-luciferase reporter and either WT or MM pCMV-NFATC1-Flag or an empty control vector. Renilla luciferase (pRLTk; Promega) was co-transfected as an internal transfection efficiency control. Part of the cells were treated with TPA and IM and/or DHPCC-9 as described above. To inhibit calcineurin activity and thereby also nuclear translocation of NFATC1, cells were treated for 24 h with 1 μM cyclosporine A (CsA; Merck) in EtOH. Luciferase assays with four parallel samples were performed on 96-well plates using the Dual-Glo® Luciferase Assay System (Promega) according to manufacturer's protocol. Luciferase activities were measured with the EnVision 2104 Multilabel Reader (Perkin Elmer, Waltham, MA, USA). The results were presented as relative luciferase activity (RLU) corresponding to the firefly luciferase light emission values normalized against renilla luciferase light emission values.

Localization assays

To determine the subcellular localizations of wild-type and mutant NFATC1 proteins, PC-3 cells plated on

coverslips were transiently transfected with Flag-tagged expression vectors. After 48 h, cells were fixed, permeabilized and stained with anti-Flag antibody (Sigma-Aldrich) and Alexa Fluor™ 488 labelled anti-mouse secondary antibody (Thermo Fisher Scientific). Samples were imaged and analysed with the Zeiss ApoTome.2 fluorescence microscope and Zen lite 2012 software. Approximately 15 images were taken from each sample.

Fluorescence-lifetime imaging method (FLIM)

To visualize interactions between RFP-tagged PIM1 and GFP-tagged NFATC1, PC-3 cells plated on coverslips were transiently transfected with the corresponding expression vectors and/or their empty controls. Part of the samples were treated overnight with DMSO or 10 μM DHPCC-9. 48 h after transfection, cell samples were fixed with 4% PFA and mounted with Mowiol. First, physical interactions between tagged proteins were measured by analysing GFP lifetime with Lambert Instruments Fluorescence Lifetime Attachment (LIFA) and LI-FLIM software as previously described [23]. Then colocalization of proteins was imaged by Zeiss LSM 780 confocal microscope and by sequential scanning with ZEN lite 2012 software. Excitation wavelengths were 488 nm (GFP) and 561 nm (RFP), and emission wavelengths 500–535 nm (GFP) and 599–651 nm (RFP). Image analyses were performed with the ImageJ® software (Wayne Rasband, NIH, USA).

Wound healing assays

PC-3 or DU-145 cells were transiently transfected with wild-type or mutant NFATC1 expression vectors. 24 h later, samples were treated with either DMSO or 10 μM DHPCC-9. To confirm that changes in cell migration were not due to changes in cell proliferation, 15 μg/ml of the anti-proliferative agent mitomycin C (Sigma-Aldrich) was used. Scratching of the wounds, microscopy and image analyses of PC-3 cells were performed as previously described [4]. Imaging of DU-145 cells was performed with CM Technologies Cell-IQ (D.I. Biotech, Korea) by using 4x objective and image analysis with the Cell-IQ software 4.3 and scratch wound measurement tool.

Boyden chamber invasion assays

One day after transfection, invasiveness of PC-3 cells was analysed using cell culture invasion inserts of 8 μm pore size (Corning BioCoat™ Matrigel® Invasion Chamber, Bedford, MA, USA) according to manufacturer's instructions. For this purpose, cells were suspended in DMEM supplemented with 1% BSA (20,000 cells/each chamber) and either DMSO or 10 μM DHPCC-9. Conditioned medium from confluent MG-63 human osteosarcoma cells was used as a chemoattractant [29]. Cells were incubated for 48 h, after which insert membranes were fixed for 2 min in methanol and stained for 10 min with 0,2% crystal violet in methanol. Then they were cut out from the inserts and mounted with immersion oil. Invaded cells on the membranes were scanned by the Olympus BX51 scanner with Surveyor software and analysed by automated image analysis. Results were verified by manual counting with the ImageJ® software from 5 random fields of each membrane.

Gelatinase activity assay

Gelatinase activity assay was performed with InnoZyme™ gelatinase (MMP-2/MMP-9) fluorogenic activity assay kit (Merck) according to manufacturer's instructions. Medium samples for the assay were collected from the upper chambers of invasion inserts after the invasion assays described above. Samples were incubated at + 37 °C for 3 h protected from light. Fluorescence was then measured with the Envision plate reader (Perkin Elmer) with an excitation wavelength of 320 nm and an emission wavelength of 405 nm.

Western blotting

Cells were lysed in 2x LSB and heated at 95 °C for 5 min. Proteins were separated by SDS-PAGE, immobilized onto PVDF-membrane (EDM Millipore, Merck) and incubated overnight with anti-PIM-1 (1:500, 12H8; Santa Cruz Biotechnology, Santa Cruz, CA, USA), anti-PIM-2 (1:1000, D1D2; Cell Signaling Technology, Danvers, MA, USA), anti-PIM-3 (1:1000, D17C9; Cell Signaling Technology), anti-NFATC1 (1:500, Santa Cruz Biotechnology), anti-V5 (1:500, Invitrogen, Carlsbad, CA, USA), anti-Flag (1:500, F1804; Sigma-Aldrich), anti-ACTB (anti-β-actin; 1:1000, 13E5, #4970S, Cell signaling Technology), anti-GAPDH (1:50000, Sigma-Aldrich), anti-β Tubulin (1:40000, Sigma-Aldrich) or anti-Fibrillarin (1:1000, Cell Signaling Technology) antibodies. After incubations with secondary antibodies, chemiluminescence reactions were generated using either Amersham™ ECL Plus or ECL Prime reagents (GE Healthcare).

Microarray analyses

For microarray analyses, PC-3 cells with or without stable PIM1 overexpression were transiently transfected with wild-type (WT) or multi mutant (MM) NFATC1 expression vectors. At the following day, total RNAs were extracted using the TRIzol reagent (Invitrogen, Carlsbad, CA, USA) according to the manufacturer's protocol. The samples were then labelled and hybridized using the Agilent whole genome oligo microarray platform on Human Gene Expression v2 4x44K Microarray slides (G4845A; Agilent Technologies, Palo Alto, CA, USA). The slides were scanned on the Agilent C-Scanner and the raw expression values were extracted

using the Agilent Feature Extraction software v. 11.0.1.1. Raw mRNA expression values were imported using limma read.maimages function. Low quality probes were filtered using the distribution of negative control probes as a reference. In particular, only probes whose raw expression values were higher than the 90th percentile of negative control probes were retained for successive analysis. Expression values were log2 transformed, quantile normalized between samples and median aggregated at the gene symbol level using Agilent annotation. A limma-based approach [30] was then applied to estimate the difference in average expression in each comparison. A fold-change cutoff (≥0.1) and *p*-value of (< 0.05) were used to determine differential gene expression.

Canonical pathway analysis

IPA (Ingenuity Pathway Analysis, Ingenuity Systems) was used for functional enrichment and detection of pathways with significant alterations based on microarray gene expressions. In canonical pathway analysis -log(*p*-values) over threshold 2.5 were considered significant.

Real-time quantitative polymerase chain reaction (qRT-PCR)

PIM, *NFATC1* and *ITGA5* expression levels were determined from total RNAs isolated from PC-3 cells as described above. Quantitative real-time PCR was performed using random hexamere primers, Maxima reverse transcriptase (Thermo Scientific), Maxima SYBR Green qPCR Master Mix (Thermo Fischer Scientific) and the CFX96™ Real-Time PCR Detection System (Bio-Rad Laboratories, Inc.). Each sample was run in triplicate, and expression values were normalized against the TATA-binding protein (TBP). Sequences of all primers (Sigma-Aldrich) for qRT-PCR are described in the Additional file 1: Table S2.

Gene correlation analyses

Three distinct clinical data sets were used to assess correlations between two different genes in clinical prostate cancer patient samples: The Cancer Genome Atlas (TCGA) - Prostate adenocarcinoma RNA-Sequencing data [31], Integrative Genomic Profiling of Human Prostate Cancer microarray data [32] and Tampere PC sequencing data [33].

Statistical analyses

The statistical significance of data from luciferase, wound healing, FLIM and cell viability assays was determined using the two-sided *t*-test. Cell invasion and gelatinase activity data were analysed by using the unpaired two-sided *t*-test or Wilcoxon matched pairs test. In RT-qPCR data validation, *P*-values were determined by the Mann-Whitney U-test. In gene correlation analyses, Pearson correlation coefficient and *P*-values were determined according to Gaussian populations. In all analyses, a *P*-value < 0.05 was considered statistically significant (*), $P < 0.01$ (**) and $P < 0.001$ (***). Error bars represent standard deviation (SD) values in each graph. Statistical analyses were performed using the GraphPad Prism version 5.02 (GraphPad Software, La Jolla, CA, USA).

Results

NFATC1 is endogenously expressed and constitutively active in PC-3 cells

As we had previously shown both PIM kinases and NFATC1 to be essential for the motility of PC-3 prostate cancer cells [4], we decided to use these cells in order to investigate in more detail the functional interactions between PIM and NFATC1 proteins. When we analysed the basal expression and transcriptional activity of NFATC1 in PC-3 cells, Western blotting with NFATC1 antibodies detected an endogenously expressed protein with the expected size of approximately 75 kDa (Fig. 1a). NFAT-dependent luciferase assays in turn revealed endogenous NFAT activity, which was dependent on the presence of NFAT binding sites (Fig. 1b), and which was enhanced by ectopic overexpression of NFATC1, but not by stimulation of cells with TPA and the calcium ionophore ionomycin (Fig. 1c). This was surprising, since usually the nuclear translocation and activation of NFATC1 is tightly regulated in a calcium- and calcineurin-dependent fashion [1, 2]. To determine the subcellular localization of NFATC1 in PC-3 cells, we transiently expressed there wild-type (WT) or mutant NFATC1 proteins (24; Table 1). While the dominant negative (DN) mutant was mostly retained in the cytoplasm and the constitutively active (mSRR) mutant in the nucleus, the WT protein could be detected in both compartments (Fig. 1d, Additional file 2: Figure S1A), suggesting that it can shuttle between the compartments of PC-3 cells. When we carried out wound healing assays to compare the effects of WT and mSRR NFATC1 on cell migration, we noticed that both of them enhanced cell motility as compared to control cells (Fig. 1e), while no major changes were observed in cell viability (Additional file 2: Figure S1B).

PIM kinases phosphorylate NFATC1 in several serine and threonine residues

As we had previously shown that the PIM1 kinase phosphorylates NFATC1 and enhances its transcriptional activity [12], we now wanted to identify the as yet unknown PIM1 target sites in NFATC1 and to investigate their physiological roles in more detail. For this purpose, we carried out in vitro kinase assays with GST-tagged PIM-1 and NFATC1 (amino acids 1–418) produced in bacteria, and cell-based assays with YFP-tagged

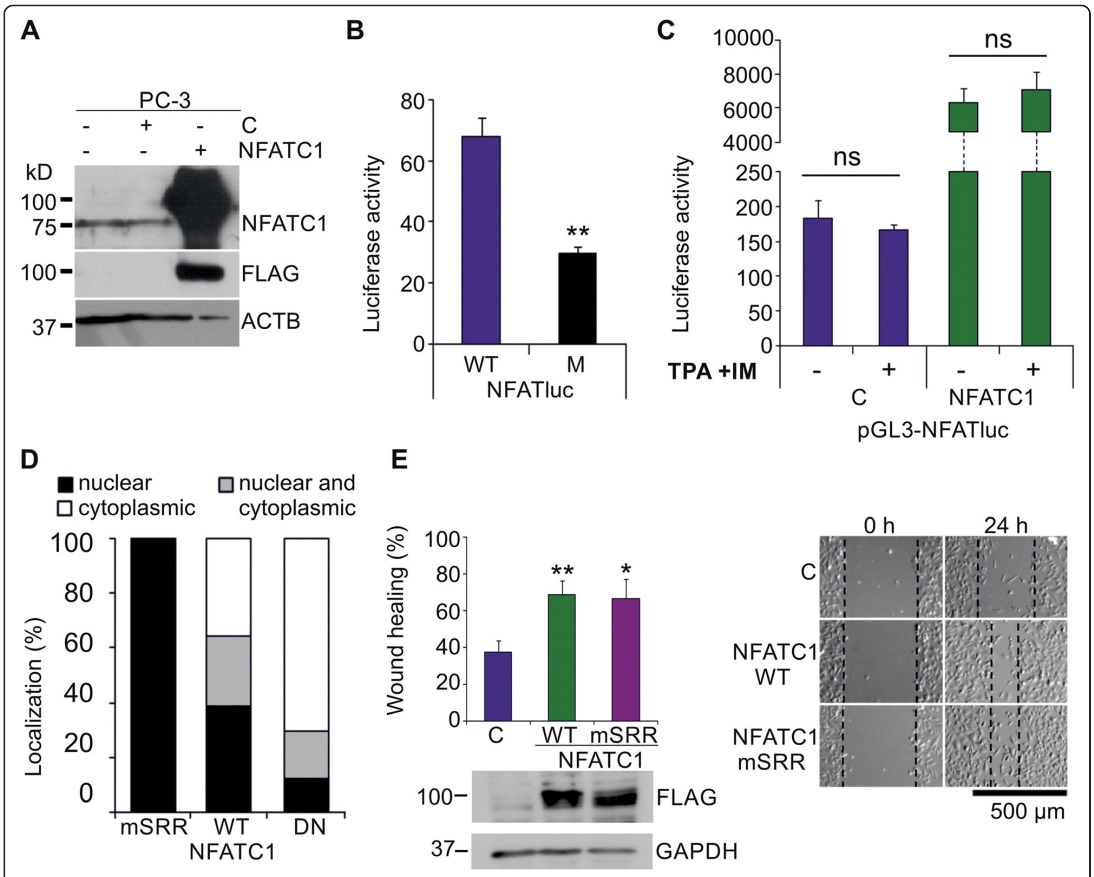

Fig. 1 NFATC1 is constitutively active in PC-3 cells. Flag-tagged NFATC1 or its mutated derivatives were transiently expressed in PC-3 prostate cancer cells. Untransfected (–) or mock-transfected cells were used as controls. **a** The endogenous or ectopic expression levels of NFATC1 were analysed by Western blotting with antibodies against NFATc1 or Flag, while ACTB staining was used as a loading control. **b** The endogenous NFAT activity of PC-3 cells was measured by luciferase assays, using transiently transfected reporters with wild-type (WT) or mutated (M) NFAT binding sites. Shown are mean luciferase activities from two independent experiments. **c** The effects of TPA and ionomycin on NFAT activity were measured by luciferase assays. Shown are luciferase activities of duplicate samples from one representative experiment. **d** Subcellular localizations of transiently expressed wild-type (WT) NFATC1, the constitutively active (mSRR) mutant and the dominant negative (DN) mutant were analysed by confocal microscopy after staining with anti-Flag antibody. Shown are average localization patterns from one experiment with three parallel samples. **e** The abilities of WT NFATC1 and the mSRR mutant to promote cell motility were analysed by wound healing assays from three parallel samples. Equivalent expression of these proteins was confirmed by Western blotting with anti-Flag antibody, while GAPDH staining was used as a loading control

Table 1 Different NFATC1 forms and mutants used in the experiments

NFATC1 proteins	Mutated sites	Length
Wild type (WT)	none	full-length
Dominant negative (DN)	none	410–680 aa
Constitutively active (mSRR)	all 11 serines mutated to alanines in the SRR (172–194)	1–418 aa
Double mutant (DM)	S245, S269	full-length
Triple mutant (TM)	S151, S153, T154, S256, S257, S335, T338, T339	full-length
Multi mutant (MM)	S151, S153, T154, S245, S256, S257, S269, S335, T338, T339	full-length

The amino acid substitutions (from serine or threonine to alanine) and other mutations in NFATC1 and the length of each mutant protein used in this study

NFATC1 protein overexpressed in PC-3 cells. When phosphorylated NFATC1-derived peptides were subjected to mass spectrometry analyses, several novel phosphorylation target sites were discovered both from the in vitro samples and from the PC-3 cell-derived samples (Fig. 2a, Additional file 1: Table S3) in addition to those in vivo sites that we had already previously identified from COS-7 cells [27]. However, since more endogenously phosphorylated cellular sites were discovered than in vitro target sites for PIM1, it was evident that many of the in vivo sites were targeted by other kinases.

To be able to evaluate the functional impact of phosphorylation at putative PIM1 target sites, we mutated multiple serine or threonine residues in NFATC1 into alanines to create phosphodeficient mutants (Fig. 2a, Table 1, Additional file 1 Table S3). The mutated sites were primarily chosen based on the presence of PIM1 consensus target sequences [34] with basic residues preceding the in vivo phosphosites observed in PC-3 cells. Those were supplemented with close-by sites that had been phosphorylated by PIM1 in vitro. Stepwise mutagenesis resulted in approximately 50% (double mutant, DM) or 90% (multi mutant, MM) reduction in the ability of PIM1 to phosphorylate NFATC1 in vitro, while the previously validated PIM-selective inhibitor DHPCC-9 [4, 26] fully abrogated PIM1 autophosphorylation and PIM1-mediated NFATC1 phosphorylation (Fig. 2b). In addition to PIM1, also PIM2 and PIM3 were able to phosphorylate WT, but not MM NFATC1 in vitro (Fig. 2c).

Both wild-type and phosphomutant NFATC1 interact with PIM1 in PC-3 cells

To assess the subcellular localization of WT versus phosphodeficient NFATC1, we transiently expressed them in PC-3 cells, where they showed similar localization patterns in the nucleus, in the cytoplasm or in both (Fig. 3a, Additional file 1: Figure S1C). As we had previously shown that NFATC1 and PIM1 can be co-immunoprecipitated with each other [12], we now wanted to determine whether the mutations in the PIM1 target sites affected either the colocalization or the physical interaction of GFP-tagged NFATC1 proteins with RFP-tagged PIM1. For these purposes, confocal microscopy and the fluorescence-lifetime imaging method (FLIM) were used as in our previous studies [23]. Both WT and MM NFATC1 showed nuclear co-localization (Fig. 3b) as well as interaction (Fig. 3c) with PIM1, as was evident from merged confocal images and from reduced lifetimes of GFP signals, respectively. Furthermore, the PIM inhibitor DHPCC-9 did not have major effects on the localizations or interactions, indicating that PIM-induced phosphorylation was not required there (Fig. 3b, c).

Phosphorylation by PIM1 promotes NFATC1 activity

To determine whether phosphorylation affects transcriptional activity of NFATC1, we transiently overexpressed WT and mutant NFATC1 proteins in three different prostate cancer cell lines, PC-3, DU-145 and LNCaP cells. Both PC-3 and DU-145 cells represent hormone-

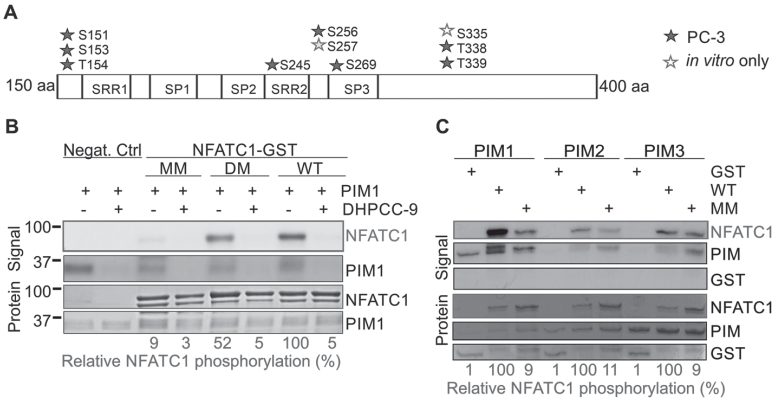

Fig. 2 PIM1 phosphorylates NFATC1 at several novel target sites. **a** A schematic representation of the phosphorylation target sites for PIM1 in NFATC1 that were detected in vivo in PC-3 cells (marked with red filled stars) or only in vitro (marked with open stars), and that were mutated in this study. **b** Wild-type (WT) NFATC1 was mutated at two in vivo sites (S245A and S269A in the double mutant, DM) or at all detected sites (multi mutant, MM), grown in bacteria as GST fusion proteins and subjected to radioactive in vitro kinase assays with human PIM1 pretreated with DMSO (–) or 10 μM DHPCC-9 (+). Shown in the upper panel are the signal intensities of phosphorylated proteins (NFATC1 phosphorylation lined red), in the lower panel the total amounts of proteins (NFAT total protein loadings lined red), and under the panels the relative levels of phosphorylation of WT NFATC1 (100%) versus those of the mutants. **c** Similar kinase assays were performed also with human PIM2 and mouse PIM3

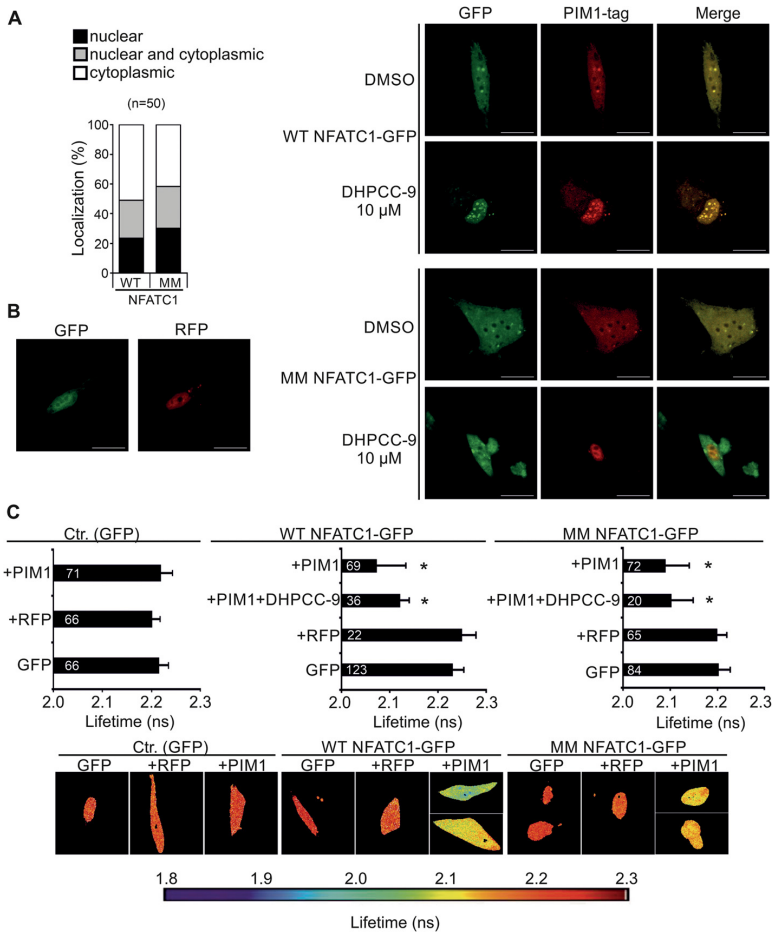

Fig. 3 PIM1 interacts with NFATC1 in PC-3 cells. **a** Wild-type (WT) or multi mutant (MM) NFATC1 were transiently expressed in PC-3 cells and their subcellular localization patterns were analysed by confocal microscopy after staining with anti-Flag antibody. Shown are means from one experiment with three parallel samples. **b** The physical interactions between RFP-tagged PIM1 and GFP-tagged WT or MM NFATC1 proteins were analysed by fluorescence-lifetime imaging microscopy (FLIM) from samples of transiently transfected PC-3 cells. 24 h after transfection, cells were treated overnight with DMSO or 10 μM DHPCC-9. Shown on the left are representative images of negative control cells with expression of empty GFP or RFP vectors, while on the right are single channel or merged images of cells co-transfected with GFP- or RFP-tagged vectors. Scale bar 20 μm. **c** Shown are average GFP lifetimes from two independent FLIM experiments along with sample numbers inside the black bars as well as representative images with a heatmap. Lowest negative control (GFP + RFP) value was set as the limit for physical interaction

insensitive tumors, while LNCaP cells are hormone-sensitive, but carry mutated androgen receptors [35]. Based on our previously published RNA-sequencing dataset [36], endogenous *PIM1* mRNA expression levels were relatively high in PC-3 cells, lower in DU-145 cells and lowest in LNCaP cells, while relatively low *NFATC1* mRNA levels were observed for all cell lines (Fig. 4a).

According to data from NFAT-luciferase assays, PC-3 cells had clearly higher basal NFAT activity than DU-145 or LNCaP cells, although in DU-145 cells the activity could be increased by stimulation with TPA and the calcium ionophore ionomycin (Fig. 4b, Additional file 1: Figure S4A). This suggests that in contrast to PC-3 cells, NFAT nuclear translocation and activation are normally regulated by calcium and calcineurin in DU-145 cells. This conclusion was further supported by the ability of cyclosporin to slightly suppress NFAT activity in stimulated DU-145 cells, but not in any other cell samples (Fig. 4c, Additional file 1: Figure S4B).

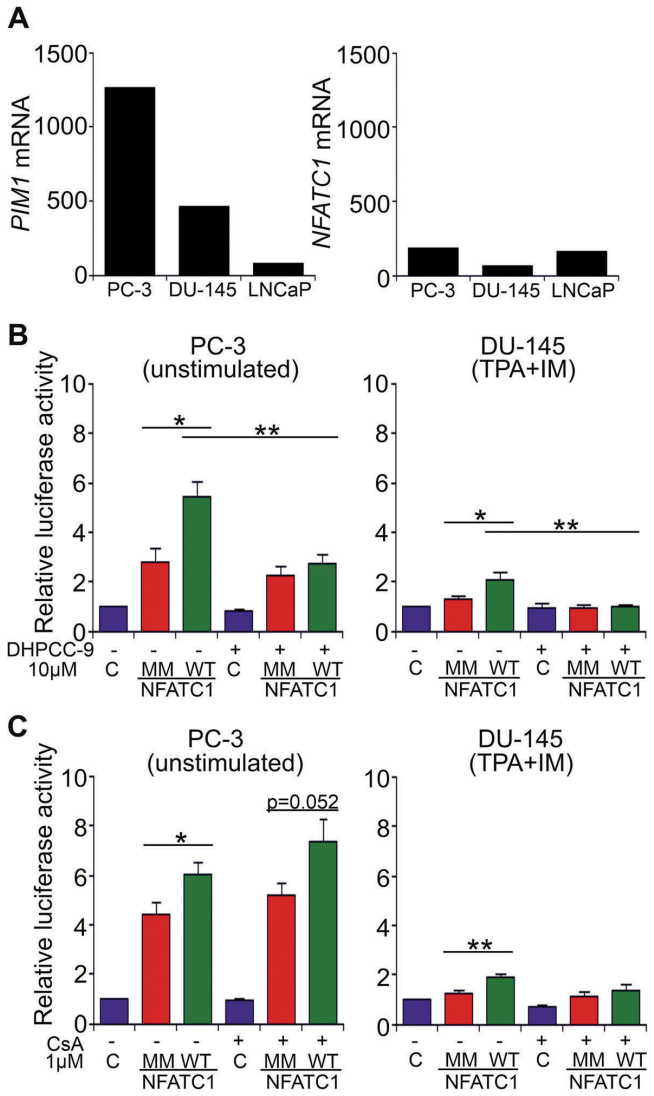

Fig. 4 Effects of PIM-dependent phosphorylation on NFAT activity. **a** The expression levels of *PIM1* and *NFATC1* mRNAs were determined from our previously published RNA-sequencing dataset from PC-3, DU-145 and LNCaP cell lines [36]. **b** The impact of PIM-dependent phosphorylation on NFAT activity was analysed by luciferase assays in PC-3 and DU-145 cells that transiently expressed wild-type (WT) or multi mutant (MM) NFATC1. Cells were treated with either DMSO (–) or 10 μM DHPCC-9 (+). In addition, DU-145 cells had been pre-treated with TPA and IM. Shown are means of relative luciferase activities from two independent experiments with four parallel samples, the results of which had been normalized against the mock-transfected control samples. **c** Similar luciferase assays were performed also with cells treated with either EtOH (–) or 1 μM CsA (+)

The presence of overexpressed WT NFATC1 strongly enhanced NFAT activity in all three cell lines, while mutations in the PIM1 target sites or treatment of cells with the PIM inhibitor DHPCC-9 resulted in significantly compromised NFAT activities in PC-3 and DU-145 cells, but not in LNCaP cells (Fig. 4b, Additional file 1: Figure S4). These results indicated that full NFAT activity was dependent on phosphorylation of PIM target sites in PC-3 and DU145 cells, but PIM-independent in LNCaP cells, where nearly negligible *PIM* mRNA levels had been observed (Fig. 4a).

Prostate cancer cell motility is regulated by NFATC1 phosphorylation

As we had previously shown that PIM inhibition blocks the pro-migratory effects of NFATC1 in PC-3 cells [4], we wanted to investigate the role of NFATC1 phosphorylation in this context. In wound healing assays with PC-3 cells transiently overexpressing WT NFATC1 or phosphomutants, mutations in the PIM target sites significantly reduced the ability of NFATC1 to promote cell migration (Fig. 5a). While there were minor effects by the DM mutant and more pronounced effects by the MM mutant, PIM inhibition by DHPCC-9 completely blocked cell migration in each case. Similar wound healing experiments were also performed with DU-145 prostate cancer cells, which transiently overexpressed WT NFATC1 or the multi mutant. As in PC-3 cells, mutations in the PIM target sites abolished the ability of NFATC1 to promote cell migration (Fig. 5b). Also DHPCC-9 diminished motility, but less efficiently than in PC-3 cells, which migrated slightly slower than DU-145 cells.

Western blotting was used to confirm equivalent protein levels of NFATC1 and PIM family members in PC-3 cells (Additional file 1: Figure S3A). DHPCC-9 slightly reduced them, but did not significantly affect cell viability (Additional file 1: Figure S3A, B). Similar viability and protein expression data were obtained also from DU-145 cells (Additional file 1: Figure S3C). Additional wound healing assays were performed in PC-3 cells in the presence of mitomycin C to exclude effects of cell proliferation on cell migration (Additional file 1: Figure S3D), but no major differences were observed as compared to its absence (Fig. 5a). More interestingly, the triple mutant (TM) NFATC1 with intact S245 and S269 sites blocked cell migration almost as efficiently as MM lacking them, suggesting that the pro-migratory

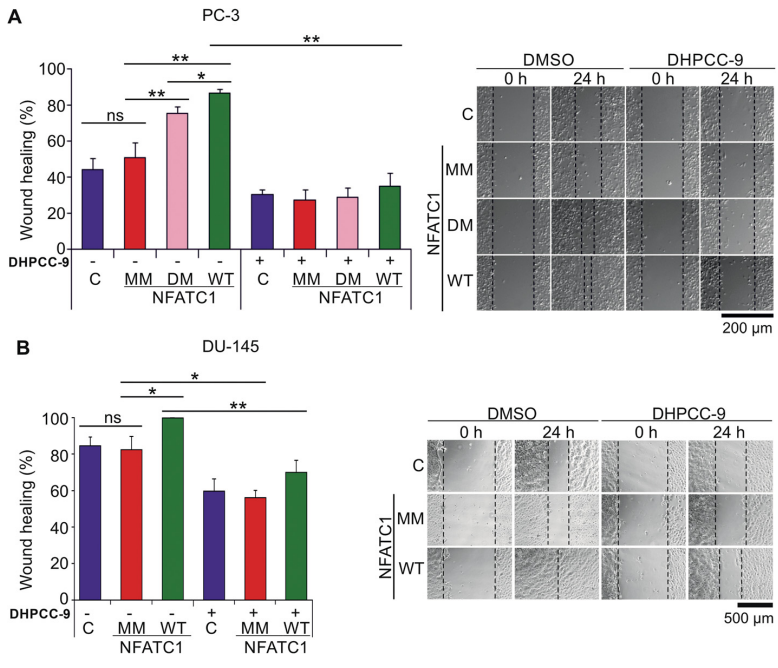

Fig. 5 Lack of PIM1 target sites reduces the ability of NFATC1 to promote migration of prostate cancer cells. Wild-type (WT), double mutant (DM) or multi mutant (MM) NFATC1 were transiently expressed in PC-3 cells (**a**) or DU-145 cells (**b**). For wound healing assays, cell layers were scratched 24 h after transfection with a 10 µl pipette tip and the wounded areas were allowed to recover for another 24 h in the presence of either DMSO or 10 µM DHPCC-9. Shown are representative pictures taken at 0 h and 24 h time-points, and average wound healing percentages

effects of NFATC1 were more dependent on phosphorylation of other PIM1 target sites.

To investigate the role of NFATC1 phosphorylation in cell invasion, we carried out matrigel-based Boyden chamber invasion assays. There WT NFATC1 increased invasion of transiently transfected PC-3 cells through the membranes, while mutations in PIM targets sites in MM NFATC1 or the presence of the PIM inhibitor DHPCC-9 decreased it (Fig. 6a). NFATC1 protein levels were also monitored by western blotting in the invasion experiments (Additional file 1: Figure S3E). No major differences were observed in cell viability, except for a slight increase by MM NFATC1 at the later 72 h timepoint (Additional file 1: Figure S3F). As activities of matrix metalloproteinases (MMPs), such as MMP-2 and MMP-9 are needed for cell invasion and may be regulated in an NFAT-dependent fashion also in our cells of interest [2], we analysed the effects of NFATC1 phosphorylation on their expression by gelatinase activity assays. The relative MMP expression levels were slightly, although not significantly reduced by MM NFATC1, while the decrease was more prominent with the PIM inhibitor DHPCC-9 (Fig. 6b). In each case, the MMP enzymatic activities correlated well with data from the invasion assays, suggesting that MMPs are relevant NFATC1 targets, whose activities can be indirectly regulated by PIM kinases.

ITGA5 is a putative target for phosphorylated NFATC1

To identify additional targets for the interplay between PIM1 and NFATC1, we designed microarray experiments, where we compared mRNA transcriptomes of PC-3 cells with or without stable overexpression of PIM1, and with or without transient overexpression of either WT or MM NFATC1. Real-time qPCR was first used to confirm overexpression of PIM1 and/or NFATC1 genes in the cell samples (Additional file 1: Figure S4A-B). With the microarrays, we performed three different types of comparisons: First, we compared parental PC-3 cells to their derivatives that stably expressed PIM1, to identify the genes that are up- or downregulated by elevated PIM1 expression. Secondly, we compared the PC-3 cells that had transiently been transfected with WT or MM NFATC1, to find genes that are controlled by the levels of NFATC1 activity. Finally, we compared PC-3 cells that both stably overexpressed PIM1 and transiently expressed WT or MM NFATC1, to unravel the genes regulated by PIM1-dependent phosphorylation of NFATC1. Genes with altered expression profiles in these three comparisons are listed in Additional file 1: Table S4.

Clustering analyses revealed that the cells overexpressing PIM1 and WT NFATC1 have a different profile as compared to the other samples (Additional file 1: Figure S4C). All the genes listed in Fig. 7a and Additional file 1: Table S4 showed higher mRNA levels in cells with WT NFATC1 than with MM, and their levels were lower also in the other control samples (Additional file 1: Figure S4C). Based on the observed gene expression profiles, we performed a canonical pathway analysis to determine, which cellular functions are primarily affected by the PIM-NFATC1 axis. We discovered five pathways that had significantly been enriched, many of which regulate cell adhesion and motility-related functions, like integrin, paxillin and FAK-signaling pathways (Additional file 2: Figure S6).

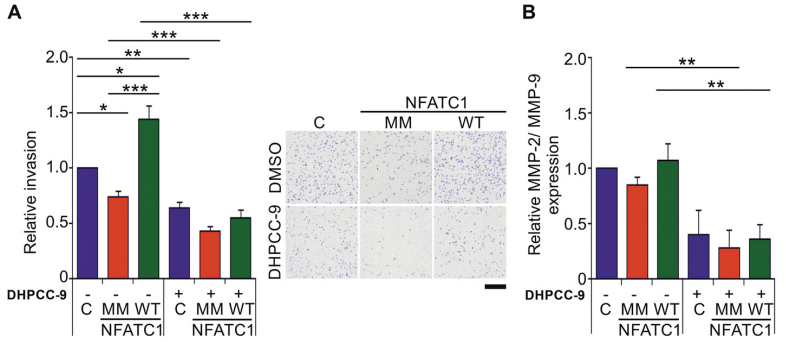

Fig. 6 Lack of PIM1 target sites reduces also the ability of NFATC1 to enhance invasiveness of prostate cancer cells. **a** For invasion assays, PC-3 cells were grown in Boyden chambers in the absence (–) or presence (+) of 10 μM DHPCC-9. After 48 h, cells that had invaded through the membranes were fixed, stained with crystal violet and counted. Shown are relative invasion rates from two separate experiments with triplicate samples, the results of which had been normalized against the mock-transfected control samples. Shown are also representative pictures of the effects of wild-type (WT) or multi mutant (MM) NFATC1 on cell invasion after 48 h. Scale bar 500 μm. **b** Matrix metalloprotease (MMP) expression levels were measured by gelatinase activity assays from invasion sample media. Shown are relative MMP-2/MMP-9 expression levels from two separate experiments with three parallel samples

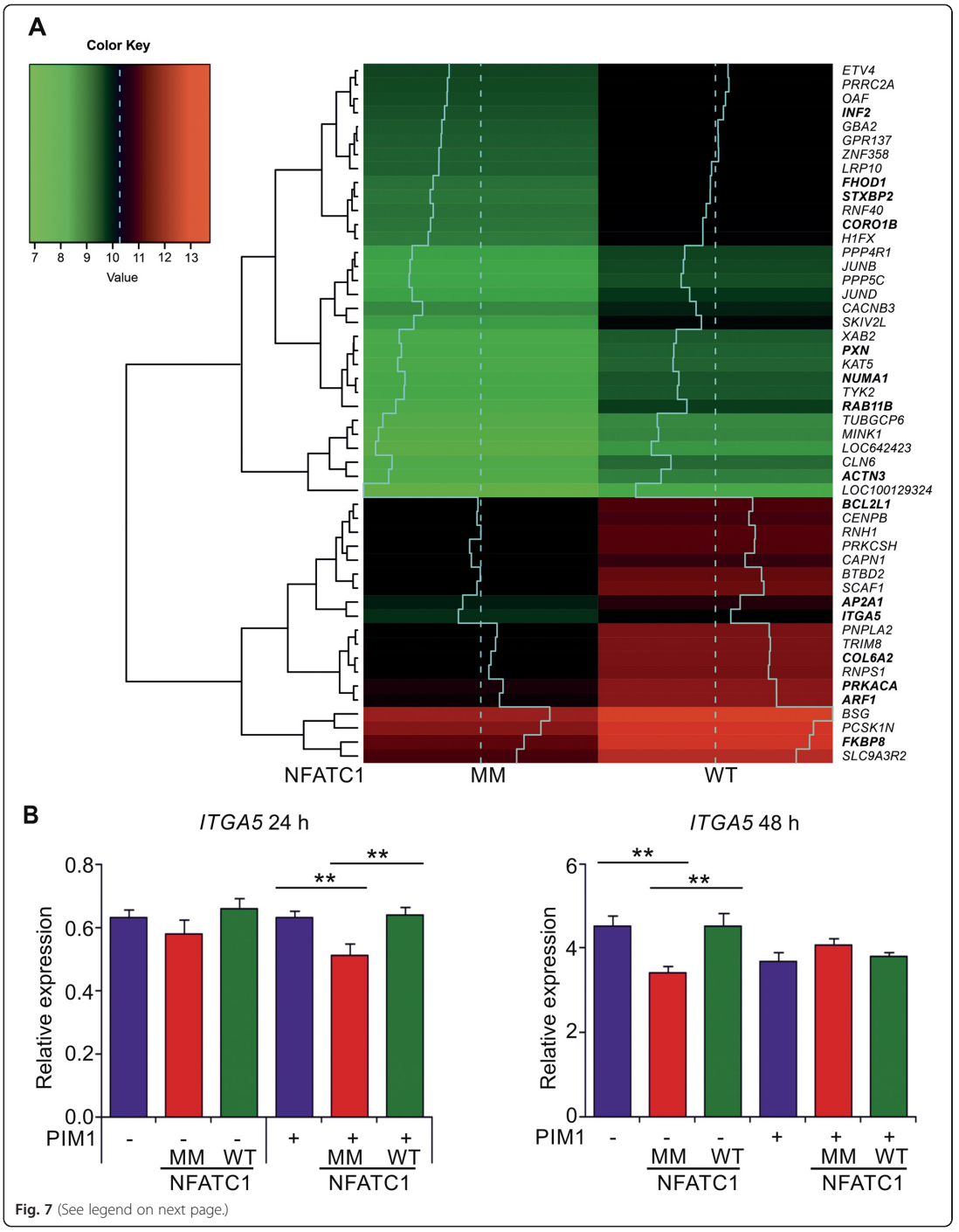

Fig. 7 (See legend on next page.)

(See figure on previous page.)
Fig. 7 Microarray analysis reveals *ITGA5* as a putative PIM1/NFATC1 target gene. **a** Heatmap of the potential PIM1/NFATC1 target genes found from microarray analysis. Shown are fifty genes with highest log2 fold changes (logFC ≥1 and *P*-value ≤0,05), when PC-3 cells expressing PIM1 plus multi mutant (MM) NFATC1 were compared to cells expressing PIM1 plus wild-type (WT) NFATC1. Dashed line indicates the median of the expression values and solid line shows the expression levels more precisely in a diagrammatic form. Genes listed in bold are reviewed in more detail in the discussion. **b** Relative expression levels of *ITGA5* mRNA were analysed by real-time qPCR from microarray samples (right panel) and from another independent data set (left panel) after transient transfections of WT or MM NFATC1 to PC-3 cells without (–) or with (+) stable PIM1 overexpression. The data were normalized against *TBP* expression levels

To validate the microarray data, we selected integrin alpha 5 (*ITGA5*) for more detailed expression analysis, as it is involved in the regulation of cell adhesion to matrices such as fibronectin [37, 38], and as we have previously connected PIM inhibition to decreased adhesion to fibronectin [39]. When we compared the expression levels of *ITGA5* mRNA between one independent data set (24 h after transfections) with microarray samples (48 h after transfections), we observed decreased expression in cells with MM NFATC1 as compared to control cells or cells with WT NFATC1 (Fig. 7b). These differences resembled those observed in MMP assays (Fig. 6b), and were statistically significant after 24 h in the cells stably overexpressing PIM1 and after 48 h in the control cell line, suggesting a role for PIM1-mediated phosphorylation and activation of NFATC1 in regulating *ITGA5* mRNA expression levels.

Our data prompted us to examine clinical prostate cancer samples for their expression levels of *PIM1*, *NFATC1* and/or *ITGA5* mRNAs. Therefore, we performed pairwise comparisons of these three genes in three independent prostate cancer patient-derived datasets [31–33]. The expression levels of *PIM1* and *ITGA5* or *NFATC1* and *ITGA5* mRNAs positively correlated in all datasets (Additional file 2: Figure S5). Most interestingly, the positive correlation between *NFATC1* and *ITGA5* increased along the Gleason score, with the strongest correlation in prostate cancer patients with Gleason ≥8.

Discussion

Here we have analysed the functional interactions of PIM and NFATC1 proteins in several prostate cancer cell lines. We have identified multiple PIM target sites in NFATC1 that are phosphorylated in vitro and/or in cells, and are essential for the transcriptional activity of NFATC1 as well as for its pro-migratory and pro-invasive effects. By contrast, the physical interactions or colocalization of PIM1 and NFATC1 are not affected by PIM-dependent phosphorylation. In addition to PIM1, also PIM2 and PIM3 can phosphorylate NFATC1, adding it to the growing list of substrates shared by all PIM family members [16].

While our study was in progress, additional kinases targeting NFATC1 were identified. Phosphorylation by the IkB kinase epsilon (IKKε) was shown to inhibit NFATC1 activity [40], whereas phosphorylation by the DYRK1A kinase increased NFATC1 protein stability by interfering with NFATC1 ubiquitination and degradation [41]. We identified two IKKε target sites (Ser151 and Ser161) and one DYRK1A site (Ser278) as cellular phosphorylation sites of NFATC1 in PC-3 cells, but our multi mutant NFATC1 protein lacked only one of them (Ser 151), suggesting that the effects of the mutant were mostly due to lack of PIM-dependent phosphorylation. This conclusion was further supported by our observations that the double mutant lacking known PKA target sites (Ser245 and Ser269; 11) promotes cell migration nearly as efficiently as wild-type NFATC1, while the triple mutant with intact PKA target sites inhibits cell motility almost as much as the multi mutant.

In this study, we have shown that the PC-3 prostate cancer cells exhibit constitutive NFAT activity. This is in contrast to most cells, where upstream activation of the calcium- and calcineurin-dependent pathway is required to allow NFAT family members to enter the nucleus and stimulate transcription there [1, 2]. This may not be a general feature of prostate cancer cells, since in another hormone-insensitive cell line, DU-145, NFAT activity could be enhanced by the calcium ionophore ionomycin and inhibited by the calcineurin inhibitor cyclosporin A. Yet in both cell lines, the transcriptional as well as pro-migratory activities of NFATC1 were similarly compromised by mutations in the PIM target sites. As the PIM-selective inhibitor DHPCC-9 blocked the activities of NFATC1 even more efficiently, this suggests that it affects additional downstream targets, only some of which are shared by PIM1 and NFATC1.

In our microarray analyses of transfected PC-3 cell samples, we were able to identify novel putative PIM1/NFATC1 target genes, which were more abundantly expressed in the presence of both PIM1 and wild-type NFATC1, but less in cells expressing the multi mutant NFATC1 or in other types of control cells. Thus, expression of all these target genes may be upregulated by PIM1-dependent phosphorylation of NFATC1. The putative PIM1/NFATC1 target genes included one encoding for the known PIM substrate NUMA1 (nuclear mitotic apparatus protein 1 [42];). Otherwise the target genes could be divided into several groups based on the

types of proteins encoded by them, including regulators of transcription, cell cycle, cell survival, cell motility, cell adhesion as well as intracellular trafficking. As expected, there were several genes involved in the NFAT signaling pathway [43], such as those encoding the catalytic subunit alpha of protein kinase A (PRKACA) and the FK506 immunosuppressant-binding immunophilin protein FKBP8. The latter protein also acts as a chaperone for the anti-apoptotic BCL2 protein, the expression levels of which have previously been shown to be upregulated by PIM kinases [44]. In addition, the BCL2 homolog BCL2L1 was listed there as also several genes encoding proteins involved in intracellular trafficking (RAB11B, STXBP2, AP2A1, ARF1). Maybe most interestingly in regard to our data on promotion of prostate cancer cell motility by PIM1 and NFATC1, there were several genes encoding regulators of the cytoskeletal actin network (INF2, FHOD1, ACTN3, CORO1B) and cell adhesion (COL6A2, PXN, ITGA5).

As signaling pathways involving integrins were highly enriched in our canonical pathway analysis, we picked ITGA5 for further expression analyses. Integrins are well-known cellular adhesion receptors that connect cells to the extracellular matrix and have been implicated in multiple steps of tumorigenesis [45]. ITGA5 has an essential role in cell adhesion, migration and tumor invasion [46–48]. Interestingly, previous experiments have linked both PIM and NFAT family members to integrin-mediated cell adhesion or motility. NFATC1 binds to the *ITGB3* promoter in osteoclast precursor cells, while NFATC2 and NFAT5 promote ITGA6/ITGB4-mediated cell invasion in breast cancer [49, 50]. Furthermore, PIM inhibition decreases cell adhesion to collagen and fibronectin matrices via different integrin subunits [38]. While no clear PIM-dependent changes in integrin activity or expression have previously been reported, we now found correlations between *PIM1* or *NFATC1* mRNA expression levels with *ITGA5*, both in PC-3 cells and in prostate cancer patient-derived samples. However, more detailed studies are needed to determine how critical *ITGA5* or other genes identified by the microarray analyses are in mediating the pro-motility effects of PIM and/or NFATC1 proteins.

Conclusions

In conclusion, we have shown that phosphorylation of PIM1 target sites stimulates the transcriptional activity of NFATC1 and enhances its ability to promote prostate cancer cell migration and invasion. Thereby, the interplay between PIM kinases and NFATC1 may also provide possibilities for therapeutic interventions against metastatic prostate cancer through combinatory approaches involving PIM-selective kinase inhibitors.

Supplementary information

Supplementary information accompanies this paper at https://doi.org/10.1186/s12964-019-0463-y.

Additional file 1: Table S1. Primers for site-directed mutagenesis in NFATC1. **Table S2.** Primers for qRT-PCR. **Table S3.** Novel NFATC1 phosphorylation sites. **Table S4**. Phosphorylation-dependent differences in the expression of PIM/NFATC1 target genes in PC-3 cells.

Additional file 2: Figure S1. Lack of PIM target sites does not affect subcellular localization of NFATC1 A. **Figure S2.** Effects of PIM-dependent phosphorylation on NFAT activity. **Figure S3.** Lack of PIM1 target sites reduces the ability of NFATC1 to promote cancer cell motility. **Figure S4.** Microarray analysis reveals phosphorylation-dependent differences in the expression of PIM/NFATC1 target genes in PC-3 cells. **Figure S5.** Integrin signaling pathway is enriched in PIM1 and NFATC1 expressing cells. **Figure S6.** ITGA5 mRNA expression levels correlates with those of *PIM1* and *NFATC1* in clinical prostate cancer samples.

Abbreviations

ACTB: ß-actin; CsA: Cyclosporine A; DHPCC-9: Pan-PIM inhibitor; DM: double mutant; DN: dominant negative; IM: Ionomycin; ITGA5: Integrin alpha 5; LSB: Laemmli sample buffer; MM: multi mutant; MMP: Matrix metalloproteinase; mSRR: constitutively active mutant of NFATC1; NFAT: Nuclear factor of activated T cells; ns: non-significant difference; TBP: TATA-binding protein; TM: triple mutant; TPA: 12–0-tetradecanoyl-phorbol-13-asetate; WT: wild-type

Acknowledgements

We thank G.R. Crabtree for the NFATC1 expression and reporter constructs, P. Moreau for DHPCC-9, O. Silvennoinen for the Renilla reporter plasmid, H. Ahlfors for helpful discussions, M. Ruuska, S. Himanen and K. Ikkala for technical assistance, and the Biocenter Finland facilities (Turku Proteomics Facility, Turku Cell Imaging and Cytometry Core, and the Tampere Imaging Facility) for assistance in mass spectrometry and microscopy.

Authors' contributions

PJK, EMR, SKE and NMS concepted and designed the study, and PJK, EMR, LL and TV supervised it. SKE, NMS, EMR, SR, PK and MS acquired data, and GC, GS, AS and DG helped to analyse and interpret them. SKE, NMS and PJK wrote the manuscript. All authors read and approved the final manuscript.

Authors' information

Not applicable.

Funding

This work was supported by grants from the Academy of Finland (grant 287040 to PJK, grants 313921 and 314558 to PR, grants 275151 and 292307 to DG), Sigrid Juselius Foundation, Cancer Society of Finland, Competitive State Research Financing of the Expert Responsibility area of Tampere University Hospital (to TV), the Pirkanmaa Fund of the Finnish Cultural Foundation (grant 0116947–3 to SE) and grant from Paulo Foundation to MS. The funding agencies had no roles in design of the study, in collection, analysis or interpretation of data, or in writing the manuscript.

Availability of data and materials

The microarray data has been deposited to the Gene Expression Omnibus (GEO, National Center for Biotechnology Information, Bethesda, MD, USA) with series entry number GSE120133, and is available from there: https://www.ncbi.nlm.nih.gov/geo/query/acc.cgi?acc=GSE120133. Other experimental data sets used and analysed during the current study as well as materials prepared are available from the corresponding author on reasonable request.

Ethics approval and consent to participate

The use of clinical material was approved by the ethical committee of the Tampere University Hospital (TAUH, Tampere, Finland).

Consent for publication

Not applicable.

Competing interests
The authors declare that they have no competing interests.

Author details
[1]Department of Biology, University of Turku, Vesilinnantie 5, FI-20500 Turku, Finland. [2]Faculty of Medicine and Health Technology, Tampere University and Tays Cancer Center, Tampere University Hospital, Tampere, Finland. [3]Turku Centre for Biotechnology, University of Turku, Turku, Finland. [4]Institute of Biomedicine, University of Eastern Finland, Kuopio, Finland. [5]University of Helsinki, Helsinki, Finland. [6]Signal processing laboratory, Tampere University of Technology, Pori, Finland. [7]Fimlab Laboratories, Tampere, Finland.

Received: 18 June 2019 Accepted: 22 October 2019
Published online: 15 November 2019

References

1. Rao A, Luo C, Hogan PG. Transcription factors of the NFAT family: regulation and function. Annu Rev Immunol. 1997;15:707–47.
2. Mancini M, Toker A. NFAT proteins: emerging roles in cancer progression. Nat Rev Cancer. 2009;9:810–20.
3. Li L, Duan Z, Yu J, Dang HX. NFATc1 regulates cell proliferation, migration, and invasion of ovarian cancer SKOV3 cells in vitro and in vivo. Oncol Rep. 2016;36:918–28.
4. Santio NM, Vahakoski RL, Rainio EM, Sandholm JA, Virtanen SS, Prudhomme M, et al. Pim-selective inhibitor DHPCC-9 reveals Pim kinases as potent stimulators of cancer cell migration and invasion. Mol Cancer. 2010;9:279.
5. Seifert A, Rau S, Küllertz G, Fischer B, Santos AN. TCDD induces cell migration via NFATc1/ATX-signaling in MCF-7 cells. Toxicol Lett. 2009;184:26–32.
6. Wang L, Wang Z, Li J, Zhang W, Ren F, Yue W. NFATc1 activation promotes the invasion of U251 human glioblastoma multiforme cells through COX-2. Int J Mol Med. 2015;35:1333–40.
7. Liu Y, Liang T, Qiu X, Ye X, Li Z, Tian B, Yan D. Down-regulation of Nfatc1 suppresses proliferation, migration, invasion, and Warburg effect in prostate cancer cells. Med Sci Monit. 2019;25:1572–81.
8. Kavitha CV, Deep G, Gangar SC, Jain AK, Agarwal C, Agarwal R. Silibinin inhibits prostate cancer cells- and RANKL-induced osteoclastogenesis by targeting NFATc1, NF-κB, and AP-1 activation in RAW264.7 cells. Mol Carcinog. 2012;53:169–80.
9. Ouyang Z, Guo X, Chen X, Liu B, Zhang Q, Yin Z, Zhai Z, Qu X, Liu X, Peng D, Shen Y, Liu T, Zhang Q. Hypericin targets osteoclast and prevents breast cancer-induced bone metastasis via NFATc1 signaling pathway. Oncotarget. 2018;9:1868–84.
10. Beals CR, Sheridan CM, Turck CW, Gardner P, Crabtree GR. Nuclear export of NF-ATc enhanced by glycogen synthase kinase-3. Science. 1997;275:1930–4.
11. Sheridan CM, Heist EK, Beals CR, Crabtree GR, Gardner P. Protein kinase a negatively modulates the nuclear accumulation of NF-ATc1 by priming for subsequent phosphorylation by glycogen synthase kinase-3. J Biol Chem. 2002;277:48664–76.
12. Rainio EM, Sandholm J, Koskinen PJ. Cutting edge: transcriptional activity of NFATc1 is enhanced by the Pim-1 kinase. J Immunol. 2002;168:1524–7.
13. Glazova M, Aho TL, Palmetshofer A, Murashov A, Scheinin M, Koskinen PJ. Pim-1 kinase enhances NFATc activity and neuroendocrine functions in PC12 cells. Brain Res Mol Brain Res. 2005;138:116–23.
14. Eichmann A, Yuan L, Bréant C, Alitalo K, Koskinen PJ. Developmental expression of Pim kinases suggests functions also outside of the hematopoietic system. Oncogene. 2000;19:1215–24.
15. Bachmann M, Möröy T. The serine/threonine kinase Pim-1. Int J Biochem Cell Biol. 2005;37:726–30.
16. Santio NM, Koskinen PJ. PIM kinases: from survival factors to regulators of cell motility. Int J Biochem Cell Biol. 2017;93:74–85.
17. Valdman A, Fang X, Pang ST, Ekman P, Egevad L. Pim-1 expression in prostatic intraepithelial neoplasia and human prostate cancer. Prostate. 2004;60:367–71.
18. Xu Y, Zhang T, Tang H, Zhang S, Liu M, Ren D, Niu Y. Overexpression of PIM-1 is a potential biomarker in prostate carcinoma. J Surg Oncol. 2005;92:326–30.
19. Cibull TL, Jones TD, Li L, Eble JN, Ann Baldridge L, Malott SR, Luo Y, Cheng L. Overexpression of pim-1 during progression of prostatic adenocarcinoma. J Clin Pathol. 2006;59:285–8.
20. Van der Poel HG, Zevenhoven J, Bergman AM. Pim1 regulates androgen-dependent survival signaling in prostate cancer cells. Urol Int. 2010;84:212–20.
21. Qu Y, Zhang C, Du E, Wang A, Yang Y, Guo J, et al. Pim-3 is a critical risk factor in development and prognosis of prostate cancer. Med Sci Monit. 2016;22:4254–60.
22. Santio NM, Eerola SK, Paatero I, Yli-Kauhaluoma J, Anizon F, Moreau P, et al. Pim kinases promote migration and metastatic growth of prostate cancer xenografts. PLoS One. 2015;10:e0130340.
23. Santio NM, Landor SKJ, Vahtera L, Ylä-Pelto J, Paloniemi E, Imanishi SY, et al. Phosphorylation of Notch1 by Pim kinases promotes oncogenic signaling in breast and prostate cancer cells. Oncotarget. 2016a;7:43220–38.
24. Beals CR, Clipstone NA, Ho SN, Crabtree GR. Nuclear localization of NF-ATc by a calcineurin-dependent, cyclosporin-sensitive intramolecular interaction. Genes Dev. 1997;11:824–34.
25. Kiriazis A, Vahakoski RL, Santio NM, Arnaudova R, Eerola SK, Rainio EM, et al. Tricyclic Benzo[cd]azulenes selectively inhibit activities of Pim kinases and restrict growth of Epstein-Barr virus-transformed cells. PLoS One. 2013;8:e55409.
26. Akué-Gédu R, Rossignol E, Azzaro S, Knapp S, Filippakopoulos P, Bullock AN, et al. Synthesis, kinase inhibitory potencies, and in vitro antiproliferative evaluation of new Pim kinase inhibitors. J Med Chem. 2009;52:6369–81.
27. Kouvonen P, Rainio EM, Suni V, Koskinen P, Corthals GL. Enrichment and sequencing of phosphopeptides on indium tin oxide coated glass slides. Mol BioSyst. 2011;7:1828–37.
28. Imanishi SY, Kochin V, Ferraris SE, de Thonel A, Pallari HM, Corthals GL, et al. Reference-facilitated phosphoproteomics: fast and reliable phosphopeptide validation by microLC-ESI-Q-TOF MS/MS. Mol Cell Proteomics. 2007;6:1380–91.
29. Virtanen SS, Väänänen HK, Härkönen PL, Lakkakorpi PT. Alendronate inhibits invasion of PC-3 prostate cancer cells by affecting the mevalonate pathway. Cancer Res. 2002;62:2708–14.
30. Ritchie ME, Phipson B, Wu D, Hu Y, Law CW, Shi W, et al. Limma powers differential expression analyses for RNA-sequencing and microarray studies. Nucleic Acids Res. 2015;43:e47.
31. The Cancer Genome Atlas Research Network. The molecular taxonomy of primary prostate Cancer. Cell. 2015;163:1011–25.
32. Taylor BS, Schultz N, Hieronymus H, Gopalan A, Xiao Y, Carver BS, et al. Integrative genomic profiling of human prostate cancer. Cancer Cell. 2010;18:11–22.
33. Annala M, Kivinummi K, Tuominen J, Karakurt S, Granberg K, Latonen L, et al. Recurrent SKIL-activating rearrangements in ETS-negative prostate cancer. Oncotarget. 2015;6:6235–50.
34. Palaty CK, Clark-Lewis I, Leung D, Pelech SL. Phosphorylation site substrate specificity determinants for the Pim-1 protooncogene-encoded protein kinase. Biochem Cell Biol. 1997;75:153–62.
35. Veldscholte J, Ris-Stalpers C, Kuiper GG, Jenster G, Berrevoets C, Claassen E, van Rooij HC, Trapman J, Brinkmann AO, Mulder E. A mutation in the ligand binding domain of the androgen receptor of human LNCaP cells affects steroid binding characteristics and response to anti-androgens. Biochem Biophys Res Commun. 1990;173:534–40.
36. Ylipää A, Kivinummi K, Kohvakka A, Annala M, Latonen L, Scaravilli M, Kartasalo K, Leppänen SP, Karakurt S, Seppälä J, Yli-Harja O, Tammela TL, Zhang W, Visakorpi T, Nykter M. Transcriptome sequencing reveals PCAT5 as a novel ERG-regulated long noncoding RNA in prostate Cancer. Cancer Res. 2015;75:4026–31.
37. Desgrosellier JS, Cheresh DA. Integrins in cancer: biological implications and therapeutic opportunities. Nat Rev Cancer. 2010;10:9–22.
38. Cai X, Liu C, Zhang TN, Zhu YW, Dong X, Xue P. Down-regulation of FN1 inhibits colorectal carcinogenesis by suppressing proliferation, migration, and invasion. J Cell Biochem. 2018;119:4717–28.
39. Santio NM, Salmela M, Arola H, Eerola SK, Heino J, Rainio EM, Koskinen P. The PIM1 kinase promotes prostate cancer cell migration and adhesion via multiple signalling pathways. Exp Cell Res. 2016b;342:113–24.
40. Zhang J, Feng H, Zhao J, Feldman ER, Chen SY, Yuan W, Huang C, Akbari O, Tibbetts SA, Feng P. IκB kinase ε is an NFATc1 kinase that inhibits T cell immune response. Cell Rep. 2016;16:405–18.
41. Liu H, Wang K, Chen S, Sun Q, Zhang Y, Chen L, Sun X. NFATc1 phosphorylation by DYRK1A increases its protein stability. PLoS One. 2017;12:e0172985.
42. Bhattacharya N, Wang Z, Davitt C, McKenzie IF, Xing PX, Magnuson NS. Pim-1 associates with protein complexes necessary for mitosis. Chromosoma. 2002;111:80–95.

43. Belinky F, Nativ N, Stelzer G, Zimmerman S, Iny Stein T, Safran M, Lancet D. PathCards: multi-source consolidation of human biological pathways. Database. 2015. https://doi.org/10.1093/database/bav006.
44. Lilly M, Sandholm J, Cooper JJ, Koskinen PJ, Kraft A. The PIM-1 serine kinase prolongs survival and inhibits apoptosis-related mitochondrial dysfunction in part through a bcl-2-dependent pathway. Oncogene. 1999;18:4022–31.
45. Hamidi H, Ivaska J. Every step of the way: integrins in cancer progression and metastasis. Nat Rev Cancer. 2018;12:533–48.
46. Akiyama SK, Yamada SS, Chen WT, Yamada KM. Analysis of fibronectin receptor function with monoclonal antibodies: roles in cell adhesion, migration, matrix assembly, and cytoskeletal organization. J Cell Biol. 1989; 109:863–75.
47. Qin L, Chen X, Wu Y, Feng Z, He T, Wang L, Liao L, Xu J. Steroid receptor coactivator-1 upregulates integrin α_5 expression to promote breast cancer cell adhesion and migration. Cancer Res. 2011;71:1742–51.
48. Wong AW, Paulson QX, Hong J, Stubbins RE, Poh K, Schrader E, Nunez NP. Alcohol promotes breast cancer cell invasion by regulating the Nm23-ITGA5 pathway. J Exp Clin Cancer Res. 2011;30:75.
49. Crotti TN, Flannery M, Walsh NC, Fleming JD, Goldring SR, McHugha KP. NFATc1 regulation of the human β3 integrin promoter in osteoclast differentiation. Gene. 2006;372:92–102.
50. Jauliac S, Lopez-Rodriguez C, Shaw LM, Brown LF, Rao A, Toker A. The role of NFAT transcription factors in integrin-mediated carcinoma invasion. Nat Cell Biol. 2002;4:540–4.

Publisher's Note

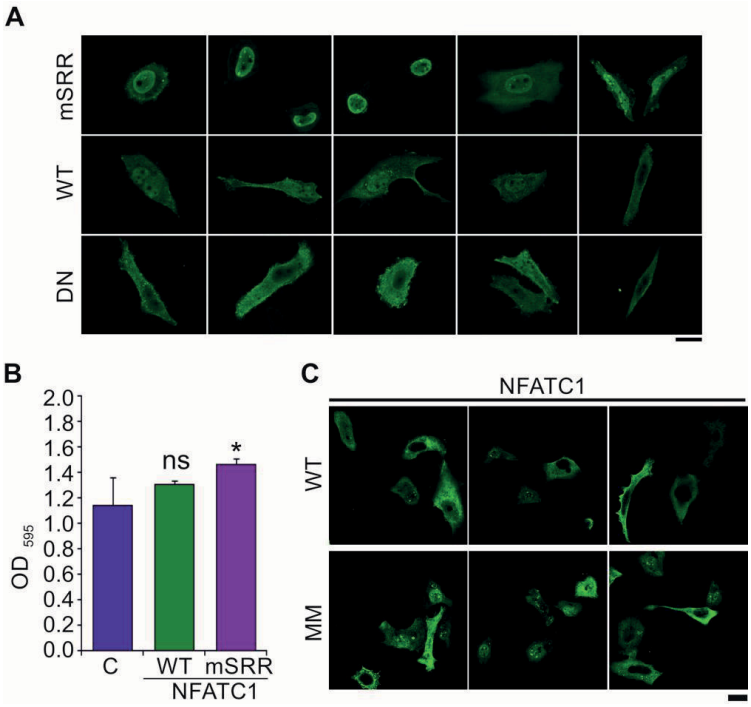

Figure S1 Lack of PIM target sites does not affect subcellular localization of NFATC1.
a Representative confocal microscopy pictures for data shown in Figure 1d on the subcellular localization patterns of transiently expressed wild-type (WT) NFATC1, the constitutively active (mSRR) mutant and the dominant negative (DN) mutant. **b** The average effects of WT NFATC1 or the mSRR mutant on cell viability were analysed by the MTT assay from three parallel samples used for Figure 1E. **c** Representative confocal microscopy pictures for data shown in Figure 3a on the subcellular localization patterns of transiently expressed WT or multi mutant (MM) NFATC1. Scale bars 20 μm.

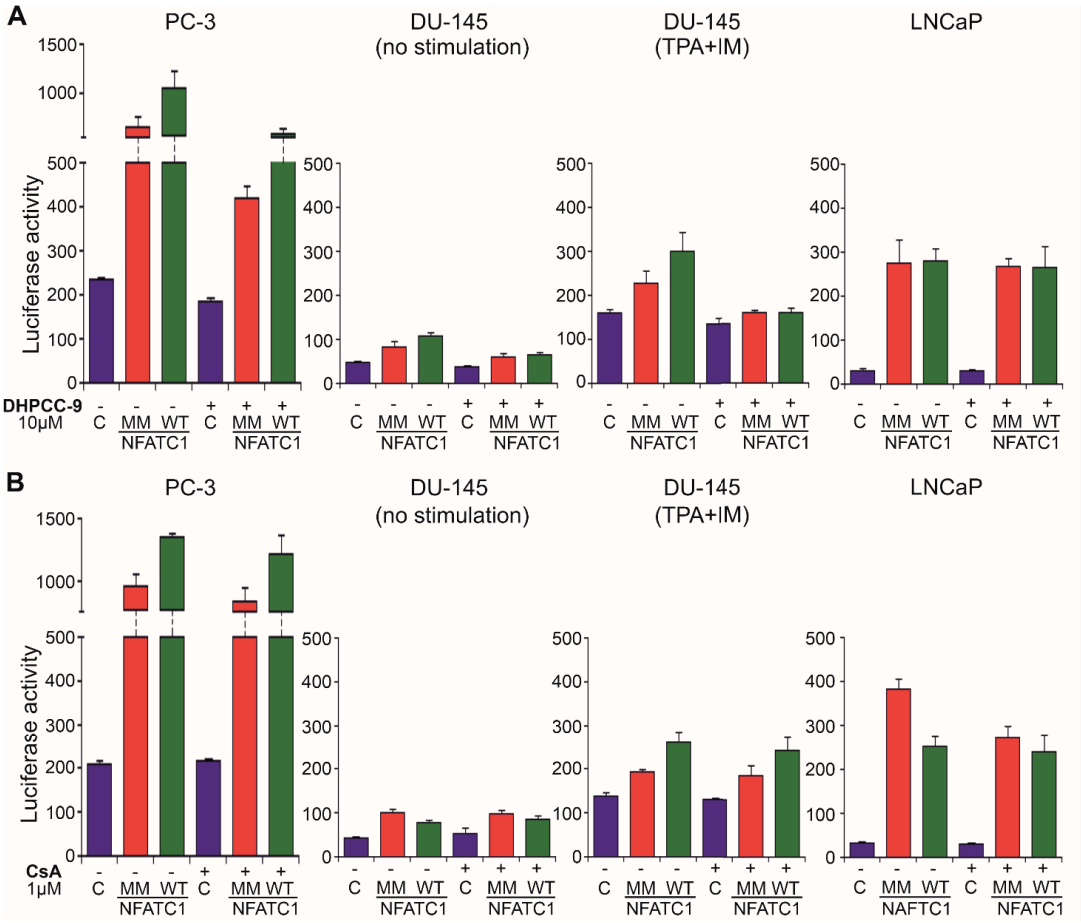

Figure S2 Effects of PIM-dependent phosphorylation on NFAT activity.
Original NFAT-dependent luciferase activities for relative data partially shown in Figure 4b and C from PC-3, DU-145 and LNCaP cell lines transiently transfected with wild-type (WT) or multi mutant (MM) NFATC1. Part of DU-145 cells were pre-treated with TPA and IM, after which all cells were treated with either DMSO (-) or DHPCC-9 (+) (**a**), or with ETOH (-) or CsA (+) (**b**).

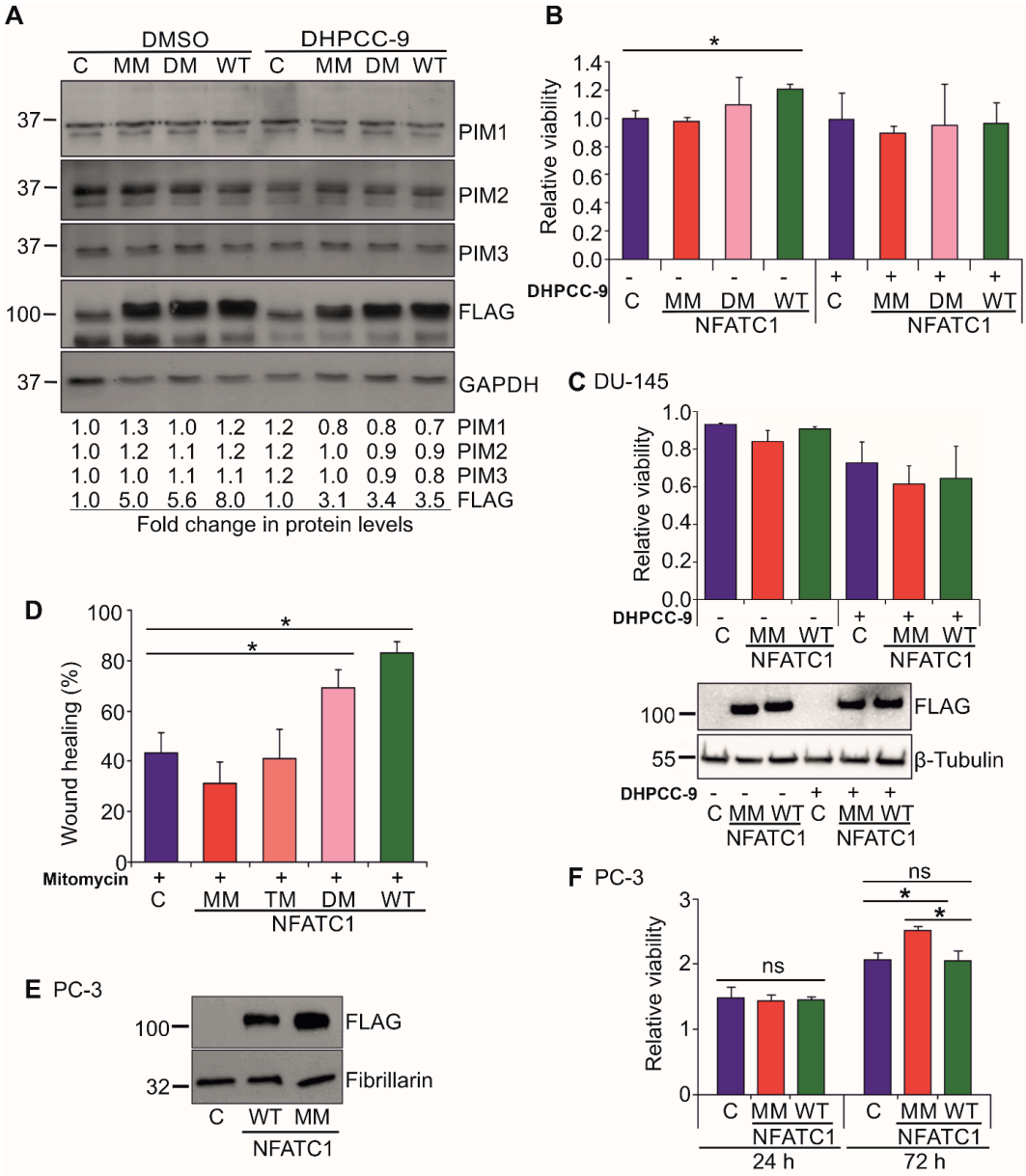

Figure S3 Lack of PIM1 target sites reduces the ability of NFATC1 to promote cancer cell motility.

a Western blotting was used to measure levels of endogenously expressed PIM family members and ectopically expressed Flag-tagged NFATC1 proteins from the experiment for Figure 5a. **b** The average relative effects of wild-type (WT), double mutant (DM) or multi mutant (MM) NFATC1 on cell viability were analysed by the MTT assay from three parallel samples used for Figure 5a. The data were normalized against mock-transfected control (C) cells. **c** The average relative effects of WT or MM NFATC1 on DU-145 cell viability were analysed by the AlamarBlue® viability assay from three parallel samples used for Figure 5b. They were

normalized against values at the starting point, and the NFATC1 protein expression levels detected by Western blotting from the same experiment. β Tubulin staining was used as a loading control. **d-e** Wound healing assays were performed in PC-3 cells also in the presence of mitomycin C to exclude effects of cell proliferation. A triple mutant (TM) of NFATC1 was included in addition to other mutants. Shown are average wound healing percentages from representative experiments with three parallel samples (**d**), and the NFATC1 protein expression levels detected by Western blotting from the same experiment (**e**). Fibrillarin staining was used as a loading control. **f** The average relative effects of WT or MM NFATC1 on cell viability were analysed by the AlamarBlue® viability assay at three time-points (0 h, 24 h and 72 h after transfection) from PC-3 cells used in invasion assays in Figure 6a, and the data were normalized against values at the starting point.

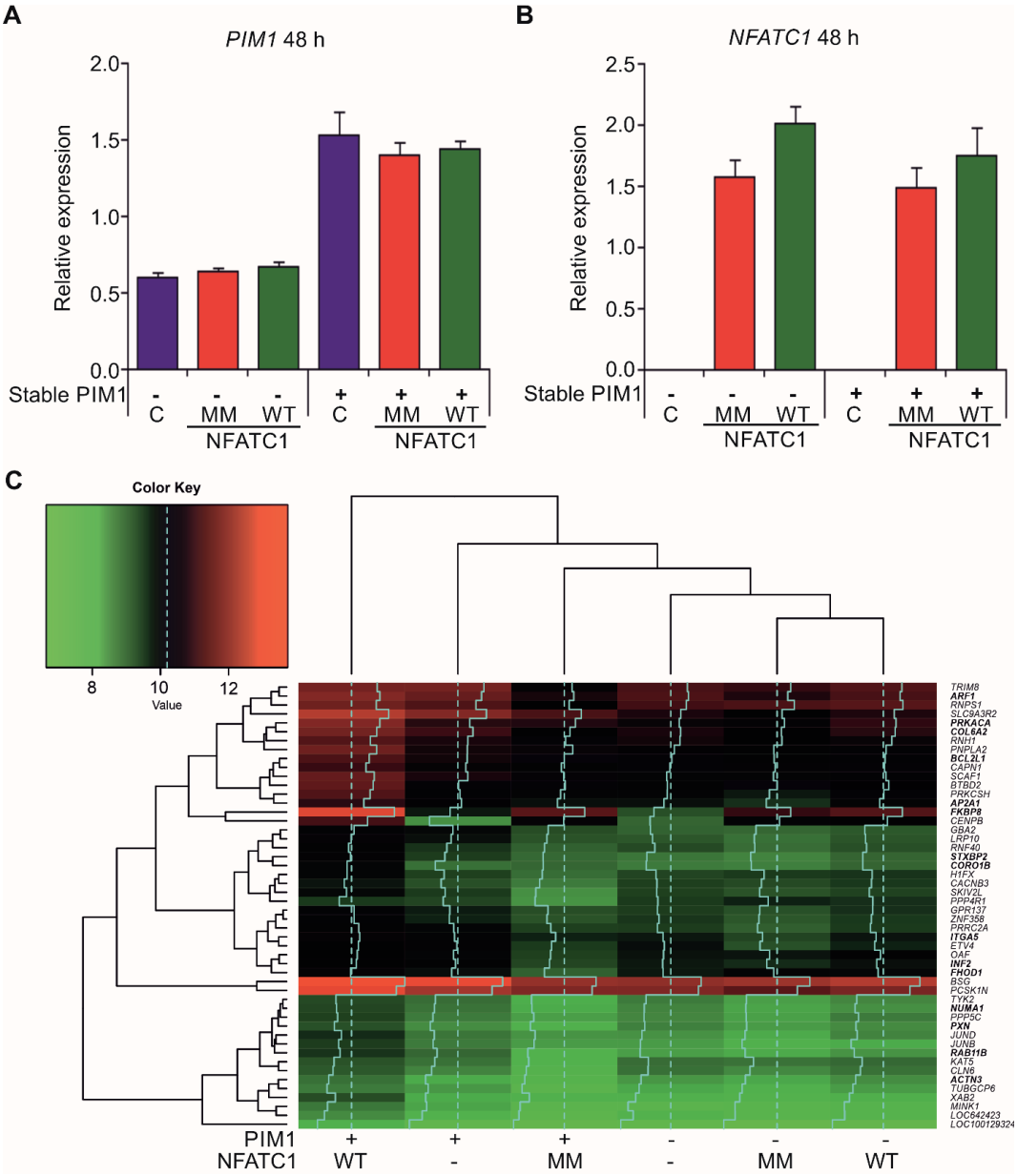

Figure S4 Microarray analysis reveals phosphorylation-dependent differences in the expression of PIM/NFATC1 target genes in PC-3 cells.

Relative expression levels of *PIM1* (**a**) or *NFATC1* (**b**) mRNAs from microarray samples, as analysed by real-time qPCR and normalized against *TBP* levels. Expression levels were measured from PC-3 cell derivatives with (+) or without (-) stable PIM1 overexpression, and with transient overexpression of wild-type (WT) or multi mutant (MM) NFATC1. **c** Heatmap of the 50 genes with highest log2 fold changes (logFC $\geq$1 and P-value $\leq$ 0,05) observed in all the three array comparisons. All genes in bold are reviewed more in detail in discussion.

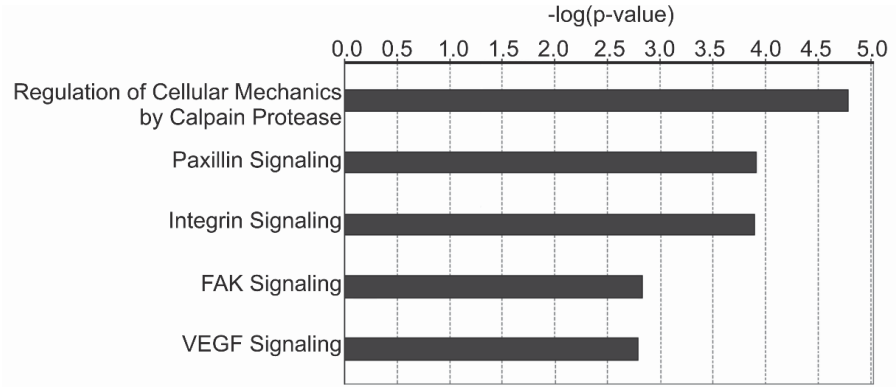

Figure S5 Integrin signaling pathway is enriched in PIM1 and NFATC1 expressing cells. IPA (Ingenuity Pathway Analysis, Ingenuity Systems) was used for functional enrichment and detection of pathways with significant alterations based on microarray gene expressions. In canonical pathway analysis -log(p-values) over threshold 2.5 were considered significant.

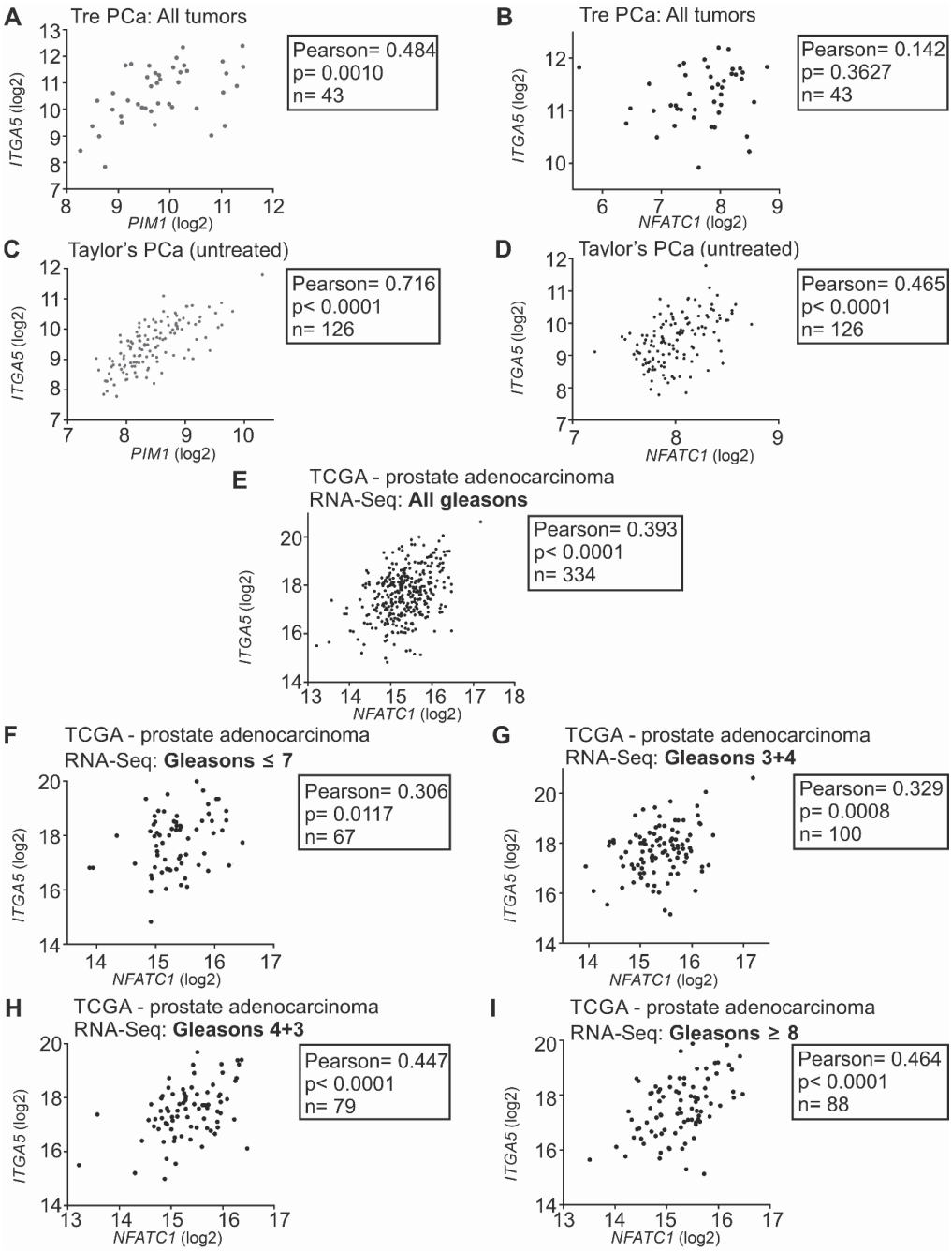

Figure S6 *ITGA5* mRNA expression levels correlate with those of *PIM1* and *NFATC1* in clinical prostate cancer samples.

ITGA5 mRNA expression levels were compared with *PIM1* or *NFATC1* mRNA levels by using three datasets of human prostate carcinomas: **a-b** Tampere PC sequencing data (Tre PCa; 33), **c-d** Integrative Genomic Profiling of Human Prostate Cancer microarray data (PCa; 32) or **e-i** The Cancer Genome Atlas (TCGA) - Prostate adenocarcinoma RNA-Sequencing data (31).

Table S1. Primers for site-directed mutagenesis in NFATC1.

Listed are primer sequences used for designed mutations in PIM1 phosphorylation target sites of NFATC1. Nucleotides in bold were mutated and the restriction sites used to help in screening of the mutations are underlined. Original sequences are listed under the mutated sequences.

Mutant primers 1.

Ser245 Restriction site PvuII = CAG/CTG (32 nt)
F : 5' CCTCGCCCCGCG<u>CA**GCT**G</u>TCACTGAGGAGAGC 3'
R : 5' GCTCTCCTCAGTGA<u>CA**GCT**G</u>CG**C**GGGGCGAGG 3'

Original sequence from first site:

F: 5' CCTCGCCCCGCGCA**AGC**GTCACTGAGGAGAGC 3'
R: 5' GCTCTCCTCAGTGACA**AGC**GCGCGGGGCGAGG 3'

Mutant primers 2.

Ser269 Restriction site *MluI* = A/CGCGT (38 nt)
F : 5' GCAACAAGAGGAAGT<u>AC**GCGT**</u>TGAACGGCCGGCAGCCG 3'
R : 5' CGGCTGCCGGCCGTTCA<u>AC**GCGT**</u>ACTTCCTCTTGTTGC 3'

Original sequence from first site:

F : 5' GCAACAAGAGGAAGTAC**AGC**TTGAACGGCCGGCAGCCG 3'
R: 5' CGGCTGCCGGCCGTTCAAC**AGC**TACTTCCTCTTGTTGC 3'

Mutant primers 3.

Ser151 + Ser153 + Thr154 Restriction site *NotI* = <u>GC/GGCCGC</u> (41nt)
F: 5' CCTAGCTCCAAACGG**G**CCCCC<u>**GC**</u>**G**<u>**GC**</u>**C**<u>GC</u>CGCCACGCTGAG 3'
R: 5' CTCAGCGTGGCG<u>GC</u>**G**<u>**GC**</u>**C**<u>GC</u>**C**GGGGG**C**CCGTTTGGAGCTAGG 3'

Original sequence from second site:

F: 5' CCTAGCTCCAAACGG**T**CCCCC**T**C**CA**C**G**GCCACCACGCTGAG 3'
R: 5' CTCAGCGTGGTGGC**C**G**TG**G**A**GGGGG**A**CCGTTTGGAGCTAGG 3'

Mutant primers 4.

Ser256 + Ser257 Restriction site *NheI* = <u>G/CTAGC</u> (33 nt)
F: 5' CTGGGTGCCCGC**G**CC**G**CCAGACCC<u>GC**TAG**C</u>CC**G** 3'
R: 5' **C**GGG<u>**GCTAGC**</u>GGGTCTGG**C**GG**C**GCGGGCACCCAG 3'

Original sequence from third site:

F 5’ CTGGGTGCCCGC**T**CC**T**CCAGACCCGC**GTC**CCC**T** 3’
R 5’ **A**GGG**GAC**GCGGGTCTGG**A**GG**A**GCGGGCACCCAG 3’

Mutant primers 5.

Ser335 + Thr338 + Thr339 Restriction site *XhoI* =C/TCGAG (36 nt)
F 5’ GTCCCTGTCAAG**G**CCCGCAAG**G**CC**G**CCCT**C**GAGCAG 3’
R 5’ CTGCTC**G**AGGG**C**GG**C**CTTGCGGG**C**CTTGACAGGGAC 3’

Original sequence from fourth site:

F 5’ GTCCCTGTCAAG**T**CCCGCAAG**A**CC**A**CCCT**G**GAGCAG 3’
R 5’ CTGCTC**C**AGGG**T**GG**T**CTTGCGGG**A**CTTGACAGGGAC 3’

Table S2. Primers for qRT-PCR.
All the primer sequences (*TPB*, *PIM1*, *NFATC1* and *ITGA5*) used for qRT-PCR analysis.

***TPB* primers for qRT-PCR**

F: 5' GAATATAATCCCAAGCGGT 3'
R: 5' ACTTCACATCACAGCTCCCC 3'

***PIM1* primers for qRT-PCR**

F: 5' CTGGGGAGAGCTGCCTAATG 3'
R: 5' GCTCCCCTTTCCGTGATGAA 3'

***NFATC1* primers for qRT-PCR**

F: 5' AAGCACCAGCTTTCCAGTCC 3'
R: 5' TGCATAGCCATAGTGTTCTTCC 3'

***ITGA5* primers for qRT-PCR**

F: 5' AGACTTCTTTGGCTCTGCCC 3'
R: 5' ACATGGTTCTGCTCCCCAAA 3'

Table S3. Novel NFATC1 phosphorylation sites.

The *in vivo* or *in vitro* PIM1 target sites in NFATC1 identified in this study have been separated from sites previously identified from COS-7 cells (27), from high-throughput (HT) analyses listed by PhosphoSitePlus® (phosphosite.org) or more specifically for other kinases, such as IKKε (40), PKA (10, 11) or DYRK1A (41). Note that the table does not include all possible phopshorylation sites of NFATC1. The mutated sites in double mutant (DM), triple mutant (TM) or multi mutant (MM) NFATC1 have been indicated with bold fonts.

Amino acid residue	*In vivo* sites in PC-3 cells	*In vivo* sites in COS-7 cells	*In vitro* site for PIM1	*In vitro* or *in vivo* sites for other kinases	NFATC1 mutant
S151	***x***	-	-	IKKε	TM, MM
S153	**x**	-	-	-	TM, MM
T154	**x**	-	-	-	TM, MM
T156	x	-	-	-	-
S158	x	-	-	HT	-
S161	x	-	-	IKKε	-
S175	x	-	-	-	-
S176	x	-	-	-	-
T178	x	-	-	-	-
T179	x	-	-	-	-
S245	**x**	**x**	**x**	PKA	DM, MM
S256	**x**	-	-	-	TM, MM
S257	**-**	-	**x**	HT	TM, MM
S269	**x**	-	**x**	PKA	DM, MM
S278	x	x	-	DYRK1A	-
S282	x	x	-	HT	-
T284	x	x	-	-	-
S286	x	x	-	-	-
S290	x	x	-	HT	-
S335	-	-	**x**	-	TM, MM
T338	**x**	-	**x**	-	TM, MM
T339	**x**	-	**x**	-	TM, MM
T359	x	x	-	HT	-

Table S4. Phosphorylation-dependent differences in the expression of PIM/NFATC1 target genes in PC-3 cells.

Top 50 genes that were differentially expressed in PC-3 cells overexpressing PIM1 and either wild-type (WT) or multi mutant (MM) NFATC1. In this table, relative gene expression changes when WT NFATC1 expressing samples were compared to MM NFATC1 expressing samples are shown. Thresholds to consider gene expression change significant, was logFC ≥1 and p-value ≤ 0,05.

Gene acronym	logFC	p-value
RAB11B	-1,66212	7,82E-06
SKIV2L	-1,5609	0,008398
SCAF1	-1,53947	0,000207
FKBP8	-1,50098	2,32E-05
PRKCSH	-1,47978	2,64E-07
BSG	-1,42546	0,000724
PRRC2A	-1,37796	2,12E-05
BTBD2	-1,37431	9,05E-08
STXBP2	-1,33762	0,00013
MINK1	-1,33609	0,00018
RNPS1	-1,32754	0,000738
SLC9A3R2	-1,32527	0,010213
ZNF358	-1,32407	1,29E-08
CLN6	-1,30607	0,000426
INF2	-1,30467	0,000231
ETV4	-1,30329	9,44E-05
COL6A2	-1,29559	4,37E-07
OAF	-1,29146	7,9E-07
JUND	-1,26384	2,41E-06
AP2A1	-1,26184	0,00019
FHOD1	-1,25799	0,010966
GPR137	-1,25276	1,25E-06
XAB2	-1,25134	1,69E-08
ARF1	-1,25123	9,47E-05
GBA2	-1,22427	0,003948
LOC642423	-1,21137	1,35E-06
KAT5	-1,19893	0,008641
TRIM8	-1,1843	0,003075
BCL2L1	-1,18013	5,27E-05
H1FX	-1,17839	3,17E-07
TUBGCP6	-1,17141	0,000119

RNH1	-1,17026	7,49E-05
NUMA1	-1,15801	7,06E-08
CAPN1	-1,1518	0,000105
CACNB3	-1,14664	0,001315
PRKACA	-1,14488	3,88E-07
TYK2	-1,14358	1,33E-07
JUNB	-1,141	2,52E-06
RNF40	-1,13097	6,91E-07
LRP10	-1,12263	0,000739
PCSK1N	-1,11936	0,000342
PPP4R1	-1,1186	0,007407
PXN	-1,11312	1,06E-08
ITGA5	-1,11235	1,32E-06
ACTN3	-1,11218	0,000303
CORO1B	-1,10961	2,97E-08
LOC100129324	-1,1086	0,00229
PNPLA2	-1,10583	5,15E-06
PPP5C	-1,10104	1,05E-08
CENPB	-1,10039	0,001016

PUBLICATION III

Expression and ERG-regulation of PIM kinases in prostate cancer

Eerola SK, Kohvakka A, Tammela TLJ, Koskinen PJ, Latonen L, Visakorpi T

Cancer Medicine, 2021; 10(10):3427–3436
DOI: 10.1002/cam4.3893

Received: 19 January 2021 | Revised: 4 March 2021 | Accepted: 23 March 2021

DOI: 10.1002/cam4.3893

ORIGINAL RESEARCH

Cancer Medicine Open Access WILEY

Expression and ERG regulation of PIM kinases in prostate cancer

Sini K. Eerola[1] | **Annika Kohvakka**[1] | **Teuvo L. J. Tammela**[1,2] | **Päivi J. Koskinen**[3] | **Leena Latonen**[4] | **Tapio Visakorpi**[1,5]

[1]Faculty of Medicine and Health Technology, Tampere University and Tays Cancer Center, Tampere University Hospital, Tampere, Finland

[2]Department of Urology, Tampere University Hospital, Tampere, Finland

[3]Department of Biology, University of Turku, Turku, Finland

[4]Institute of Biomedicine, University of Eastern Finland, Kuopio, Finland

[5]Fimlab Laboratories Ltd, Tampere University Hospital, Tampere, Finland

Correspondence
Tapio Visakorpi, Faculty of Medicine and Health Technology, Tampere University, Kalevantie 4, 33100 Tampere, Finland.
Email: tapio.visakorpi@tuni.fi

Funding information
This study was supported by the Sigrid Juselius Foundation (TV, LL), the Cancer Society of Finland (TV, LL), the Foundation of the Finnish Cancer Institute (LL), the Competitive State Research Financing of the Expert Responsibility area of Tampere University Hospital (TV), the Academy of Finland (LL 317871, PJK 287040), and the Doctoral Programme in Medicine, Biosciences and Biomedical Engineering (SKE).

Abstract

The three oncogenic PIM family kinases have been implicated in the development of prostate cancer (PCa). The aim of this study was to examine the mRNA and protein expression levels of PIM1, PIM2, and PIM3 in PCa and their associations with the *MYC* and *ERG* oncogenes. We utilized prostate tissue specimens of normal, benign prostatic hyperplasia (BPH), prostatic intraepithelial neoplasia (PIN), untreated PCa, and castration-resistant prostate cancer (CRPC) for immunohistochemical (IHC) analysis. In addition, we analyzed data from publicly available mRNA expression and chromatin immunoprecipitation sequencing (ChIP-Seq) datasets. Our data demonstrated that PIM expression levels are significantly elevated in PCa compared to benign samples. Strikingly, the expression of both PIM1 and PIM2 was further increased in CRPC compared to PCa. We also demonstrated a significant association between upregulated PIM family members and both the ERG and MYC oncoproteins. Interestingly, ERG directly binds to the regulatory regions of all *PIM* genes and upregulates their expression. Furthermore, ERG suppression with siRNA reduced the expression of PIM in PCa cells. These results provide evidence for cooperation of PIM and the MYC and ERG oncoproteins in PCa development and progression and may help to stratify suitable patients for PIM-targeted therapies.

KEYWORDS

castration-resistant prostate cancer, ERG, MYC, PIM kinases, prostate cancer

1 | BACKGROUND

PIM kinases form a family of serine/threonine kinases consisting of three members, namely PIM1, PIM2, and PIM3, which have partially overlapping functions and expression patterns.[1–3] PIM kinases are known to affect cancer progression by promoting proliferation, preventing apoptosis, and regulating the activities of several transcription factors. Increased expression of PIM family members has been detected both in hematopoietic malignancies and in solid tumors of epithelial origin, such as prostate cancer (PCa). PIM1 levels are elevated in PCa compared to benign prostatic epithelium,[4–7] with partially contrasting conclusions on

whether PIM1 expression correlates with prostate tumor aggressiveness. Both PIM2 and PIM3 expression levels have been positively correlated with Gleason scores,[8–10] although for PIM3, this has not yet been verified at the protein level. Furthermore, the expression levels of PIM kinases have not been determined in CRPC or characterized for all PIM family members in parallel in any prostate samples.

The *ERG* (ETS-related gene 1) gene belongs to the ETS family of transcription factors and is fused with the prostate-specific and androgen-responsive *TMPRSS2* (transmembrane protease, serine 2) gene in approximately 50% of PCa cases, resulting in ERG overexpression.[11] Additionally, two other *ERG* gene fusions can contribute to its increased expression, *SLC45A3*:*ERG* (solute carrier family 45, member 3) and *NDRG1*:*ERG* (N-myc downstream regulated 1), which occur in less than 5% of PCa cases.[12] Based on recent studies, *ERG* and *PIM1* are associated at the transcriptional level in PCa specimens. Moreover, ERG can directly bind to the *PIM1* promoter and thereby induce PIM1 expression.[13]

Overexpression of the *MYC* oncogene is one of the most common alterations in PCa.[14,15] PIM1 levels have been shown to be increased together with MYC levels during androgen ablation therapy.[16] Furthermore, *PIM1* has been observed to enhance MYC-induced tumorigenicity in human PCa in a mouse xenograft model,[17] while coexpression of PIM1 and MYC in human PCa is associated with higher Gleason scores, suggesting that these oncoproteins synergize to induce advanced prostate carcinoma.[17,18] By contrast, there is no information available on the similar synergism of PIM2 or PIM3 with ERG or MYC oncoproteins.

The aim of this study was to systematically investigate in parallel how different PIM family members are expressed in primary and advanced PCa. In addition, we wanted to assess whether their expression levels are associated with those of the *MYC* or *ERG* oncogenes or with the prognosis of patients with PCa. We found that all PIM kinases are overexpressed in primary PCa and that PIM1 and PIM2 expression further increases in CRPC. Moreover, the expression of PIM kinases is regulated by ERG and associated with *MYC* expression.

2 | MATERIALS AND METHODS

2.1 | Patient samples

Altogether, 254 prostate tissue microarray (TMA) samples, including benign samples ($n = 23$) from adjacent tissue of untreated primary PCa prostatectomy samples, untreated primary PCas ($n = 186$), and locally recurrent CRPCs ($n = 45$), were obtained from Tampere University Hospital (TAUH, Tampere, Finland). The mean age of patients at diagnosis was 63.5 years (range: 49–72), and the mean prostate-specific antigen (PSA) concentration was 14.3 ng/ml (range: 1.5–78.2) (Table S1). Biochemical progression was defined as two consecutive samples with PSA ≥0.5 ng/ml. The use of clinical material was approved by the Ethics Committee of the Tampere University Hospital and the National Authority for Medicolegal Affairs. For prospective sample collection, informed consent was obtained from all the subjects.

2.2 | Gene correlation analyses

Two distinct clinical datasets were used to assess the gene expression levels of *PIM* genes and their associations with the *ERG* and *MYC* oncogenes in PCa patient samples: Tampere PCa RNA-seq dataset[19] and Integrative Genomic Profiling of Human Prostate Cancer microarray dataset.[20]

2.3 | Immunohistochemical staining

PIM protein expression levels in prostate carcinomas were validated by immunohistochemical (IHC) analysis from formalin-fixed paraffin-embedded (FFPE) TMA samples. Primary antibodies against PIM1 (1:200, ab224772; Abcam), PIM2 (1:50, TA501166; OriGene Technologies Inc.), PIM3 (1:200, TA351349; OriGene), and ERG (1:200, EPR3864; Epitomics, Inc.) were used with the Histofine Simple Stain MAX PO multi; containing both Universal Immunoperoxidase Polymer Anti-Mouse and Anti-Rabbit (Nichirei Biosciences Inc.) secondary antibody according to the manufacturer's instructions. TMA sections were deparaffinized, and antigen retrieval was performed by autoclaving in TE buffer (5 mmol/L Tris-HCl/ 1 mmol/L EDTA, pH 9) at 98°C for 15 min. The primary antibody was diluted in Antibody Diluent (ImmunoLogic). Staining was performed using a Lab Vision Autostainer 480S (Thermo Fisher Scientific). Sections were counterstained with Mayer's hematoxylin (Histolab AB) for 2 min and mounted with Neo-Mount (Merck KGaA).

For negative controls, the primary antibody was omitted, and for positive controls, FFPE samples of tonsil, glioma, and/or colon tissues were used. Slides were scanned with an Olympus BX51 scanner with a 20× objective and Slide Strider software (Jilab Inc.) or with a NanoZoomer S60 Digital slide scanner (C13210-01, Hamamatsu Photonics, K. K.) with a 20× objective. Nuclear scoring of the figures was performed with ImageJ® software (Wayne Rasband, NIH, USA) and its cell counter tool. Nuclear and cytoplasmic staining intensities of PIM proteins were classified on a scale from 0 to 3 with negative (0), weak (1), moderate (2), or strong (3) staining in proportion to the stained cancerous area. In the case of nuclear staining, if possible, a minimum of 200 cells were calculated from carcinogenic areas. The Histoscore (H-score/HS) was calculated by a semiquantitative assessment

of both the intensity of staining with the 0 to 3 scale and the percentage of positive PCa cells/area. The range of possible scores was from 0 to 300 or from 0 to 600 when both the cytoplasmic and nuclear scores were combined or summed. Samples stained against ERG antibody were categorized into ERG-positive and ERG-negative (Table S2 and Figure S1). The results from 85 ERG-stained samples were already published in Leinonen et al. 2013,[21] while 38 additional samples were stained and analyzed for these studies.

2.4 | Cell culture

VCaP PCa cells (RRID:CVCL_2235) were kindly provided by Dr. Jack Schalken (Radboud University Nijmegen Medical Center). Cells were cultured as recommended by the suppliers and tested for mycoplasma contamination regularly.

2.5 | Transfections for gene knockdown

siRNAs targeting *ERG* (sense: UGAUGUUGAUAAAGC CUAUU; antisense: UAGGCUUUAUCAACAUCAUU) or a negative control siRNA (MISSION siRNA Universal Negative Control #2) were purchased from Sigma-Aldrich. The transfection reagent Lipofectamine RNAiMAX (Invitrogen) was used for transfecting siRNAs according to the manufacturer's instructions. VCaP PCa cells were reverse-transfected with 25 nM siRNA and grown for 72 h before RNA and protein extraction.

2.6 | Quantitative reverse transcription PCR (qRT-PCR)

For determination of *ERG* and *PIM* mRNA expression levels, total RNA was extracted using TRIzol reagent (Invitrogen, Carlsbad, CA, USA) according to the manufacturer's protocol. qRT-PCR was performed using random hexamer primers (Thermo Fisher Scientific, Waltham, MA, USA), Maxima reverse transcriptase (Thermo Fisher Scientific), Maxima SYBR Green qPCR Master Mix (Thermo Fisher Scientific), and the CFX96™ Real-Time PCR Detection System (Bio-Rad Laboratories, Inc.). The expression levels were measured from three biological and technical replicates and normalized against mRNA of the TATA-binding protein (*TBP*). All primers are presented in Table S3.

2.7 | Western blot analysis

After knockdown experiments, cells were lysed in Triton-X lysis buffer containing 50 mM Tris-HCl, pH 7.5, 150 mM NaCl, 0.5% Triton X-100, 1 mM PMSF, 1 mM DTT, and 1× Halt protease inhibitor cocktail (Thermo Fisher Scientific), after which the lysates were sonicated four times for 30 s at medium power with Bioruptor equipment (Diagenode Inc.), and cellular debris was removed by centrifugation. Samples were resuspended in 2× Laemmli sample buffer and heated at 95°C for 5 min. Proteins were separated by Mini-PROTEAN TGX Precast Gels (Bio-Rad), and immobilized onto PVDF membranes (Immobilon-P, Millipore, Merck). Primary antibodies against PIM1 (1:2000, Abcam, ab224772), PIM2 (1:2000, OriGene, TA501166), PIM3 (1:1000, OriGene, TA351349), ERG (1:5000, EPR3864; Epitomics), β Tubulin (1:40 000, Sigma-Aldrich), or Fibrillarin (1:1000, Cell Signaling Technology) were used together with anti-mouse HRP-conjugated antibody produced in rabbit (1:10 000; DAKO) or anti-rabbit HRP-conjugated antibody produced in swine (1:5000; DAKO). Chemiluminescence reactions were generated using either Amersham™ ECL Plus or ECL Prime reagents (GE Healthcare Life Sciences).

2.8 | Statistical analyses

Statistical analyses for IHC protein expression levels were performed using the Mann-Whitney U test. Gleason scores were divided into three groups: low (scores <7), intermediate (scores equal to 7), and high (scores >7 [from 8 to 10]). Correlations between PIM1/PIM2 or PIM3 expression and MYC were tested using Pearson's correlation coefficient. Grubbs' test, also called the extreme studentized deviate (ESD) method, was used to analyze possible outliers from the *PIM-MYC* gene correlation dataset, and a p-value of 0.05 was used as a cutoff for the significance of the outliers. Associations between PIM1/PIM2 or PIM3 expression and ERG were tested with the Chi-square test or Fisher's exact test depending on the form of data suitable for each analysis. Kaplan–Meier survival analysis and the log-rank (Mantel-Cox) test were used to estimate the progression-free (PSA-free) time (survival) between samples divided by their median expression into PIM low and PIM high expression groups. Unpaired two-tailed Student's t-test was used to calculate the significance between the control and experimental conditions in qRT-PCR. All statistical analyses were performed using GraphPad Prism version 5.02 (GraphPad Software Inc). p-values <0.05 (*), p-values <0.01 (**), and p-values <0.001 (***) were considered statistically significant.

To investigate the binding sites of ERG in all *PIM* promoter areas, we used a publicly available dataset (GSM353647[22]) with Integrative Genomics Viewer (IGV) version 2.5.0 (Broad Institute) to observe ERG ChIP-seq

peaks compared to *PIM* regulatory regions in VCaP PCa cells.

3 | RESULTS

3.1 | *PIM* gene expression is elevated in prostate cancer

To study the expression of all *PIM* family members in PCa, we first utilized our RNA-seq-based mRNA expression dataset of PCa patient samples (Tampere PCa sequencing data[19]). Of all the *PIM* members, the overall expression of *PIM3* was the highest, and *PIM2* was the lowest (Figure S2A). Similar results were observed in another dataset [20] (Figure S2B). Next, we analyzed transcriptional expression levels according to pathology (BPH, PCa, and CRPC). In our Tampere PCa dataset, there was a significant increase in *PIM1* and *PIM3* but not *PIM2* gene expression in PCa compared to BPH patient samples (Figure 1A–C). When the primary tumors were categorized according to Gleason scores (GS < 7, GS = 7, and GS > 7), a slight but not statistically significant increase was detected for *PIM2* in samples with Gleason scores higher than 7 when compared to samples with lower Gleason scores (Figure 1E), while no association with Gleason scores was observed for *PIM1* or *PIM3* expression levels (Figure 1D and F). We analyzed also larger Taylor et al. microarray dataset and the results were parallel with our own cohort but not statistically significant (Figure S3).

3.2 | PIM protein expression increases during the prostate cancer progression

Next, we wanted to assess PIM expression levels at the protein level using a sample cohort containing 23 benign adjacent tissue samples from the primary PCa samples, 186 primary PCa samples, and 45 CRPC samples. Our results from IHC analysis showed a significant increase in PIM1 and PIM2 protein expression levels in primary PCa compared to benign patient samples ($p = 0.0002$, $p = 0.007$; Figure 2A and B). However, the expression levels of either PIM1 or PIM2 had no association with progression-free survival ($p = 0.77$, $p = 0.07$; Figure S4A and B). To our knowledge, PIM3 protein expression levels in PCa have not been reported before. Our results show that the PIM3 levels were significantly higher in PCa than in benign samples ($p = 0.02$; Figure 2C). Additionally, in this case, the expression levels did not correlate with progression-free survival ($p = 0.8$; Figure S4C). When primary PCa samples of different Gleason score groups were compared, a statistically significant increase was observed in PIM1 expression with Gleason scores higher than 7 when compared to Gleason scores lower than 7 ($p = 0.04$; Figure 2D). However, no statistically significant differences in the PIM2 and PIM3 protein expression levels were observed within the different Gleason score groups (Figure 2E and F).

In CRPC samples, both PIM1 and PIM2 expression levels were significantly upregulated compared to those in primary PCa patient samples ($p<0.0001$, $p<0.0001$; Figure 2A and

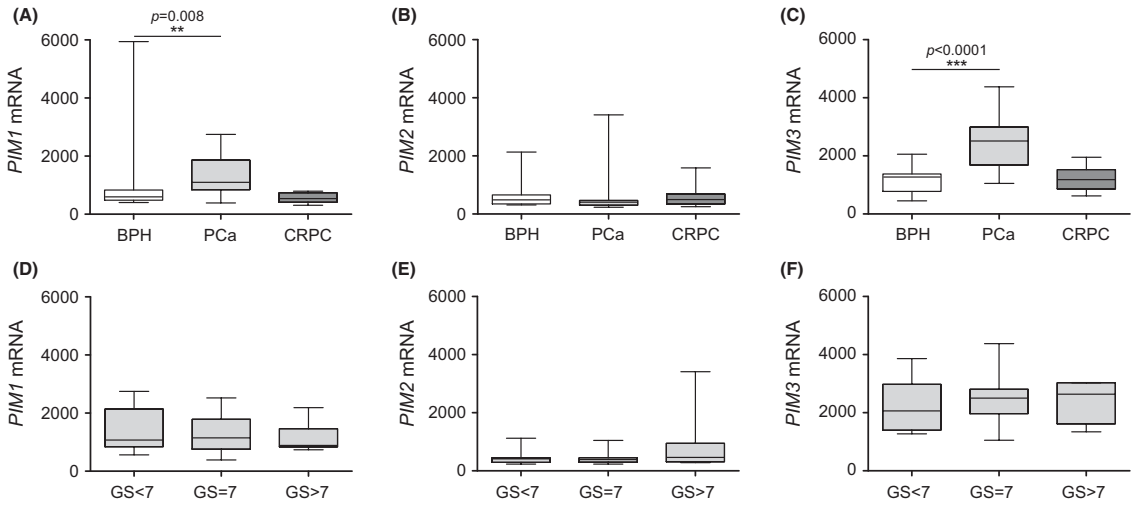

FIGURE 1 Expression of *PIM1* and *PIM3* is elevated in primary PCa. The Tampere PCa sequencing dataset[19] was used to assess the mRNA expression levels of the *PIM1* (A, D), *PIM2* (B, E), and *PIM3* (C, F) genes. The results were first categorized into BPH ($n = 12$), primary PCa ($n = 30$), and CRPC ($n = 13$) samples (A–C). Primary PCa samples were further divided based on Gleason scores GS<7 ($n = 7$), GS = 7 ($n = 7$), and GS>7 ($n = 15$) (D–F). Error bars display the minimum and maximum values, and the line inside the boxes displays the median in the dataset range. *p*-values <0.05 (*), *p*-values <0.01 (**), and *p*-values <0.001 (***) were considered statistically significant

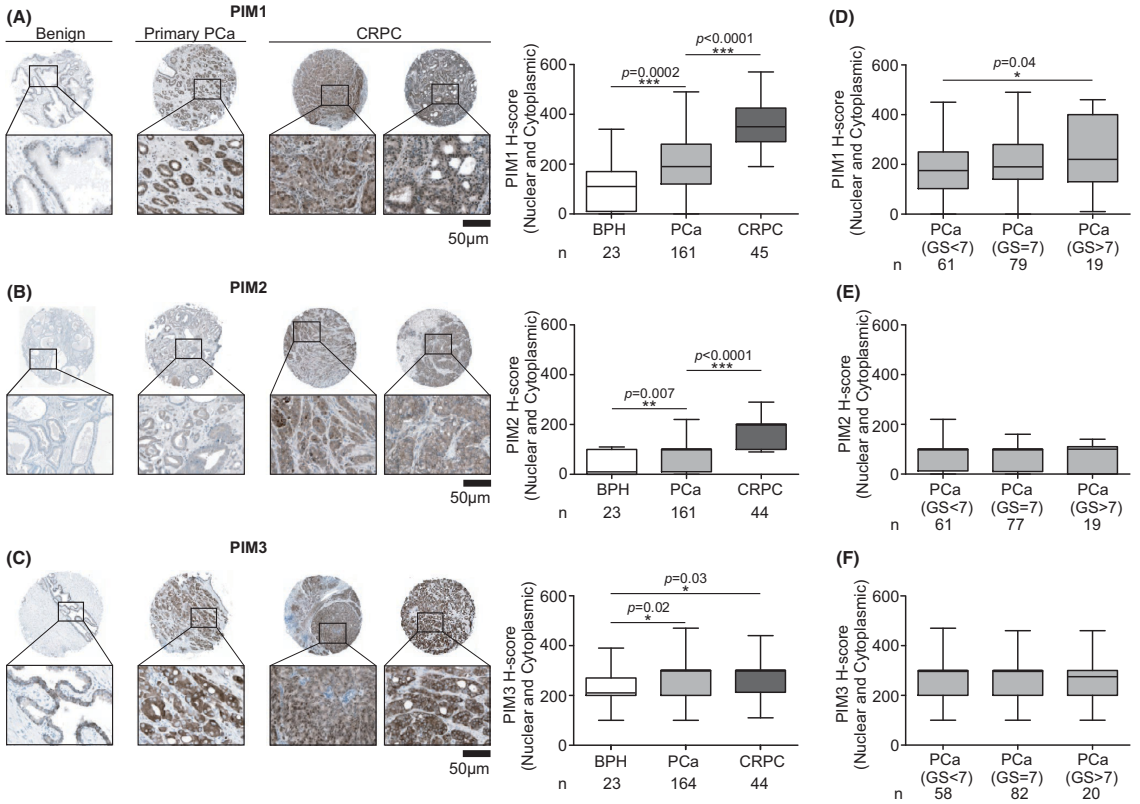

FIGURE 2 PIM protein levels are upregulated during PCa progression. IHC staining was performed for FFPE TMA samples of 23 benign prostate, 186 primary PCa, and 45 CRPC samples. Representative IHC figures of whole TMA spots with 5x and 20x enlargement of the refined area are shown from benign prostate, primary PCa and CRPC samples stained with PIM1 (A), PIM2 (B), and PIM3 (C) antibodies. Boxplots were made from IHC staining results by combined Histoscore numbers of nuclear and cytoplasmic staining of the samples. Primary PCa samples were categorized by Gleason scores (GS<7, GS = 7, and GS>7) and PIM1 (D), PIM2 (E), and PIM3 (F) protein expression levels. Error bars display the minimum and maximum values, and the line inside the boxes displays the median in the dataset range. Sample numbers (*n*) and *p*-values (*p*) are marked in the figures. *p*-values <0.05 (*), *p*-values <0.01 (**), and *p*-values <0.001 (***) were considered statistically significant

B). The PIM3 expression level was significantly higher in CRPC than in BPH ($p = 0.03$), while no further increase was observed from primary PCa to CRPC (Figure 2C). Thus, our data indicate that the expression of PIM1 and PIM2 increases during the progression of the disease.

3.3 | Expression of *PIM1 or PIM3* and *MYC* oncogene positively correlate in prostate cancer

As PIM1 kinase has been shown to cooperate with the MYC oncoprotein to induce advanced PCa,[17] we wanted to investigate the possible associations between the expression of distinct *PIM* family genes and the *MYC* oncogene. We observed correlations between *PIM1* ($r = 0.43$; Figure 3A), *PIM2* ($r = 0.29$, Figure 3B), and *PIM3* ($r = 0.41$; Figure 3C) with *MYC* mRNA in the Taylor et al. 2010 dataset. This correlation was confirmed in our smaller Tampere PCa cohort for *PIM3* but not for *PIM1* or *PIM2* (Figure S5A–C). These results suggest for the first time that not only PIM1, but also PIM3 may cooperate with MYC in prostate tumorigenesis.

3.4 | Expression of PIM genes and proteins is associated with ERG

Next, we assessed *PIM* associations with *ERG* at the transcriptional level in primary tumors. No significant association at the transcriptional level was detected between *PIM1* and *ERG* in the Tampere PCa dataset (Figure 4A), while the association between *PIM2* and *ERG* was significantly negative (Figure 4B). Interestingly, *PIM3* and *ERG* showed a significant positive association (Figure 4C). In contrast, in the larger Taylor et al. dataset, *ERG* showed

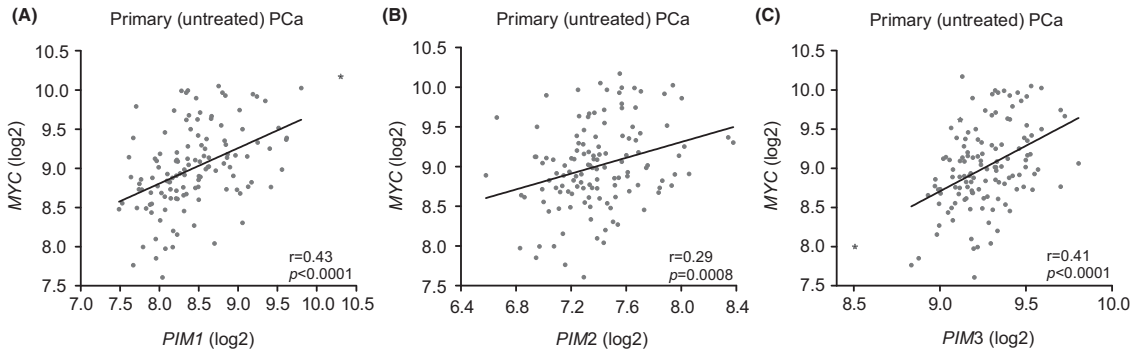

FIGURE 3 *PIM* and *MYC* oncogene expression is associated with human PCa. The Integrative Genomic Profiling of Human Prostate Cancer microarray dataset[20] ($n = 126$) was used to assess the mRNA expression of the *PIM1* (A), *PIM2* (B), and *PIM3* (C) genes and their correlations with *MYC* oncogene in logarithmic scale in untreated prostate cancer patient samples. Possible outliers of the dataset were calculated with Grubbs' test and marked as a black star in the dot blot. *p*-values (*p*) and Pearson correlation values (r) are marked in the figures. *p*-values <0.05 (*), *p*-values <0.01 (**), and *p*-values <0.001 (***) were considered statistically significant

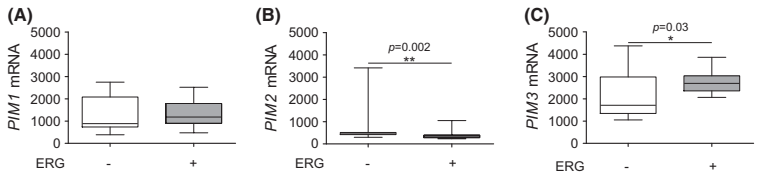

FIGURE 4 Association of the *PIM* and *ERG* oncogenes. Using the Tampere PCa cohort,[19] *PIM1* (A), *PIM2* (B), and *PIM3* (C) mRNA expression levels were compared in *ERG*-negative ($n = 15$) and *ERG*-positive ($n = 15$) samples. The cutoff for *ERG*-negative and *ERG*-positive expression values was calculated from the *ERG* expression average of BPH samples by adding double the standard deviation to this value. Error bars display the minimum and maximum values, and the line inside the boxes displays the median in the dataset range

a significant association with *PIM1* but not with *PIM2* or *PIM3* gene expression in primary untreated PCa samples (Figure S6A–C). Taken together, these results suggest a cooperative or regulatory role between the *PIM* and *ERG* oncogenes.

Next, we wanted to investigate the possible associations of PIM and ERG at the protein level. Based on IHC staining, all PIM family members showed an association with ERG in PCa patient specimens. Higher nuclear, cytoplasmic, or both nuclear and cytoplasmic PIM1 expression was associated with ERG positivity ($p = 0.0004$, $p = 0.0009$, $p<0.0001$, Figure 5A). Moreover, significantly higher combined cytoplasmic and nuclear PIM2 expression were associated with the expression of ERG ($p = 0.001$; Figure 5B), and higher cytoplasmic and combined cytoplasmic and nuclear PIM3 expression were significantly associated with ERG expression ($p = 0.03$, $p = 0.01$; Figure 5C), while for PIM2 and PIM3, an association was not observed in samples with only nuclear staining (Figure 5B, C). Altogether, these results at both the mRNA and protein levels indicate that in addition to PIM1, PIM2 and PIM3 are also associated with the expression of the ERG oncogene.

3.5 | Expression of all *PIM* family members is regulated by ERG

The strong associations between ERG and PIM kinases led us to further investigate the nature of the cooperation between them. Previous data by Magistroni et al. 2011 demonstrated direct binding of the TMRSS2:ERG fusion protein to the *PIM1* promoter, enabling ERG-mediated regulation of *PIM1* expression in benign RWPE-1 prostate cells. Therefore, we used a publicly available ERG ChIP-seq dataset from VCaP PCa cells[22] to assess the possible ERG binding sites at the *PIM1*, *PIM2*, and *PIM3* loci. This analysis revealed multiple ERG binding sites not only at *PIM1* but also at the *PIM2* and *PIM3* promoter regions (Figure 6A–C).

To assess the effect of ERG on the transcriptional regulation of *PIM* genes, we performed qRT-PCR of VCaP cells transfected with *ERG* siRNA (siERG) or scrambled negative control (NC) siRNA. The results showed significant transcriptional downregulation of all *PIM* mRNAs in *ERG*-silenced samples compared to control samples (Figure 6D). This downregulation was also evident at the protein level in

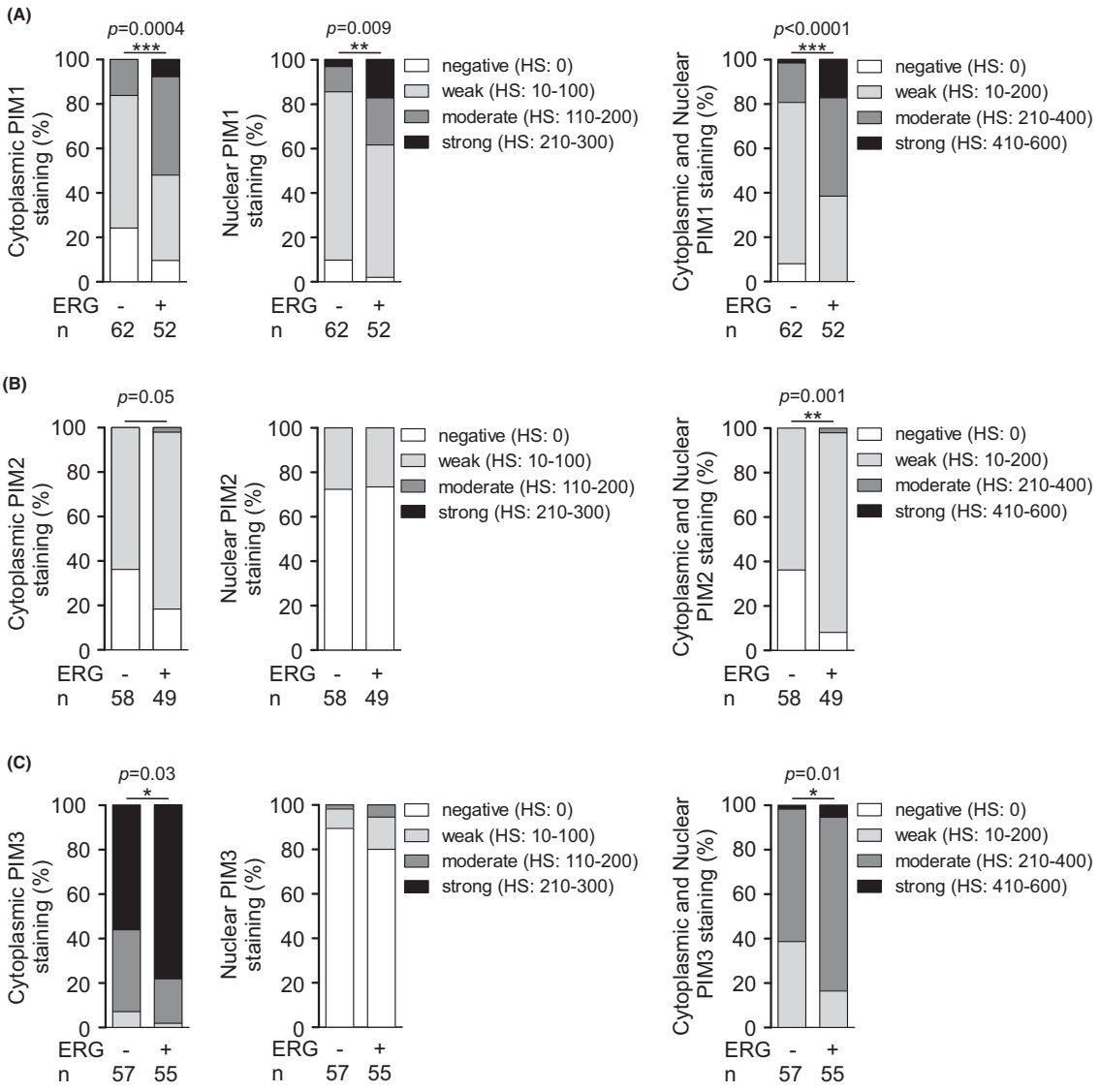

FIGURE 5 PIM kinases are associated with the ERG oncoprotein. Histograms of PIM1 (A), PIM2 (B), and PIM3 (C) protein expression levels in the cytoplasmic, nuclear, or both compartments were categorized into negative, low, moderate, and strong staining intensities and compared between ERG-negative and ERG-positive samples

immunoblotted samples (Figure 6E). Altogether, these results indicate that ERG regulates the expression of not only PIM1 but also PIM2 and PIM3.

4 | DISCUSSION

To be able to improve PCa therapies, it is important to identify the critical oncogenes that promote cancer development toward a more aggressive and possibly lethal form. This in turn may help to recognize high-risk CRPC patients from localized PCa at an earlier stage and thereby choose the right types of therapies to increase patient survival. To achieve this goal, new molecular biomarkers and drug targets are needed.

This study provides novel insights into the role of different PIM family kinases together with other effective oncoproteins involved in PCa progression. Here, we have for the first time compared the mRNA and protein expression of all PIM family members in PCa patient samples in parallel.

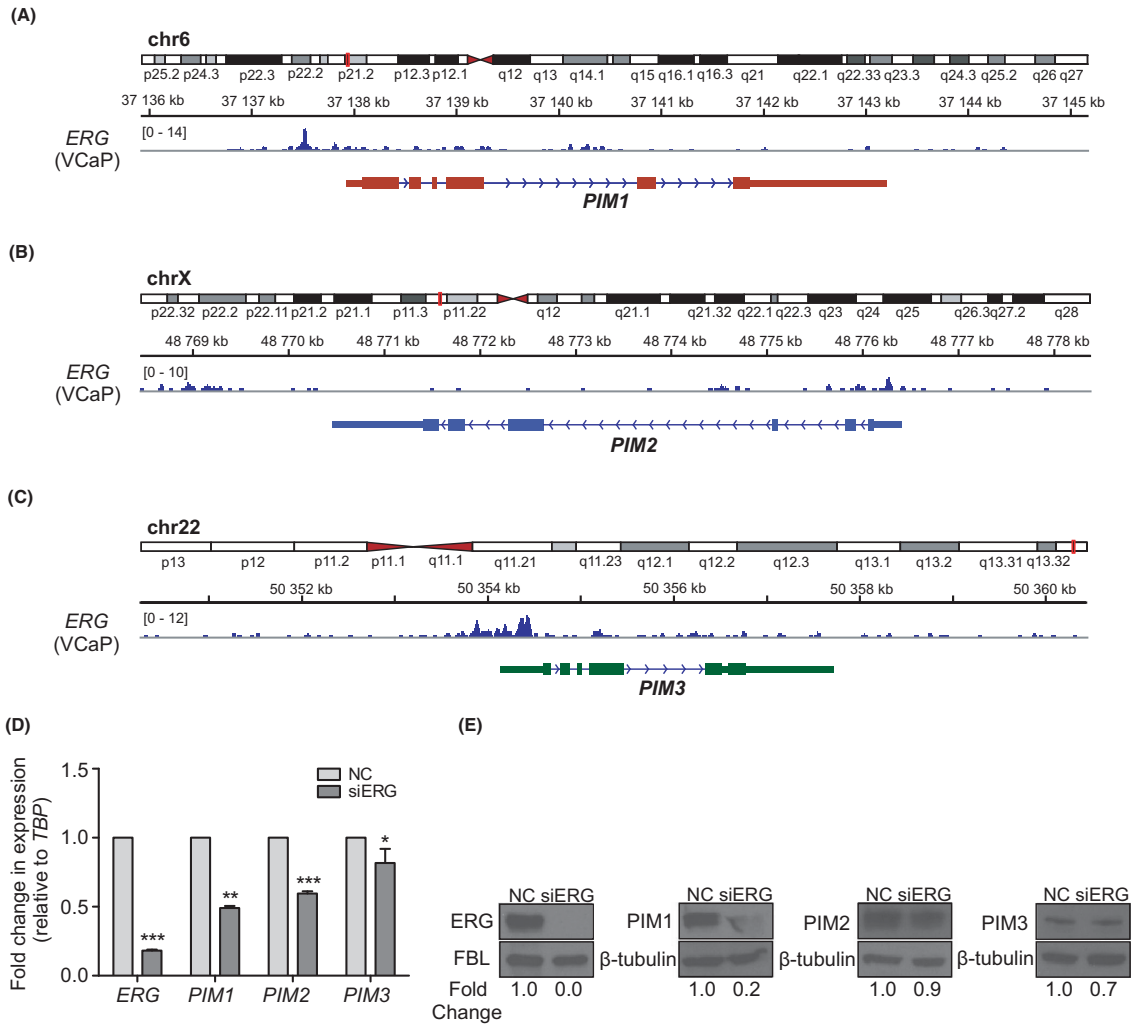

FIGURE 6 ERG binds to the regulatory regions of all PIM genes and regulates their expression. Publicly available ChIP-seq data were used to determine the binding sites for ERG on the *PIM1* (A), *PIM2* (B), and *PIM3* (C) promoter areas. D. qPCR was performed on ERG-silenced (siERG; 25 nM) VCaP cells from which *ERG*, *PIM1*, *PIM2*, and *PIM3* transcriptional expression levels were determined after 72 h and compared with cells transfected with control siRNA (NC). *TBP* was used as a reference gene to normalize the data. E. Western blot analyses of *ERG*-silenced (siERG; 25 nM) VCaP cells, from which ERG, PIM1, PIM2, and PIM3 protein expression levels were determined after 72 h and compared with cells transfected with control siRNA (NC). Fold changes in protein expression levels were normalized against fibrillarin (FBL) or β-tubulin, which were used as loading controls

This is important, as expression analyses focusing on only one of the functionally fairly redundant family members may underestimate the overall contribution of PIM kinases to PCa progression. At the transcriptional level, there was a slight increase in *PIM1* and a more robust upregulation of *PIM3* mRNAs in primary PCa patient samples compared to normal or BPH samples in our PCa cohort.[19] At the protein level, however, the expression levels of all PIM kinase family members are elevated in primary PCa compared to benign prostate samples and are further increased in CRPC samples for both PIM1 and PIM2. PIM1 protein levels also increased in a Gleason score-dependent manner. To our knowledge, PIM3 protein levels have not been analyzed in PCa before, nor have the levels of any PIM family proteins in CRPC. However, there was no association between any PIM expression and progression-free survival in our dataset.

In addition to our Tampere PCa RNA-seq data, we utilized Integrative Genomic Profiling of Human Prostate Cancer microarray data.[20] When overall *PIM* mRNA

expression levels were compared with this larger dataset, the results were fairly similar to our Tampere PCa dataset, although no significant differences were detected between the samples from normal prostates and primary prostate tumors or metastasized CRPC tumors, and no Gleason score-dependent differences were detected. These discrepancies may partly be due to differences between the platforms used (RNA-seq vs. microarray) or in the samples assessed (BPH vs. normal prostate tissue and CRPC vs. metastasized CRPC). Further clinical datasets will undoubtedly shed more light on the matter.

Based on earlier results, both PIM1 and MYC levels are elevated in human PCas,[4–7,14,15] suggesting that they may cooperate in prostate carcinogenesis. Moreover, it has been discovered that PIM1 can enhance the transcriptional activity of MYC and thereby promote tumorigenicity.[17] Aligned with the previously published data, we observed positive correlation of *PIM1* and *MYC* expression within Taylor et al. dataset. However, in our own dataset, the correlation between *PIM1* and *MYC* was not statistically significant. *PIM2* and *MYC* showed only weak positive correlation in Taylor et al. cohort and no significant correlation was detected in our own dataset. The discrepancies between the two datasets in case of *PIM1*/*PIM2* and *MYC* may partly be due to the different size of the cohorts (Taylor et al. $n = 126$ and our cohort $n = 30$) and differences between the platforms used (RNA-seq vs. microarray) or in the samples assessed. Further clinical validation will undoubtedly shed more light on the matter. However, in this study, we show a positive correlation between the expression levels of *PIM3* and *MYC* mRNAs within the two human PCa datasets, suggesting that PIM3 and MYC also cooperate in PCa progression. While MYC is a challenging target for therapies, patients overexpressing both PIM and MYC proteins may benefit from PIM-targeted therapy.

In addition to the *MYC* oncogene, it is known that the transcription factor *ERG* is often coexpressed with PIM1 and that ERG binds to the *PIM1* promoter and directly induces its expression.[13] Here we also show a significant association between *ERG* and *PIM3* gene expression in our PCa RNA-seq dataset and demonstrate that all PIM kinases are associated to a significant extent with ERG at the protein level. Furthermore, we show that there are ERG binding sites on the regulatory regions of all the *PIM* family members and that ERG regulates their expression levels, as confirmed by reduced PIM mRNA and protein levels by RNA interference-mediated *ERG* knockdown. This regulation in turn may be relevant for ERG-induced prostate tumorigenesis.

In a novel publication by Luszczak and others,[23] it was reported that both the PIM and PI3 K/AKT/mTOR pathways are overlapping and cross-impact each other. Luszczak and others[23] also suggested that more effort should be put into identifying the associating oncogenes/biomarkers of each patient and targeted combinatorial treatments against them. Indeed, there are already promising results from combinatorial treatment against PIM and PI3 K in PIM-upregulated and TMPRSS:ERG-fusion-positive PCa cells.[24] Based on our findings, these combinatorial treatments against PIM, ERG, and MYC signaling pathways in relevant patients may be helpful.

5 | CONCLUSIONS

In this study, we demonstrate for the first time that the mRNA and protein expression levels of all three PIM family kinases can be upregulated during PCa progression and can thereby significantly contribute to this process, especially in cooperation with other co-overexpressed oncoproteins, such as MYC and ERG, as shown here. The increased PIM expression levels may in turn be explained by our observation that ERG can induce transcription of all PIM family genes. As ERG itself is often overexpressed in PCa due to oncogenic gene fusions, our data suggest that it is important to identify patients who express high levels of any PIM kinase together with other oncoproteins, such as MYC or ERG, as those patients may benefit most from targeted and combinatorial therapies.

ACKNOWLEDGMENTS

The authors want to thank Hanna Rauhala, Aurora Halkoluoto, Sari Toivola, Marja Pirinen, and Päivi Martikainen for their technical assistance and the Tampere Imaging Facility (TIF) for their service.

CONFLICT OF INTEREST

The authors declare that they have no conflict of interest.

ETHICS APPROVAL AND CONSENT TO PARTICIPATE

The use of clinical material was approved by the ethics committee of the Tampere University Hospital (Tampere, Finland) and the National Authority for Medicolegal Affairs. For prospective sample collection, informed consent was obtained from the subjects.

DATA AVAILABILITY STATEMENT

The Integrative Genomic Profiling of Human Prostate Cancer microarray dataset[20] is available at https://www.ncbi.nlm.nih.gov/geo/query/acc.cgi?acc=GSE21036 under the accession number GSE21036. To investigate the binding sites of ERG oncogene in all PIM kinase promoter areas, we used a publicly available dataset https://www.ncbi.nlm.nih.gov/geo/query/acc.cgi?acc=GSE14092 under the accession number GSM353647[22]; Tampere PCa RNA-seq data[19] and datasets for IHC analysis are mainly available in the Supplementary Information, and additional information related to these

datasets are available from the corresponding author upon reasonable request.

ORCID

Tapio Visakorpi https://orcid.org/0000-0002-5004-0364

REFERENCES

1. Eichmann A, Yuan L, Bréant C, Alitalo K, Koskinen P. Developmental expression of Pim kinases suggests functions also outside of the hematopoietic system. *Oncogene*. 2000;19:1215-1224.
2. Nawijn MC, Alendar A, Berns A. For better or for worse: the role of Pim oncogenes in tumorigenesis. *Nat Rev Cancer*. 2011;11:23-34.
3. Santio NM, Koskinen PJ. PIM kinases: from survival factors to regulators of cell motility. *Int J Biochem Cell Biol*. 2017;93:74-85.
4. Dhanasekaran SM, Barrette TR, Ghosh D, et al. Delineation of prognostic biomarkers in prostate cancer. *Nature*. 2001;412:822-826.
5. Valdman A, Fang X, Pang S, Ekman P, Egevad L. Pim-1 expression in prostatic intraepithelial neoplasia and human prostate cancer. *Prostate*. 2004;60:367-371.
6. Xu Y, Zhang T, Tang H, et al. Overexpression of PIM-1 is a potential biomarker in prostate carcinoma. *J Surg Oncol*. 2005;92:326-330.
7. Cibull TL, Jones TD, Li L, et al. Overexpression of Pim-1 during progression of prostatic adenocarcinoma. *J Clin Pathol*. 2006;59:285-288.
8. Dai H, Li R, Wheeler T, et al. Pim-2 upregulation: biological implications associated with disease progression and perinueral invasion in prostate cancer. *Prostate*. 2005;65:276-286.
9. Qu Y, Zhang C, Du E, et al. Pim-3 is a critical risk factor in development and prognosis of prostate cancer. *Med Sci Monit*. 2016;22:4254-4260.
10. Ren K, Gou X, Xiao M, He W, Kang J. Pim-2 cooperates with downstream factor XIAP to inhibit apoptosis and intensify malignant grade in prostate cancer. *Pathol Oncol Res*. 2019;25:341-348.
11. Tomlins SA, Rhodes DR, Perner S, et al. Recurrent fusion of TMPRSS2 and ETS transcription factor genes in prostate cancer. *Science*. 2005;310:644.
12. Pflueger D, Rickman DS, Sboner A, et al. N-myc downstream regulated gene 1 (NDRG1) is fused to ERG in prostate cancer. *Neoplasia*. 2009;11:804-811.
13. Magistroni V, Mologni L, Sanselicio S, et al. ERG deregulation Induces PIM1 over-expression and aneuploidy in prostate epithelial cells. *PLoS One*. 2011;6:e28162.
14. Ellwood-Yen K, Graeber TG, Wongvipat J, et al. Myc-driven murine prostate cancer shares molecular features with human prostate tumors. *Cancer Cell*. 2003;4:223-238.
15. Gurel B, Iwata T, Koh CM, et al. Nuclear MYC protein overexpression is an early alteration in human prostate carcinogenesis. *Mod Pathol*. 2008;21(9):1156-1167.
16. van der Poel HG, Zevenhoven J, Bergman AM. Pim1 regulates androgen-dependent survival signaling in prostate cancer cells. *Urol Int*. 2010;84:212-220.
17. Wang J, Kim J, Roh M, et al. Pim1 kinase synergizes with c-MYC to induce advanced prostate carcinoma. *Oncogene*. 2010;29:2477-2487.
18. Wang J, Anderson PD, Luo W, Gius D, Roh M, Abdulkadir SA. Pim1 kinase is required to maintain tumorigenicity in MYC-expressing prostate cancer cells. *Oncogene*. 2012;31:1794-1803.
19. Annala M, Kivinummi K, Tuominen J, et al. Recurrent SKIL-activating rearrangements in ETS-negative prostate cancer. *Oncotarget*. 2015;6:6235-6250.
20. Taylor BS, Schultz N, Hieronymus H, et al. Integrative genomic profiling of human prostate cancer. *Cancer Cell*. 2010;18:11-22.
21. Leinonen KA, Saramäki OR, Furusato B, et al. Loss of PTEN Is associated with aggressive behavior in ERG-positive prostate cancer. *Cancer Epidemiol Biomarkers Prev*. 2013;22:2333.
22. Yu J, Yu J, Mani R, et al. An integrated network of androgen receptor, polycomb, and TMPRSS2-ERG gene fusions in prostate cancer progression. *Cancer Cell*. 2010;17:443-454.
23. Luszczak S, Kumar C, Sathyadevan VK, et al. PIM kinase inhibition: co-targeted therapeutic approaches in prostate cancer. *Signal Transduct Target Ther*. 2020;5:7
24. Mologni L, Magistroni V, Casuscelli F, Montemartini M, Gambacorti-Passerini C. The novel PIM1 inhibitor NMS-P645 reverses PIM1-dependent effects on TMPRSS2/ERG positive prostate cancer cells and shows anti-proliferative activity in combination with PI3K inhibition. *J of Cancer*. 2017;8:140-145.

SUPPORTING INFORMATION

Additional supporting information may be found online in the Supporting Information section.

How to cite this article: Eerola SK, Kohvakka A, Tammela TL, Koskinen PJ, Latonen L, Visakorpi T. Expression and ERG regulation of PIM kinases in prostate cancer. *Cancer Med*. 2021;10:3427–3436. https://doi.org/10.1002/cam4.3893

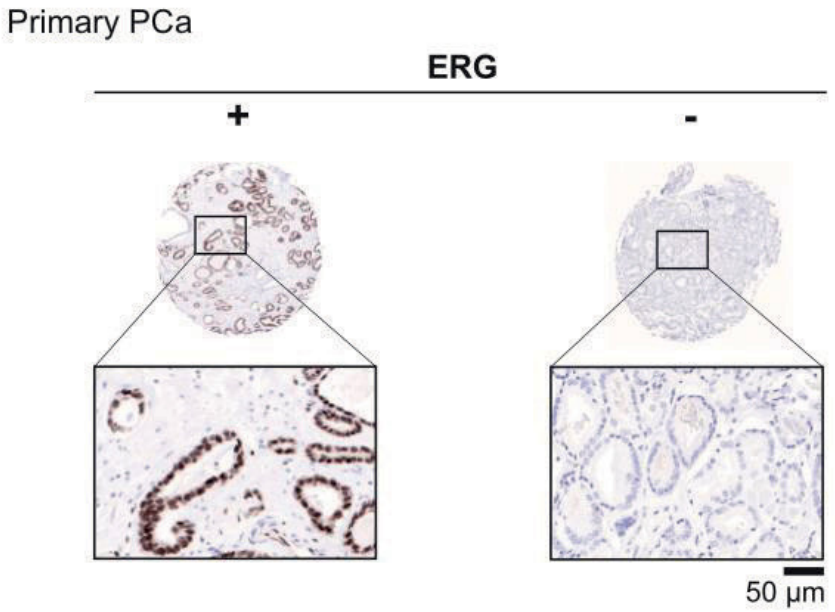

Supplementary Figure S1. ERG positive and negative IHC staining.

IHC staining was performed for FFPE TMA samples of 85 ERG-stained primary PCa samples which were already published in 'Blinded per Author Guidelines' [21], while 38 additional primary PCa samples were stained and analyzed for these studies. Primary PCa samples stained with ERG antibody were categorized into ERG-positive and ERG-negative samples and representative IHC figures of whole TMA spots with 5x and 40x enlargement of the refined area are shown.

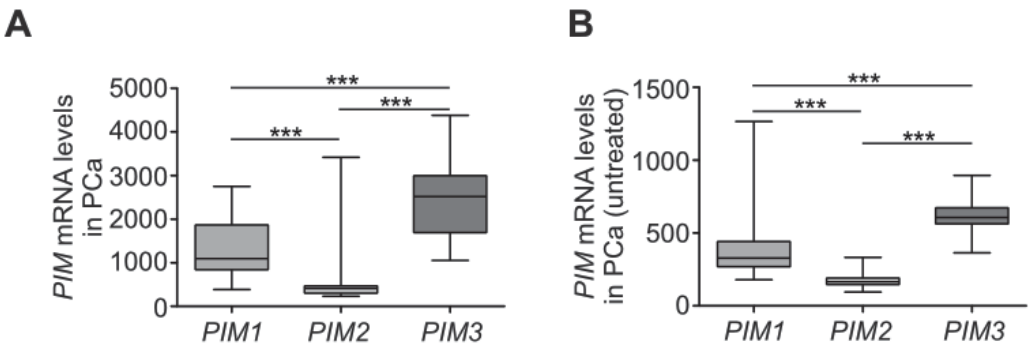

Supplementary Figure S2. Transcriptional levels of *PIM* oncogenes in PCa patient cohorts

A. The <city> PCa sequencing dataset [19] (n=30) and **B.** Integrative Genomic Profiling of Human Prostate Cancer microarray data set [20] (n=126) were used to assess overall gene expression levels of *PIM1*, *PIM2* and *PIM3* in primary prostate cancer. Error bars display the minimum and maximum values, and the line inside the boxes displays the median in the dataset range. *P*-values < 0.05 (*), *p*-values < 0.01 (**) and *p*-values < 0.001 (***) were considered statistically significant.

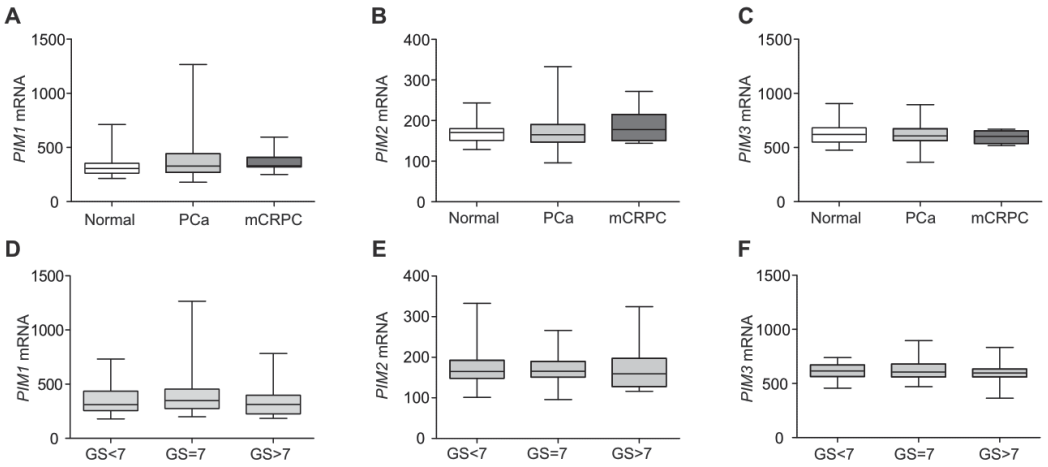

Supplementary Figure S3. *PIM gene* expression in progression of PCa

The Taylor et al. 2010 microarray dataset [20] was used to assess the mRNA expression levels of the *PIM1* (**A,D**), *PIM2* (**B,E**) and *PIM3* (**C,F**) genes. The results were first categorized into Normal (n=28), primary PCa (n=126) and metastasized CRPC (mCRPC) (n=8) samples (**A-C**). Primary PCa samples were further divided based on Gleason scores GS<7 (n=41), GS=7 (n=71) and GS>7 (n=14) (**D-F**)**.** Error bars display the minimum and maximum values, and the line inside the boxes displays the median in the dataset range.

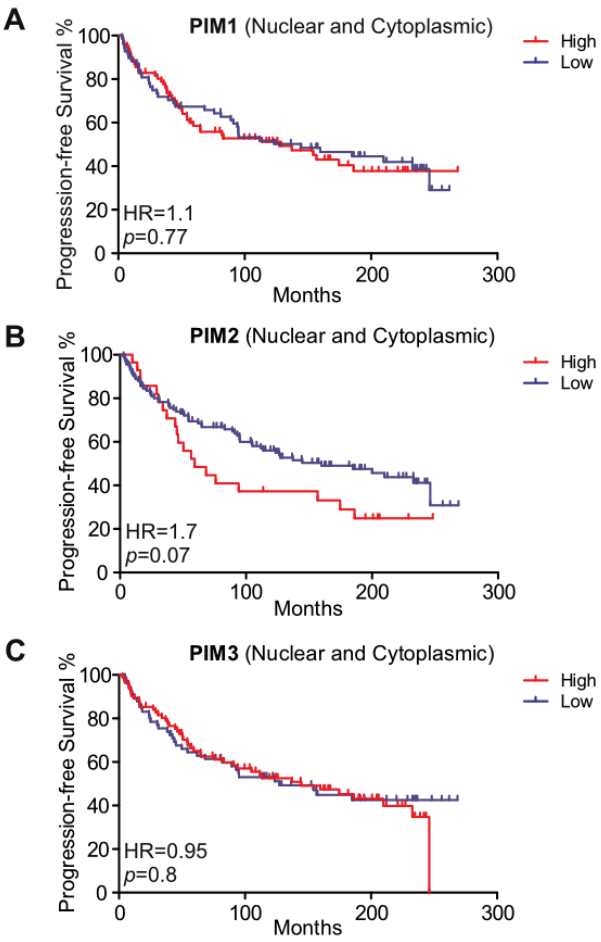

Supplementary Figure S4. PIM protein expression-related survival of patients with PCa

Kaplan–Meier analysis was used to measure the progression-free survival of patients with primary PCa who were grouped into low PIM expression and high PIM expression groups based on the median expression of **A.** PIM1, **B.** PIM2 and **C.** PIM3 proteins. *P*-values were calculated by the log-rank test. HR, hazard ratio.

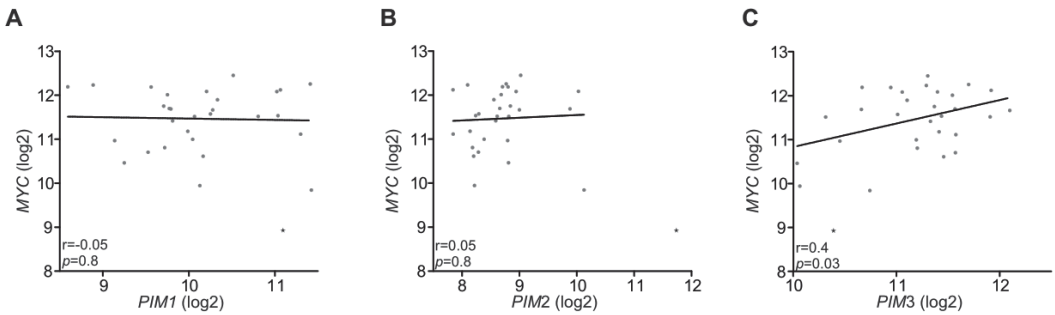

Supplementary Figure S5. Association of the *PIM* and *MYC* oncogenes in patients with PCa

<City> PCa sequencing data [19] (n=30) were used to assess the gene expression of the *PIM1* (**A**), *PIM2* (**B**) and *PIM3* (**C**) genes and their correlations with the *MYC* oncogene on a logarithmic scale in prostate cancer patient samples. *P*-values (*p*) and Pearson correlation values (r) are marked in the figures. Possible outliers of the dataset were calculated with Grubbs' test and marked as a black star in the dot blot. *P*-values < 0.05 (*), *p*-values < 0.01 (**) and *p*-values < 0.001 (***) were considered statistically significant.

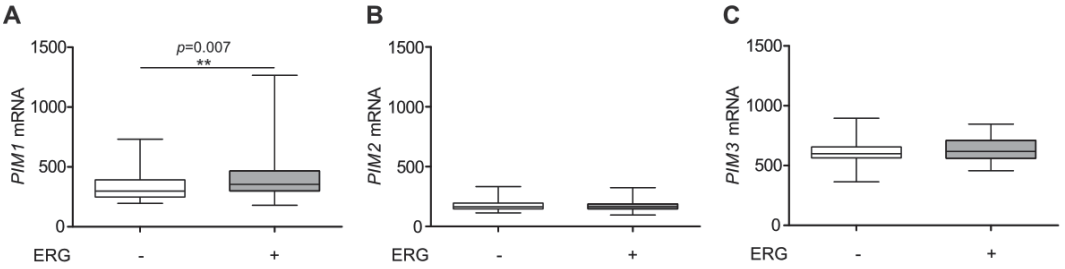

Supplementary Figure S6. *PIM* gene associations with the *ERG* oncogene

Taylor et al. dataset [20] (n=126). **A.** *PIM1*, **B.** *PIM2* and **C.** *PIM3* mRNA expression levels compared to *ERG*-negative (n=67) and ERG-positive (n=59) samples. Cutoffs for *ERG*-negative and *ERG*-positive expression values were calculated from the ERG expression average of normal prostate samples, and double the standard deviation was added to this value. Error bars display the minimum and maximum values, and the line inside the boxes displays the median in the dataset range. *P*-values (*p*) are marked in the figures. *P*-values < 0.05 (*), *p*-values < 0.01 (**) and *p*-values < 0.001 (***) were considered statistically significant.

Supplementary Table S1. PCa patient data

The number and clinicopathological description of the primary PCa prostatectomy samples used in the study.

PCa prostatectomy specimens, n	**186**
Gleason score, n (%)	
<7	67 (36)
7	95 (51)
>7	22 (12)
pT stage, n (%)	
pT1	1 (0.5)
pT2	115 (62)
pT3	68 (37)
pT4	1 (0.5)
Mean age at diagnosis 63.5 years	(median 64.0, range 49.0–72.0 years)
Mean PSA at diagnosis 14.3 ng/mL	(median 10.5, range: 1.5–78.2 ng/mL)
Median follow-up time 94.9 months	(range 2.8–268.6 months)

Supplementary Table S2. IHC data

Number of the immunohistochemical staining description of the prostatectomy samples. † HS, Histo-Score.

PIM1

Adjacent benign prostate sample, n = 23

	Cytoplasmic HS	Nuclear HS	both Cytoplasmic and Nuclear HS
Range:	0–200	0–240	0–340
Median:	70	10	110
Mean:	56	10	105

Primary PCa samples, n = 161

	Cytoplasmic HS	Nuclear HS	both Cytoplasmic and Nuclear HS
Range:	0–300	0–300	0–490
Median:	100	70	190
Mean:	114	88	202

CRPC samples, n = 45

	Cytoplasmic HS	Nuclear HS	both Cytoplasmic and Nuclear HS
Range:	100–300	0–300	190–570
Median:	200	200	350
Mean:	178	183	361

PIM2

Adjacent benign prostate sample, n = 23

	Cytoplasmic HS	Nuclear HS	both Cytoplasmic and Nuclear HS
Range:	0–100	0–10	0–110
Median:	70	10	110
Mean:	40	0	45

Primary PCa samples, n = 161

	Cytoplasmic HS	Nuclear HS	both Cytoplasmic and Nuclear HS
Range:	0–200	0–60	0–220
Median:	100	0	100
Mean:	69	5	74

CRPC samples, n = 44

	Cytoplasmic HS	Nuclear HS	both Cytoplasmic and Nuclear HS
Range:	90–210	0–90	90–290
Median:	200	0	200
Mean:	160	3	164

PIM3

Adjacent benign prostate sample, n = 23

	Cytoplasmic HS	Nuclear HS	both Cytoplasmic and Nuclear HS
Range:	100–200	0–120	100–390
Median:	200	10	210
Mean:	190	39	228

Primary PCa samples, n = 164			
	Cytoplasmic HS	Nuclear HS	both Cytoplasmic and Nuclear HS
Range:	100–300	0–210	100–470
Median:	300	0	300
Mean:	254	13	267
CRPC samples, n = 44			
	Cytoplasmic HS	Nuclear HS	both Cytoplasmic and Nuclear HS
Range:	100–300	0–240	110–440
Median:	300	0	300
Mean:	251	11	262
ERG			
Primary PCa samples, n 123			
	ERG negative		ERG positive
n:	67		56

Supplementary Table S3. Primers for qRT-PCR.

Sequences of all the primers used in the study.

***PIM1* primers for qRT-PCR**

F: 5’ CTGGGGAGAGCTGCCTAATG 3’
R: 5’ GCTCCCCTTTCCGTGATGAA 3’

***PIM2* primers for qRT-PCR**

F: 5’ TGACTTTGATGGGACAAGGGT 3’
R: 5’ GGAATGTCCCCACACACCAT 3’

***PIM3* primers for qRT-PCR**

F: 5’ ACCGACTTCGACGGCAC 3’
R: 5’ TATCGTAGAGAAGCACGCCC 3’

***TPB* primers for qRT-PCR**

F: 5’ GAATATAATCCCAAGCGGT 3’
R: 5’ ACTTCACATCACAGCTCCCC 3’